# CRYSTALLIZATION BEHAVIOR OF POLY (P-PHENYLENE SULFIDE): KINETICS AND MORPHOLOGY

by

Leonardo C. López

Dissertation submitted to the Faculty of the

Virginia Polytechnic Institute and State University

in partial fulfillment of the requirements for the degree of

DOCTOR OF PHILOSOPHY

in

Materials Engineering Science

APPROVED:

Garth L. Wilkes, Chairman

Thomas C. Ward

James E. McGrath

James P. Wightman

Edmund G. Henneke

October, 1987

Blacksburg, Virginia

# CRYSTALLIZATION BEHAVIOR OF POLY (P-PHENYLENE SULFIDE): KINETICS AND MORPHOLOGY

by

Leonardo C. López

Garth L. Wilkes, Chairman

Materials Engineering Science

(ABSTRACT)

The crystallization behaviour of poly (p-phenylene sulfide) (PPS) has been studied. Isothermal rates of bulk crystallization, spherulitic radial growth rates, and nucleation densities were analyzed as functions of molecular weight of PPS, branching agent concentration, and chemical nature of the endgroup counter-atom. The overall rate of bulk crystallization was described by an Avrami equation with exponent ~3. As molecular weight increased in the 24,000-63,000 range, the rates of spherulitic growth and bulk crystallization decreased by a factor of 4. The nucleation density of PPS with $<M_w>$ =24,000 was 32-fold lower than those of the higher molecular weight polymers. Introduction of 0.2% by weight of branching agent trichlorobenzene in the synthesis vessel reduced the spherulitic growth rate to 1/2, and the rate of bulk crystallization and the nucleation density to 1/4 of those of the linear polymer of the same molecular weight. The decreasing order of crystal growth rates for the endgroup counter-atoms is Ca > H > Zn > Na with calcium providing growth rates two-fold higher than the sodium counter-atom. The rates of overall bulk crystallization (K) followed the decreasing trend H > Zn > Ca > Na. For hydrogen, K was 17-fold higher than that of sodium counter-atom. The nucleation densities presented a different trend, H > Na > Zn > Ca.

The spherulitic growth rates were analyzed in terms of equations proposed to explain the molecular weight dependence. The logarithm of the crystal growth rate followed a linear function of the logarithm of the number average molecular weight proposed by Cheng and Wunderlich.

Since most processing operations occur under non-isothermal conditions, the non-isothermal crystallization of PPS was also studied. Differential scanning calorimetry data followed a model proposed by Ozawa for non-isothermal kinetics of crystallization. This model allowed the determination of the Avrami exponent under non-isothermal conditions. The values of the Avrami exponent obtained were in good agreement with values determined isothermally.

The morphological textures of semicrystalline poly (p-phenylene sulfide) (PPS) were investigated utilizing two etching techniques to enhance the finer details. One technique was based on the partial attack of chromic acid solutions at high temperature (100°C), whereas the other used suspensions of anhydrous aluminum chloride at lower temperature (35°C). The aluminum chloride approach was shown to be more appropriate and successful in enhancing the fine details in textures of PPS. This reagent selectively attacked amorphous PPS enhancing the crystalline textures to a greater extent than the chromic acid approach. This technique allowed the observation of the spherulitic growth habit and the "interconnectivity" between impinged spherulites.

The morphology of PPS in composite materials containing few carbon fibers was analyzed. Low crystallization temperatures, slow cooling rates, low molecular weight polymer and local orientation favored the nucleation of transcrystallinity at the carbon fiber surface. T300U carbon fibers were the most effective in nucleating transcrystallinity. Fiber anodization in $H_2SO_4$ and NaOH electrolytes decreased the nucleating ability of the fibers possibly due to an increase of polarity at the fiber surface. Utilization of the aluminum chloride etching technique in conjunction with scanning electron microscopy confirmed that PPS was nucleating at the fiber surface and showed the radial growth habit and cylindrical symmetry of the transcrystalline regions.

*Lovingly dedicated to Virginia*

# Acknowledgements

I wish to express my sincere appreciation and deep gratitude to Professor Garth L. Wilkes for his understanding, support and suggestions throughout the course of this dissertation. I also wish to extend my gratitude to Professors J. E. McGrath, T. C. Ward, J. P. Wightman and E. G. Henneke for their critical comments and helpful suggestions on this work.

My gratitude goes to Drs. C. J. Stacy, J. F. Geibel and T. W. Johnson of the Phillips Petroleum Company for providing the polymer samples utilized in this investigation and for very helpful discussions. I would also like to convey my appreciation to Dr. T. A. Devilbiss for spawning my interest in composite materials through his contagious enthusiasm and also for sharing some of his carbon fiber samples and characterization data.

I am grateful to the Graduate School and the University for my selection as a Cunningham Dissertation Year Fellow for the 1986-87 academic year. Financial support from the Phillips Petroleum Company is gratefully acknowledged. I would also like to acknowledge the financial support of the American Chemical Society that made possible the presentation of parts of this dissertation at the 194th National Meeting of the American Chemical Society in New Orleans, in August 1987.

Deep appreciation goes to all my colleagues and friends that made graduate school a wonderful experience.

My heartfelt thanks go to my parents, and for their ever present love and support, and for teaching me the value of education. My parents in law and have also been very loving and supportive throughout my graduate career and I certainly appreciate their devotion. Finally, without the love and

support of , my wife, none of this would have been possible. She has been my inexhaustible source of strength and inspiration.

# Table of Contents

# List of Illustrations

# List of Tables

# CHAPTER I

# INTRODUCTION

Amongst the various high temperature polymers, those based on aromatic units, such as poly (2,6-dimethylphenylene oxide) (PPO), poly (phenylene sulfide) (PPS), poly (ether ether ketone) (PEEK), and poly (ether sulfone) (PES) have attracted much attention in the last few years due to their good thermal and chemical resistance. One of these polymers, Poly (p-phenylene sulfide) (PPS) is also an important high strength/high temperature engineering thermoplastic that is finding increasing use in technological applications such as molding resins, fibers and matrices for thermoplastic composites. PPS consists of para-phenylene units alternating with sulfide linkages. The first known report of its synthesis was by Grenvesse in 1898 (1). However, interest in the synthesis of PPS only began in 1948 when Macallum (2) described the preparation of (phenylene sulfide) polymers by the melt reaction of p-dichlorobenzene with sodium carbonate and sulfur. Further investigation on the synthesis of PPS by Lenz and coworkers (3,4,5), and later by Edmonds and Hill (6) developed PPS into a commercial reality. After their synthesis, the polymer is an off-white powder that has a glass transition temperature ($T_g$) at 85°C and melting point at about 285°C. The off-white coloration is known to be due to the presence of $Fe^{+3}$ ions in the form of $FeCl_3$ that arise from the steel reactor utilized to synthesize PPS. However, this problem has been avoided by utilizing a titanium reactor instead of a steel one. Therefore, "white" or purer polymer can be obtained

(7). The study of the structure and molecular weight distribution of PPS has been precluded by its intrinsic high chemical resistance. Only recently, a gel permeation chromatographic system (GPC) capable of determining molecular weights and molecular weight distribution of PPS has been developed (8). The GPC experiments are conducted utilizing α-chloronaphthalene as the solvent at 210°C in order to maintain PPS in solution. Typical polydispersity ratios of PPS synthesized by the method of Edmonds and Hill are in the order of 1.5-2.0.

One of the important characteristics of PPS is its ability to undergo reactions upon heating in air to produce a "cured" polymer. The mechanisms involved in this "curing" process are not fully understood. However, it is accepted that the process consists of oxidative crosslinking, chain-extension and chain-scission reactions (9). In addition, it is known that the substitution of the oxygen atmosphere by nitrogen slows down the curing process to an unnoticeable level. As will be explained later, the "curing" process can be performed by two different methods. One comprises a melt process, and the other is a solid state process. The former process can produce a dark infusible solid material, while the latter has been utilized to moderately increase the molecular weight of PPS. This "curing" behaviour of PPS has been considered an advantage for many applications. In particular, the coating industry has used the "curing" of PPS as a processing variable. For example, PPS coatings can be applied to substrates by techniques such as water-dispersed slurry spraying, and fluidized-bed coating, followed by a bake cycle at high temperature (350°C) in order to cure the polymer and form a hard, tough coating with excellent chemical resistance (10).

Other important properties of PPS include superior mechanical properties, thermal stability, excellent chemical resistance, flame resistance, and precision moldability (11,12). The mechanical properties are represented by a tensile strength of 65 MPa (ASTM D638), an elongation of 1.1% (ASTM D638), and a flexural strength of 96 MPa (ASTM D790). Its chemical resistance is evidenced by a high degree of insolubility in most organic solvents below 200°C. PPS is adversely attacked by high temperature exposure to a few organic solvents, strong

oxidizing environments and mineral acids. The thermal stability is manifested by a weight loss of less than 5% when PPS is heated up to 500°C in air. This unusual combination of properties allows the use of PPS in pump impellers, ball valves, wear rings, electrical sockets, battery and telephone components, chip carriers, optical-fiber cables, electronic component encapsulants, and as a thermoplastic matrix for composite materials. In addition, the para-phenylene structure of PPS has attracted physicists very much due to the possibility of electron transfer mechanisms that can take place. Therefore, great emphasis has been placed in this topic, and as a result, PPS has been rendered electrically conductive through the addition of dopants such as arsenic pentafluoride (13,14).

The next chapter will be concerned with a review of the state of knowledge on poly (p-phenylene sulfide) synthesis, structure, and properties. It will become apparent to the reader that there are still quite a few areas in need of systematic studies in order to achieve a better understanding of the phenomena occurring. One of these areas is the crystallization behaviour of PPS; i.e., the kinetics of crystallization and crystalline morphology. These two areas are very important because many properties of polymers depend on them. For example, the properties of a semicrystalline polymer that developed a superstructure quiescently are different from those of a polymer that developed a superstructure under an applied strain. In the latter case, the modulus in the direction of the straining force will be higher than those in the other two perpendicular directions. A similar effect occurs with the optical properties. However, this is not the case with superstructures obtained quiescently. Furthermore, the kinetics of formation of the superstructure may affect the morphology obtained. This is a critical point to take into account for the processing of thermoplastic composites with semicrystalline polymer matrices. Therefore, a fundamental investigation of the crystallization behaviour of PPS was undertaken. In particular, the effects of molecular weight, branching agent content, and chemical nature of the endgroup counter-atom on the kinetics of crystallization of PPS were studied. Furthermore, the morphological textures of semicrystalline PPS, and PPS in carbon fiber composites were investigated. In the next two chapters, two

reviews will be presented to introduce the reader to the subject. The first review will be concerned with PPS, whereas the second one will address some of the fundamental principles of polymer crystallization.

# CHAPTER II

# POLY (P-PHENYLENE SULFIDE) - A LITERATURE REVIEW

## *2.1 SYNTHESIS OF POLY (P-PHENYLENE SULFIDE)*

The structure of poly (phenylene sulfide) was first assigned to a largely insoluble material "melting" at 295°C by Grenvesse in 1898 (1). The product was obtained by heating benzene with sulfur in the presence of aluminum chloride. Similar descriptions were given by other workers by the turn of the century. For example, Deuss (15) obtained similar products by reacting thiophenol with aluminum chloride. Hilditch (16) produced a cream colored, insoluble powder by self-condensation of thiophenol in concentrated sulfuric acid with the empirical formula $C_6H_4S$ . Glass and Reid (17) also obtained a resinous product by heating benzene with sulfur at 350°C. In all cases, however, ill defined polymers were obtained, and the presence of many by-products such as thiophenol, phenyl sulfide, phenyl disulfide, and thianthrene caused very low polymer yields.

Interest in the synthesis of poly (phenylene sulfide) only began in 1948 when Macallum (2) obtained this polymer by condensation polymerization. Macallum synthesized phenylene

sulfide polymers from the melt reaction of p-dichlorobenzene with alkali and alkaline earth metal sulfides catalyzed by sulfur. The reaction occurred at about 300°C and under pressure. In particular, most of this authors' work was based on the condensation of p-dichlorobenzene with sodium carbonate and sulfur, where the composition and properties of the polymers obtained were very much dependent on the ratio of reactants,

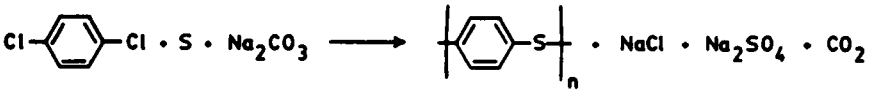


A molar ratio of sulfur and sodium carbonate to p-dichlorobenzene of 1.5:1 produced polymers with empirical formulas close to the theoretical for poly (phenylene sulfide); i.e., $x \cong 1.0$. However, due to the nature of the melt reaction, it was very difficult to control. Therefore, Lenz and coworkers (3,4,5) undertook a detailed study of the Macallum polymerization in order to understand it and control it. Lenz and Carrington (3) proposed a mechanism for the Macallum polymerization that consisted of several steps. The reaction would start by the formation of polysulfides by a series of nucleophilic substitution type of oxidation-reduction reactions between $Na_2CO_3$ and sulfur. Initiation of the polymerization would occur through radical attack by sulfur on the aromatic ring to form a polysulfide side chain. This polysulfide would cleave by nucleophilic substitution to form a thiophenoxide anion. Since the thiophenoxide anion is a much stronger nucleophile than the sulfide or polysulfide anions, the thiophenoxide anion would initiate the polymerization by forming the first diaryl sulfide linkage (Fig. 1a). Subsequently, propagation of the reaction would result from successive nucleophilic substitutions by sulfide and thiophenoxide anions on the haloaryl sulfides (Fig. 1b).

Later, Lenz and Handlovits (4) studied the structure of poly (phenylene sulfide)s obtained by the Macallum polymerization. These authors compared the Macallum polymers with a "linear" poly (phenylene sulfide) of low molecular weight prepared by self-condensation of sodium p-chlorothiophenoxide. Crystalline melting points in the range of 270-285°C were found

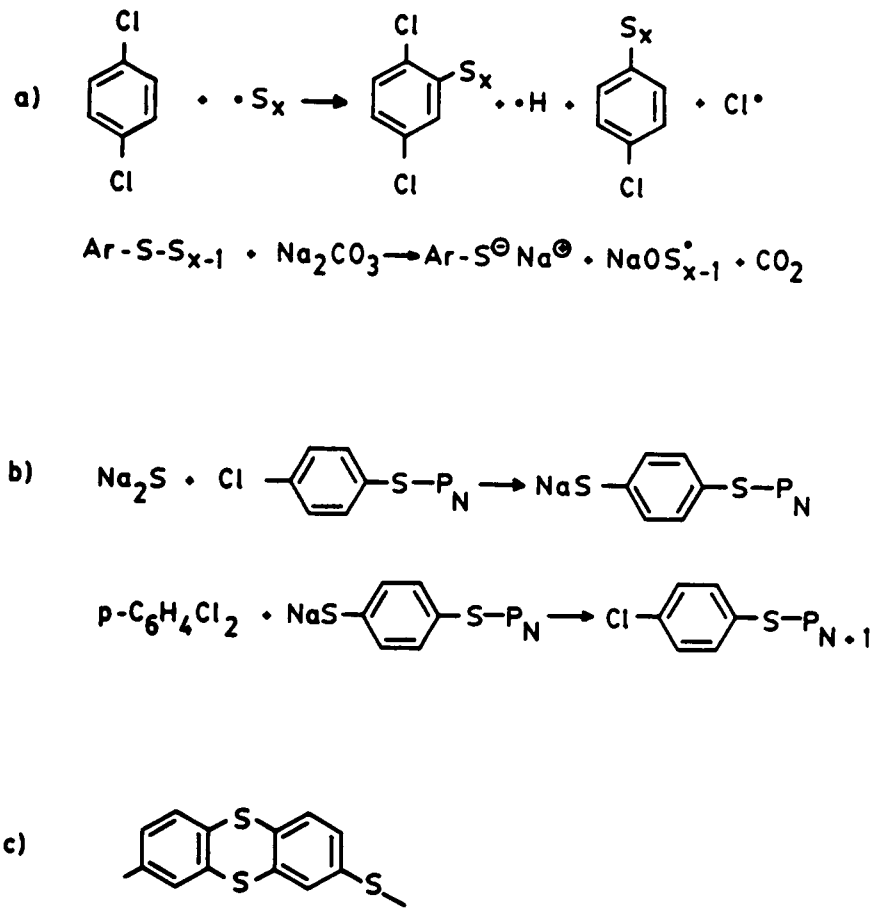


**Figure 1.** **Reaction mechanism proposed for the Macallum polymerization. (from 3):** $P_N$ represents a polymer chain with degree of polymerization N.

for both polymers. The x-ray diffraction patterns were also very similar. However, infrared spectra showed a significant difference in the 860-900 $cm^{-1}$ wavenumber range. The Macallum polymers presented a band in this region characteristic of 1,2,4-trisubstitution on the benzene ring, indicating the branched (and possibly partially crosslinked) nature of the Macallum polymers. This branching was attributed to radical attack of sulfur on the benzene rings of the aromatic monomers or repeating units during the early stages of the reaction. Elemental analysis showed a sulfur content of 15-20% higher in the Macallum polymers. However, this could not be attributed to a high incidence of polysulfide groups since the polymers were stable up to 460°C and polysulfide bonds would cleave homolytically at temperatures well below 300°C. Therefore, the higher sulfur content was explained in terms of the formation of thianthrene-type repeating units (Fig. 1c).

Finally Lenz, Handlovits and Smith (5) investigated other routes for the synthesis of poly (p-phenylene sulfide). They prepared linear poly (phenylene sulfide) by the condensation polymerization of alkaline metal salts of p-halothiophenols in pyridine. Salts of I, Br, F, and p-Cl-thiophenols were utilized. The sodium salt of p-bromothiophenol gave more quantitative results. However, complete control of side reactions was not achieved, producing low molecular weight polymers (degree of polymerization $\cong$ 20).

Using an approach similar to Macallum (2), Hortling and Lindberg (18) studied the effect of substituents of chlorobenzene on their melt reaction with sulfur at 200-350°C for the synthesis of poly(phenylene sulfide). The monomers investigated included 1,4-dichlorobenzene, 4-chlorobenzoic acid, 4-chlorophenol, 4-chloroaniline, 4-chlorotoluene and chlorobenzene. They found that higher reaction temperatures, longer reaction times and greater chlorine content in the monomers increased the conversion, yield and molecular weight of the polymer. Moreover, the amount of crosslinks and insoluble products was increased by the same factors. However, when no chlorine was present in the monomers, the reactions occurred at higher temperatures and the products were of low molecular weight. These same authors suggested that the reactions were initiated by a substitution of the chlorine atoms by sulfur to

form diaryl polysulfanes. Propagation would continue by homolytic dissociation of disulfide and polysulfide bonds at high temperatures, with formation of more condensed structures containing monosulfide bonds through radical reactions.

A commercially feasible synthetic route for poly (p-phenylene sulfide) (PPS) was first developed by Edmonds and Hill (6). The process involved the polycondensation of p-dichlorobenzene with sodium sulfide in N-methyl pyrrolidone at 260°C and pressures in the order of 160psi. This reaction produced PPS with molecular weight in the range of 15,000-20,000. The mechanism of the reaction is believed to be a series of nucleophillic displacement reactions that lead to the formation of PPS and sodium chloride as a by-product (19). Recently, a similar reaction scheme has been investigated by Rajan, Ponrathman and Nadkarni (20). These authors studied the kinetics of the polycondensation reaction of p-dichlorobenzene and $Na_2S$ in N-methyl pyrrolidone at 195°C and 30psi. The reaction followed second-order kinetics and had a bimodal rate. There was a slow initial rate up to 50% conversion followed by a faster rate at higher conversions ($\cong$2.5 times faster). The slow initial rate was partially attributed to the limited solubility of sodium sulfide in N-methyl pyrrolidone. They also analyzed the development of the degree of polymerization with reaction time by intrinsic viscosity measurements. Figure 2 shows a plot of intrinsic viscosity as a function of reaction time. It was observed that the intrinsic viscosity reached a plateau after a reaction time of six hours, indicating that the molecular weight of PPS did not increase after 6 hours of reaction time. Furthermore, Radhakrishnan et al. (21) studied the effect of reaction time and stirring speed on the crystallinity, particle size and morphology of PPS synthesized by the same method. The crystallinity determined by x-ray diffraction techniques decreased from 74% to 68% after 6 hours of reaction. These values may be attributed to the presence of low molecular weight species at the beginning of the reaction that can easily crystallize and at higher rates. The particle size and polymer yield increased with reaction time in a very similar way. The particles seemed to have a porous structure with a generally spherical shape containing a "sheaf-like" structure or "lettuce-like" structure as these authors described it. The

stirring speed affected the morphology by producing bigger and more compact particles as the speed was increased. Moreover, the particle size distribution was sharpened.

The structure of the species present in PPS synthesized by the Edmonds and Hill (6) process has been studied (22,23,24). Reents and Kaplan (22) utilized methylene chloride extraction, high performance liquid chromatography and solid probe mass spectroscopy (MS) to analyze the oligomers present after synthesis. These authors found the presence of cyclic , as well as linear (p-phenylene sulfide) oligomers. The linear species were chlorine terminated, single chlorine terminated, and with no chlorine endgroups. They also noticed the presence of dibenzothiophene. Similarly, Battiste et al. (23) utilized a combination of laser desorption Fourier transform MS, field ionization MS, and gas-chromatography MS to determine the oligomers present in PPS. These authors reported that the major components were cyclic oligomers; the pentamer, hexamer and heptamer were the most abundant. Linear oligomers of the kind Reents and Kaplan (22) found were also observed. In addition, Battiste et al. (23) identified nitrogen substituted pyrrolidone, substituted methyl amines and phenolic ethers. A comparative study of the oligomers present in the synthesis of poly (o-phenylene sulfide) (o-PPS), poly (m-phenylene sulfide) (m-PPS), and poly (p-phenylene sulfide) (p-PPS) was performed by Montaudo et al. (24). The o-PPS isomer presented mostly thianthrene species. The m-PPS isomer showed cyclic oligomers from trimers to heptamers, with the cyclic trimer as the most abundant. These authors, however, reported that only traces of cyclic oligomers were observed in p-PPS.

Recently, Campbell (25) developed an improved process for the synthesis of PPS with higher molecular weight (35,000-65,000). The scheme involves the reaction of p-dichlorobenzene with $Na_2S$ in N-methyl pyrrolidone with an alkaline metal salt of acetic acid, propanoic acid, benzoic acid or phenol at 245°C and 5.4-9.5 atm. It has been claimed that by using 1,2,4-trichlorobenzene as a comonomer in this reaction scheme, the molecular weight of PPS can be increased to 200,000 (26). Another method utilized to increase the molecular weight of PPS is *curing*, a phenomenon that will be addressed in a following section (27). The

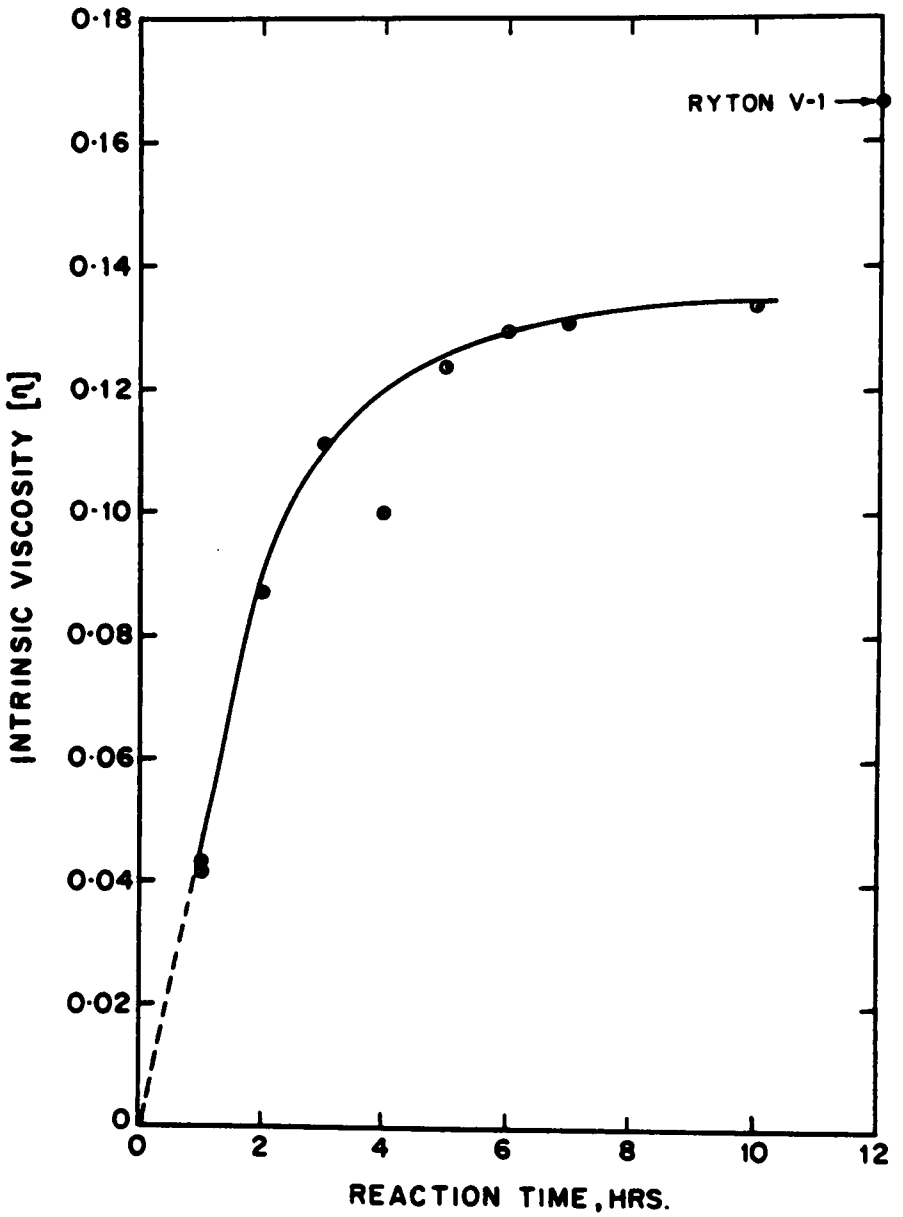


**Figure 2. Plot of intrinsic viscosity as a function of synthesis reaction time for PPS. (from 20)**

mechanism of the Campbell reaction was traditionally considered to be a nucleophillic substitution. However, Koch and Heitz (28) proposed a one-electron-transfer process with radical cations as reactive intermediates as shown in Fig. 3 (Reactive Intermediate Polycondensation). This mechanism involves five types of reactive intermediates: sulfenyl radicals (A), aromatic radicals (B and B'), and radical cations (C and C'). Generation of any of these would provide entry into the propagation cycle. The chain is initiated by a one-electron-transfer process to form $HS^{\bullet}$ . Formation of the disulfide D is inherent to the mechanism, and explains its presence as a by-product. Furthermore, it indicates the need of high temperature in order to cleave the disulfide linkage homolytically, otherwise, the chain propagators would be destroyed. The chain propagation occurs by the reaction of the sulfenyl radicals (A) with 1,4-dichlorobenzene, and with oligomers (F) formed by electron transfer of $HS^{-}$ to the radical cation (Fig. 4a). As opposed to polycondensation, the formation of PPS would not require equal reactivity of the endgroups irrespective of chain length due to the formation of reactive intermediates C,C' which are of higher reactivity than the monomer. This reactivity decreases with increasing chain length due to increasing conjugation (Fig. 4b), and leads to products with intermediate molecular weight at the beginning of the reaction even if the reactants are not added in stoichiometric amounts. For example, Fig. 5 presents schematically the dependence of molecular weight on the conversion for four types of polymerizations. In the Reactive Intermediate Polycondensation proposed by Koch and Heitz (28), high molecular weight products are obtained near the end of the reaction, similar to condensation polymerizations.

Other synthesis methods for the preparation of PPS have been investigated. For example, Wejchan-Judek and Rogal (29) studied the preparation of poly (phenylene sulfide)s by oxidation of thiophenol with thionyl chloride in the presence of $FeCl_3$, $BF_3$, $ZnCl_2$, $TiCl_4$, and Sn $Cl_4$; and Wejchan-Judek (30) used $WCl_6$, $SbCl_5$, and $H_2SO_4$ as catalysts. The synthesis with Sb $Cl_5$ was not successful, no polymer was obtained. The rest of the catalysts produced polymers that contained partly cyclic structures. Polymers synthesized in the presence of $FeCl_3$ , $ZnCl_2$,

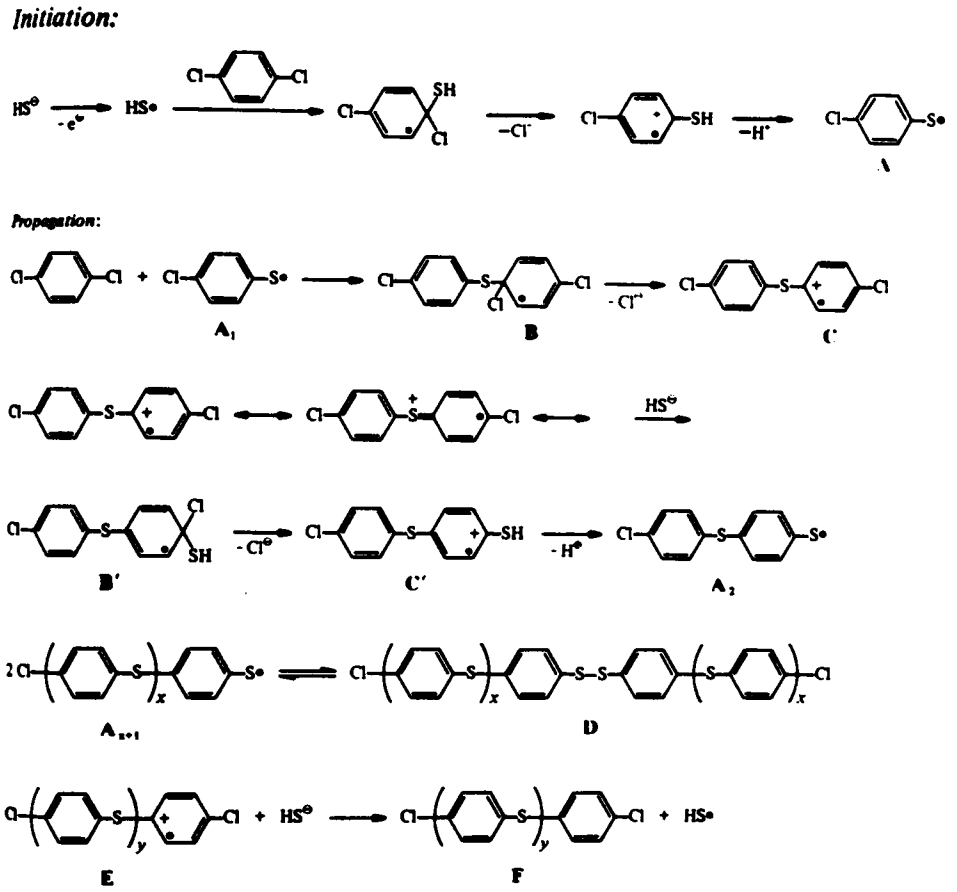


**Figure 3. Reaction mechanism proposed for the synthesis of PPS by the method of Campbell. (from 28)**

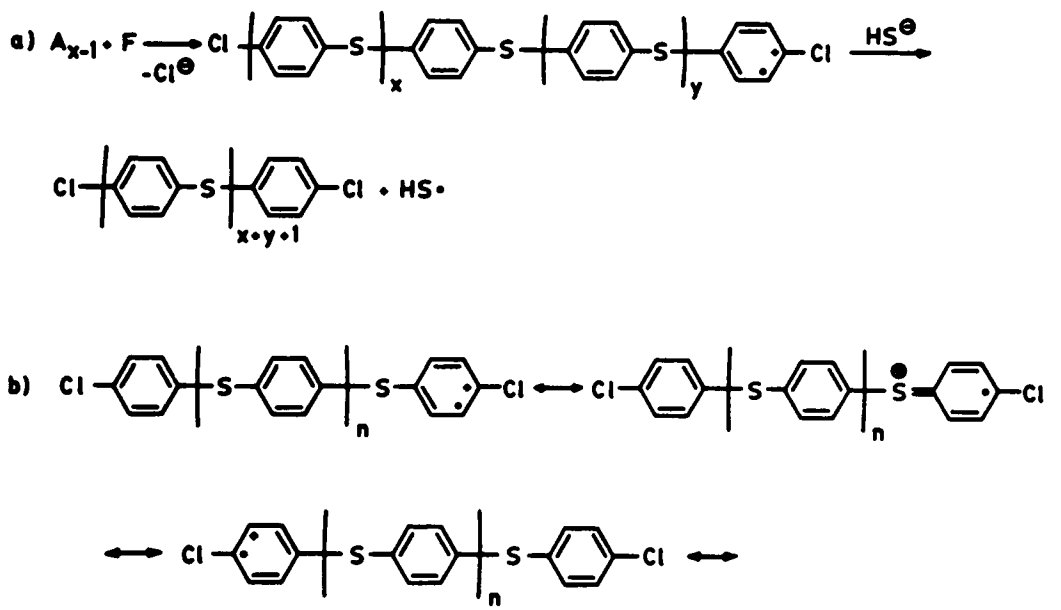

**Figure 4.** **Reaction mechanism proposed for the synthesis of PPS by the method of Campbell. (from 28):** a) Electron transfer from HS to the radical cation. b) Stabilization of the reactive intermediate C by conjugation.

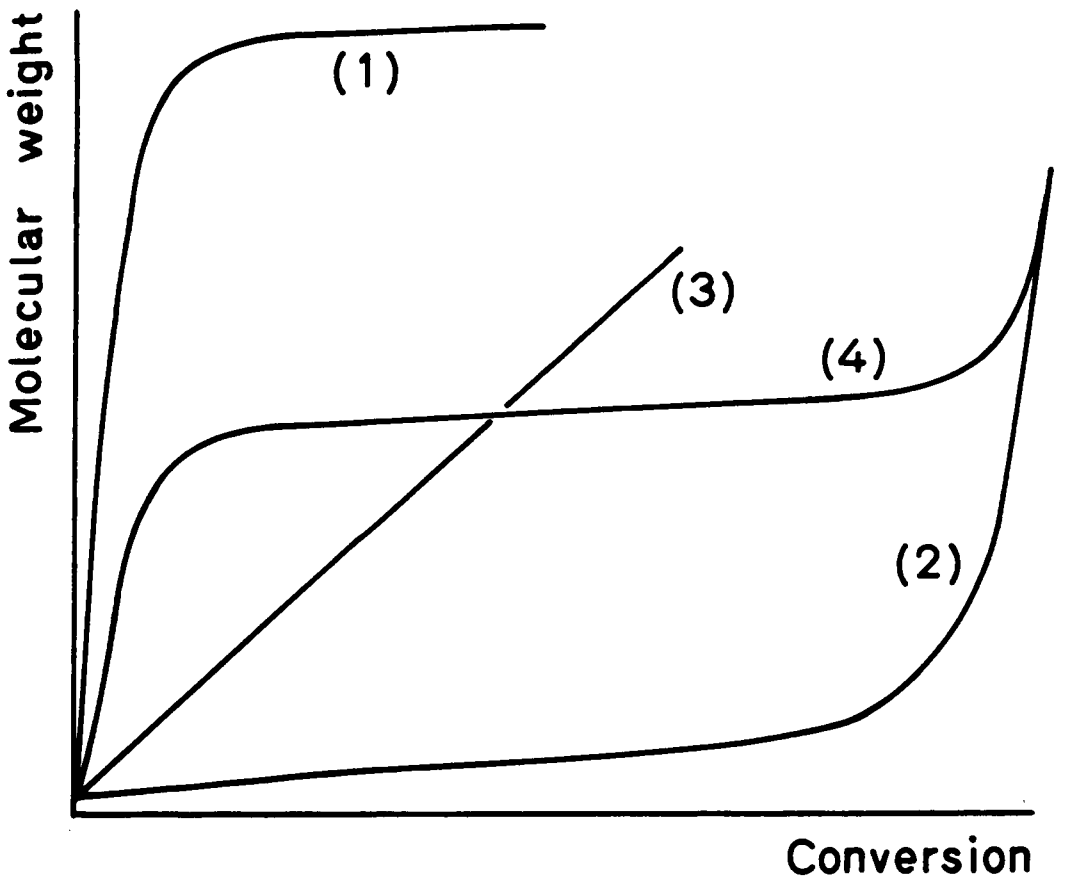


**Figure 5.** **Schematic representation of the dependence of molecular weight on conversion for four types of polymerizations. (from 28):** (1) Radical Polymerization; (2) Polycondensation; (3) Living Polymerization; (4) Reactive Intermediate Polycondensation.

$SnCl_4$, and $TiCl_4$ were amorphous. Polymer synthesized with $BF_3$ catalyst had crystallinity of the order of 68% (by x-ray diffraction) and showed sequences of a unit cell similar to that of Ryton® made by Phillips Petroleum Co. Elemental analysis showed that significant amounts of oxygen were present in all polymers, with the exception of those synthesized in the presence of $BF_3$. It was suggested that oxygen was present in the form of sulfoxide groups. Kreja et al. (31) synthesized poly (phenylene sulfide)s utilizing a modified version of the Grenvesse reaction. They utilized the reaction of benzene, elemental sulfur and aluminum chloride at 80°C under an inert atmosphere. However, they obtained polysubstituted poly (phenylene sulfide)s containing linear, cyclic and crosslinked species. Solution polymerization of PPS by reaction of cuprous 4-bromothiophenoxides in quinoline-pyridine has also been reported (32). Nevertheless, none of these methods are commercially feasible as the methods of Edmonds and Hill (6), and Campbell (25) mentioned above.

Recently, a very different approach to synthesize PPS has been taken by Novi et al. (33). These authors synthesized PPS by polymerization of sodium p-bromobenzenethiolate in DMSO at room temperature utilizing catalytic amounts of a diazonium salt (solid arenediazonium tetrafluoroborate) via a radical, radical-anion chain pathway. The reaction was carried out in argon. The step sequence of the reaction proposed by Novi et al. is shown in Fig. 6 . It consists of a single-electron transfer from the thiolate to the initiator to form an aryl radical (A); growth of the chain occurs by radical/anion coupling (B) and expulsion of bromide with formation of a new radical (C). Chain growth may be terminated by oxidation of a radical anion by residual initiator, or radical/radical coupling, or H-atom transfer to a radical from the medium.

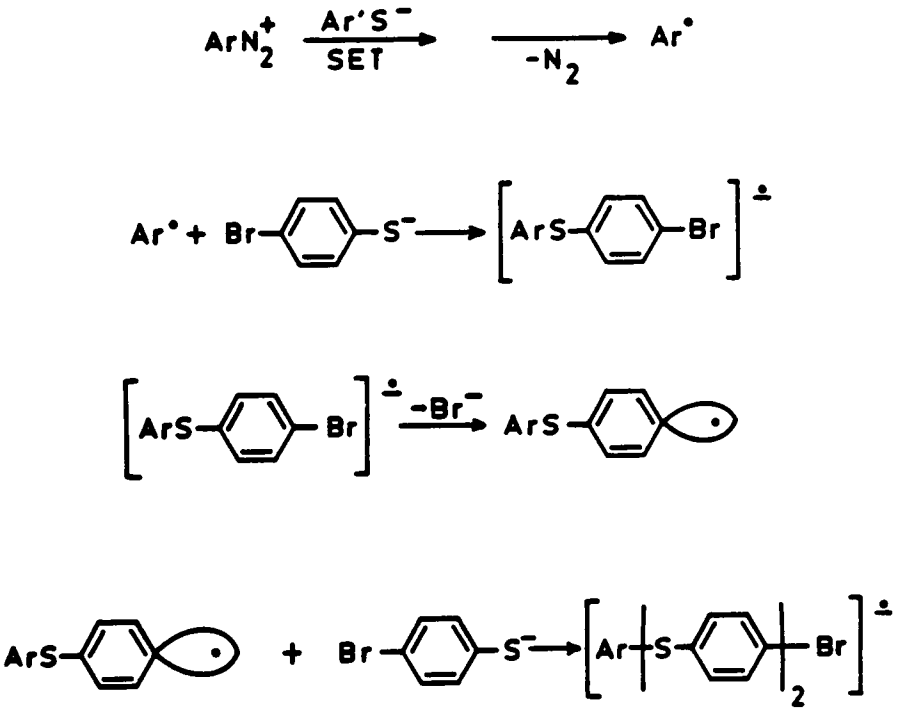

Figure 6. Reaction sequence proposed by Novi et al. (from 33)

## 2.2 *PROPERTIES*

### 2.2.1 "Curing" of PPS

It was mentioned above that PPS has the unique characteristic of being classified as a thermosetting-thermoplastic. This means that PPS can undergo "curing" reactions upon heating in the presence of oxygen. It has been stated that by curing PPS, the molecular weight of the polymer is increased and the toughness, the ductility and insolubility can be increased to a certain extent (12). This curing behavior has been amply utilized , especially in the coatings industry where by curing PPS films, very hard and chemically resistant coatings can be developed. For example, coatings can be applied to substrates by techniques such as water-dispersed slurry spraying, and fluidized-bed coating, followed by a bake cycle at high temperature to cure the polymer (10). Although the curing behaviour has been viewed as an advantage for most processes, several patents have been issued concerning the stabilization of PPS with respect to curing (34). The curing process of PPS has been performed by two different methods (35). The first one is a melt process in which PPS is heated at temperatures above the melting point (315-425°C). The polymer melts and upon continued heating, it darkens and thickens. After several hours of heating, it gels and eventually solidifies to a dark infusible solid. This curing route is slow, therefore, negligible changes occur when PPS is processed under typical conditions. The second curing method involves a solid state process in which PPS is heated in air at temperatures below its melting point (175-280°C). This method has been utilized to increase the molecular weight of the polymer. Figure 7 (35) shows the change in melt flow of PPS with reaction time as PPS is cured at different temperatures. The melt flow decreases as the curing time increases, indicating an increase in molecular weight. Furthermore, the rate of cure of PPS is faster at higher temperatures.

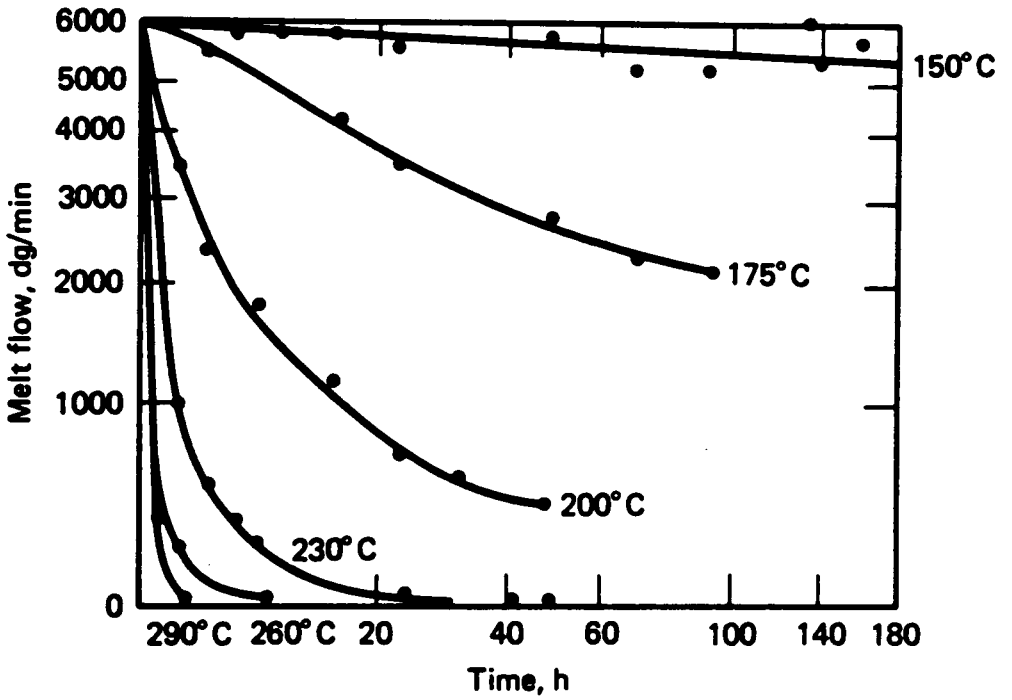


**Figure 7.** **Plot of melt flow as a function of curing time at different curing temperatures. (from 35)**

As may be expected, the properties of PPS are affected by the curing process. However, very few systematic studies of the effect of curing on the properties of PPS have been reported. For example, Wejchan-Judek and Zuk (36) studied the curing of PPS with sulfur at 290°C in an argon atmosphere. They indicated that the impact resistance, thermal stability and crystallization behaviour was affected by the amount of sulfur linked during the curing reaction. The impact resistance increased from 52,800 J/m² to 85,600 J/m² as the sulfur linked during the curing reaction changed from 0 to 0.94% by weight. Further increase of sulfur linked during the reaction to 3.44% by weight caused a decrease of the impact resistance to 54,000 J/m². Thermogravimetric analysis showed a lower thermal stability of samples containing larger amounts of sulfur linked during the curing reaction. These same authors reported that the degree of crystallinity as measured from x-ray diffraction measurements decreased from 79% (uncured PPS) to 0 for PPS containing 5.4% sulfur linked during the reaction. However, Brady (37) stated that curing of semicrystalline PPS at 260°C for 24 hours did not change the crystallinity index. Nevertheless, upon melting and recrystallization, the crystallinity index was reduced from 61% to 31%; i.e., the ability of the polymer to crystallize was reduced by the curing treatment. Similarly, Zeng and Ho (38) studied the effect of curing on the spherulitic textures of PPS. Observations in the polarized light microscope showed spherulites with diameter of 20-30 μm in uncured PPS. On the other hand, PPS solid-state cured at 270°C for 22 hours and crystallized from the melt formed only minute superstructures that did not present Maltese Cross patterns. These authors also indicated that there was no difference in the average crystallite size of uncured and solid-state cured PPS, implying that solid-state curing impeded the formation of a superstructure, namely spherulites, but had little effect on the size of the crystallites. These authors also studied the effect of curing on the corrosion resistance to chromic acid. They reported that solid-state curing at 270°C for 22 hours reduced the corrosion resistance of PPS, presumably due to the decrease of crystalline content and lack of superstructure formation. However, melt-cured PPS (370°C) presented a higher corrosion resistance than uncured PPS due to the formation of an amorphous network structure (crosslinking). Joshi and Radhakrishnan (39) also studied the effect of curing tem-

perature on the crystallinity of PPS coatings. Figure 8 shows a plot of crystallinity as a function of curing temperature for PPS cured for 30 minutes. The percent crystallinity decreases as a function of curing temperature and it reaches zero for PPS cured above the melting point (300°C). Moreover, they reported that annealing at 200-205°C for 3-4 hours produced crystallinities of about 15%. However, no crystallinity was observed on samples cured at temperatures above 370°C even after extended annealing. The influence of the time of melt-curing on the heat of melting has been studied (40). It was reported that the heat of fusion decreased from 5.12 cal/g to zero as PPS was heat treated at 320°C in air from zero to 96 hours. Also, there was a simultaneous reduction of the melting temperature of the polymer.

The understanding of the mechanisms involved in the curing process has been precluded by the insolubility of PPS. Early workers in this subject suggested the occurrence of chain-extension reactions, crosslinking processes, chain-scission processes, and oxidation reactions (41,42,43). A somewhat detailed study of the cure of PPS in air was performed by Hawkins (9). An increase of 0.90% by weight of oxygen was found in PPS cured at 370°C for 24 hours. Furthermore, infrared spectra of cured PPS had several differences with that of uncured PPS. The differences were interpreted by Hawkins as increasing aryl C-O species, increasing 1,2,4-trisubstitution in benzene rings, decreasing para-substitution, and decreasing C-S bond number. Decrease of para-substitution was in agreement with the increase of 1,2,4-trisubstitution in the benzene ring, and the decrease of C-S bond number was also consonant with the observation of $SO_2$ loss during the curing reaction. Therefore, Hawkins proposed that four types of reactions occurred during the cure of PPS:

1. chain-extension reactions, as showed in Fig. 9(1)

2. oxidative crosslinking to form tri-substituted species as those showed in Fig. 9(2)

3. thermal crosslinking to produce also tri-substituted species as shown in Fig. 9(3)

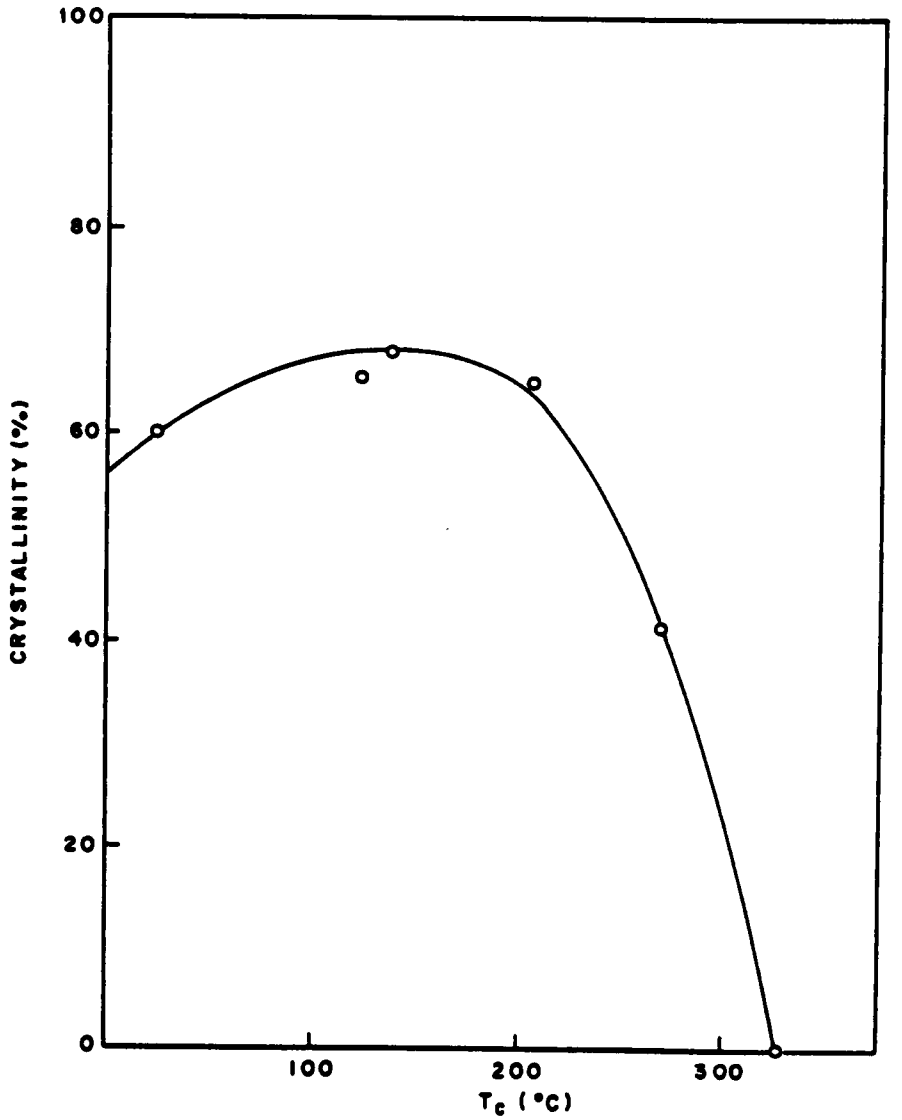


**Figure 8. Percent crystallinity as a function of curing temperature for PPS. (from 39)**

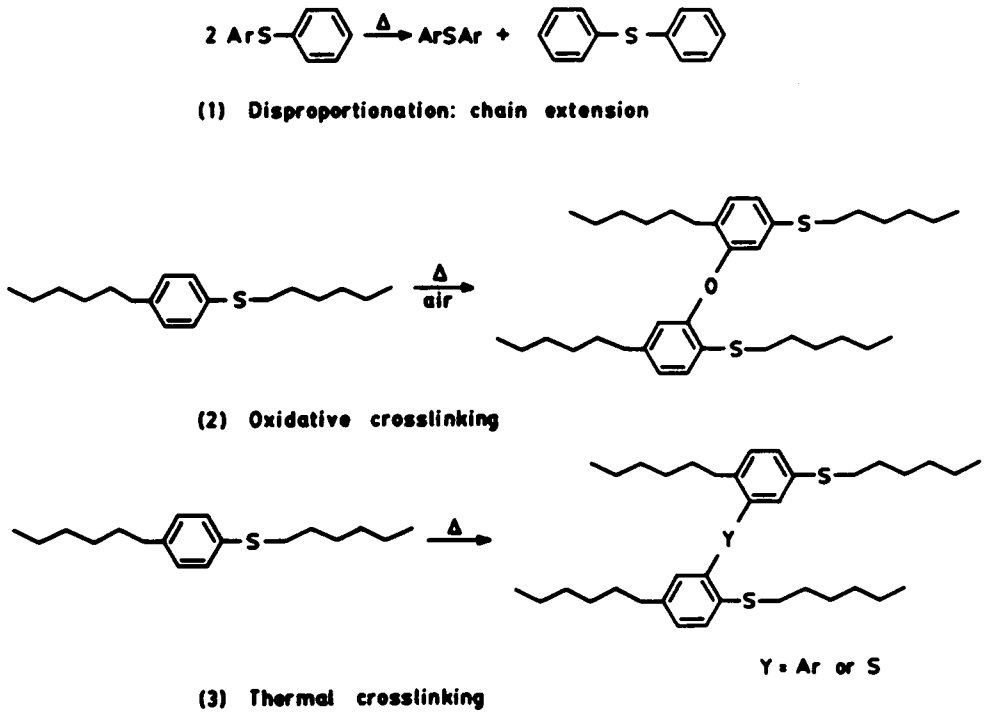


**Figure 9. Reactions proposed to occur during the curing processes. (from 26)**

4. oxygen uptake followed by loss of $SO_2$.

Mass spectroscopy studies on PPS solid-state cured in air (22) support reactions (1) and (2). PPS solid-state cured in air showed a reduction in the amount of chlorine terminated linear chains and presented the appearance of (phenyl biphenyl ether) presumably formed during the curing reaction in air. To the author's knowledge, no other study giving a more detailed description of the mechanisms of curing has been reported.

### 2.2.2 Crystallization Behaviour

When the crystallization behaviour of polymers is studied, two aspects to be concerned with are 1) the morphological and structural aspects, and 2) the kinetics of the crystallization events. This section will be concerned with these two aspects of the crystallization behaviour of PPS.

The first report on crystal spacings of PPS was given by Tsunawaki and Price (44). The crystal structure of PPS was determined by Tabor et al. (45) utilizing x-ray diffraction methods. The unit cell is orthorhombic with dimensions a = 8.67Å, b = 5.61Å, and c = 10.26Å, being parallel to the chain axis. The cell comprises four monomer units, with two polymer chains passing through it; i.e., one chain passing through the center and the other through a corner. Figure 10 shows the crystal structure of PPS projected onto two different planes. It can be observed that the sulfur atoms are arranged in a zig-zag manner in the (100) plane. Furthermore, the planes of the phenylene groups are alternately rotated +45° and -45° with respect to the basal plane and the sulfur bond angle is 110°. Somewhat different results on the crystalline structure of PPS were reported by Garbarczyk (46). This author claimed that the crystalline structure of PPS determined by Tabor et al. (45) may have been affected by the stretched nature of the samples. Garbarczyk calculated the inter- and intra-molecular inter-

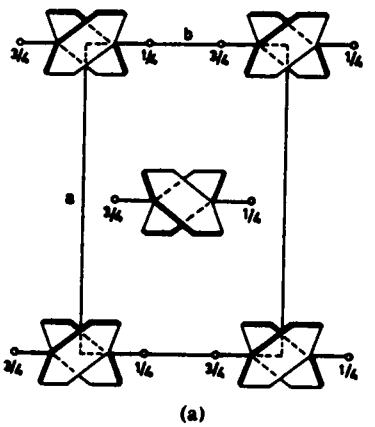


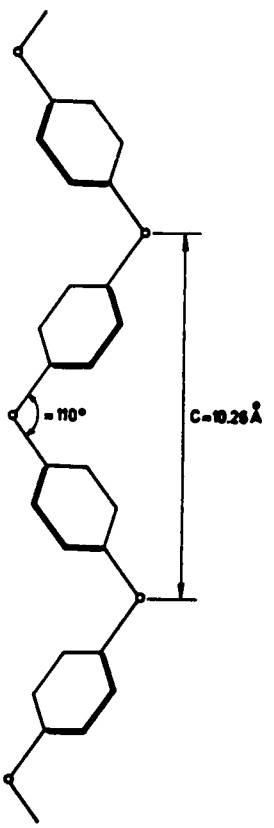


**Figure 10.** **The crystal structure of Poly (p-phenylene sulfide). (from 45):** a) crystal structure projected on the basal plane. b) conformation of a polymer chain in the crystal.

action energies and determined a C-S-C angle of 105.4° for PPS instead of 110° found by Tabor et al. (45). In addition, Garbarczyk suggested a more planar conformation for PPS molecules. He proposed a structure such that alternate phenyl rings are nearly coplanar with the C-S-C plane, and neighboring phenyl rings form a 60° angle between them. Some preliminary x-ray data reported by Garbarczyk seem to indicate a difference with the crystalline structure of PPS determined by Tabor et al. (45). However, Waddon et al. (47) arrived at similar conclusions as Tabor et al. (45) and extended the analysis to compare PPS with poly (ether ether ketone) (PEEK) and poly (ether ketone) (PEK). The crystal unit cell of the three polymers is orthorhombic with two molecules traversing each unit cell. The cell extends over two phenyl groups in the chain direction or c-axis. Table 1 presents the cell dimensions of PPS, PEEK and PEK for comparison.

It is interesting to mention at this point a study performed by Jones et al. (48) to determine conformational and packing information on glassy PPS by means of wide-angle x-ray scattering and model semi-empirical calculations. These authors performed a conformational energy analysis of the isolated chain partitioning the energy into non-bonded and dipole interactions, and an intrinsic rotation barrier. They concluded that in glassy PPS the lowest energy conformation is one with each phenylene ring rotated about the bridging sulfur atom by 40°, away from the all-planar conformation. In addition, this conformation was found to persist over lenghts of the order of 15Å, or three repeat units. These findings would suggest that the conformation of the isolated chain is very similar in the crystalline and glassy states. The 5° difference in the rotation angle of the phenylene ring with respect to the crystalline conformation was suggested to indicate an enhancement of the interchain interactions in the crystalline state (48). The investigation on the packing of chains indicated no parallel-chain packing. However, these authors reported a limited range of "face-to-face" pairwise phenylene correlation within an otherwise random chain packed system. Comparison of the conformation of the PPS polymer chains to the trans zig-zag conformation of polyethylene would explain the lower modulus of PPS. The "kinked" conformation of the PPS polymer chains in the amor-

**Table 1. Comparison of the unit cell parameters of PPS, PEEK and PEK.**

| polymer | unit cell | a-axis | b-axis | c-axis |
|---|---|---|---|---|
| PPS | orthorhombic | 8.67 | 5.61 | 10.26 |
| PEEK | orthorhombic | 7.75 | 5.86 | 10.00 |
| PEK | orthorhombic | 7.63 | 5.96 | 10.00 |

PPS

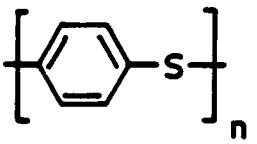


PEEK

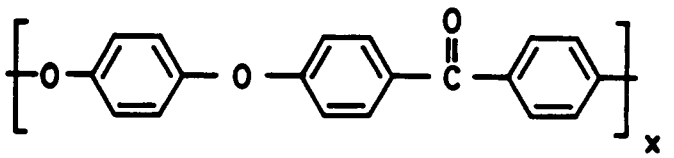


PEK

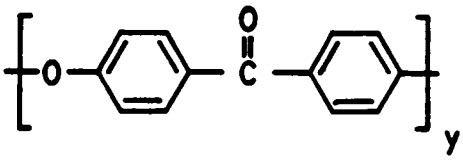

phous and crystalline states, would give place to lower bond angle bending energies than polyethylene when stretched. In addition, the larger cross-section of the PPS polymer chain is another factor in providing PPS with a lower modulus (≅3000MPa) than polyethylene (≅8000MPa) (49).

The morphological features of solution grown crystals of PPS have been studied (47,50). Figure 11 shows PPS crystals grown from a solution in α-chloronaphthalene at 167°C. These crystals had an elongated, fibrillar type of morphology. The crystals had 30-40nm in width, and SAXS experiments revealed a crystal thickness of 11.5nm. Electron diffraction patterns indicated that the c-axis (chain axis) is perpendicular to the basal plane of the crystals. Furthermore, the growth direction of the crystals is parallel to the b-axis, and during growth, the crystals change their orientation around the b-axis. Waddon et al. (47) observed the same phenomena in PPS, PEEK and PEK. The solution grown crystals of the 3 polymers were elongated, multilayered, sheaf-like lamellae with rough edges which suggested chain folded crystallization. In addition, the jagged edges, and layer splitting along the spear direction also suggested that the fold plane was parallel to the long dimension or growth direction of the crystal. Indeed, x-ray diffraction experiments indicated that the molecular axis ( c-axis) was perpendicular to the layers, and that the long crystal dimension was always along the b-axis. Moreover, these findings on solution grown crystals were related to the growth of melt crystallized spherulites. Therefore, these authors identified the crystal orientation within spherulites as radial, symmetrical texture elements with the b-axis as the fiber axis aligned radially to the spherulite. Uemura et al. (50) performed lattice imaging with high resolution microscopy. The 200 (0.43nm spacing), 110 (0.47nm spacing), and the -110 (0.47nm spacing) lattice fringes were observed. Such an image is presented in Fig. 12 with the corresponding diffraction pattern. Since the polymer chain was determined to be normal to the crystal surface, the dark ellipsoids in Fig. 12 were attributed to polymer chains projected on the a-b plane along the chain direction. Also, analysis of films in the polarized light transmission microscope revealed all spherulites with negative birrefringence; i.e., the direction of highest

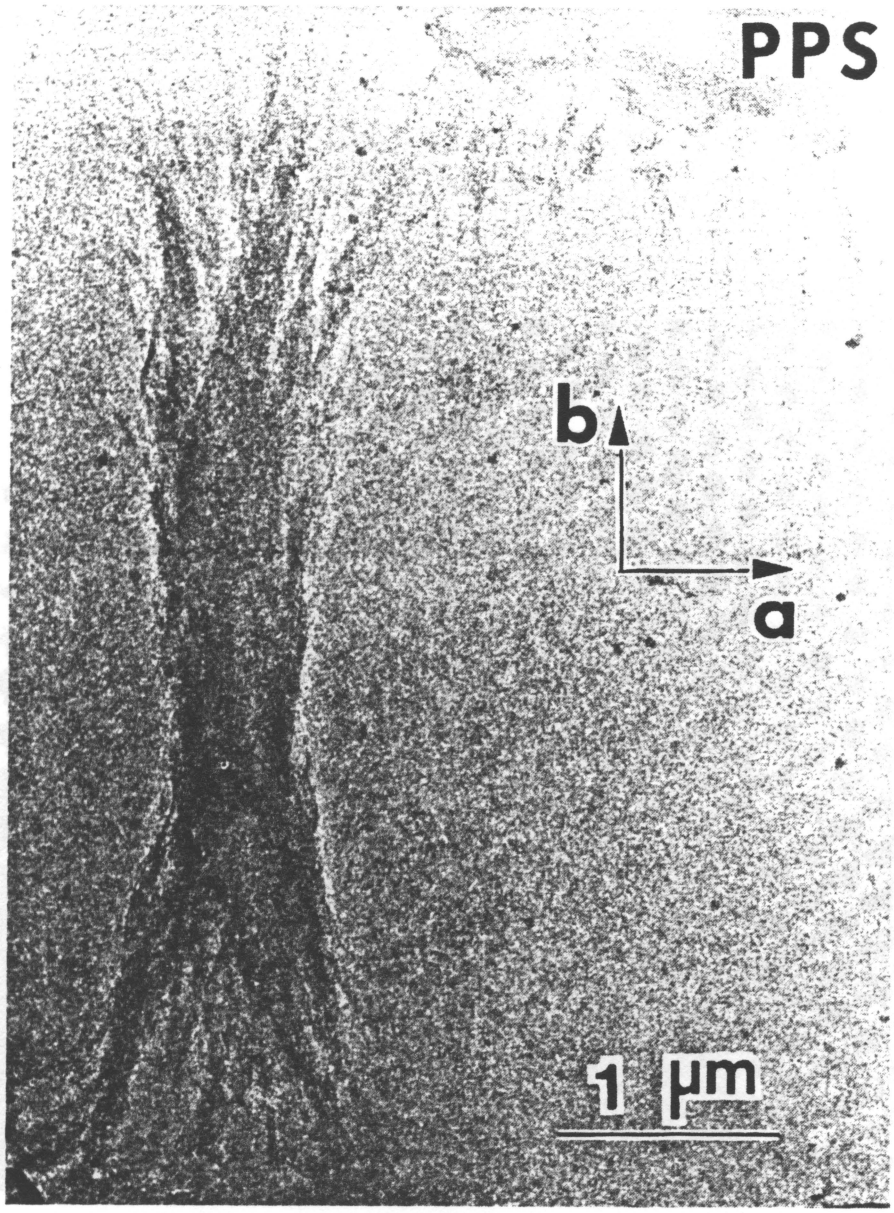


**Figure 11.** PPS crystals grown from α-chloronaphthalene solution at 167°C. (from 50)

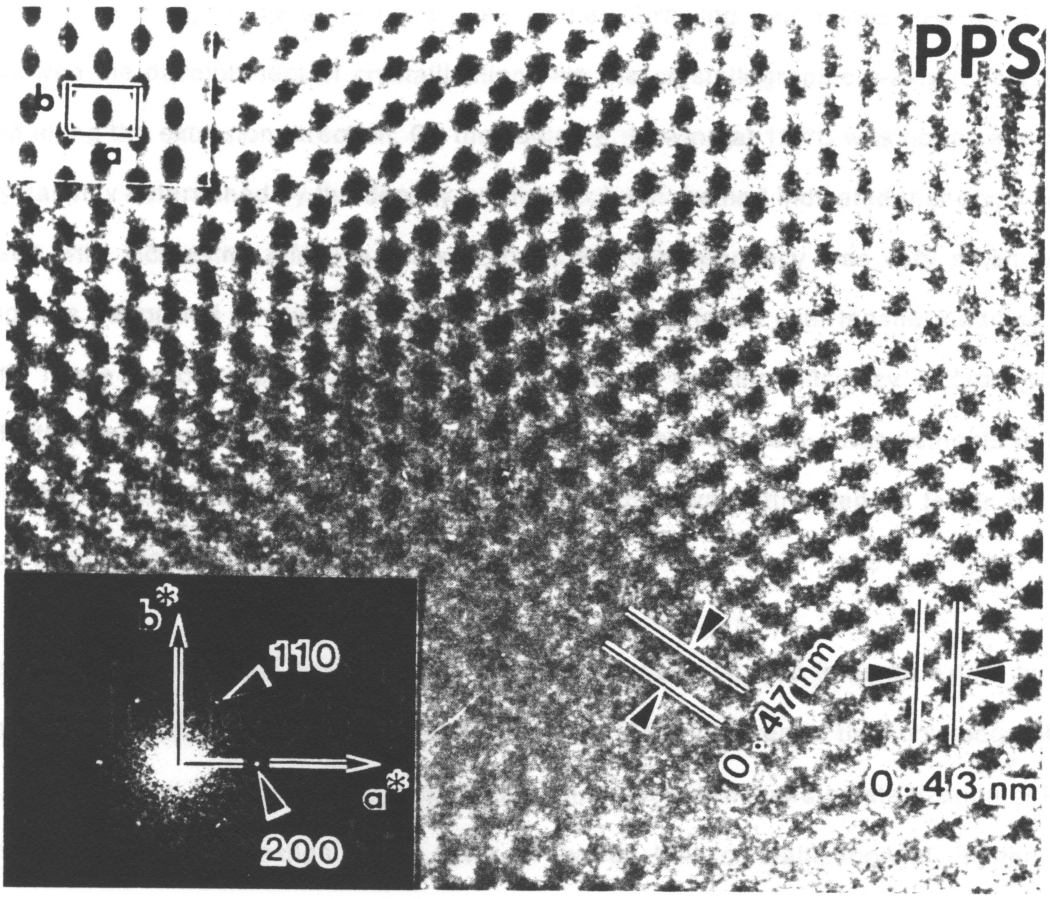


**Figure 12.** High resolution lattice image of a solution grown crystal of PPS showing the interplanar spacings. (from 50)

refractive index is along the c-axis, implying that the chain axis is perpendicular to the radial direction (47,50). Furthermore, electron diffraction patterns from a spherulite showed that the b-axis is parallel to the radial direction, the growing direction of the crystal (50).

The development of crystallinity in PPS upon drawing has been reported (51). Moreover, the effects of drawing temperature have been studied. Drawing amorphous PPS at 75° and 95°C showed the development of crystallization with the crystallographic c-axis (chain axis) oriented along the extrusion direction. On the contrary, drawing at 110°C was not as effective. The crystallinity determined by the density gradient column method indicated that crystallinity increased with increasing effective draw ratio (EDR). This tendency was very small when drawing was performed at 110°C. A similar correlation was found with tensile modulus and strength. These authors rationalized the results in terms of drawing efficiency. In order to obtain effective chain orientation by drawing, a certain number of chain entanglements is necessary. Therefore, the lower drawing efficiency at 110°C. was attributed to fewer or less effective chain entanglements or network points.

The kinetics of quiescent crystallization of PPS have been studied to some extent by Jog and Nadkarni (52), and by Lovinger, Davis and Padden (53). However, to the knowledge of the author, there has not been any studies published on the strain induced crystallization of PPS. Jog and Nadkarni (52) investigated the rates of overall bulk crystallization of unfilled and glass-fiber reinforced PPS by differential scanning calorimetry. In both cases, they found that the maximum crystallization rate occurred at 170°C. At a given temperature, the glass-fiber reinforced PPS crystallized at faster rates than unfilled PPS. This was related to the faster heterogeneous nucleation that takes place in the filled polymer as opposed to homogeneous nucleation that may occur in unfilled PPS. This hypothesis was supported by the fact that the rate difference is more pronounced at higher crystallization temperatures. The kinetic data was analyzed in terms of an Avrami equation for bulk crystallization. Both polymers followed the Avrami equation. Furthermore, the Avrami exponents were determined to be 2.5 for glass

filled PPS and 2.2 for unfilled PPS which would be controversial with the argument of heterogeneous versus homogeneous nucleation expressed above.

The spherulitic growth rates of PPS crystallized from the melt and the quenched glass were analyzed by Lovinger et al. (53). PPS with $<M_w> = 15{,}000$ and $<M_w> = 51{,}000$ were studied. Plots of the spherulite growth rate as a function of crystallization temperature are shown in Fig. 13. This figure makes clear the wide range of temperatures in which PPS can crystallize. The maximum growth rates were located at about 180°C, which are at similar temperatures to the maximum bulk rate found by Jog and Nadkarni(52). Lovinger et al. (53) analyzed the growth rate data in terms of the kinetic theory of crystallization of Hoffman (54,55) in search of Regime behaviour. The regime behaviour proposed by Hoffman (54,55) is determined by the mechanism of growth of molecular layers adsorbed on the surface of a lamellar crystal. Regime I behaviour occurs at the highest crystallization temperatures. At these temperatures, the rate of molecular nucleation is small; consequently, adsorbed molecules can deposit by chain-folding along the width of the lamellar growing front before another nucleation event takes place. Furthermore, the overall growth rate is proportional to the rate of molecular nucleation. Regime III occurs at the lowest crystallization temperatures and represents a similar situation. In this case, the rate of nucleation is so high that crystallization proceeds almost exclusively through nucleation events. Therefore, the overall growth rate is also proportional to the rate of nucleation. Finally, Regime II occurs at intermediate temperatures and represents an intermediate situation between Regimes I and III. In Regime II, the rate of molecular nucleation is intermediate. As a result, there is competition between adjacent nuclei to spread along the lamellar growing front and the crystal growth rate is proportional to the square root of the rate of molecular nucleation. Performing this kind of analysis, Lovinger et al (53) found that PPS with $<M_w> = 55{,}000$ had a Regime II→III transition at 208°C. Furthermore, they estimated the activation energy for chain motion to be 1400 cal/mol, the lateral-surface free energy to be 16.9 erg/cm$^2$, and the end or fold-surface free energy to be 125 erg/cm$^2$ for Regime II, and 130 erg/cm$^2$ for Regime III. PPS with $<M_w> = 15{,}000$ presented

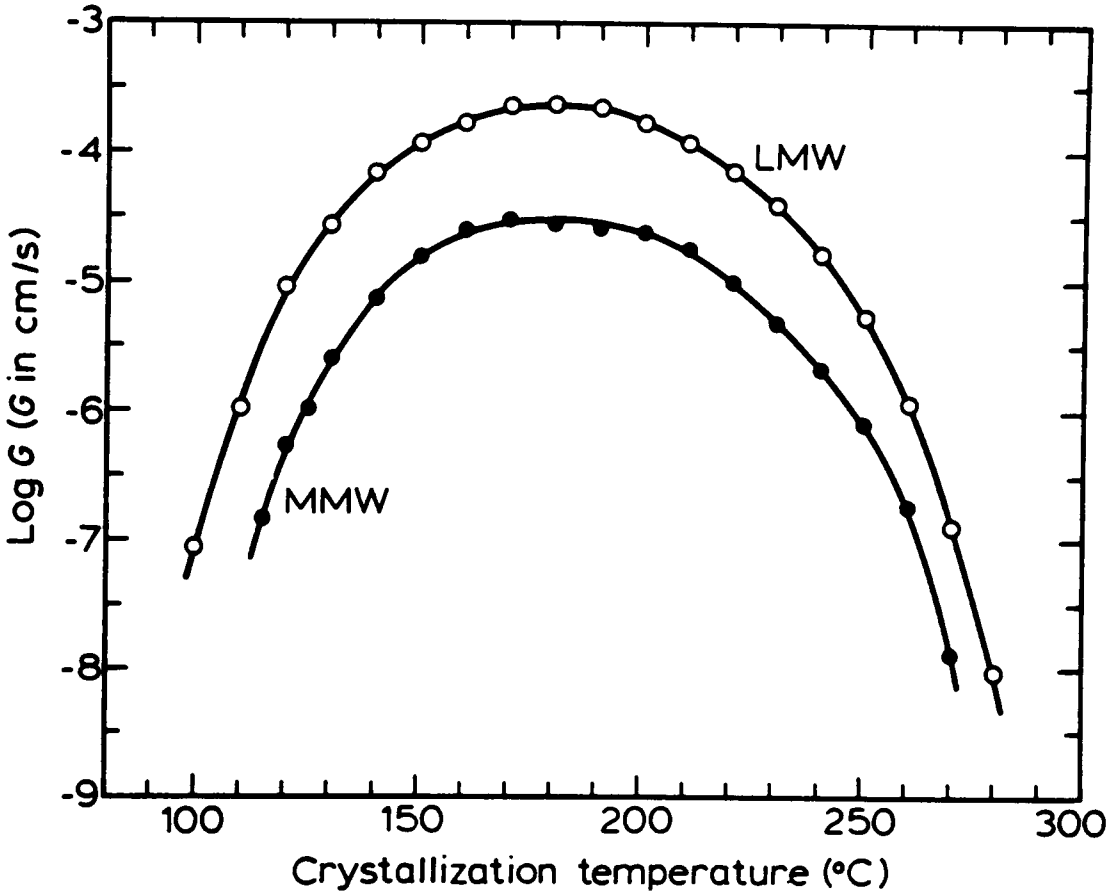


**Figure 13.** **Plot of spherulite growth rates as functions of crystallization temperature for PPS. (from 53):** LMW represents PPS with MW = 15,000; whereas MMW represents PPS with MW = 51,000.

Regime III kinetics at low temperatures. At higher temperatures, the behaviour departed continuously from Regime III without attaining Regime II kinetics.

### 2.2.3 Thermal Characteristics

As has been mentioned, poly (p-phenylene sulfide) has a glass transition temperature ($T_g$) at about 85°C and a melting point ($T_m$) at 285°C. In addition, the good thermal resistance of PPS was pointed out. The thermal resistance of a polymeric material is defined as the ability to maintain its dimensional stability, mechanical stability, weight, and appearance when exposed to high temperatures. Therefore, the thermal resistance can be measured by studying the mechanical properties and the weight of the polymer when exposed to high temperature. For example, variation of the flexural modulus with temperature may be a useful method. Figure 14 presents such a plot for PPS, nylon 6-6 and polyimide thermoplastics, in addition to glass-filled PPS, polycarbonate and polysulfone composites (56). This comparative study indicates that unfilled PPS retains good mechanical properties to higher temperatures than nylon 6-6; however, polyimide (Vespel SP-1) seems to perform better at higher temperatures. In the case of the glass-filled polymers presented in Fig. 14, PPS shows overall higher flexural modulus than polysulfone and polycarbonate. Nevertheless, it must be noted that the glass load is higher in the PPS composite, and that a semicrystalline matrix (PPS) is being compared to two glassy ones.

Traditionally, the resistance to thermal decomposition has been probed by thermogravimetric analysis. Hill and Edmonds (43) utilized such a method to obtain comparative data for PPS and other thermoplastics in a nitrogen atmosphere. Figure 15 shows that no appreciable weight loss is observed in PPS up to about 500°C. In air, degradation of PPS is complete at 700°C. On the other hand, in nitrogen, there is a 40% weight retention at 1000°C. Comparison with polyvinyl chloride, poly (methylmethacrylate), polystyrene,

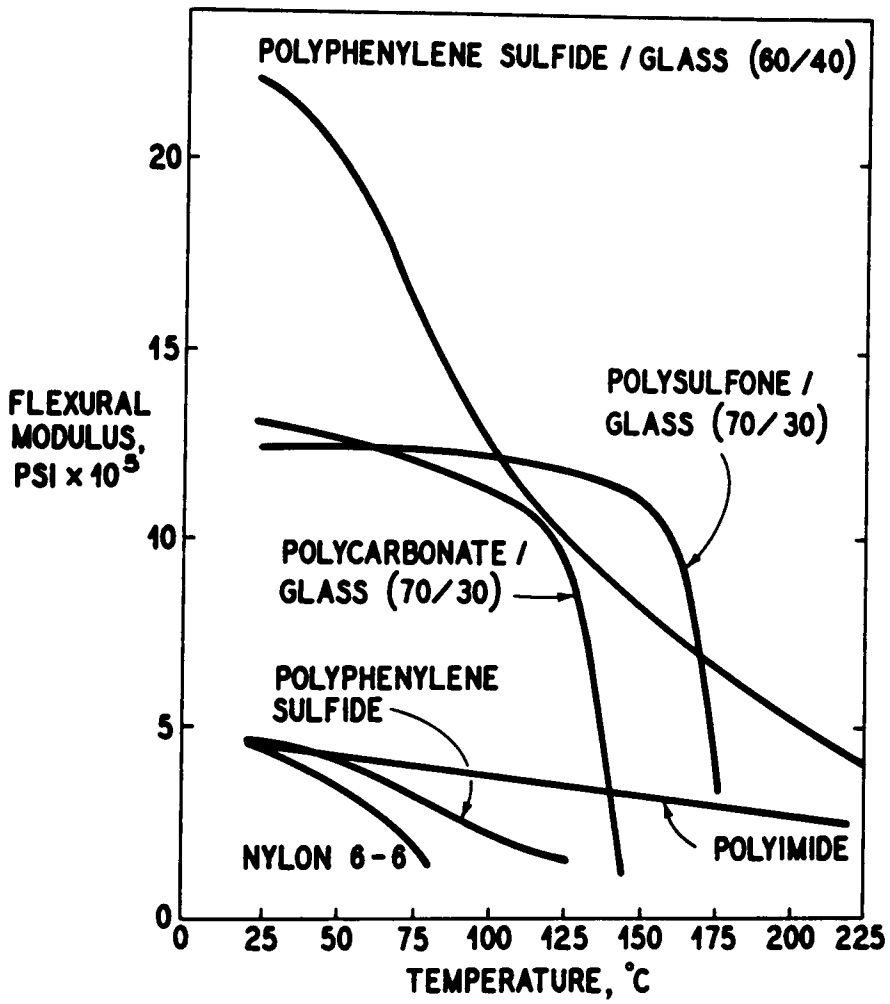


**Figure 14. Flexural moduli of thermoplastic polymers as functions of temperature. (from 56)**

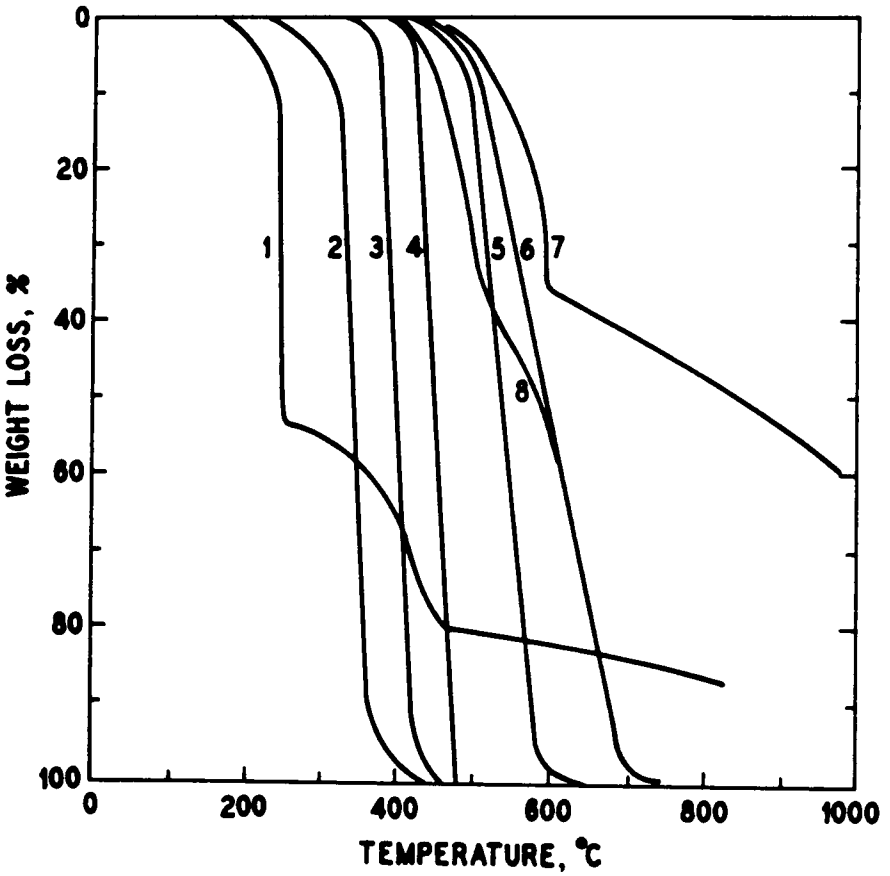


**Figure 15.** Comparative thermogravimetric analysis for several thermoplastic polymers. (from 43)

polyethylene and poly (tetrafluoroethylene) indicated a higher thermal resistance for PPS. A similar study was performed by Black et al. (41). However, these authors analyzed the thermal stability of polymers synthesized by the Macallum method (2) and by the Lenz method (5) (linear PPS). In the Macallum polymerization, 1,2,4-trichlorobenzene was added to obtain branched copolymers and compare their thermal stability to that of the linear polymer in air. These authors found that the logarithm of the weight loss as a function of time had a linear relationship with three stages in the reaction. The initial stage was a rapid weight loss with evolution of sulphur compounds to form a crosslinked polymer. The second stage involved slow oxidation with weight loss proportional to time to the power 0.1-0.5. The last part consisted of a more rapid stage in which the weight loss was proportional to the time, and the oxygen content of the polymer increased proportionally to the weight loss. Contrary to these findings, Christopher et al. (42) indicated only two stages in the thermal decomposition curve of PPS in vacuum. The weight loss curves showed a slow rate of weight loss, followed by a much faster rate of degradation. Similarly, Markert and coworkers (57) reported that the thermal degradation of PPS in oxygen was a two step process that started at 400°C and finished at 750°C. These same authors also indicated that the addition of lithium carbonate (acid acceptor) caused an increase in the thermal stability of PPS. The degradation process of PPS containing lithium carbonate started at 450°C instead of 400°C as observed in PPS without the additive(57,58).

The effects of structural variables on the thermal stability of PPS have been studied to a certain extent. Black et al. (41) reported that branched polymers seemed to be more stable than the linear one. In addition, the molecular weight did not have any obvious effects on the thermal stability of the (p-phenylene sulfide) polymers. The effect of substituents on chlorobenzene used to synthesized (phenylene sulfide) polymers by reaction with sulfur has been investigated (59). Hortling (59) utilized 1,4-dichlorobenzene, 4-chlorophenol, 4-chloroaniline, and 4-chlorotoluene. The curves of weight loss as a function of temperature indicated that the decreasing order of thermal stability was 1,4-dichlorobenzene >

4-chlorotoluene > 4-chlorophenol > 4-chloroaniline. The infrared spectra of the pyrolisis products indicated the presence of 1,2,4-trisubstitution in the benzene ring. In addition, pyrolisis in a 95/5 nitrogen/oxygen atmosphere showed absorption bands in the 1050-1400 $cm^{-1}$ region of the IR spectrum presumably due to oxidation reactions and formation of CO and SO bonds. The thermal degradation of poly (phenylene sulfide) synthesized by the method of Lenz (5) has also been studied by mass spectroscopy (42,60). Christopher et al. (42) analyzed the products of pyrolysis of PPS in vacuum at 350°C by mass spectroscopy. Mass spectral analysis indicated trace amounts of $SO_2$, $CO_2$, and COS in the products of pyrolisis. In addition, peaks corresponding to $C_6H_5Br$ , $C_6H_4Br_2$, $C_6H_5SC_6H_5$ , $BrC_6H_4SC_6H_5$ , $BrC_6H_4SC_6H_4Br$ , and dibenzothiophene were identified. Higher temperature pyrolisis (460°C) showed, in addition to all these products, the elimination of H. A similar study was performed by Ehlers et al. (60), who reported that the major decomposition product was a condensate composed of dimeric and trimeric chain fragments, dibenzothiophene and thianthrene. Other products consisted of $H_2S$, $H_2$ , and a residue that suggested to be a crosslinked species. Moreover, Fig. 16 represents a simplified version of the reaction mechanism of the thermal degradation of PPS proposed by Ehlers et al. (60). The breakdown mechanism would start by cleavage of carbon-sulfur bonds and abstraction of hydrogen to form chain fragments with phenyl and phenylmercapto endgroups. Further cleavage of C-SH bonds and abstraction of H would lead to the elimination of $H_2S$. The radicals formed by abstraction of H would cause recombination and crosslinking, and low molecular weight dimers and trimers would be removed at these high temperatures to form a condensate. The dibenzothiophene structure would form from free diphenylsulfide or within the polymer chain; whereas thianthrene would originate from phenylmercaptan or phenylmercapto endgroups.

Recently, Montaudo et al. (24) studied the thermal degradation of poly (o-phenylene sulfide) (o-PPS), poly (m-phenylene sulfide) (m-PPS), and poly (p-phenylene sulfide) (p-PPS) by gel permeation chromatography and mass spectrometry. Mass spectra corresponding to o-PPS showed the presence of thianthrene oligomers and cyclic trimers; m-PPS presented

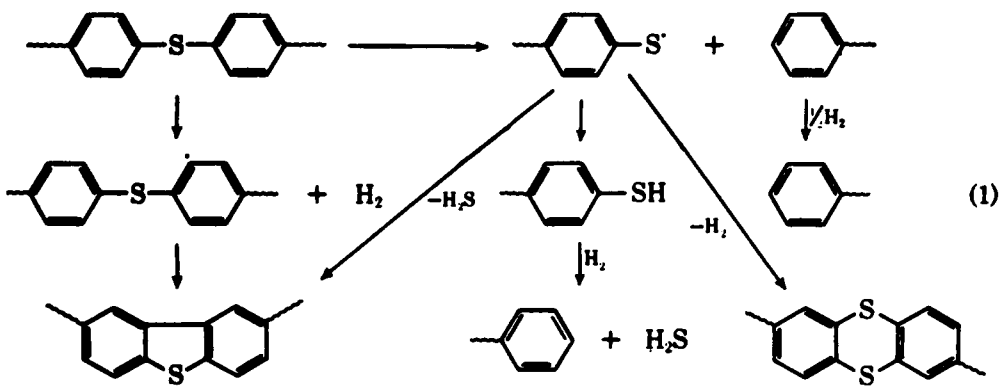


**Figure 16. Reaction mechanism for the thermal degradation of PPS proposed by Ehlers et al. (from 60)**

cyclic oligomers from trimer to heptamer; and p-PPS had peaks corresponding to the molecular ions of cyclic oligomers from tetramer to heptamer. Since the formation of cyclic compounds is favored at higher temperatures, these authors suggested that the thermal fragmentation of the polymer chains may take place through a ring-chain equilibration process that creates the series of cyclic oligomers. Furthermore, there was a structural effect on the distribution of cyclic oligomers generated during degradation. For example, o-PPS produced mostly cyclic dimer (thianthrene); whereas m-PPS generated cyclic trimer and tetramer predominantly over pentamer, hexamer and heptamer, and in p-PPS the cyclic pentamer was the most abundant.

### 2.2.4 Chemical Properties

Similar to the definition of thermal resistance, chemical resistance of a polymer is defined as the ability to maintain its dimensional stability, mechanical properties, weight and appearance when exposed to chemicals at high temperatures. Most of the information available on the chemical resistance of PPS arises from studies performed by scientists at Phillips Petroleum Co. Table 2 presents some comparative data on the short term chemical resistance of PPS and other selected thermoplastics (11). In short term chemical resistance, PPS seems to have performed better than poly (2,6-dimethylphenylene oxide), polysulfone, polycarbonate and nylon 6-6. Bromine and butylamine seemed to have attacked PPS harshly at 93°C in 24 hours. These two cases present 36% and 50% loss of the tensile strength, respectively. The long term chemical resistance of PPS is also very good. Table 3 shows data corresponding to PPS treated at 93°C for 24 hours and 3 months with different solvent systems. The table indicates that PPS has good chemical resistance to sulfuric and phosphoric acids, sodium hydroxide, water, butyl alcohol, butylether, etc. However, hydrochloric acid, nitric acid and butylamine were very detrimental for PPS. It has been reported that the solubilization of PPS in acidic media requires the simultaneous action of a strong acid and a strong oxidant (61). It

**Table 2. Comparative chemical resistance of various polymers at 93°C/24 hr. (from 11)**

**Percent tensile retained**

| Chemical | Nylon 6-6 | Polycar-bonate | Polysul-fone | Modified PPO | PPS |
|---|---|---|---|---|---|
| 37% HCl | 0 | 0 | 100 | 100 | 100 |
| 10% $HNO_3$ | 0 | 100 | 100 | 100 | 96 |
| 30% $H_2SO_4$ | 0 | 100 | 100 | 100 | 100 |
| 85% $H_3PO_4$ | 0 | 100 | 100 | 100 | 100 |
| 30% NaOH | 89 | 7 | 100 | 100 | 100 |
| 28% $NH_4OH$ | 85 | 0 | 100 | 100 | 100 |
| $H_2O$ | 66 | 100 | 100 | 100 | 100 |
| $FeCl_3$ | 13 | 100 | 100 | 100 | 100 |
| NaOCl | 44 | 100 | 100 | 100 | 84 |
| Bromine | 8 | 48 | 92 | 87 | 64 |
| Butyl alcohol | 87 | 94 | 100 | 84 | 100 |
| Phenol | 0 | 0 | 0 | 0 | 100 |
| Butylamine | 90 | 0 | 0 | 0 | 50 |
| Aniline | 85 | 0 | 0 | 0 | 96 |
| 2-Butanone | 87 | 0 | 0 | 0 | 100 |
| Benzaldehyde | 98 | 0 | 0 | 0 | 84 |
| Chlorobenzene | 73 | 0 | 0 | 0 | 100 |
| Chloroform | 57 | 0 | 0 | 0 | 87 |
| Ethyl acetate | 89 | 0 | 0 | 0 | 100 |
| Butyl phthalate | 90 | 46 | 63 | 19 | 100 |
| p-Dioxane | 96 | 0 | 0 | 0 | 88 |
| Butyl ether | 100 | 61 | 100 | 0 | 100 |
| Gasoline | 80 | 99 | 100 | 0 | 100 |
| Diesel fuel | 87 | 100 | 100 | 36 | 100 |
| Toluene | 76 | 0 | 0 | 0 | 98 |
| Benzonitrile | 88 | 0 | 0 | 0 | 100 |
| Nitrobenzene | 100 | 0 | 0 | 0 | 100 |

**Table 3. Long term chemical resistance of PPS moldings at 93°C. (from 11)**

| | Percent tensile retained | |
|---|---|---|
| Chemical | 24 hrs | 3 months |
| 37% HCl | 93 | 56 |
| 10% $HNO_3$ | 96 | 31 |
| 30% $H_2SO_4$ | 100 | 100 |
| 85% $H_3PO_4$ | 100 | 100 |
| 30% NaOH | 100 | 100 |
| $H_2O$ | 100 | 100 |
| 5% NaOCl | 84 | 90 |
| Butyl alcohol | 100 | 100 |
| Cyclohexanol | 96 | 81 |
| Butylamine | 50 | 0 |
| Aniline | 96 | 87 |
| 2-Butanone | 100 | 70 |
| Benzaldehyde | 84 | 90 |
| $CHCl_4$ | 100 | 77 |
| Chloroform | 87 | 79 |
| Ethyl acetate | 100 | 100 |
| Butyl ether | 100 | 100 |
| p-Dioxane | 88 | 75 |
| Gasoline | 100 | 87 |
| Toluene | 98 | 74 |
| Benzonitrile | 100 | 77 |
| Nitrobenzene | 100 | 85 |
| Phenol | 100 | 100 |
| N-Methyl-pyrrolidone | 94 | 74 |
| air | - | 90 |

was suggested that the oxidant oxidizes the polymer to a polymeric cation which dissolves in the acid to form a complex. Therefore, the acid has to be sufficiently strong to stabilize the electrophilic polymeric cation which may be attacked easily by any species with basic character. In this respect, the result of oxidation of PPS by peroxy-formic acid was reported to create sulfoxide and sulfone groups (62,63). Oxidation in basic media has been shown to produce a decrease of the flexural strength by 60% after 1171 hours of exposure (64). Other solvents such as cyclohexanol, carbon tetrachloride, chloroform, toluene, gasoline, oil, brake fluid, transmission fluid, and nitrobenzene produced moderate attack on PPS after a three-month exposure at 93°C (65). However, aluminum chloride in hydrocarbon media attacks PPS rather strongly. Johnson (66) utilized the attack of a suspension of aluminum chloride in toluene to depolymerize PPS in PPS/C fiber composites and determine the fiber content in the composite.

### 2.2.5 Viscoelastic Properties of PPS

The viscoelastic response of PPS has been studied over a wide range of frequencies, involving torsional pendulum measurements (67), dielectric measurements (68), and nuclear magnetic resonance (69). However, there are limited data and the interpretation of the data may not be precise. Although these studies comprised a wide range of frequencies, all of the authors attributed the relaxation phenomena observed to oscillatory motions of the phenylene groups. The lowest frequency analysis involved the use of the torsional pendulum (0.5Hz). Eisenberg (67) investigated the viscoelastic properties of amorphous and semicrystalline PPS. Figure 17a shows the tan$\delta$ behaviour of PPS at 0.5Hz for a quenched sample and a specimen annealed at 250°C for 1 hr. The $\beta$ relaxation observed in amorphous PPS at $\sim$-110°C was attributed to hindered torsional oscillatory motions (rotational) of the phenylene groups in the backbone around the S-$\Phi$-S bond axis. An activation energy of $11 \pm 2$ Kcal/mol was determined. This energy barrier was attributed to intermolecular effects due to the arrangement

of neighboring but nonbonded segments. Comparison of this β-relaxation of PPS with that of poly(phenylene oxide) (PPO) reveals the similarity of these two polymers in their viscoelastic properties at low temperatures. PPO also presents a β-relaxation at -113°C with an activation energy of 12±2 Kcal/mol at a frequency of 0.9Hz, that has also been attributed to hindered torsional oscillatory motions of phenylene units in the backbone (67). The presence of this transition at low temperature may be an important factor in determining the toughness of PPS, since the absorption of mechanical energy by relaxation mechanisms in the glassy state is important in providing toughness and resistance to fracture (70). Eisenberg and Cayrol (67) also analyzed the effect of crystallinity on the β-relaxation of PPS. The crystallinity of PPS seemed to only lower the intensity of the β-relaxation and perhaps shift it to somewhat higher temperature, which would strengthen its attribution to hindered rotations of phenylene groups in the amorphous phase. These same authors also recognized the presence of another relaxation below -200°C whose origin was not clear.

The low temperature dielectric relaxation of PPS was also studied (68). The dielectric loss tangent, tanδ, measured at various frequencies is shown in Fig 17b as a function of temperature. The relaxation region from 80 to 190K, termed the γ-relaxation, was assigned to the reorientation of the phenylene ring, probably coupled with torsional rotational motions of nearby units. An activation energy of 8.8 Kcal/mol was calculated for this γ-relaxation. Furthermore, this relaxation seemed to be independent of frequency in the range of frequency of 60-$10^5$ Hz. These results are rather surprising. Only first order transitions are independent of frequency. The second order relaxations such as this γ-transition should be frequency dependent. However, the data of Rigby and Dew-Hughes do not show such an effect (68). These authors also indicated that crosslinking would not change substantially the position of the relaxation, however, the magnitude of it would be decreased.

Pulsed-$^1$H NMR spectroscopy was also utilized to investigate the dynamics of PPS at low temperature (69). Analysis of spin lattice relaxation times ($T_1$) showed a relaxation process with an activation energy of 2.8 Kcal/mol that was attributed to phenylene rotation about the

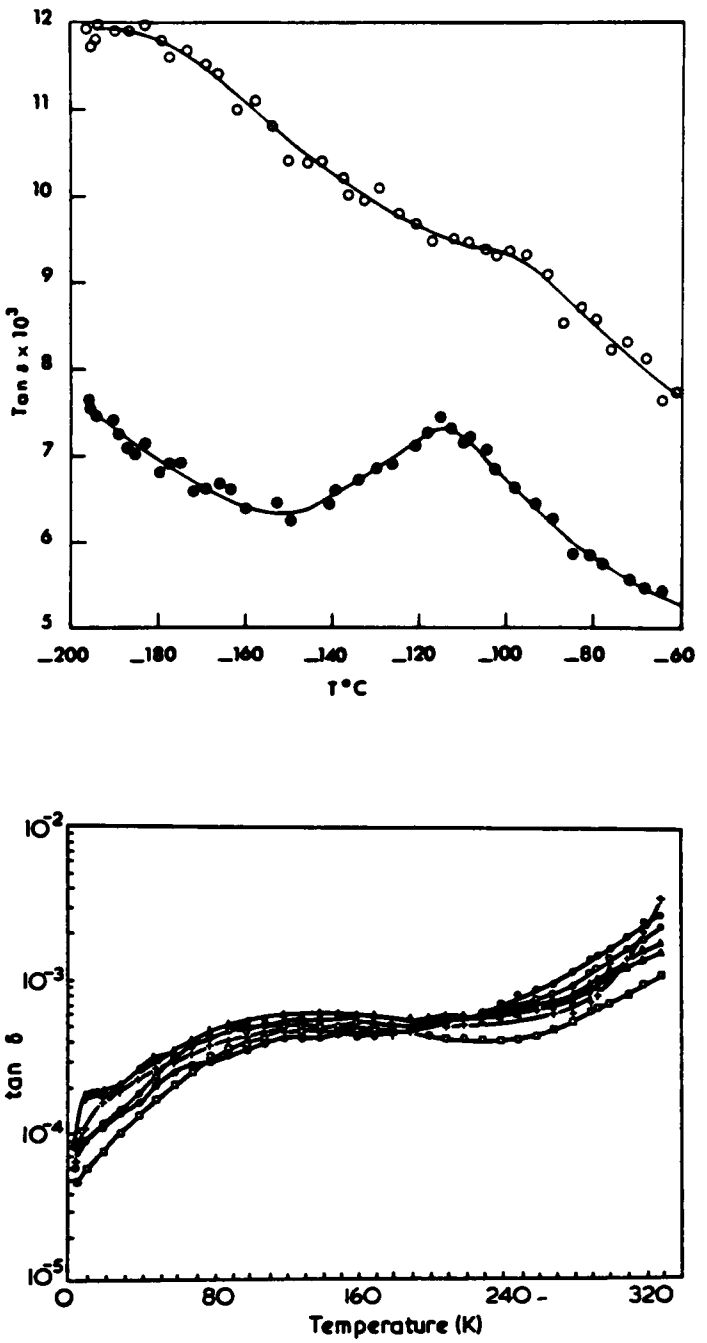


**Figure 17. Dynamics of PPS:** a) Torsional pendulum measurements: • amorphous, o semi-crystalline; b) dielectric measurements: + 62Hz; o 255Hz; • 1kHz; △ 4kHz; ▲ 10kHz; □ 100kHz. (from 67,69)

S-S direction. Nevertheless, analysis of linewidth and second moments indicated two relaxation phenomena with activation energies $1.4 \pm 0.3$ and $3.4 \pm 0.3$ Kcal/mol. These authors suggested that the two values of activation energy obtained from linewidth analysis might indicate the different ease for phenylene rotation in the amorphous and the crystalline phases. Moreover, they suggested that spin diffusion might have washed out this effect in the spin lattice relaxation time measurements. In summary, this studies of the dynamics of PPS indicated that the relaxation processes observed at low temperature are due to rotational motions of the phenylene units about the S-Φ-S bond axis.

### 2.2.6 Electrical properties

PPS has a dielectric constant of 3.1 at $10^6$ Hz and at 27-150°C, and a resistivity of $10^{17}$ Ωcm (12) which indicate the insulating properties of the polymer. However, the transport of electrical charge in PPS studied by Yoshino et al. (72), Saito and coworkers (73), and by Tsutsui and collaborators (74) revealed some interesting properties. The predominant charge carrier in PPS was determined to be the hole (75). The temperature dependence of the electrical conductivity has been shown to have an activation type behaviour (72,74). The activation energy changed remarkably from 0.3 eV to 2.0 eV at 90°C ($\sim T_g$ of PPS). The small activation energy below $T_g$ indicated the predominance of electronic conduction at low temperatures. Whereas, the large activation energy at temperatures above $T_g$ seemed to suggest ionic conduction at high temperatures. Furthermore, annealing at 160°C produced a decrease in the apparent conductivity of one order of magnitude and UV-light irradiation at room temperature increased the apparent conductivity of the film by about three orders of magnitude (73,76). However, this higher conductivity state was extinguished by annealing PPS at temperatures above $T_g$ (74). This decrease in conductivity was attributed to electronic carriers being thermally released from deep trap sites, which were generated by photo-irradiation.

As mentioned earlier, PPS can be rendered electrically conductive through the addition of dopants such as $AsF_5$, $SbF_5$, and $SO_3$ . Many other polymers, in particular those with $\pi$-conjugated structures in their skeletal chain have been doped with strong electron acceptors to produce conductive polymers. Examples are polyacetylene (77), poly (p-phenylene) (78) and polypyrrole (79). All of these polymers, however, lack adequate processibility; i.e., they are intractable and infusible. As PPS has the advantage of being melt processable and solution processable, a great deal of attention has been placed in the study of doped PPS. The first two reports on conductive PPS doped with $AsF_5$ were presented by Rabolt et al. (80) and by Chance et al. (81). In general, it is agreed that to have an electrically conductive polymer, a network of overlapping intra- or inter-molecular orbitals is needed. PPS seems to have such a characteristic, although the aromatic rings are essentially perpendicular to each other (45,48). Apparently, the sulfur atoms contribute to delocalize the electronic structure due to significant overlap between the sulfur p-orbitals and the aromatic $\pi$-orbitals of aryl rings (71). A doping process, that is, the addition of an oxidizing or reducing agent will produce the partially filled electron bands that are needed for conduction. Arsenic pentafluoride has been used as a doping agent for PPS to form a p-type conductor, i.e., the charge carriers are holes (82,83). Doping of PPS with $AsF_5$ at room temperature has been shown to introduce changes in the structure of the polymer (84). Upon doping PPS with $AsF_5$, crystallinity was lost presumably due to dopant-induced structural disorder (85). In adition, $AsF_5$ induced the formation of dibenzothiophene linkages in PPS by joining adjacent aromatic rings. Eventually, poly (benzothiophene) (PBT) would be formed. The formation of PBT would cause the adjacent aromatic rings to be constrained to a coplanar structure, which would enhance the conductivity and suggest the importance of the "p" orbitals for conduction in PPS. This is further stressed by the effect of the position of the sulfur atom in the phenyl ring. If poly (m-phenylene sulfide) (m-PPS) is doped with $AsF_5$ at -76°C, the polymer will not form a highly conductive complex (86). The conductivity of such a complex is $10^{-7}$ S/cm, as opposed to 2.7S/cm measured for doped PPS. At -76°C, the doping process does not produce any chemical changes in m-PPS. Consequently, the structure of m-PPS does not provide sufficient

electron delocalization to form a highly conductive complex. If doping is conducted at -25°C, however, a complex with conductivity of 0.08 S/cm is obtained. Infrared spectra indicated some evidence consistent with intra-molecular bridging of adjacent aryl rings to form thiophene rings, causing species with higher p-orbital overlapping that lead to higher electron delocalization and conductivity. Tripathy et al. (87) performed a conformational analysis of segments of PPS molecules. They reported that a quasi-planar structure is energetically accesible to PPS. In addition, these authors indicated that there is not a significant loss in packing energy in changing from a nonplanar to a quasi-planar structure. Therefore, upon doping, it is possible for the phenyl rings of PPS to take a quasi-planar structure to allow hydrogen abstraction and formation of the thiophene bridges reported (85). Frommer et al. (88) reported that the penetration of $AsF_5$ in PPS films was not complete for films of 0.025 cm thick. However, the penetration of $AsF_5$ was facilitated by previous exposure of the films to $AsF_3$. These same authors suggested that the role of $AsF_3$ was that of a plasticizer for PPS, increasing the rate of diffusion of $AsF_5$ into the interior of the film and enhancing the doping homogeneity (89). Furthermore, a theoretical treatment of the thermodynamic and transport behaviour of $AsF_3$ and $AsF_5$ in PPS based on effects due to the conducting polymer's hole-electron equilibria was performed (90). Another interesting result was observed with arsenic trifluoride (91). Treating a suspension of PPS in liquid $AsF_3$ with $AsF_5$ at room temperature produced rapid doping and dissolution of the polymer with formation of a dark blue conductive solution. Moreover, upon removal of the solvent, the cast films had good strength and flexibility, with conductivities that ranged from $5x10^{-3}$ to 200 S/cm. Dissolution of doped PPS in $AsF_3$ is very surprising since undoped PPS in insoluble in $AsF_3$, and doping with $AsF_5$ was shown to produce crosslinking. Nevertheless, the solutions were reported to be clear and indefinitely stable in dry air, which indicated that no crosslinking was occurring.

Other dopant systems have been used. Antimonium pentafluoride was indicated as a dopant for PPS; but, the conductivities were lower than those observed for $AsF_5$ (84). The study of such a complex by X-ray Photoelectron Spectroscopy suggested the formation of a

charge transfer structure as $(PPS)^+(SbF_6)^-$ for $SbF_5$ doped PPS (92). However, when antimonium pentachloride was utilized to dope PPS, infrared spectroscopy indicated that the structure of the polymer did not change (93). Schoch (94) utilized $SO_3$ to dope PPS. The doped films had conductivities of 0.3 S/cm with better stability to moisture than $AsF_5$-doped PPS. Infrared and elemental analysis showed that in addition to changing the electronic structure of PPS, $SO_3$ produced sulfonation and possibly crosslinking. Shimizu et al. (92) also reported the sulfonation reaction when studying $SO_3$-doped PPS by X-ray Photoeletron Spectroscopy. On the contrary, Kazama et al. (95) excluded the possibility of a sulfonation reaction. $^1H$ NMR, $^{13}C$ NMR and IR spectroscopy seemed to indicate that a direct intramolecular crosslink between neigboring phenyl rings was the most probable modification. X-ray diffraction indicated the introduction of extensive disorder in PPS upon doping with $SO_3$ due to the crosslinking reactions and insertion of dopants species between chains. The doped films were amorphous regardless of the crystallinity of the initial films. Nevertheless, the initial crystallinity affected the rate of doping (96). The temperature dependence of $SO_3$ -doped PPS followed a $1/T^{1/2}$ dependence which is consistent with tunneling of charge carriers between conducting regions or with a one-dimensional hopping mechanism. Rubner et al. (97) reported the successful doping of PPS with solutions of nitrosyl salts in nitromethane/methylene chloride to render it electrically conductive. The nitrosyl salts used were $NOPF_6$ , $NOSbF_6$, and $NOHSO_4$. $NOPF_6$ dopant seemed to be the best of the three salts. A maximum conductivity of 1 $1/\Omega cm$ is obtained with 38 mole % of $NOPF_6$ incorporated into the polymer. The amount of dopant absorbed was a function of the film crystallinity. The conductivity changed from $4x10^{-2}$ $1/\Omega cm$ to less than $10^{-12}$ $1/\Omega cm$ as the crystallinity of the films previous to doping varied from 5% to 65%. The doped films were described as very rigid and brittle and the deterioration of the mechanical properties was proportional to the extent of doping. In addition, DSC indicated that the peaks associated with the glass transition temperature, recrystallization and melting gradually disappear as the dopant content was increased which may suggest the occurrence of a crosslinking reaction.

Organic acceptors have also been investigated as doping agents for PPS. Tetracyanoethylene (TCNE), dichloro-dicyanobenzoquinone (DDQ), chloranil, tetracyanodimethane (TCNQ), and trinitrofluorenone (TNF) have been used to dope PPS. However, only TCNE and DDQ were fairly effective in raising the conductivity of PPS to ~ $10^{-10}$ S/cm (73). Saito et al. (73) proposed that the main effect of doping PPS was the enhancement of the charge carrier mobility, although doping in the beginning stages produced an increase in the carrier density. Furthermore, Tokito et al. (98) suggested that the carrier transport is due to a hopping mechanism. The charge carriers are expected to move by hopping between localized states in the polymer which include large portions of amorphous regions. Since the $\pi$-electrons on the phenyl rings of PPS seemed to be delocalized throughout several repeating units, the charge should be transfered by hopping between delocalized regions. Consequently, the rate determining step should be the inter-chain hop. Kawano and coworkers (99) indicated that x-ray diffraction and fluorescence experiments suggested the presence of TCNE dopant in the amorphous regions. Similar results were proposed for PPS doped with $AlCl_3$, $FeCl_3$, and $TaF_5$ (100). It has also been reported that in PPS doped with TCNQ the predominant charge carriers are holes (101). The hole mobility increased with increase in TCNQ concentration, by a decrease of the activation energy of hole mobility. A double doping technique of TCNQ and iodine has been reported (102). By doing a melt doping technique of PPS with TCNQ and subsequently exposure to $I_2$ gas higher conductivities than those of TCNQ doped PPS were obtained at lower concentration of TCNQ.

A different method to induce conductivity in PPS was utilized by Mazurek et al. (103). They performed ion-implantation of arsenic, krypton and bromine in PPS. Films implanted with either arsenic or krypton became increasingly conductive with a maximum conductivity of ~ $1.5 \times 10^{-5}$ $1/\Omega cm$. In contrast to chemically doped PPS, the conductivities of ion-implanted PPS films remained stable when exposed to natural ambient; i.e., they were not affected by desorption in the presence of water vapor, which happens with chemically doped PPS. Since krypton is normally inert and produced conductivities similar to those of arsenic-implanted

PPS, these authors suggested that conductivity was a consequence of structural arrangements brought about by "ion-implantation-induced-disorder". That is, bond-breaking and bond formation may have occurred upon ion-implantation that pressumably make charge carriers available for conduction. Furthermore, infrared spectroscopy suggested increased substitution on the aromatic rings to form crosslinked species, and intrachain crosslinking to form a polybenzothiophene structure. Electron Spin Resonance measurements gave further evidence supporting this argument (104). Bromine implantation in PPS produced higher conductivities than arsenic and krypton ($4x10^{-4}1/\Omega cm$ at $3.46x10^{16}$ $cm^{-2}$ fluence); however, unlike arsenic and krypton implanted PPS, the bromine-implanted samples did not exhibit implant saturation, i.e., the bromine-implanted PPS had a linear relationship between conductivity and ion flux. Schoch and Bartko (105) also irradiated PPS films with high energy lithium, fluorine and iodine ions to obtain conductive materials. Conductivities up to 0.7 $Scm^{-1}$ were measured. However, the conductivity values were dependent on the irradiation conditions. Infrared and electron paramagnetic resonance (EPR) spectroscopies suggested the creation of free radicals during irradiation. Furthermore, increase in the dose of ions lead to increase of the number of free radicals and increase of the bulk conductivity of the films. A DSC study showed that PPS films experiment substantial crystallization during irradiation. X-ray diffraction experiments, on the contrary, did not indicate changes in crystallinity.

## *2.3 COMPOSITE MATERIALS BASED ON PPS*

The technique of making composite materials has provided an effective means to tailor materials to achieve a specific balance of properties, processing characteristics, and in many cases reduce costs. In a very broad sense, the expression "composite material" defines materials that consist of more than one phase. However, this term is usually understood as materials that are composed of more than one component or ingredient. In this section the author

will deal with materials that comprise more than one component or ingredient. In particular, attention will be placed in the use of PPS as a thermoplastic matrix for advanced thermoplastic composites, since it is an area of major importance for the applications of PPS. Therefore, blends of PPS with other polymers, glass fibers and carbon fibers will be described.

Blends of PPS with bisphenol-A polysulfone (PSF) have been studied (106,107). The PSF/PPS blends were obtained by evaporation of α-chloronaphthalene solutions of the polymers. The solutions appeared to be homogeneous; however, in the dry blends, the polymers were incompatible. In this case, the blend consists of a crystallizable polymer (PPS) and an amorphous one (PSF); therefore, not only the mechanical and thermal properties are expected to be affected, but also the crystallization behaviour of PPS. In this respect, the crystalline morphology of PPS/PSF blends was investigated by optical microscopy (107). It was reported that the textures of the blends changed from a continuous PPS phase to a continuous PSF phase as the PSF content was increased in the blend. Furthermore, the spherulitic morphology of PPS was deteriorated by the PSF presence until it became irregular. Torsional braid analysis was utilized to observed the effect of heat treatments on the phase separation behaviour of these blends (106). Previous to heat treatment, the glass transition temperatures of PPS at 95°C and of PSF at 190°C were observed. The $T_g$ of PSF and the $T_g$ and $T_m$ of PPS were almost independent of the blend composition. Heat treatment of the blends at 300°C or 350°C produced increases in the $T_g$ of PPS and PSF due to the occurrence of an oxidative crosslinking reaction. Furthermore, after heating the blends at 350°C for 3 hours, the melting point of PPS disappeared which indicated the formation of a network. At a higher temperature treatment (~400°C), the $T_g$ corresponding to PSF was not observed. In addition, blends containing more than 70% weight of PPS treated at 400°C presented a higher $T_g$ (125-180°C) that increased with increasing PSF content, suggesting mixing of the two components. Acetylene terminated sulfones (bis(4-(4-ethynylphenoxy)phenyl)sulfone EST) were blended with PPS in an attempt to raise the $T_g$ of PPS for applications as a matrix for structural composites (108). Solution blending in α-chloronaphthalene at 200°C produced a uniformly dispersed system.

The $T_g$ increase would be achieved by formation of interpenetrating networks of PPS and EST upon curing. Torsional braid analysis indicated that a blend containing 40% by weight of EST produced the highest rigidity and minimum of damping. Using this 40/60 EST/PPS blend, Zeng et al. (108) determined that the $T_g$ of PPS can be raised to 180°C by curing at 370°C for 9hs in air. The presence of one $T_g$ only suggested that the two components are well mixed. However, a 50/50 blend cured for 1hr at 320°C produced a microphase separated system with two glass transition temperatures, one at 100°C due to a PPS-rich phase, and the other at 165°C corresponding to an EST-rich phase. Therefore, although the $T_g$ of PPS can be increased by blending with EST, composition and, in particular, curing process are critical variables to consider. Zeng et al. (108) also reported that the flexural modulus and interlaminar shear strength of continuous unidirectional carbon fiber composites with EST/PPS = 10/90 matrix were 80% and 15% higher than those of composites with pure PPS matrix.

Blends of PPS with other crystallizable polymers have also been studied. For example, Fisher and Balow (109) made composite materials of Nylon 6.6/PPS with 20% chopped glass fibers in order to improve the chemical resistance and stability at high temperatures of Nylon 6.6 composites. These same authors reported that the tensile strength of the composite decreased by about 50% when the PPS content increased from zero to 60% by weight. The flexural modulus, however, increased by 40% in the same range of composition. The chemical resistance of the composite to water, acids, strong alkali solutions, hexane and toluene was improved by the addition of PPS. Similarly, Nadkarni and Jog (110) melt-compounded PPS/glass fibers with high density polyethylene (HDPE) to accelerate processing, obtain lower costs and improve the toughness of PPS/short glass fiber composites. Since their major concern was the processing of the composites, these authors studied the thermal behaviour and isothermal crystallization of these materials. The melting peak temperatures reported for PPS in the blends varied erratically with the blend composition; however, the heat of fusion per gram of PPS in the blend decreased from 7.8 cal/gram to 5.0 cal/gram as the composition changed from 100/0 to 37/63 volume ratio of PPS/HDPE, suggesting lower degree of

crystallinity of PPS. Furthermore, the PPS melting temperature range became narrower as the HDPE content increased. Since the melting temperature range is an indication of the crystallite size distribution, the narrower melting range suggested that PPS has a narrower crystallite size distribution in the blend. The time needed for isothermal crystallization of PPS was reduced by alloying with HDPE for compositions in which PPS was the major component. At a volume ratio of 37/63 PPS/HDPE the time for crystallization of PPS was longer than those of PPS/glass samples. It was suggested that this effect was due to the different number average molecular weights of PPS (21,000) and HDPE (70,000-85,000). At low volume contents of HDPE, a nucleating effect of molten HDPE would accelerate crystallization. However, at high volume contents (37/63 PPS/HDPE), the higher molecular weight HDPE would impose a higher diffusion barrier to PPS decreasing the growth rate, therefore, increasing the time needed to complete isothermal crystallization.

As expressed before, the addition of other components to PPS allows the tailoring of many properties for specific applications. In particular, the formation of composite materials with long fiber reinforcing agents such as long glass fibers or continuous carbon filaments produces an enhancement of the impact strength of PPS (111). A somewhat systematic study of the effects of sample thickness, impact speed, temperature, fiber length and content on the impact resistance of PPS-glass fiber composites was performed by Lou (112). The impact energy and specimen thickness had a linear relationship up to 0.4cm, followed by a very rapid decrease of the impact energy with increasing thickness. Similarly, the energy and load necessary to initiate failure propagation also increased linearly with specimen thickness up to samples 0.4cm thick. The impact energy showed a maximum at impact speeds of 127cm/sec. Furthermore, analysis of impacted samples at 127 cm/sec indicated a global damage pattern with substantial fiber pull-out. At higher impact speeds, the damage zone was smaller with very little fiber pull-out; i.e., at high impact speeds the impact time is too short to allow relaxation of the energy throughout a large area in the composite. The energy absorbed during impact decreased with increasing temperature in long glass-fiber PPS composite, with the

glass fibers having a major influence on the impact performance. However, a different dependence was observed in the chopped-fiber PPS composites. In this material, the impact energy goes through a maximum at 40°C and at higher temperatures it decreases. The impact resistance increased with increasing glass content and reached a plateau at 20% glass content. Lhymn (113,114) indicated that the impact fatigue lifetime of PPS/40% short glass fiber composites was a function of the impact load direction, and that there was a minimum impact energy for failure to occur. Moreover, the detailed microstructure of impact-fatigued composites showed that the fracture occurred along the fiber/matrix interface and along the matrix. In addition, failure by fiber pull-out was abundant while fiber fracture was a minor event (115). The mechanical lifetime of these composites in air, NaOH and HCl was studied by stress-rupture testing (116,117). The mechanical lifetime of the composites in air and HCl was very similar, and that in NaOH was significantly lower. SEM studies revealed that in NaOH ruptured samples, the fiber/matrix interface was attacked by the chemical agent.

Presently, composites containing long carbon fibers are receiving attention in the aerospace industry for structural applications. One of the very important properties for this type of utilization is the interlaminar fracture toughness. That is, the energy necessary to separate layers of unidirectional fiber matts from a part composed of several layers. This property is mainly dependent on the polymer matrix and on the polymer-fiber interaction. Ma et al (118) studied the interlaminar fracture toughness of uniaxial carbon fiber/PPS composites by a double cantilever beam Mode I delamination test. This kind of test measures the critical strain energy release rate, $G_{IC}$, which is a measure of the delamination resistance of a composite system. Table 4 shows the critical strain energy release rates for a few materials utilized as matrices for unidirectional carbon fiber composites. The comparison of PPS with epoxy and polysulfone matrices indicates the superior interlaminar fracture toughness of the PPS based composite laminates. However, comparison of PPS with poly ether ether ketone (PEEK) shows that both polymers present about the same values (7.8 inlb/in$^2$ versus 8.0 inlb/in$^2$, respectively). This good interlaminar fracture toughness has been attributed to the formation of good

bonding of PPS to the carbon fibers (119). In this respect, Johnson (120) has reported that carbon fibers induced the nucleation of crystallization of PPS at the fiber surface. Similarly, composites based on PEEK have also been shown to form transcrystalline regions (121); i.e., nucleation of crystallization at the fiber surface. However, it is important to realize that these morphological features are extremely dependent on the processing conditions (122,123,124).

In summary, although a sizeable amount of investigation has been performed on PPS, it is evident that many areas require the utilization of systematic studies in order to better understand the behaviour of this polymer. The crystallization behaviuor of PPS is one of these areas. In the oncoming chapters, a systematic study of the crystallization behaviour of PPS will be presented. The kinetics of isothermal crystallization of PPS as a function of the molecular weight, the branching agent content, and the nature of the endgroup counter-atom will be addressed. Furthermore, the kinetics of non-isothermal crystallization will be studied, and the morphological textures of neat PPS and PPS in composites with carbon fibers will be investigated.

**Table 4. Interlaminar fracture toughness for unidirectional carbon fiber composites. (from 118)**

| polymer | $G_{IC}$(inlb/in$^2$) |
|---|---|
| Epoxy | 0.6 |
| Polysulfone | 3.8 |
| PPS | 7.8 |
| PEEK | 8.0 |

# CHAPTER III

# THE KINETICS OF QUIESCENT CRYSTALLIZATION OF BULK POLYMERS

In studying the crystalline state of polymers, scientists have to be concerned with the equilibrium situations, which can be described by equilibrium thermodynamics, and with non-equilibrium situations. For example, the development of a crystalline phase quiescently occurs at a finite rate only at temperatures well below the equilibrium melting temperature, $T_m^0$, under supercooling conditions often far removed from $T_m^0$. Therefore, the morphology and properties of such a phase are the result of a competition between the kinetics factors of the transformation and the requirements of thermodynamic equilibrium.

The development of a crystal within a liquid phase involves two processes, namely the formation of the crystalline phase, and its subsequent development. The former process is called nucleation and the latter growth. The starting crystalline nuclei are presumed to have large specific surface area, in order to stimulate growth (Wunderlich). With this in mind, the free energy of a crystal ($G_{crystal}$) can be written as follows,

$$G_{crystal} = G_{bulk} + \Sigma \gamma A \tag{3.1}$$

where $G_{bulk}$ is the free energy of the crystal disregarding surface effects, $\gamma$ represents the specific surface energy, and A is the corresponding surface area. Therefore, the free energy change upon crystallization is,

$$\Delta G = \Delta G_c + \Sigma \gamma A \tag{3.2}$$

with $\Delta G_c$ representing the bulk free energy change. The specific surface free energies are positive for the crystallization temperatures of interest. At temperatures below the melting point, then, $\Delta G_c$ is negative and $\Delta G$ presents a maximum value. This process is called primary nucleation, and it leads to the formation of a growing crystal. Figure 18 shows a schematic representation of $\Delta G$ as a function of the nucleus size. At the beginning of crystallization, a primary nucleus must be formed through a positive $\Delta G$, until it reaches a maximum $\Delta G$ at a critical size (critical nucleus). Nuclei smaller than the critical nucleus are called embryos, and larger nuclei are called supercritical as long as $\Delta G$ is positive. Upon subsequent growth of the nucleus, $\Delta$ G becomes negative, at which point the nucleus is called a stable nucleus and then, growth is continued. The $\Delta G$ energy barrier for crystallization can be overcome only by random local fluctuations of order; consequently, the larger the required stable nucleus, the longer it will take for the nucleation process. If no preformed nuclei or foreign surfaces are present during nucleation, the primary nucleation is called *homogeneous* nucleation. If a foreign surface is present, the nucleus size needed for crystal growth is frequently decreased because the creation of interface between polymer crystal and substrate may be less hindered than the creation of the corresponding free polymer crystal surface. Therefore, an enhanced nucleation process occurs that is called *heterogeneous* nucleation.

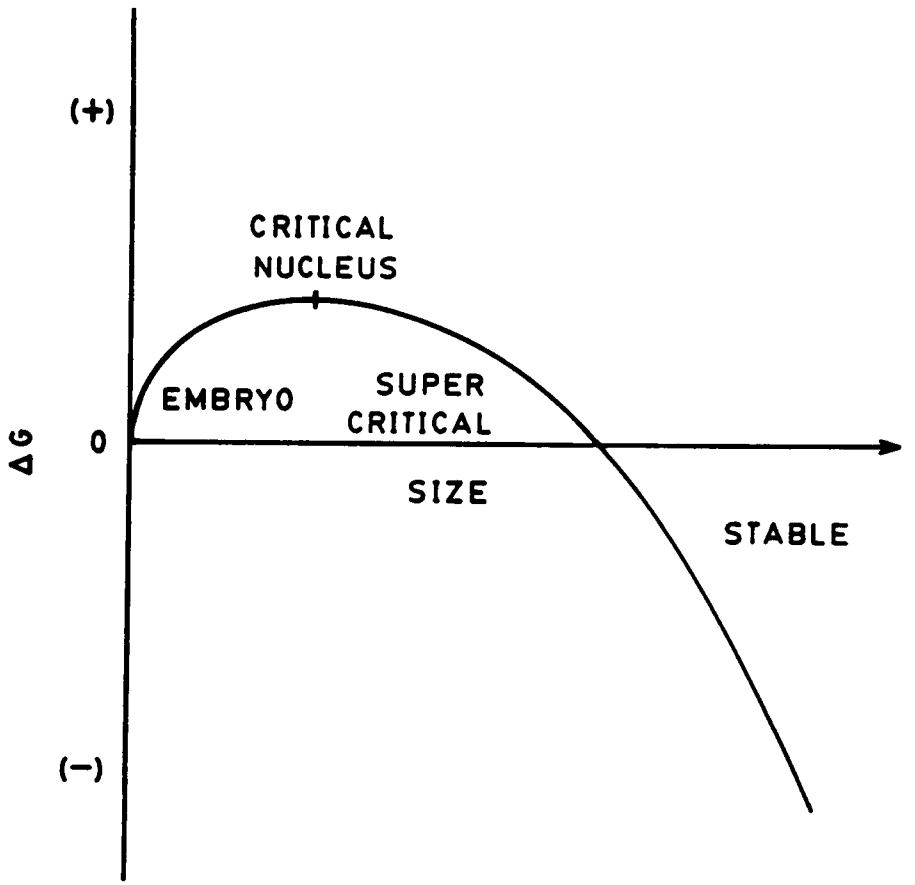


**Figure 18. Schematic representation of the change in free energy as a function of nucleus size.**

## 3.1 OVERALL RATE OF BULK CRYSTALLIZATION

The idea of separating nucleation and growth is by no means exclusive to polymers, and it was originally developed for low molecular weight materials. Several theories have been presented that describe isothermal crystallization in terms of a nucleation frequency or density (N) and the growth rates of the various crystallographic planes (G). For example, the free growth approximation of Von Goler and Sachs (126) describes the evolution of an individual growth center assumed to be independent of the mass already transformed as well as the growth of other centers. The main objection to this formulation is the lack of natural termination of the crystallization process, i. e., mutual impingement of growing entities. More exact descriptions of the kinetics of phase transformation in metallic systems considering the mutual impingement of growing centers were forwarded by Johnson and Mehl (127), Evans (128) and Avrami (129).

A rigorous mathematical formulation was given by Avrami (129) assuming that nucleation occurs according to a certain probability function P(t), and growth of the nuclei is linear with time. In addition, the growth of a real center is assumed to be retarded as it encounters other regions of already transformed material (impingement). The theory was developed as an analogy of expanding circles of waves which intersect at the end of the process. Avrami expressed the probability $p_x$ that a point is crossed by x growing waves (spherulitic fronts) in terms of Poisson's distribution,

$$p_x = \frac{e^{-E}E^x}{x!} \tag{3.3}$$

where E is the average number of fronts. The probability that no front is going to cross that point (or x=0) is $p_0 = e^{-\epsilon}$. Interpreting $p_0$ as the volume fraction of amorphous material, 1-X(t), and considering E as the volume of crystalline material (at low degrees of crystallization), Eq. 3.3 is written as follows,

$$1 - X(t) = \exp(-V_t) \tag{3.4}$$

At this point, the volume fraction of crystalline material, $V_t$, is calculated by considering that 1) nucleation is instantaneous, or 2) there is nucleation sporadic in time. In the first case, for N spherical nuclei growing at constant rate G, the volume increase in crystallinity is given by,

$$dV_t = 4\pi r^2 N dr \tag{3.5}$$

Substituting Gt for the spherulite radius, r, in Eq. 3.5, and integrating in the interval (0,t), the following expression is reached,

$$V_t = \frac{4}{3}\pi G^3 N t^3 \tag{3.6}$$

For sporadic nucleation, the number of nuclei is considered to increase linearly with time; therefore, for spherulites nucleated at time $t_i$, the volume increase in crystallinity is given by,

$$dV_t = 4\pi G^2 (t - t_i)^2 N G dt \tag{3.7}$$

that upon integration yields,

$$V_t = \frac{4}{3}\pi G^3 N t^4 \tag{3.8}$$

In a general form, the right hand side of Eqs. 3.6 and 3.8 are written as follows,

$$V_t = K t^n \tag{3.9}$$

Consequently, the general equation derived by Avrami considering a constant volume transformation reads as follows,

$$X(t) = 1 - \exp(K t^n) \tag{3.10}$$

where X(t) is the volume fraction of crystalline material at a given time t; K is a kinetic constant which is a function of the crystallization temperature $T_c$ and a combination of nucleation and growth parameters; and n is the Avrami exponent. The value of n has been utilized to deduce information regarding the details of the nucleation and growth processes. Table 5 shows the dependence of n on the dimensionality of the growth. However, it is apparent that extracting information regarding growth geometry and type of nucleation processes based solely on specifying the values of n is not fully justified (130). For example, an increase in crystallinity of the spherulites through thickening of lamellae will produce a fractional component to the Avrami exponent (131,132). Furthermore, Price (133) showed that variations of the Avrami exponent of as much as 0.3 could arise from the inability of achieving a constant volume transformation, an assumption imposed in the derivation of Eq. 3.10.

Comparison of Eqs. 3.6 and 3.9 indicates that the rate constant K is written in terms of the crystal growth rate, G, and the nucleation density N,

$$K = \frac{4\pi N G^3}{3} \tag{3.11}$$

Therefore, by determining the values of the rate constant K, and the radial growth rate G, the number of active nuclei, N, can be estimated.

## 3.2 CRYSTAL GROWTH RATE OF CHAIN-FOLDED LAMELLAR SPHERULITES

The theories utilized to describe the overall rate of bulk crystallization are not concerned with the mechanisms involved in the crystallization events. In other words, these theories

**Table 5. Values of the Avrami exponent for various types of nucleation and growth habits.(from 130)**

| | Homogeneous Nucleation | | Heterogeneous nucleation |
|---|---|---|---|
| Growth Habit | Linear Growth | Diffusion Controlled Growth | Linear growth |
| 3-dimensional | 4 | 5/2 | $3 \leq n \leq 4$ |
| 2-dimensional | 3 | 2 | $2 \leq n \leq 3$ |
| 1-dimensional | 2 | 3/2 | $1 \leq n \leq 2$ |

model only the transformation from a liquid state to a solid state regardless of the mechanisms. In polymers, however, the mechanisms of nucleation and growth are very important because they determine the superstructures that will be generated. The spherulitic superstructure is one of the most common superstructures observed in polymers crystallized from the molten state under quiescent conditions. Spherulites in bulk polymers grow from a nucleation site that is generally of heterogeneous nature. The spherulite is formed by stacks of blade-like lamellae that grow outward from the nucleation center. These lamellae are chain-folded lamellae with the thin dimension of the order of 50-250Å (lamellar thickness) (134); i. e., the polymer chains enter a crystal and fold on themselves to continue growth. The reentry mechanisms, adjacent versus nonadjacent or random reentry has been the topic of much argument (135,136). Nevertheless, it is known that the polymer chains in the crystalline matter in spherulites are approximately normal to the spherulite radius. Early studies with microcamera x-ray diffraction have provided evidence that indicated that the chain axes are nearly normal to the flat lamellar surfaces in polyethylene (137), a fact that is widely accepted. Figure 19 shows a schematic representation of a spherulite and the chain orientation in the lamellae.

The radial growth rate of a spherulite is the variation of its radius as a function of time. The radial growth rate results from the formation of the lamellar crystals, therefore, it is the same as the rate of growth of the lamellar crystals. In this section, the crystal growth rate of chain-folded lamellar spherulites will be analyzed to a certain extent.

As expressed above, most of the crystallization theories are based on the consideration of nucleation and growth steps. The modern theories of polymer crystallization of Hoffman et al. (54,138) also make use of this concept. The theory of Lauritzen and Hoffman (54) predicts the crystal growth rates and the lamellar thicknesses of polymers under certain conditions of supercooling. This theory assumes the model for surface nucleation and growth shown in Fig. 20. Several points are implied in Fig. 20:

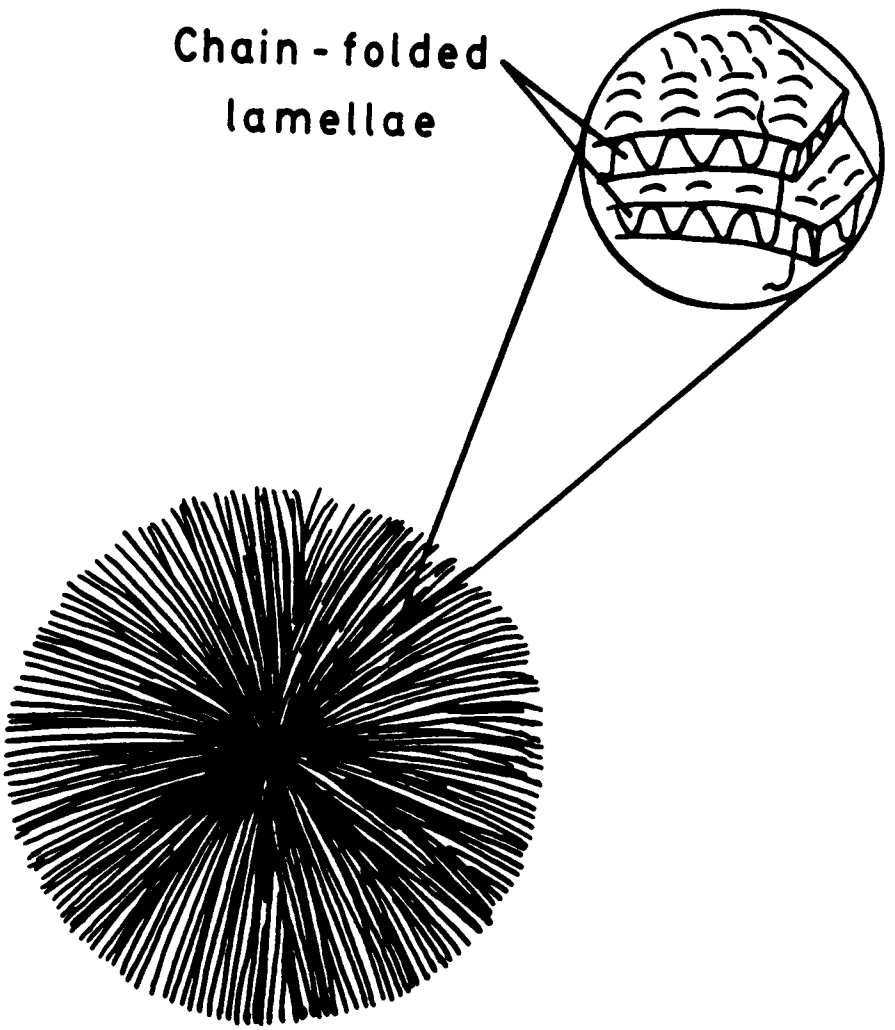


**Figure 19.** Schematic representation of a spherulitic superstructure showing the chain-folded lamellar crystals.

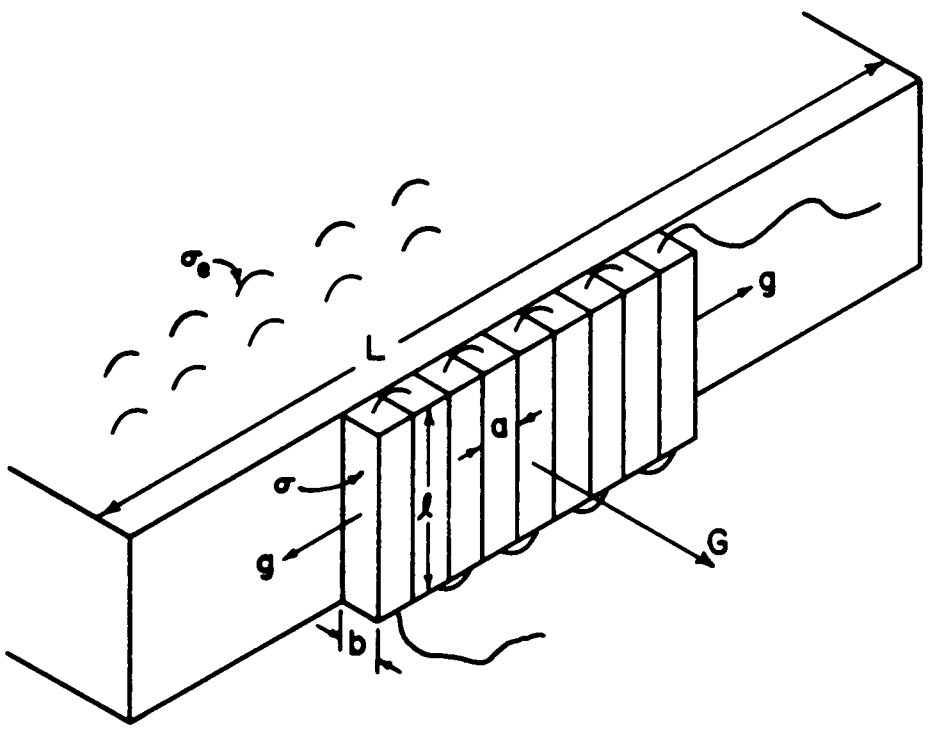


**Figure 20. Model for surface nucleation and growth of chain folded crystal. (from 54)**

1. the lamellar fold period is constant, which is not very realistic;

2. the polymer molecule is represented by a tetragonal body of cross-sectional area ab;

3. adjacent reentry after folding is considered to occur only, a subject of extensive discussion;

4. the effect of chain ends is ignored by assuming that the number of folds per molecule in the growth surface is large.

The model consists of the formation of a surface nucleus composed of a number of stems of length l, thickness b, and width a on the substrate and development of this nucleus in the g direction. Subsequently, the nucleus would complete a layer of thickness b by spreading over the crystal width L, causing the crystal to grow in the G direction.

The problem was approached by Lauritzen and Hoffman (54) as a nucleation-controlled process with a large energy barrier that has to be surpassed to initiate the nucleus with subsequent steps leading to a stable region. The free energy of formation of such a process can be depicted as a serrated curve. The number of nucleation events was calculated as the flux over the energy barrier in terms of two reaction rates: one for species passing the barrier, and another for species returning over the barrier. Furthermore, it was assumed that the rates for the first barrier were different than those corresponding to the following barriers, and the rates for the "secondary" barriers were all the same. In the steady-state approximation, Lauritzen and Hoffman (54) expressed the total flux $S_T$ as follows,

$$S_T = N_0(\beta/l_u)P \exp(2ab\sigma_e\psi/kT) \exp(-4b\sigma\sigma_e/\Delta fkT) \tag{3.12}$$

with

$$P = \frac{kT}{2b\sigma - ab(\Delta f)\psi} - \frac{kT}{2b\sigma + (1-\psi)ab(\Delta f)} \tag{3.13}$$

The significance of a and b is evident in Fig. 20; $\sigma$ represents the lateral surface free energy and $\sigma_e$ is the fold surface free energy; $l_u$ is the monomer repeat length; $\Delta f$ is the free energy of fusion; $\beta$ represents a retardation factor that accounts for the rate of transport of polymer molecules; k is the Boltzmann constant; T is the absolute temperature ; $N_0$ is the occupation number; and $\psi$ is concerned with the path by which the first element of the surface nucleus is attached to the surface; if the polymer segment goes from subcooled melt directly to the face without any intermediate state, $\psi = 1$. However, it is believed that there is usually an adsorption step before nucleation, therefore, $\psi$ takes values between 0 and 1.

The retardation factor $\beta$ is very important since at high supercoolings the rate of transport of polymer molecules will be the controlling factor of the flux. This factor can be expressed as follows,

$$\beta = (kTl_u)J_1 \exp[\frac{-U^*}{R(T - T_\infty)}] \qquad (3.14)$$

The exponential factor represents the temperature dependence of the segmental jump rate in polymers; $U^*$ is the activation energy for the segmental jump; $J_i$ is a preexponential factor regarded as essentially independent of temperature; $T_\infty$ represents a hypothetical temperature at which all motion associated with viscous flow ceases; and R is the universal gas constant. The values of $U^*$ and $T_\infty$ for bulk fluidity can be obtained from a William-Landel-Ferry type of equation. "Universal" values of $U^*$ are considered to be within 10-15% of 4100 cal/mole, and similarly, $T_\infty$ is within 5-10K of $T_g - 52$ K. However, values obtained from data on growth rates indicate that $U^*$ is in the vicinity of 1000-1600 cal/mole and $T_\infty \cong T_g - 30$ K (53,54).

At this point in the discussion it is important to invoke Fig. 21. This figure shows two different morphologies that may develop upon nucleation that need be considered. The diagrams at the left of Fig. 21 represent the morphology of the growing front for "Regime I" crystallization. Regime I occurs at high crystallization temperatures (small supercoolings). In

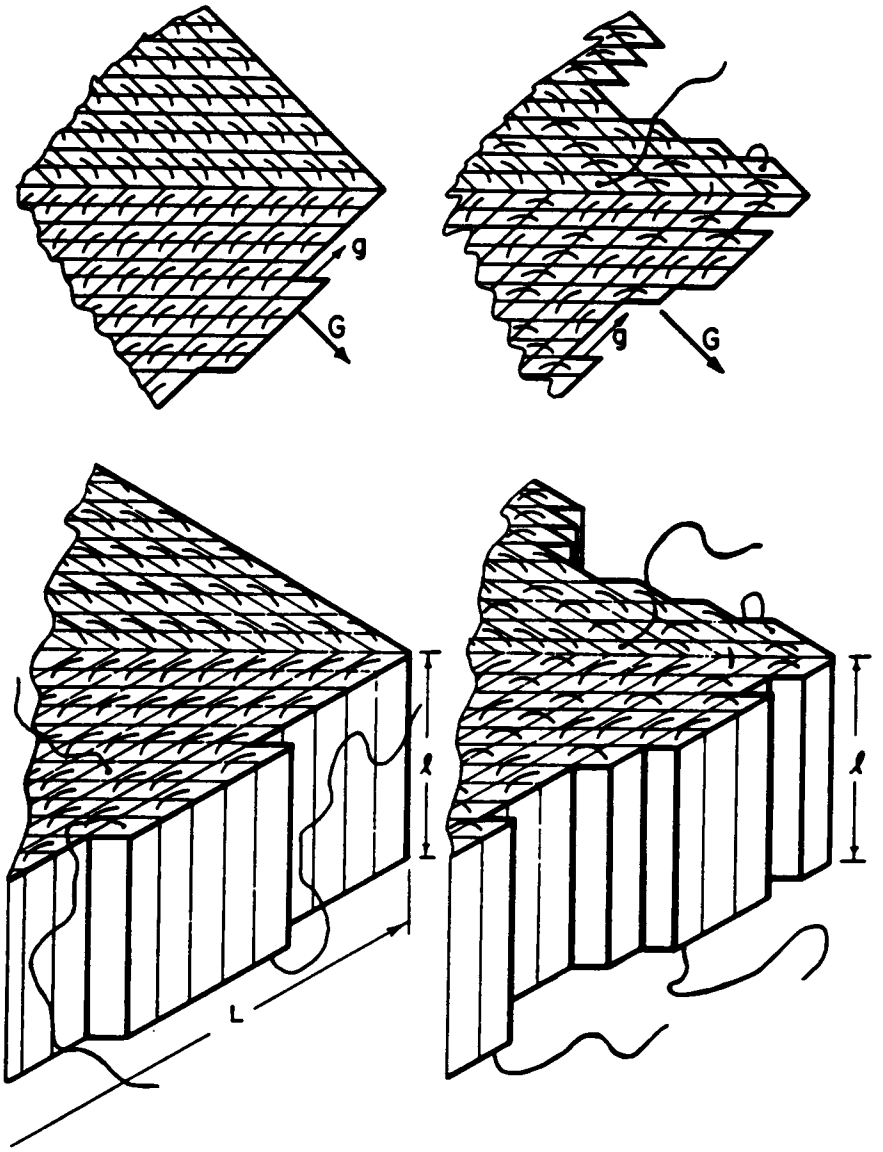


**Figure 21.** Morphology of the growth front for Regime I (diagrams at left) and Regime II (diagrams at right). (from 54)

this Regime, each surface nucleation event quickly completes the growth on the front of length L, annexing a layer of thickness b before another nucleation event can occur. In this situation, the growth rate is given by,

$$G = ibL \tag{3.15}$$

where i is the net surface nucleation rate given by $S_T/aN$ with N = Avogadro's number. Substituting $S_T$ by Eq. 3.12, the rate of growth for Regime I is written as follows,

$$G = G_0 \exp[\frac{-U^*}{R(T - T_\infty)}] \exp[\frac{-4b\sigma\sigma_e}{(\Delta f)kT}] \tag{3.16}$$

where the preexponential factor $G_0$ gathers the factors not strongly dependent on temperature,

$$G_0 = b(kT/h)n_s J_1 \exp(2ab\sigma_e \psi kT) \tag{3.17}$$

"Regime II" growth occurs at lower temperatures than Regime I. In the case of Regime II, surface nuclei form in large numbers on the substrate at a rate given by i. However, the lateral spread velocity g (Fig. 20) is small. This would lead to a rough growth front on a molecular scale. In this case, the polymer crystal growth rate is proportional to the square root of the surface nucleation rate (54), $G \propto (gi)^{1/2}$. Consequently, the growth rate is given by,

$$G = b(S_T g/aN)^{1/2} \tag{3.18}$$

$$G = G_0 = \exp[\frac{U^*}{R(T - T_\infty)}] \exp[\frac{-2b\sigma\sigma_e}{(\Delta f)kT}] \tag{3.19}$$

$$G_0 = b(\frac{kT}{h})J_l \exp[ab\sigma_e(2\psi - 1)kT] \tag{3.20}$$

Comparison of Eqs. 3.16 and 3.19 indicates that a general expression can be written for both regimes,

$$G = G_0 \exp[\frac{-U^*}{R(T - T_\infty)}] \exp[\frac{-K_g}{T(\Delta T)f}] \qquad (3.21)$$

In Eq. 3.21, $K_g$ has different values depending on the regime considered,

$$\textit{Regime I} \qquad K_{gI} = \frac{4b\sigma\sigma_e T_m^0}{(\Delta h_f)k} \qquad (3.22a)$$

$$\textit{Regime II} \qquad K_{gII} = \frac{2b\sigma\sigma_e T_m^0}{(\Delta h_f)k} \qquad (3.22b)$$

In this equations, $\Delta f$ has been substituted by $\frac{\Delta h_f(\Delta T)}{T_m^0 f}$, with $\Delta h_f$ = enthalpy of fusion; $T_m^0$ = melting point of an equilibrium crystal; $\Delta T = T_m^0 - T_c$, the supercooling; and f is a correction factor for departures of the approximation of the entropy of fusion to $\Delta h_f/T_m^0$ at high supercoolings. The factor f is close to unity at high temperatures, but becomes important at high supercoolings; it is given empirically by $f = 2T_c/T_m^0 + T_c$. It is important to point out that the relationship between $K_{gI}$ and $K_{gII}$ is a factor of 2; i. e., $K_{gI} = 2K_{gII}$. This relationship is utilized to test the validity of Eqs. 3.15, 3.16a and 3.16b.

The assumption of the different mechanisms of growth at the molecular level allowed the prediction of the two different regimes for crystallization, Regime I at high temperatures (low supercoolings), and Regime II at lower temperatures (high supercoolings). In a later publication, Hoffman (138) extended the previous analysis to account for Regime III kinetics. Regime III occurs at lower temperatures than Regime II. At this lower temperatures (higher supercoolings), the rate of nucleation is so high that adsorbed molecular stems have little probability of spreading laterally. Therefore, crystallization occurs almost exclusively through the accumulation of nucleation events. Under these circumstances, the crystal growth rate G is controlled by the rate of deposition of nuclei on the substrate, i, the same as Regime I. Consequently, the expression for the rate of crystal growth G is given by Eqs. 3.16 and 3.17, or Eqs.

3.21 and 3.22a. Similarly, the relationship between $K_{gII}$ and $K_{gIII}$ is a factor of 2, i.e., $K_{gIII} = 2K_{gII}$. Regime III would produce a high kinetic roughness at the growth fronts.

The validity of Eqs. 3.15, 3.16a and 316b has been tested for several polymeric systems. For example, Hoffman et al. (54) determined a transition from Regime I→Regime II at about 127°C in polyethylene. Allen and Mandelkern (131) indicated that the transition temperature can be found when overall crystallization kinetics are analyzed. These authors also reported that the transition temperature seems to have a decreasing trend with increasing molecular weight of polyethylene. Hoffman (55) and Martínez-Salazar et al. (140) showed that polyethylene crystallized at unusually high supercoolings presents a Regime II→Regime III transition. Poly (oxymethylene) (141), isotactic polypropylene (142), poly(phenylene sulfide) (53), and synthetic cis-polyisoprene (143,144) were also shown to present a Regime II→Regime III transitions.

Newer theories have been proposed that avoid making assumptions (1) and (3) of the theory of Hoffman and Lauritzen (54). For example, Lauritzen and Passaglia (145) considered the growth of a new layer of polymer crystal to be composed of a row of step elements such as those shown in Fig. 20. Although these authors considered adjacent reentry of the polymer segments, the element length, however, was considered a variable. Therefore, the lamellar thickness was an average quantity. Lauritzen, DiMarzio and Passaglia (146) have developed a theory that describes the formation of a one-dimensional, multicomponent chain under non-equilibrium conditions. This theory allowed the investigation of certain kinetic aspects of polymer crystallization such as crystal thickness fluctuations, impurity rejection, nonadjacent reentry, and molecular weight fractionation. A more recent development by Sanchez and DiMarzio (147) also takes into account the effect of chain ends. By considering that chain-end groups can be rejected, these authors were able to investigate the effect of polymer molecular weight and concentration on the nucleation rates of single crystals formed from solution.

### 3.2.1 Molecular Weight Dependence of the Crystal Growth Rate

In a general form, Eq. 3.21 can be rewritten as follows,

$$\ln G = \ln G_0 - \frac{\Delta E}{kT} - \frac{\Delta F^*}{kT} \tag{3.23}$$

where $\Delta E$ represents the free energy of activation for the transport of units across the phase boundary; $\Delta F^*$ is the free energy of activation for the formation of a critical size nucleus; k is the Boltzman constant; and T represents the absolute temperature. $G_0$ gathers the factors that are not strongly dependent on temperature.

Equation 3.23 *per se* does not include a molecular weight dependence. However, there have been several attempts to introduce a molecular weight dependence into Eq. 3.23. For example, Devoy and Mandelkern (148) analyzed the effect of $<M_n>$ on the spherulitic growth rate at temperatures in the vicinity of the melting temperature. In this temperature range, crystallization is a nucleation controlled process, therefore, these authors considered the effect of molecular weight or chain length on the critical free energy for nucleation, $\Delta F^*$, in Eq. 3.23. For a 2-dimensional growth process that involves the unimolecular deposition of chain units on a crystalline face, Devoy and Mandelkern (148) expressed the critical free energy for nucleation as follows,

$$\Delta F^* = 2\sigma\xi^* \tag{3.24}$$

$$\xi^* = \frac{2\sigma_e - RT_c \ln[(x - \xi^* + 1)/x]}{\Delta f_u - (RT_c/x)} \tag{3.25}$$

where $\sigma_e$ is the interfacial free energy per sequence at the fold plane; $\sigma$ is the lateral surface free energy; $\xi^*$ is the number of units in the nucleus along the chain axis; x represents the number of repeating units per molecule; R is the gas constant, and $\Delta f_u$ is the free energy of fusion per unit at $T_c$. According to Eqs. 3.23, 3.24 and 3.25, plots of lnG *versus* $\Delta F^*/2\sigma T_c$ should

produce straight lines for all molecular weights that intercept the lnG axis at a common point. Devoy and Mandelkern (148) showed that data corresponding to fractions of linear polyethylene, poly (tetramethyl-p-silphenylene) siloxane, and trans-1,4-polyisoprene followed the molecular weight dependence expressed by Eqs 3.24 and 3.25. It was also suggested by Hoffman and Weeks (149) and by Magill (150) that the spherulitic growth rate is inversely proportional to the molecular weight. Following this suggestion, Lovering (151) added a ln $<M_n>$ term to the left hand side of Eq. 3.23 obtaining the following,

$$\ln G + \ln <M_n> + \frac{\Delta E}{kT} = \ln G_0 - \frac{\Delta F^*}{kT} \tag{3.26}$$

This same author plotted data corresponding to t-1,4-polyisoprene as lnG + ln$<M_n>$ *versus* $T_m/T_c T_m^0 - T_c$ and found all molecular weight fractions from $<M_n>$ = 12,000 to $<M_n>$ = 165,000 were represented by a single straight line.

In contrast, Hoffman and Weeks (149) proposed that the preexponential factor $G_0$ should be dependent on molecular weight. In particular, they stated that $G_0$ would be proportional to $1/<n_n>^y$, where $<n_n>$ is the number average degree of polymerization and y has values between zero and unity. Recently, Hoffman (152) presented an adapted nucleation theory to include a molecular weight dependence of the crystal growth rate. This author included the effect of reptation in the expression of the retardation parameter β. As mentioned previously, β represents the resistance of the molecule in the melt to being pulled onto the substrate. Therefore, Hoffman expressed β in the following form,

$$\beta = (\frac{\kappa}{n})(\frac{kT}{h}) \exp[\frac{-Q_D^*}{RT}] \tag{3.27}$$

Comparison of this equation with Eq. 3.14 brings out some important points. The activation energy for segmental jump rate $U^*$ has been substituted in Eq. 3.27 by $Q_D^*$, the activation energy for the reptation process. In addition, a κ/n factor is included in Eq. 3.27 to represent the effect of chain length (molecular weight) on the reptation rate in the melt; κ would represent

the number of chain units that act as the effective segment length in the liquid state. Analysis of data corresponding to fractions of polyethylene (152) indicated that in the 1/n dependence of G, n needs to be considered as $<n_z>$, the z-average degree of polymerization.

Some empirical functions have also been suggested as attempts to express the molecular weight dependence of G. As an example, Magill and Li (153) proposed a semiempirical equation of the form,

$$\ln G = \frac{a}{<M_n>^{\alpha}} \tag{3.28}$$

where a is a constant, $<M_n>$ is the number average molecular weigth and $\alpha$ has values $0.5<\alpha<1.2$.

Recently, Cheng and Wunderlich (154) presented a logarithmic function to fit the molecular weight dependence of the crystal growth rate of poly (ethylene oxide) in the very wide range of $<M_w>$ 3,500-5,000,000,

$$\ln G = b \ln <M_n> + a \tag{3.29}$$

This model also seemed to fit other literature data corresponding to polyethylene, poly (hexamethylene oxide), poly (ethylene terephthalate), poly (tetramethyl-p-silphenylene) siloxane, and trans-1,4-poly (2-methyl butadiene). The connotations behind this model, as stated by Cheng and Wunderlich, indicate that molecular nucleation controls the crystal growth rather than crystal secondary nucleation. Molecular nucleation refers to the process which establishes the first part of a macromolecule in the crystalline phase. The term molecular nucleation has to be distinguished from crystal nucleation which describes the initiation of a new crystal or new crystal layer regardless of the parts of macromolecules contributing to the growth of the nucleus. However, these two terms may be closely related. For example, since the primary nucleus of a polymer crystal is normally smaller than a molecule length, molecular and crystal nucleation must occur simultaneously. For crystal growth to occur,

nucleation of segments of polymer molecules at the growing front of the crystal is necessary; therefore, molecular nucleation would control the crystal growth. Moreover, since the $\exp[1/(T_m^0 - T_c)]$ and $\exp[1/T_c(T_m^0 - T_c)]$ dependences describe surface nucleation, these same authors suggested that a molecular nucleus involves "a surface patch of increased surface area and a cooperative molecular weight dependent term".

# CHAPTER IV

# MATERIALS AND EXPERIMENTAL METHODS

## *4.1 MATERIALS*

The polymer samples utilized for the study of the effect of molecular weight and branching agent content on the crystallization kinetics of PPS were kindly donated and characterized by Dr. C. J. Stacy from Phillips Petroleum Co. Table 6 shows the sample designation and characteristics. The characterization of molecular weight and molecular weight distributions was performed by means of a gel permeation chromatographic technique in α-chloronaphthalene at 210°C developed by Dr. C. J. Stacy (8). Polymer specimens PPS24, PPS49, and PPS63 were used to investigate the effect of molecular weight on the crystallization rates. The polydispersity ratio of these samples is ~1.4, indicating fairly narrow molecular weight distributions.

Table 6 also shows the characteristics of the specimens used for the study of the effect of branching on the crystallization rates. Due to the high insolubility of PPS, the analysis of the branching characteristics by conventional techniques such as Nuclear Magnetic Resonance

**Table 6. Characteristics of samples utilized to study the quiescent crystallization kinetics of PPS.**

| Sample Designation | $<M_w>$ | $<M_w>/<M_n>$ |
|---|---|---|
| PPS24 | 24,000 | 1.4 |
| PPS49 | 49,000 | 1.4 |
| PPS63 | 63,000 | 1.5 |

| Sample Designation | TCB content (weight %) | $<M_w>$ | $<M_w>/<M_n>$ |
|---|---|---|---|
| PPS00 | 0.00 | 63,000 | 1.5 |
| PPS13 | 0.13 | 75,000 | 1.5 |
| PPS20 | 0.20 | 65,000 | 1.7 |

has been precluded to date. Therefore, the content of branching agent trichlorobenzene (TCB) in the reaction vessel was utilized as characterization of the concentration of branches in the polymer. This would imply a linear proportion between TCB content and branch concentration.

The similar molecular weight and molecular weight distribution of samples PPS00 and PPS20 allows the investigation of the effect of TCB content on the kinetics of crystallization with a very small contribution by the effect of molecular weight. In contrast, polymer PPS13 will present the mixed effects of branching and molecular weight differences.

The specimens utilized to study the "endgroup" effect were prepared by Dr. J. F. Geibel of Phillips Petroleum Co. using an effective ion-exchange procedure that presumably takes place at the endgroups of the polymer, as follows. One lot of high molecular weight linear PPS was utilized for the ion exchange procedures. Selectively introducing a specific metal counter ion to the polymer requires rigorous removal of all other metal ions normally present in the polymer. An efficient method to remove residual metal ions from PPS involves charging the PPS and a dilute solution of acetic acid (1%, v:v) to a stainless steel autoclave. The reaction mixture was degassed by pressurizing to 200 psig with nitrogen and then releasing the pressure. This pressurization/release cycle was repeated six times. Degassing in this manner eliminates oxygen from the autoclave and minimizes the possibility of adventitious oxidative chain extension. The reaction mixture was then heated to 235°C with agitation and held at that temperature for one hour. The polymer slurry was then cooled, filtered and the recovered polymer was washed with glass-distilled water at room temperature to remove any residual adsorbed acetic acid solution. A sample of the acid washed polymer was analyzed for residual metal ions. To introduce specific metal ions to the polymer, an aliquot of the acid-washed polymer was charged to the autoclave along with a dilute metal acetate solution (1%, w:v). Degassing was accomplished as previously described. The reaction mixture was heated to 235°C for 30 minutes, cooled and the polymer recovered as described above. All samples of PPS were dried in a vacuum oven at 100°C prior to analysis. Table 7 summarizes the samples, their designation and metal analyses obtained by plasma emission spectroscopy of acid

digestates of residual polymer ash. Utilization of such a method to prepare the polymer samples allows one to avoid the effect of molecular weight, since the same PPS is ion-exchanged. However, the procedure inherently produces samples that have higher nucleation densities, as will be shown in a forthcoming section.

## *4.2 EXPERIMENTAL METHODS*

### 4.2.1 Growth Rate Measurements

PPS specimens were molded into thin films between glass cover slips to measure spherulitic growth rates. A Zeiss polarizing microscope equipped with a Leitz 350 heating stage and a 35mm camera was utilized. Temperature calibration of the heating stage was performed with naphthalene, indium, anthraquinone and sodium nitrate.

PPS is known to undergo chemical reactions at high temperature in the presence of oxygen that involve chain extension, branching and crosslinking (9). These reactions alter the molecular weight of PPS. Therefore, the residence times of samples at high temperature need to be minimized. Moreover, the crystallization studies must be conducted under a nitrogen atmosphere to minimize the extent of these reactions. For this reason, the samples were held at 320°C for 4 minutes prior to crystallization. Crystallizations were performed in the temperature range of 220°C to 260°C minimizing the residence times of the samples at high temperatures as much as possible. No crystallization time was longer than 90 minutes. This limitation on the temperature range impaired a further detailed analysis of the growth rates in terms of the Regime theory proposed by Hoffman and coworkers (54,55,138).

**Table 7. Sample Designation and Analyses for PPS Specimens Used to study the effect of the Nature of the Endgroup Counter-atom.**

| Sample Designation | Counter-atom | Metal Analyses (ppm) Ca | Na | Zn |
|---|---|---|---|---|
| PPS As Received | — | 786.0 | 77.3 | 20.3 |
| PPSH | Hydrogen | 15.7 | BDL* | BDL |
| PPSZn | Zinc | BDL | BDL | 1950.0 |
| PPSCa | Calcium | 417.0 | BDL | 54.4 |
| PPSNa | Sodium | 9.0 | 268.0 | 24.7 |

* Below Detection Limits

Spherulite growth was followed by taking photographs with a 35mm camera at fixed time intervals. The spherulite diameters were measured from these optical micrographs. The values of the radius were plotted versus time and provided straight lines whose slope represented the growth rate, G. The values of these slopes were then utilized to obtain curves of the growth rates as functions of crystallization temperature. The error introduced by the determination was estimated by calculating the relative error as follows,

$$\Delta E = \frac{\Delta G}{G} \tag{5.1}$$

where $\Delta G$ is the maximum difference in the slope determined by the measurement of 10 spherulites on the same photograph, and G represents the average of the 10 slopes. The values obtained showed a relative error no larger than 10%.

### 4.2.2 Rate of Bulk Crystallization

A Perkin-Elmer DSC-4 differential scanning calorimeter was utilized to obtain bulk crystallization isotherms. The temperature calibration was performed with an indium standard and anthraquinone. The PPS samples were weighed in aluminum pans (2-3mg) and were crystallized from the melt after being held at 320°C for 4 minutes.

Crystallization from the melt was only possible in the temperature range 220°C-260°C. Two factors contributed to limit this temperature range. The upper end was set by the long residence time needed to complete crystallization at high temperatures which may induce chemical reactions. The lower limit was imposed by the high nucleation densities encountered. For this reason, the cooling rates available in the DSC-4 were not sufficiently fast to permit the achievement of temperatures lower than 220°C prior to the initiation of crystallization.

In order to obtain crystallization data in the diffusion controlled part of the crystallization rate-temperature curve, thin amorphous PPS films were formed. These were prepared by compression molding PPS at 320°C for 4 minutes at 2000psi, and quenching in ice water. Similar to crystallization from the melt, the temperature range for crystallization from the glassy state was very limited.

## 4.3 DATA ANALYSIS

The overall rate of bulk crystallization was analyzed in terms of the well known Avrami equation (129),

$$x_c(t) = 1 - e^{-Kt^n} \tag{5.2}$$

In this equation, $X_c(t)$ is the volume fraction of crystals at time t; K is a rate constant that includes the temperature dependent terms, and contains information regarding diffusion and nucleation rates; n, the Avrami exponent is a constant dependent on the types of processes occurring during nucleation and growth. Assuming that nucleation results in three-dimensional spherulites, and that the increase in crystal dimensions is linear with crystallization time, the nucleation density N (number of nuclei per cubic centimeter) can be estimated by,

$$N = \frac{3K}{4\pi G^3} \tag{5.3}$$

where K is obtained from Eq. 5.2, and G is the linear crystal growth rate. Therefore, the combination of K obtained from DSC experiments, and G obtained from polarized light microscopy experiments on spherulitic growth rates allows the estimation of the nucleation density as a function of crystallization temperature.

The parameters in Eq. 5.2 can be determined by taking the logarithm of this equation two times,

$$\ln[ - \ln(1 - X_c(t))] = \ln K + n \ln t \tag{5.4}$$

Consequently, a plot of the double logarithm of the amorphous content as a function of the logarithm of time (a classical Avrami plot) permits the determination of K from the intercept, and n from the slope of the straight line. However, due to the lack of sensitivity of a double logarithmic plot, the method would be suspected of not being highly accurate.

A potentially more precise method to determine n and K involves the use of the crystallization half-time. Referring to Fig. 22, the whole area under the exothermic curve represents a normalized crystalline content of unity. On a normalized basis, the crystallization half-time, $t_{1/2}$, is defined as the time at which the normalized crystalline content is 0.5. The crystallization half-time method consists on the determination of the crystallization half-time, $t_{1/2}$, from a graph of the amorphous content as a function of time, and the calculation of the slope , S, of the curve of amorphous content as a function of logarithm of time at $t = t_{1/2}$.

Taking the logarithm of Eq. 5.2 at $t = t_{1/2}$, one obtains (125),

$$K = \frac{ln2}{t_{1/2}^n} \tag{5.5}$$

The slope of the curve (1- $X_c(t)$) as function of ln(t) can be written as follows,

$$S = t\frac{\partial(1 - X_c(t))}{\partial t} \tag{5.6}$$

Utilizing Eq. 5.2, $\partial(1- X_c(t))/\partial t$ can be calculated,

$$\frac{\partial(1 - X_c(t))}{\partial t} = - Knt^{n-1}e^{-Kt^n} \tag{5.7}$$

At $t = t_{1/2}$ it can be shown that,

$$S_{t_{1/2}} = \frac{n \ln 2}{2} \tag{5.8}$$

Therefore, using Eqs. 5.5 and 5.8 the two parameters of the Avrami equation, K and n, can be determined.

Both methods discussed so far were utilized to determine the parameters of the Avrami equation. As shown in Table 8, the Avrami exponents calculated with both methods compare very favorably. This indicates that either method is surprisingly equally precise, and adds a greater degree of confidence in the values obtained. Furthermore, reproducibility of the determination of the rate constant, K, indicated a standard deviation of 10%.

In particular, when differential scanning calorimetry is used to follow bulk crystallization, the weight fraction of material that has crystallized at time t, $X_c(t)$, is given by,

$$X_c(t) = \frac{\int_0^t (\frac{dH}{dt})dt}{\int_0^\infty (\frac{dH}{dt})dt} \tag{5.9}$$

where dH/dt is the rate of heat evolution as a function of time. This is achieved by determining the area under the crystallization isotherm point by point, and taking the ratio of the areas at each time interval to the total area. This method is depicted schematically in Fig. 22.

**Table 8. Avrami exponent determined by the double logarithmic, and by the crystallization half-time methods for PPS49.**

| *Temperature (°C)* | *Avrami Exponent* | |
|---|---|---|
| | ln[-ln(1-X)] vs lnt | $t_{1/2}$ method |
| 255 | 2.9 | 3.0 |
| 250 | 3.0 | 3.1 |
| 245 | 2.8 | 2.6 |
| 240 | 2.7 | 2.9 |
| 235 | 2.7 | 2.8 |
| 230 | 2.7 | 2.8 |
| 225 | 2.8 | 2.9 |
| 220 | 2.8 | 2.8 |

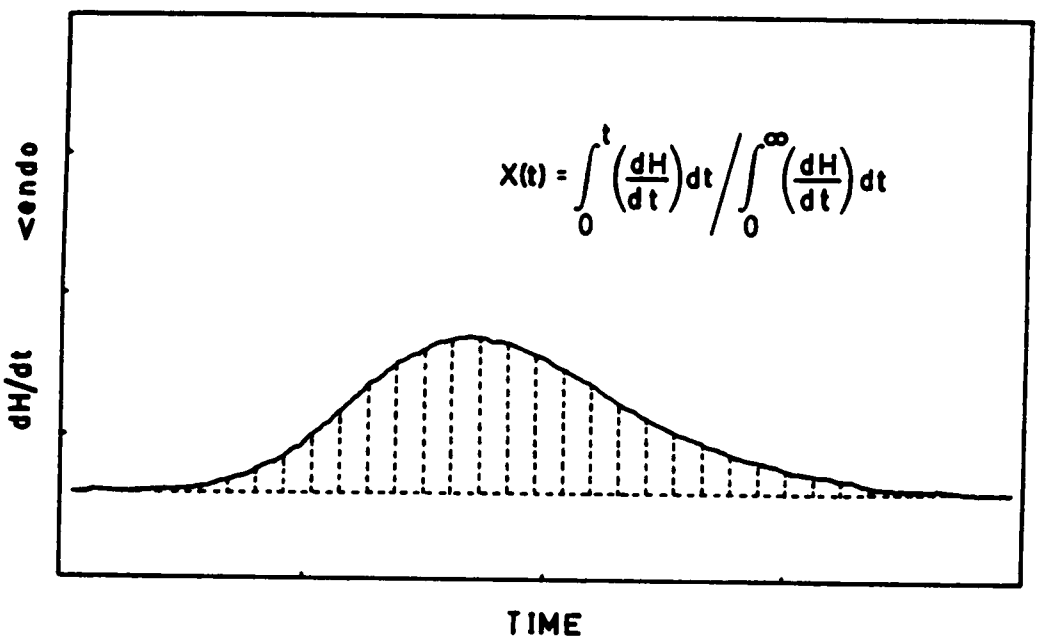


**Figure 22.** Typical crystallization endotherm for PPS63 showing the method utilized to calculate the normalized crystalline content.

# CHAPTER V

# KINETICS OF ISOTHERMAL CRYSTALLIZATION OF PPS

In this chapter, the kinetics of isothermal crystallization of PPS in quiescent conditions will be addressed. The effect of molecular weight, branching agent content and chemical nature of the end-group counter-atom on the kinetics of crystallization will be discussed in terms of experimental data obtained by optical microscopy and differential scanning calorimetry. Therefore, this chapter will consist of three sections devoted to each of the variables investigated. In addition, the dependence of the crystal growth rate on the molecular weight will be modelled utilizing equations previously proposed by other authors.

## *5.1 EFFECT OF MOLECULAR WEIGHT*

Crystal growth rates are presented in Fig. 23 in the form of plots of the logarithm of growth rate as function of crystallization temperature. Two limiting factors contributed to make the crystallization temperature range shown in Fig. 23 (220-260°C) rather narrow. At high temperatures, PPS may undergo curing reactions that cause chain-extension, branching and possibly

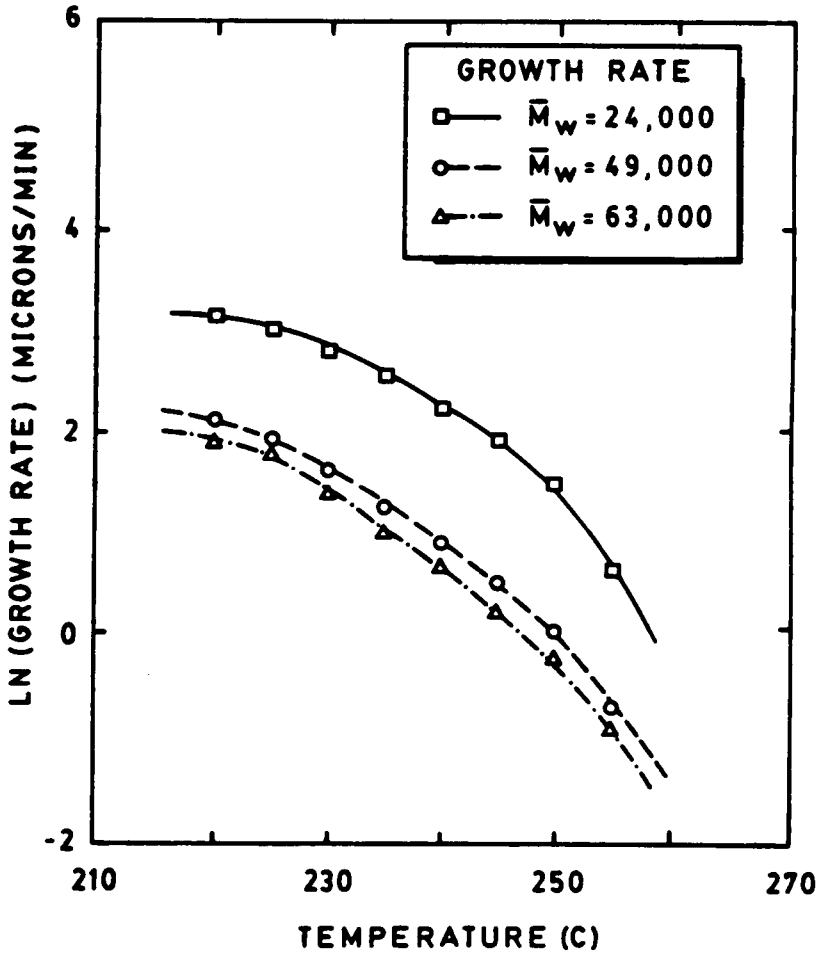


**Figure 23. Relationship between linear crystal growth rate and crystallization temperature for PPS samples crystallized from the melt.**

crosslinking. These reactions would change the molecular weight and molecular weight distribution of the polymer; consequently, the residence time of the polymer at high temperatures had to be minimized. As the maximum residence time at high temperature was determined to be 2.5 hs. by optical microscopy (darkening of samples), the kinetics of crystallization could only be studied up to a temperature of 260°C. Above 260°C, crystallization occurs too slowly to avoid curing of PPS samples. At the lower temperature end, a different problem arouse. At temperatures below 220°C, the nucleation density and growth rate were too high to obtain reproducible measurements.

Slower crystal growth rates are observed as the molecular weight of PPS increases. This is reasonable since increasingly longer chains need more cooperative displacements to go from the melt to the crystalline structure. Therefore, the time necessary to crystallize increases, and the crystal growth rate decreases. At a supercooling of 70°C, the lowest molecular weight PPS24 ($<M_w>$ = 24,000) has a crystal growth rate four times faster than the highest molecular weight PPS63 ($<M_w>$ = 63,000). However, the difference between PPS49 ($<M_w>$ = 49,000) and PPS63 is only a factor of 0.5. This may indicate that the decrease in growth rate due to increased molecular weight may be approaching a limiting value. A similar behaviour has been observed in trans-1,4-polyisoprene (151). In this case, the crystal growth rate was virtually independent of molecular weight for samples with number average molecular weight higher than 150000. In the present case of PPS, it seems that the "critical" molecular weight may be lower than that of trans-1,4-polyisoprene.

Figure 24 shows a plot of the normalized crystalline content of PPS49 crystallized from the melt as a function of the logarithm of time, and an Avrami plot, i.e., a graph of $\ln[-\ln(1- X_c(t))]$ versus logarithm of time. These graphs were calculated utilizing equations (5.9) and (5.4), respectively. As can be observed in part b) of Fig. 24, the DSC data follow almost perfectly the Avrami equation for the overall rate of bulk crystallization. The values of the Avrami exponents corresponding to samples crystallized from the melt are shown in Fig. 25 as functions of the crystallization temperature. It is clear that PPS49 and PPS63 present Avrami exponents very

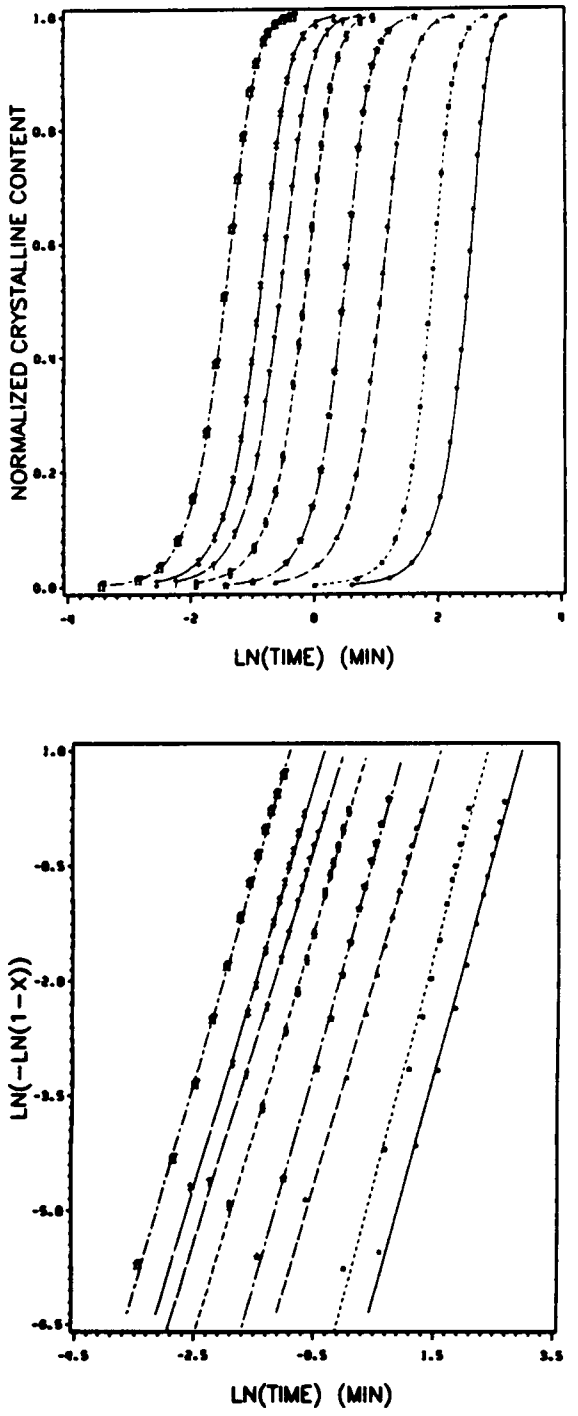


**Figure 24. Crystallization isotherms corresponding to PPS49:** a) Normalized crystalline content as a function of ln(time). b) Double logarithmic plot of amorphous content versus ln(time), following the Avrami equation. • T=255°C; ▪ T=250°C; ▲ T=245°C; ★ T=240°C; § T=235°C; † T=230°C; ‡ T=225°C; ff T=220°C.

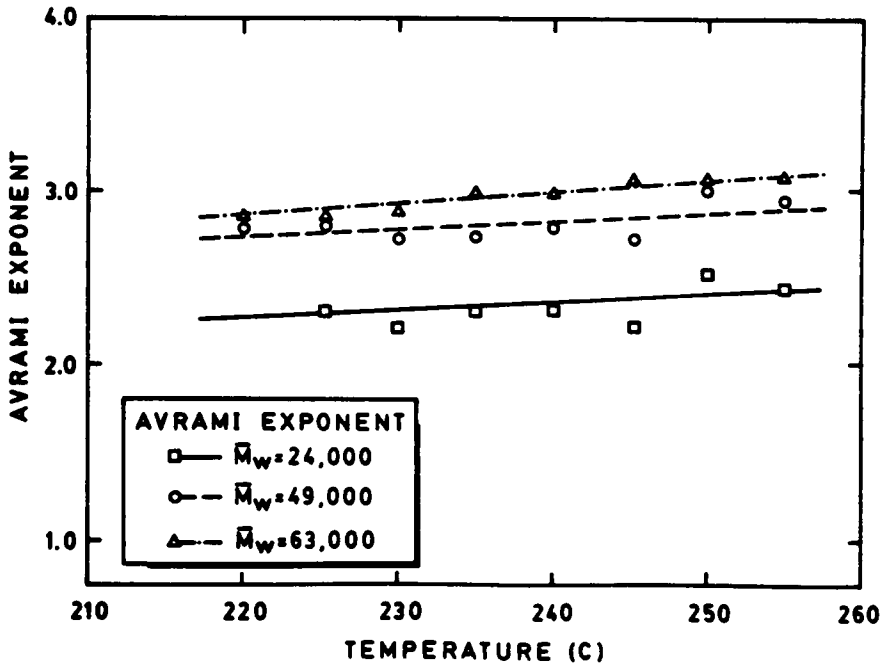


**Figure 25.** Avrami exponent as a function of crystallization temperature for PPS crystallized from the melt.

close to 3. This strongly indicates the assumption behind Eq. (5.3), namely 3-dimensional spherulites are formed, is valid for the calculation of the nucleation densities. PPS24, however, shows lower values of n, in the order of 2.5. These lower values may be attributed to growth that is not 3-dimensional which lowers the value of the Avrami exponent. Consider Fig. 26 which presents a schematic representation of the development of a spherulite from a single lamella (step 1) to a 3-dimensional spherulite (step 5). The intermediate sheaf-like structures such as those in steps 3 and 4 in Fig. 26 would decrease the Avrami exponent from the value of 3. Consequently, the presence of these structures would contribute to the lowering of n in PPS24. A very high nucleation density may induce the presence of these structures upon crystallization. However, the nucleation density values obtained in PPS24 are lower than those of PPS49 and PPS63, as will be shown. In addition, observations in the optical microscope indicated the formation of spherulitic textures in PPS24. Another possible cause of a somewhat lower Avrami exponent exists. Specifically, it has been shown that n may be lowered as much as 0.3 due to the impossibility of achieving a constant volume transformation, an assumption imposed in the derivation of Eq.(5.2) (131).

In Fig. 27, the logarithm of K and the logarithm of $t_{1/2}$ are represented as functions of the crystallization temperature for specimens crystallized from the melt (data on the right hand side of plots) and specimens crystallized from the glassy state (data on the left hand side of plots). The complete curves are presented. However, as expressed in the Chapter 4, there were limitations in the temperature ranges studied. No reliable data points could be gathered in the region of fast crystallization rates due to the start of crystallization at rapid rates before temperature stabilization could be achieved. Therefore, the curves were constructed following a third-order polynomial regression. Although from a statistical point of view these curves should be considered cautiously in their central part, the rate maxima located at 170°C for PPS24 and PPS49, and at 180°C for PPS63 are in good agreement with the values obtained by Jog and Nadkarni (52), and by Lovinger, Davis and Padden (53). Figure 27 shows that lnK and $\ln t_{1/2}$ curves also present the effect of molecular weight. At a supercooling of 70°C, the

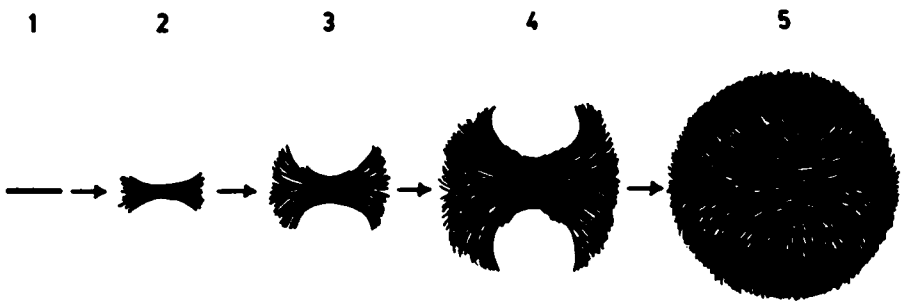


**Figure 26. Schematic representation of the development of a spherulitic superstructure.**

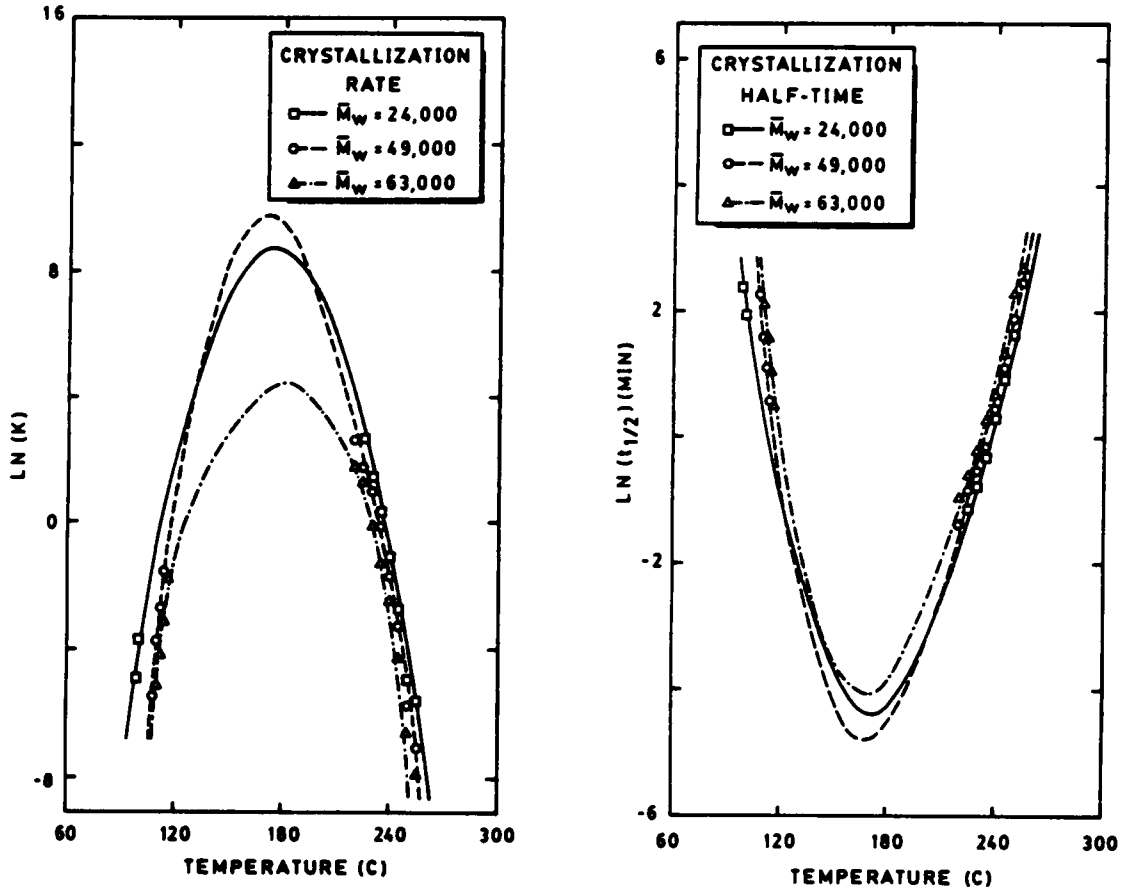


**Figure 27. Kinetic data determined from the Avrami analysis:** a) Relationship between rate constant, K, and crystallization temperature; b) relationship between crystallization half-time and crystallization temperature, for different molecular weight materials.

overall rate of bulk crystallization decreases by a factor of 3.5 as the molecular weight of PPS increases from 24,000 to 63,000. Similarly, the crystallization half-time increases by a factor of 3.5 as the molecular weight increases. It is of interest to compare these factors to those corresponding to poly (ethylene terephthalate) (PET) in view of their similar window for crystallization. PET has a glass transition temperature ($T_g$) at about 69°C and a melting temperature ($T_m$) at about 265°C. Therefore, the temperature range in which PET can crystallize is similar to that of PPS ($T_g$ = 85°C , $T_m$ = 285°C). In addition, PPS can potentially substitute PET in many applications, especially if chemical resistance is of importance. Van Antwerpen and van Krevelen (155) studied the effect of molecular weight on the crystallization kinetics of PET in a similar range of $<M_n>$ as that of PPS reported here. They observed that at a supercooling of 90°C, the overall rate of crystallization as measured by the crystallization half-time decreased by only a factor of 2.5 as the $<M_n>$ of PET increased from 19,000 to 35,400. In the case of PPS, the overall rate of bulk crystallization decreased by a factor of 4 as $<M_n>$ increased from 17,100 to 42,000. Therefore, the effect of molecular weight on the overall rate of bulk crystallization seems to be more important in PPS than in PET.

Combination of the growth rate data and overall rate of bulk crystallization data permits the calculation of the nucleation density by means of Eq. (5.3). The results of these calculations are plotted in Fig. 28 as a function of the crystallization temperature for samples crystallized from the melt. These show that the nucleation density decreases as the crystallization temperature increases in all cases. At lower crystallization temperatures, the critical size of the nucleus for crystallization is smaller; therefore, more nuclei can be activated; whereas at high crystallization temperatures, the critical size of nucleus for crystallization is larger and less nuclei can be activated for further growth. Consequently, a decrease of the nucleation density is expected as the crystallization temperature increases. The lower molecular weight PPS24 has nucleation density values that are 32-fold lower than the higher molecular weight PPS49 and PPS63. This indicates that the faster overall rate of bulk crystallization of PPS24 is due primarily to rapid crystal growth rates and is not due to higher nucleation densities. As ex-

pressed above, these results are not in agreement with having Avrami exponents of 2.5 for PPS24. In other words, the explanation of having species that are not three dimensional spherulites does not seem to agree with the lower nucleation density of PPS24.

Figure 29 presents a plot of the normalized overall heat of crystallization as a function of $T_c$ for PPS crystallized from the melt. The heat of crystallization follows the usual increasing trend with crystallization temperature. As the temperature increases, although crystallization occurs slowly, the extent of crystallization is higher. Since the heat of crystallization is proportional to the extent of crystallization, the heat of crystallization is expected to increase as crystallization temperature increases. There is about a 30% increase of the heat of crystallization as temperature varies from 220°C to 255°C for all samples studied.The higher molecular weight PPS, PPS49 and PPS63 have similar values for the heat of crystallization. However, PPS24 shows somewhat higher values of $\Delta H$ at low crystallization temperatures, indicating a higher crystalline content. At temperatures above 250°C the heats of crystallization have similar values.

### 5.1.1 Crystal Growth Rate as a Function of Molecular Weight

As expressed in Chapter 3, the crystal growth rate is expressed by Eq. (3.23),

$$\ln G = \ln G_0 - \frac{\Delta E}{kT} - \frac{\Delta F^*}{kT} \tag{3.23}$$

where $\Delta E$ represents the free energy of activation for the transport of units across the phase boundary; $\Delta F^*$ is the free energy of activation for the formation of a critical size nucleus; k is the Boltzmann constant; and T represents the absolute temperature. Several attempts have been made to introduce a molecular weight dependence into Eq. (3.23). For example, Devoy

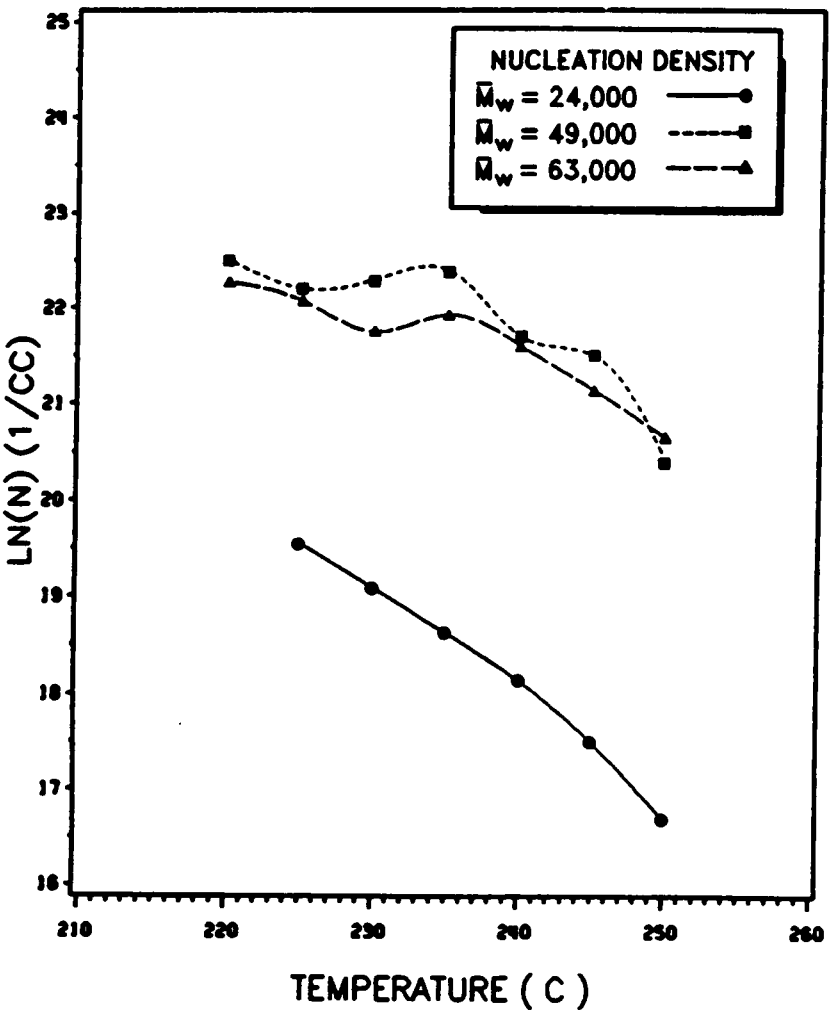


**Figure 28.** Plot of nucleation density as a function of crystallization temperature for different molecular weights of PPS crystallized from the melt.

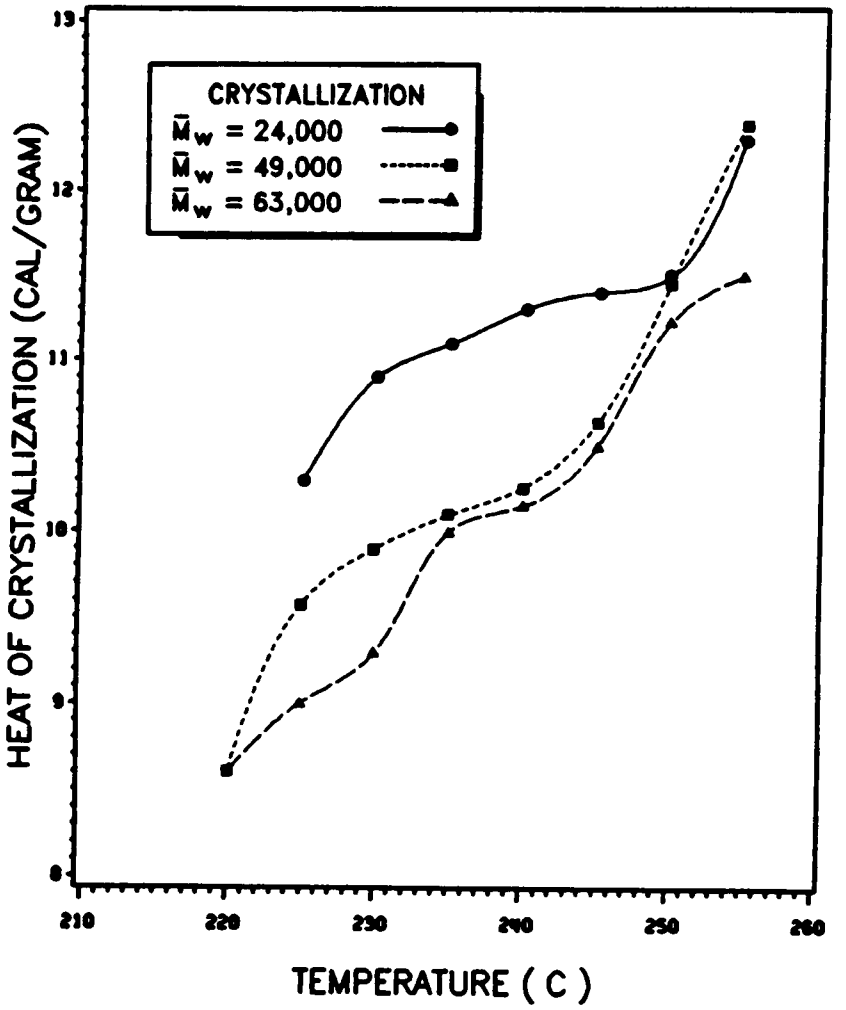


**Figure 29.** Heat of crystallization as a function of crystallization temperature for different molecular weights of PPS crystallized from the melt.

and Mandelkern (148) analyzed the molecular weight dependence of G considering the effect of chain length on the free energy of fusion. That is, only the last term in Eq. (3.23), $\Delta F^*$, was considered a function of molecular weight. It was also suggested that the growth rate is inversely proportional to $<M_n>$. Therefore, Lovering (151) added a $-\ln<M_n>$ term to the righthand side of Eq. (3.23) to explain the molecular weight dependence of G. This same author showed that a plot of $\ln G + \ln<M_n>$ as a function of $T_m/T_c(T_m^0 - T_c)$ should provide a straight line with all his data for different molecular weights falling on the same line. In contrast, Hoffman and Weeks (149) suggested that the term $G_0$ was the molecular weight dependent parameter. They proposed that $G_0$ was proportional to $(1/<n>)^y$, where $<n>$ is the number average degree of polymerization, and y takes values between zero and unity. Recently, Hoffman (152) stated that the linear crystal growth rate (G) was found to be inversely proportional to $<n_z>$, the z-average degree of polymerization.

Some empirical functions have also been suggested as attempts to express the molecular weight dependence of G. As an example, Magill and Li (153) proposed an equation of the form,

$$\ln G = \frac{a}{<M_n>^{\alpha}} \tag{3.28}$$

where a is a constant, $<M_n>$ is the number average molecular weight and $\alpha$ has values $0.5 < \alpha < 1.2$.

Recently, Cheng and Wunderlich (154) presented a logarithmic function to fit the molecular weight dependence of the crystal growth rate of poly (ethylene oxide) in the very wide range of $<M_w>$ 3,500-5,000,000,

$$\ln G = b \ln <M_n> + a \tag{3.29}$$

This model also seemed to fit other literature data corresponding to polyethylene, poly (hexamethylene oxide), poly (ethylene terephthalate), poly (tetramethyl-p-silphenylene) siloxane, and trans-1,4-poly (2-methyl butadiene). The significance of the slope, b, and intercept, a, in Eq. 3.29 is not understood yet. However, Cheng and Wunderlich (154) showed that the slope increases and the intercept decreases as the supercooling ($\Delta T = T_m^0 - T_c$) increases, for data corresponding to poly (ethylene oxide). Furthermore, these authors showed that the slope, b, was a linear function of the reciprocal of the supercooling, and the intercept, a, was a linear function of $\ln T_c - (\frac{T_m^0}{\Delta T T_c})x10^2$ .

Although the range of molecular weights studied in the present report is rather narrow, the molecular weight dependence of G was studied in terms of the models described previously. The data were analyzed in terms of the models by Lovering (151), Hoffman (152), Magill and Li (153), and Cheng and Wunderlich (154). Only the latter model seems to conform to the data well as will be demonstrated.

Since, the thermodynamic melting points, $T_m^0$, were needed for this analysis, they were determined by the method of Hoffman and Weeks (156). The equilibrium or thermodynamic melting temperature represents the melting temperature of the most perfect crystal. The method of Hoffman and Weeks (156) to determine the equilibrium melting temperatures combines the model of chain-folded crystallization with the finding that a plot of melting temperature as a function of crystallization temperature from the melt yields a straight line relationship at the higher crystallization temperatures (157). The technique assumes that upon isothermal crystallization, the fold length has a fixed value proportional to the reciprocal of the supercooling. Hoffman and Weeks (156) derived an expression for the experimental melting point, $T_m$, as follows,

$$T_m = \frac{[T_m^0(2\beta - 1) + T_c]}{2\beta} \qquad (6.1)$$

where $T_m^0$ is the extrapolated equilibrium melting temperature, $T_c$ is the crystallization temperature, and $\beta$ represents the lamellar fold length expressed in terms of multiples of the primary, homogeneous nucleus. As the fold length depends on the crystallization conditions, molecular weight and molecular weight distribution, Eq (6.1) defines a family of straight lines for the different values of $\beta$ that intersect when $T_m = T_c = T_m^0$. Therefore, the determination of $T_m^0$ by this method involves the crystallization of polymer samples from the melt at different supercoolings. Then, the experimental melting points are plotted as functions of the crystallization temperature. At the higher crystallization temperatures a straight line relationship between melting and crystallization temperatures is found. This line is extrapolated to $T_c = T_m$, and this point represents $T_m^0$. Figure 30 shows typical Hoffman-Weeks plots, i.e., plots of melting point as function of crystallization temperature. It is observed that straight line relationships are obtained at high crystallization temperatures as indicated by Lauritzen and Hoffman (157). Upon extrapolation, the values obtained for the thermodynamic melting points are 304°C for PPS24, 308°C for PPS49, and 312°C for PPS63, presenting an increasing trend of $T_m^0$ with increasing molecular weight. The relationship between $T_m^0$ and molecular weight or molecular length is simple in monodisperse polymer samples. As the molecular weight increases, the crystal thickness would increase in the direction of the chain axis, causing an increase in the equilibrium melting point. However, when a distribution of molecular weights is present, a more complicated situation arises that involves separation of different molecular weight species. Since this process would be controlled by the kinetics of crystallization, the relationship between $T_m^0$ and the molecular weight is not simple. In addition, the chain folding effect that occurs, allows the incorporation of molecules with different chain lengths in the same crystal making the situation even more complicated. Nevertheless, in a polymer with a distribution of molecular weights, as the higher molecular weight component concentration increases, the equilibrium melting temperature increases, and viceversa. Therefore, a polymer sample with higher $<M_n>$ will present a higher equilibrium melting temperature than one with lower $<M_n>$ as is observed in the data reported here.

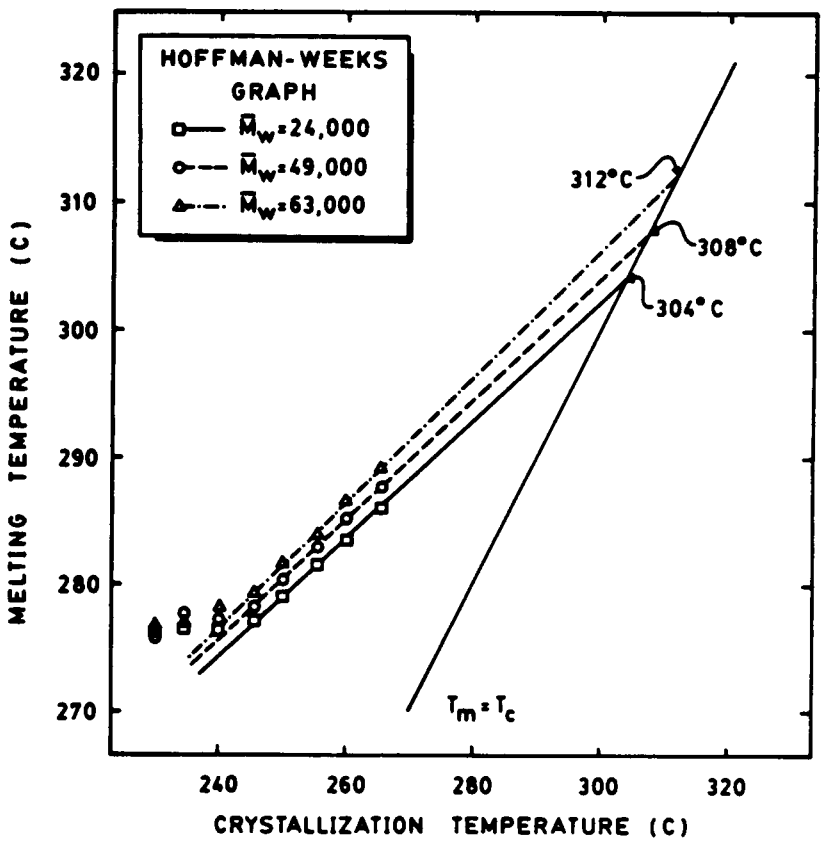


**Figure 30.** Hoffman-Weeks plots utilized to determine thermodynamic melting points of different molecular weight fractions of PPS.

To analyze the crystal growth rate data in terms of their molecular weight dependence, the growth rate values at constant supercooling are needed, instead of values at constant temperature. Utilization of these values eliminates the thermodynamic effects. At a constant crystallization temperature, a polymer with higher molecular weight will crystallize at a higher supercooling ($\Delta T$) than a lower molecular weight sample, due to the higher $T_m^0$ of the former. Consequently, the driving force for crystallization is higher in the high molecular weight polymer. By utilizing values of crystal growth rate at the same supercooling, then this effect is accounted for, and only the effect of molecular weight will be observed. Figure 31 presents a graph of linear crystal growth rate as a function of supercooling $\Delta T = T_m^0 - T_c$. This curves show the effect of lower crystal growth rates as the molecular weight of the polymer increases. By taking values of G at constant supercooling for the different molecular weights from Fig. 31, the different models were fitted.

As expressed before, Lovering's model (151) implies that a plot of $\ln G + \ln \langle M_n \rangle$ as a function of $T_m / T_c(T_m^0 - T_c)$ should give a straight line with all the data for different $\langle M_n \rangle$ on the same line. The present data are plotted in this way in Fig. 32. The data fall into straight lines; however, the lines were far from being coincident. The slopes of the straight lines differ by a factor of 2. Therefore, the model of Lovering does not seem to conform to the experimental data. When the data are analyzed in terms of Hoffman's (152) model ($G \propto 1/\langle n_z \rangle$), the data do not conform to this relationship. Gel permeation chromatography data (8) which provided $\langle n_z \rangle$ showed that the exponents on $\langle n_z \rangle$ were higher than 1.7 in all cases, and the correlation coefficients were very low, i.e., the linear relationship was very poor. Figure 33 presents a plot of the crystal growth rate as a function of the reciprocal of $\langle n_z \rangle$ at different supercoolings. It is clear that the data do not follow straight lines as suggested by Hoffman (152). Consequently, this model does not fit the experimental data. Similarly, in the case of the model by Magill and Li (153), the values of the exponent $\alpha$ were very high, and the relationship was very poor, as was observed in low values of the correlation coefficients. Figure 34 shows

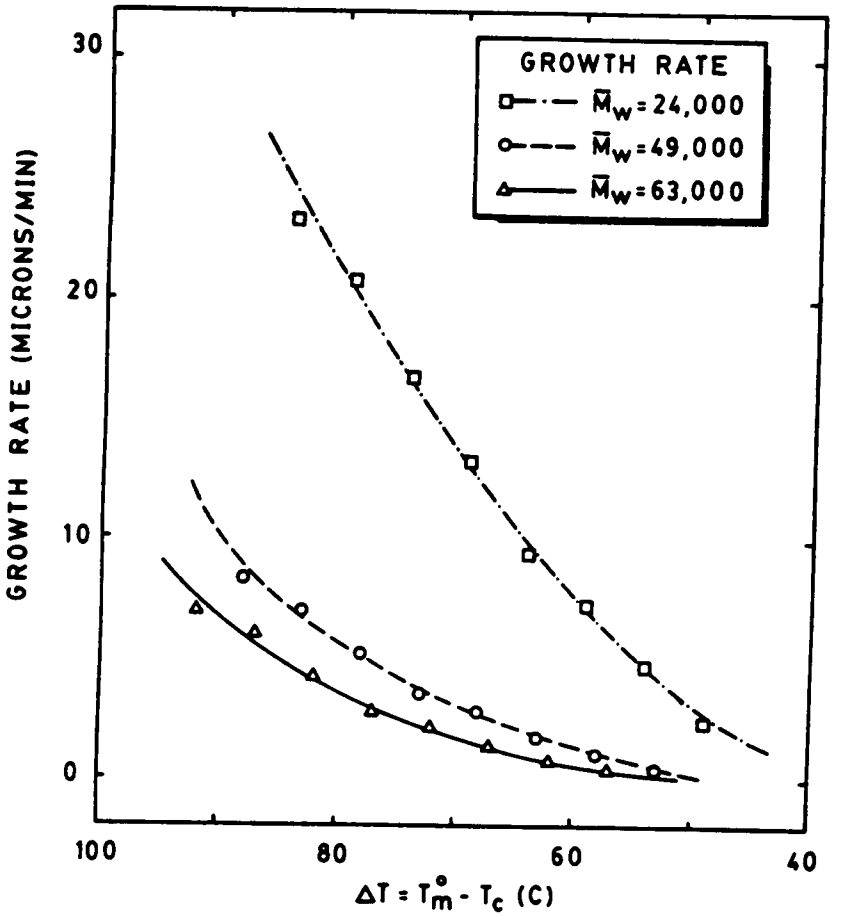


**Figure 31. Linear crystal growth rates of PPS as functions of the supercooling**

a plot of the ln[ln(growth rate)] as a function of $\ln < M_n >$ following Eq. (3.28). Except for data at the lowest supercooling, the rest of the data does not follow Eq. (3.28).

Figure 35 shows a plot of the logarithm of G as a function of logarithm of $< M_n >$ for a series of supercoolings following the model by Cheng and Wunderlich (154). The data fall very well on straight lines that conform with Eq. (3.29). Furthermore, Fig. 36 indicates that the slope increases and the intercept decreases as the supercooling increases in a similar way to the data of Cheng and Wunderlich on poly (ethylene oxide) (154). In addition, the slope and the intercept are linear functions of $1/\Delta T$ and $1/ T_c\Delta T$, respectively (Fig. 37). Therefore, it seems that the data presented in this report is another example that follows the model proposed by Cheng and Wunderlich (154) and gives further support to their hypothesis regarding the dependence of the linear crystal growth rate on molecular weight. The connotations behind this model, as stated by Cheng and Wunderlich, indicate that molecular nucleation controls the crystal growth rather than crystal secondary nucleation. Moreover, since the $\exp[1/(T_m^0 - T_c)]$ and $\exp[1/T_c(T_m^0 - T_c)]$ dependences describe surface nucleation, these same authors suggested that a molecular nucleus involves "a surface patch of increased surface area and a cooperative molecular weight dependent term". Molecular nucleation refers to the process which establishes the first part of a macromolecule in the crystalline phase. The term molecular nucleation has to be distinguish from crystal nucleation which describes the initiation of a new crystal or new crystal layer regardless of the parts of macromolecules contributing to the growth of the nucleus. However, these two terms may be closely related. For example, since the primary nucleus of a polymer crystal is normally smaller than a molecule length, molecular and crystal nucleation must occur simultaneously. Molecular nucleation would also play an important role in secondary nucleation, that is, in the nucleation steps necessary for growth to occur. For crystal growth to occur, nucleation of segments of polymer molecules at the growing front is necessary; therefore, molecular nucleation would have much importance.

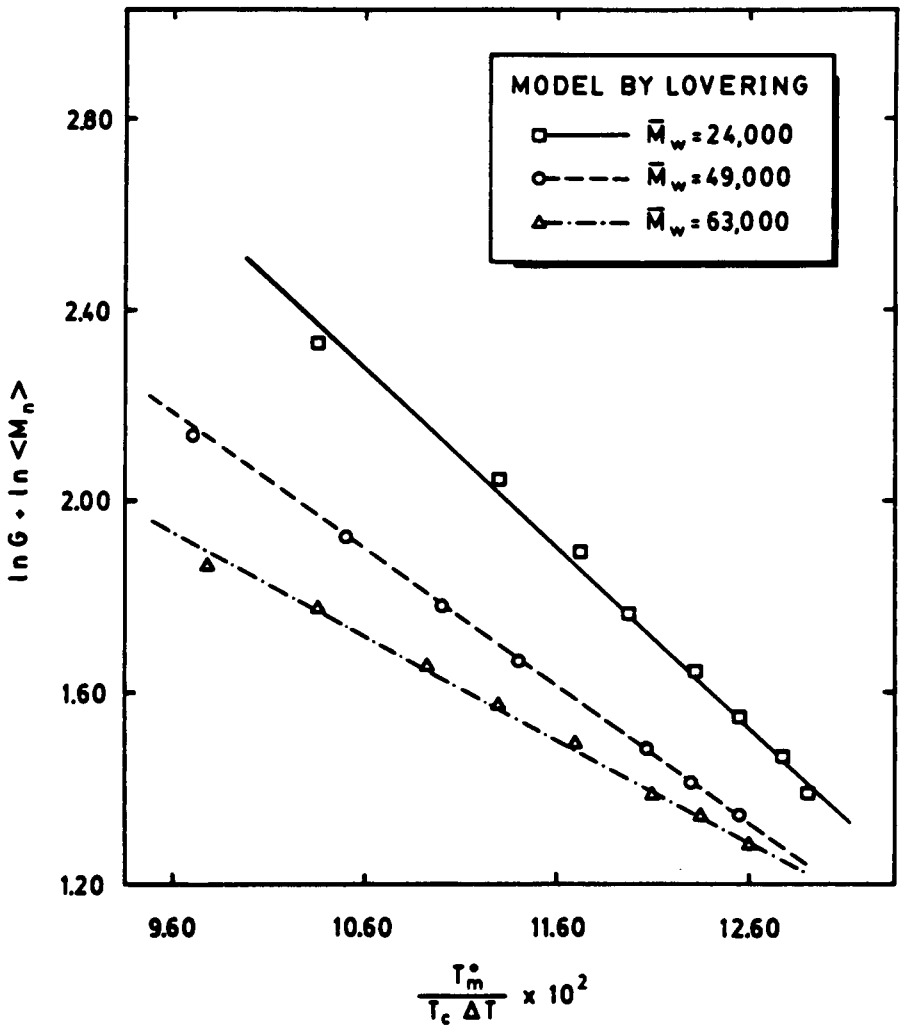


**Figure 32.** **Linear crystal growth rates of PPS plotted following the model of Lovering (151).**

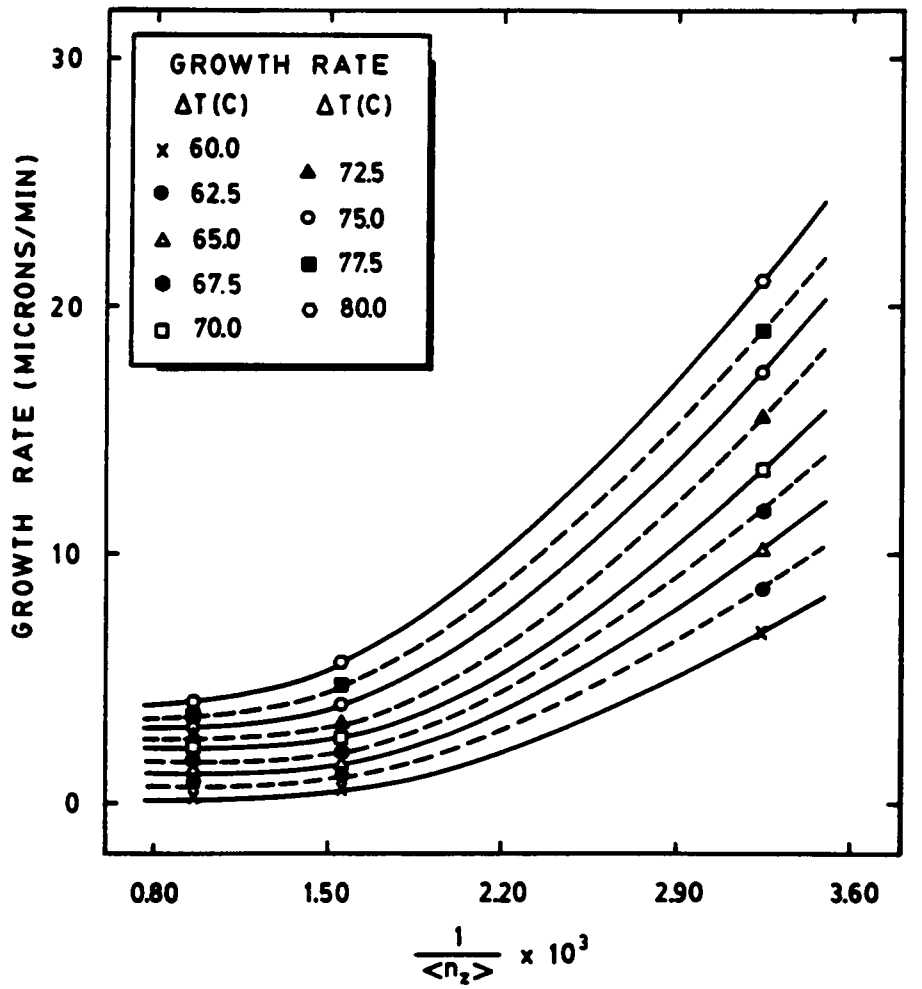


**Figure 33.** **Plot of crystal growth rate following the model by Hoffman (152):** crystal growth rate as a function of the reciprocal of $\langle n_z \rangle$ .

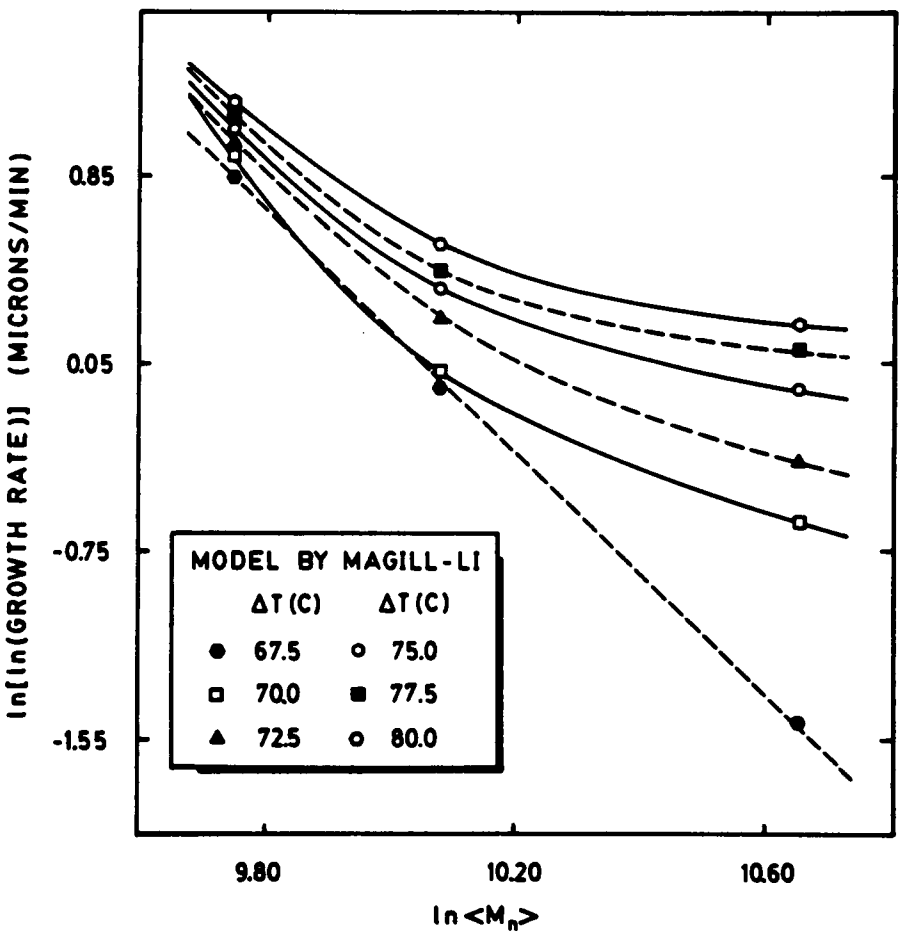


**Figure 34.** **Plot of crystal growth rate following the model by Magill and Li (153):** graph of ln[ln(growth rate)] as a function of $\ln < M_n >$.

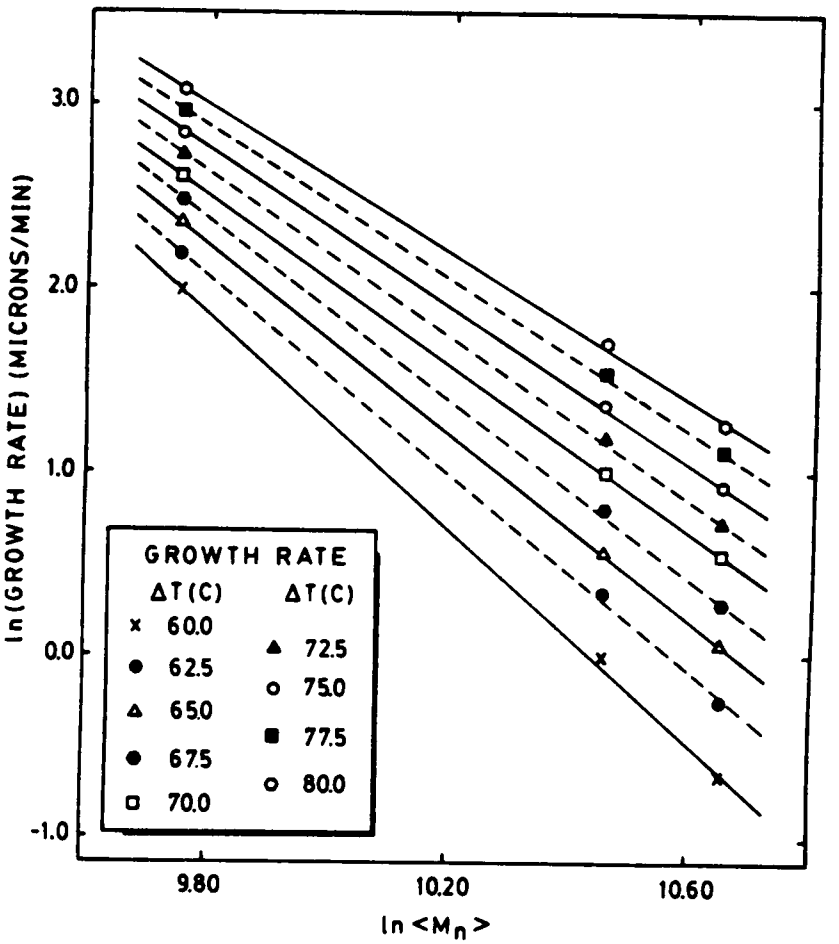


**Figure 35. Relationship between crystal growth rate and the logarithm of the number average molecular weight at several supercoolings:** data plotted following the model by Cheng and Wunderlich (154).

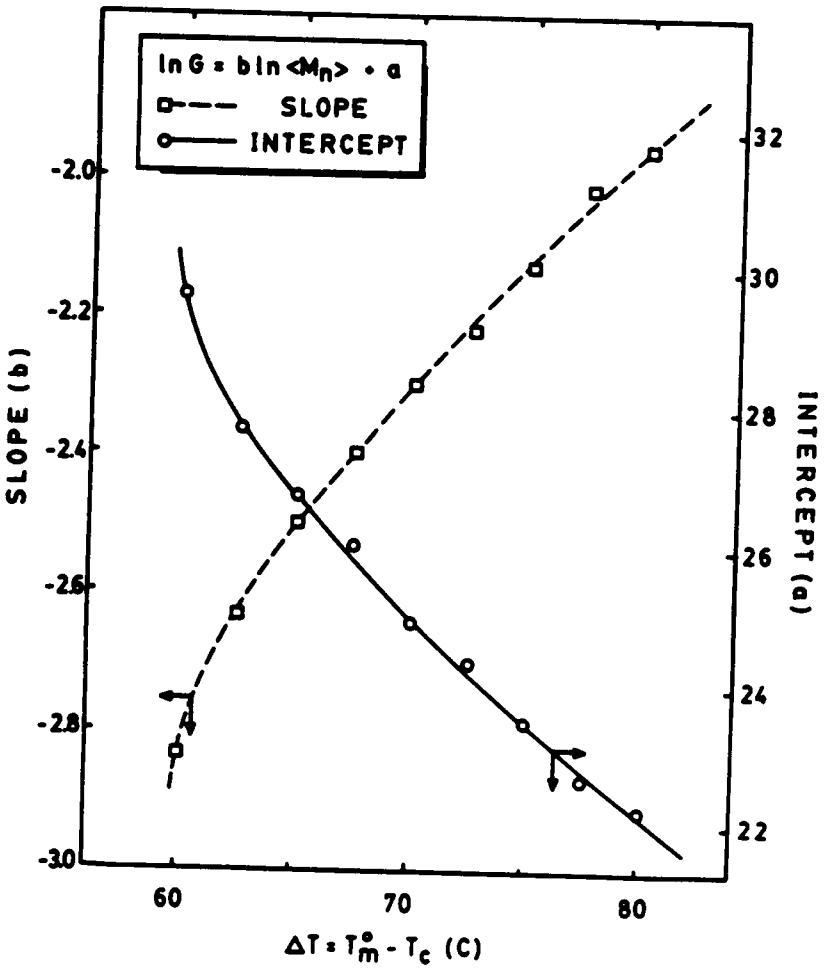


**Figure 36.** **Slopes and intercepts of the linear relationship between logarithm of crystal growth rate and logarithm of the number average molecular weight extracted from Fig. 36:** slope and intercept vs supercooling, $\Delta T$.

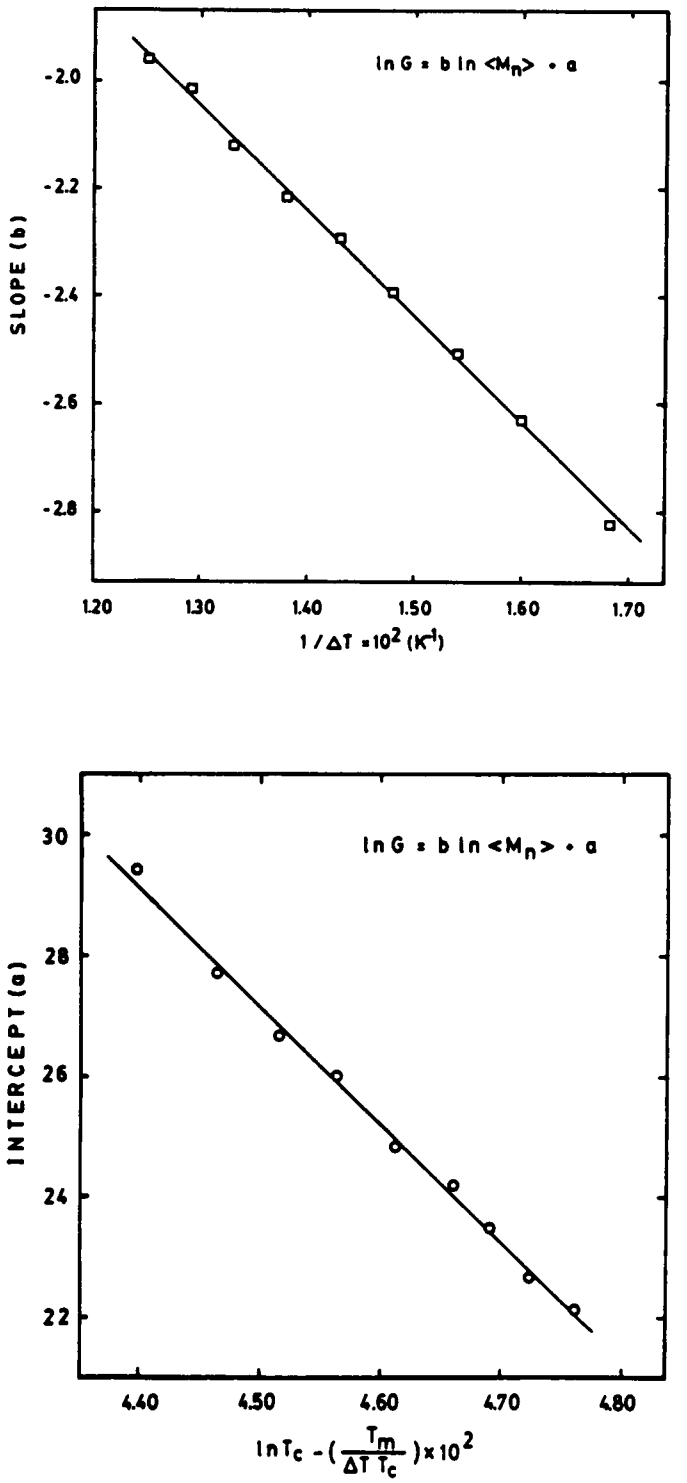


**Figure 37.** **Slopes and intercepts of the linear relationship between logarithm of crystal growth rate and logarithm of the number average molecular weight extracted from Fig. 36** a) slope vs $1/\Delta T$, b) intercept vs ln $T_c - (T_m^0/\Delta T T_c)\times 10^2$.

## 5.2 *EFFECT OF BRANCHING AGENT CONTENT*

As mentioned in the Chapter 2, Hill (27) stated that the molecular weight of PPS can be increased further during polymerization by the addition of small amounts of 1,2,4-trichlorobenzene (TCB), producing a lightly branched polymer (long branches) with molecular weight that can reach the order of 200,000. The introduction of branches has been shown to influence the crystallization behavior of polyethylene, not only with regard to the morphology (158-162), but also the kinetics of crystallization (163-165). For example, Voight-Martin et al. (162) observed that the lateral dimensions of lamellae in hydrogenated polybutadiene became smaller as the branch content increased. An increase in the ethyl-branch content from 2.2 mole % to 3.2 mole % produced a decrease of the crystallite thickness from 70Å to 40Å. Further increase in the branch content to 4.5 and 5.7 mole % produced small crystallites that did not present the lamellar characteristics. In the case of the kinetics of bulk crystallization, it has been shown that low density polyethylene (short branches) presents crystallization isotherms which can not be explained in terms of a simple Avrami equation (163-165). Moreover, Strobl, Schneider and Voight Martin (166) proposed a model to explain some of these effects in LLDPE by considering that branch points remained in the amorphous interlamellar layers, and that the distribution of branch points was one of the important controlling factors of the kinetics of crystallization. An important point worth considering is the difference between LLDPE and PPS studied in the present report. LLDPE presents short side-chains, such as ethyl, butyl, and hexyl groups. However, branched PPS synthesized by the addition of small amounts of 1,2,4-trichlorobenzene in polymerization produces long branches. Consequently, different crystallization behavior might be expected as compared to that of LLDPE.

In this section, the effect of the branching agent content, trichlorobenzene (TCB), on the kinetics of crystallization of PPS will be described. Since the high insolubility of PPS has precluded, to date, the study of the branching characteristics with traditional techniques such as

nuclear magnetic resonance (NMR), the TCB content in the reaction vessel is utilized as characterization of the concentration of branches in the polymer.

Linear crystal growth rate data obtained via polarizing optical microscopy are presented in Fig. 38 as plots of the logarithm of growth rate versus crystallization temperature. Slower crystal growth rates are observed as the trichlorobenzene content increases, i.e., as the concentration of branches increases. Quantitatively for PPS, the crystal growth rates decreased by a factor of 2.2 when the TCB content increased from zero to 0.2% by weight. Since the molecular weight of samples PPS00 and PPS20 are very similar, the decrease in the crystal growth rate is fully attributed to the long chain branches introduced upon the addition of TCB in polymerization. An intermediate value of the TCB content (0.13% by weight) produces the lowering of the growth rate by a factor of 1.4. However, polymer PPS13 has a higher molecular weight than PPS00. Consequently, PPS13 presents contributions due to branching and possibly due to a slightly different molecular weight. Nevertheless, the contribution of the molecular weight to the lowering of the crystal growth rate can be estimated if it is assumed that branched PPS follows the same molecular weight dependence than linear PPS. It was shown in the previous section that the crystal growth rate of linear PPS followed a logarithmic function of the number average molecular weight,

$$\ln G = b \ln <M_n> + a \tag{3.29}$$

Considering the effect of molecular weight on G, and taking values for b and a from the previous section, a crystal growth rate of 2.98μm/min is estimated for PPS13 at a supercooling of 70°. Growth rate data extracted from Fig. 38 give G = 3.32μm/min for PPS00, and G = 2.36μm/min for PPS13 at the same supercooling. Comparison of these results indicates that the molecular weight contribution to the lowering of the growth rate is only one fourth of the total decrease. Therefore, the effect of branching on the growth rate seems to be far more important than that of molecular weight for PPS13. Although crystal growth rate and lamellar

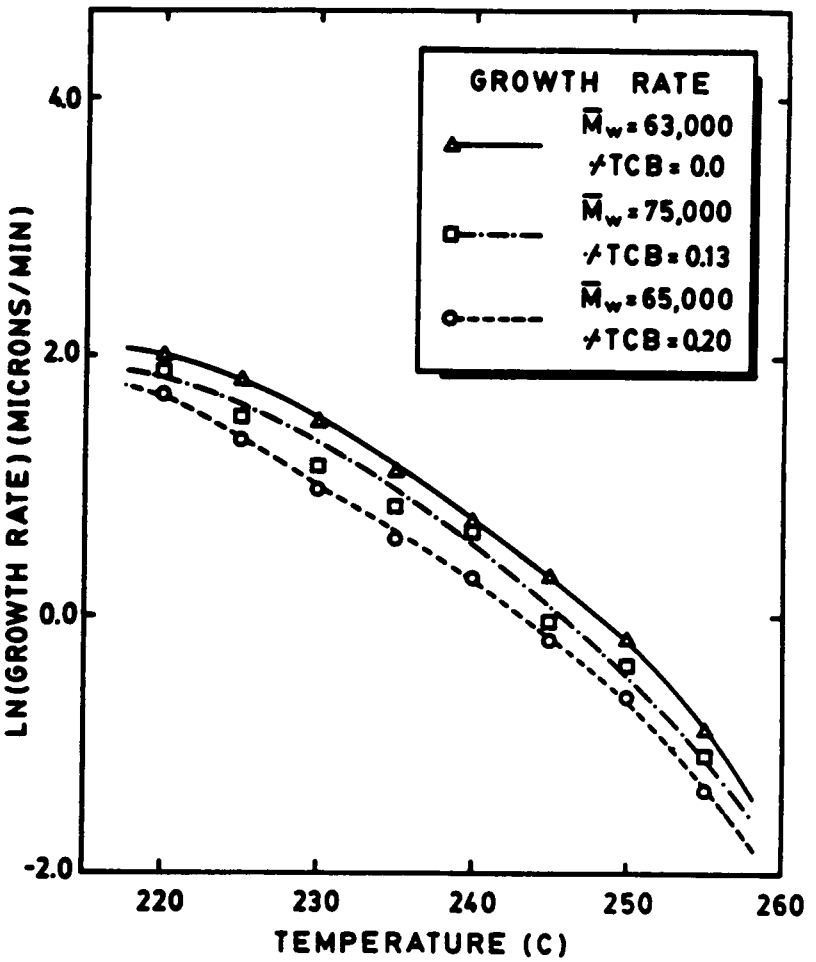


**Figure 38.** **Relationship between crystal growth rate and crystallization temperature for PPS samples crystallized from the melt as a function of the branching agent content.**

thickness can not be directly related, it is interesting to note that Maderek and Strobl (164) concluded that branching had a larger effect on the lamellar thickness of LLDPE (short branches) than molecular weight and molecular weight distribution. These authors found that the lamellar thickness ($d_c$) of fractions remained constant as the viscosity average molecular weight changed from 20,000 to 80,000. Furthermore, $d_c$ was the same for fractions and for unfractionated polymer. That is, the contribution of molecular weight and molecular weight distribution to the crystallization behavior of LLDPE were negligible. This is the same kind of effect observed in the case of PPS13; i.e., branching has a more important effect on the growth rate than the molecular weight difference between PPS13 and PPS00.

Figure 39 presents a graph of the normalized crystalline content of PPS20 crystallized from the melt as a function of the logarithm of time, and an Avrami plot, i.e., a plot of $\ln [ - \ln (1 - X_c(t))]$ versus logarithm of time. The Avrami plot in part b) of Fig. 39 shows that the DSC data corresponding to PPS20 follow almost perfectly an Avrami equation for the overall rate of bulk crystallization. Furthermore, Fig. 40 displays the values of the Avrami exponent (n) as a function of the crystallization temperature corresponding to samples crystallized from the melt. The values of n are all very close to 3. This behavior is in contrast to that found for LLDPE (163). In LLDPE, the overall rate of bulk crystallization could not be interpreted by a single Avrami equation. In addition, the Avrami exponents derived from crystallization isotherms of LLDPE took on unusually low values, as low as $n \sim 1$. However, there is an important difference between the topology of LLDPE and PPS studied. The PPS samples analyzed in the present report have long branches, as opposed to short ones in LLDPE. In particular, since PPS has long branches and the number of branch-points is not very high, the crystallization mechanism does not seem to be disrupted to cause lower Avrami exponents. In addition, the long branches may be able to crystallize into lamellar crystals. Therefore, a different behavior of the overall rate of bulk crystallization might well be expected.

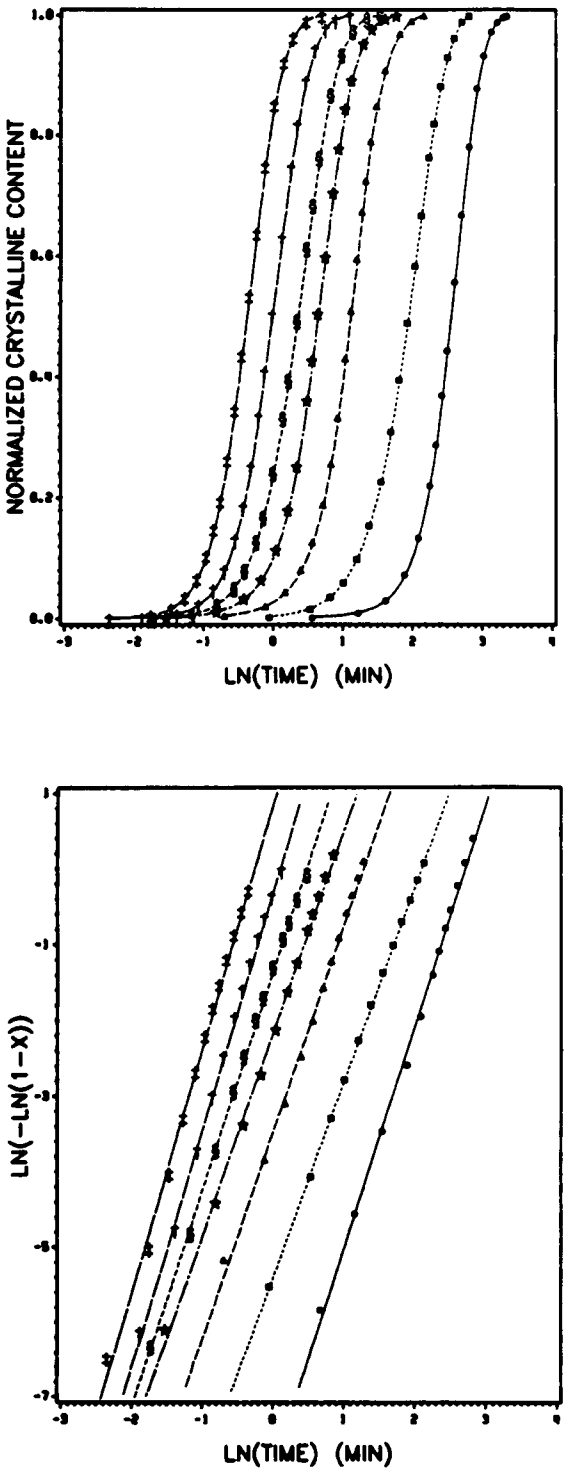


**Figure 39. Crystallization isotherms corresponding to PPS20:** a) Normalized crystalline content as a function of ln(time). b) Double logarithmic plot of amorphous content versus ln(time) following the Avrami equation. • T=250°C; ▪ T=245°C; ▲ T=240°C; ★ T=235°C; § T=230°C; † T=225°C; ‡ T=220°C.

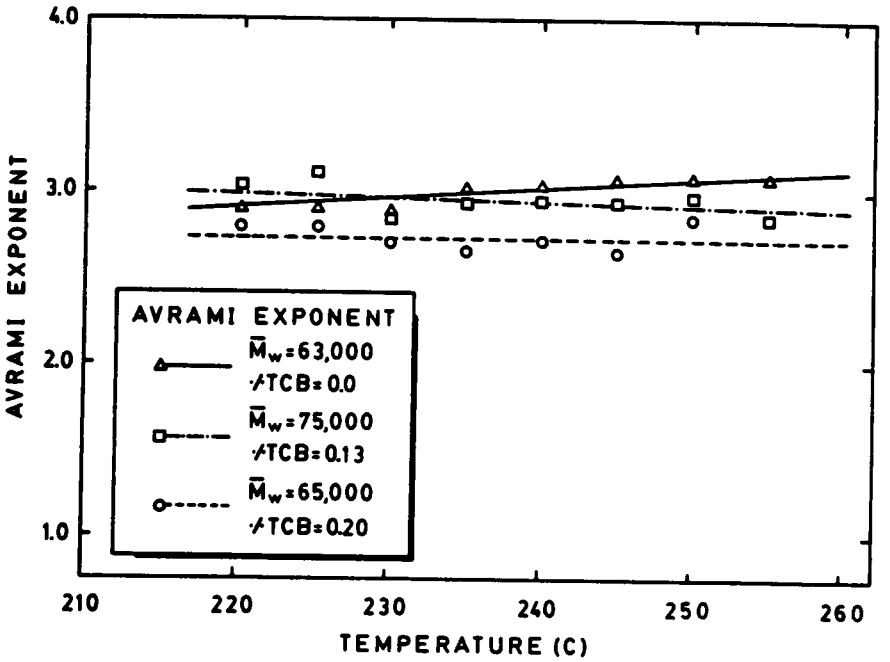


**Figure 40.** **Avrami exponent as a function of crystallization temperature for PPS crystallized from the melt.**

Figure 41 shows plots of the logarithm of the rate constant K and the logarithm of crystallization half-time as functions of the crystallization temperature. As expressed in the Chapter 4, there were limitations in the temperature ranges studied. Due to the start of rapid crystallization before temperature stabilization, no reliable data points could be gathered in the region of fast crystallization rates. Therefore, the curves were constructed following a third-order polynomial regression. The rate maxima are located in the range 170-180°C, in agreement with values previously reported for linear PPS (52,53). At 230°, the overall rate of bulk crystallization, K, decreases by a factor of 2 as the TCB content varies from zero to 0.13% by weight, and by a factor of 5 as %TCB changes to 0.20. The crystallization half-time varies accordingly. There is an increase in $t_{1/2}$ by a factor of 1.8 as the TCB content increases to 0.13% by weight. Further increase of TCB concentration to 0.20% by weight produces an increase in $t_{1/2}$ by a factor of 4. These factors are higher than those found for the linear crystal growth rate, especially for sample PPS20, indicating a more important effect of branching on the overall rate of bulk crystallization than that on the linear crystal growth rate. Consequently, the results would lead to indicate that nucleation density is playing an important role. Figure 42 presents a graph of the logarithm of nucleation density as a function of the crystallization temperature calculated by means of Eq. (5.3) for PPS with different trichlorobenzene contents. The nucleation density of PPS13 is only 25% lower on the average than that of PPS00. However, PPS20 shows nucleation densities that are lower than those of PPS00 by a factor of 3.5. These values suggest that the introduction of branches in PPS produces a decrease in the ability of the polymer to nucleate crystallization, in addition to affect the crystal growth rates. If the molecular nucleation concept of Wunderlich (125) is invoked, it can be pictured that branched molecules will have more difficulty in getting in the right conformation to nucleate crystallization. Furthermore, if growth is controlled by molecular nucleation, the rate of secondary nucleation needed for growth will also be slowed down producing slower growth rates.

Figure 43 shows a graph of the normalized overall heat of crystallization as a function of crystallization temperature for PPS crystallized from the melt. The heat of crystallization pre-

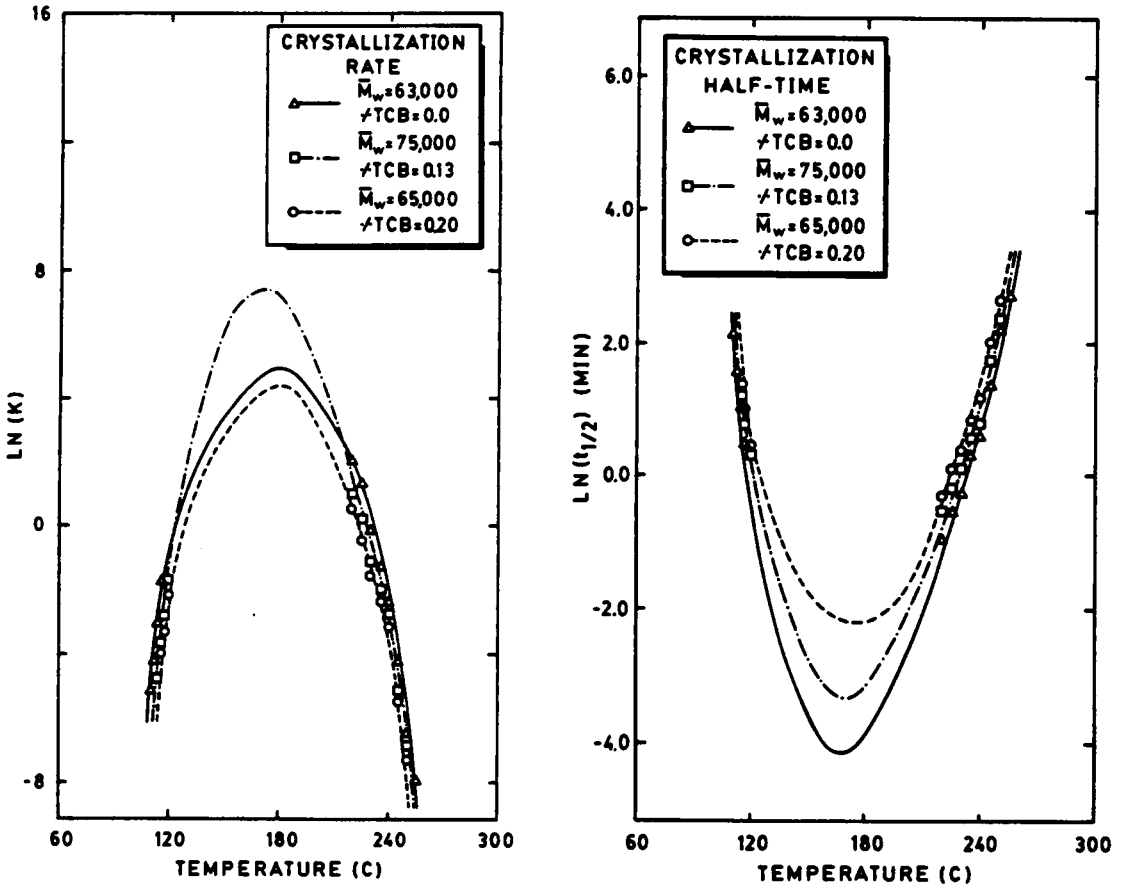


**Figure 41.** **Kinetics data determined from the Avrami analysis for PPS with different branching agent content:** a) Relationship between rate constant, K, and crystallization temperature. b) Relationship between crystallization half-time and crystallization temperature.

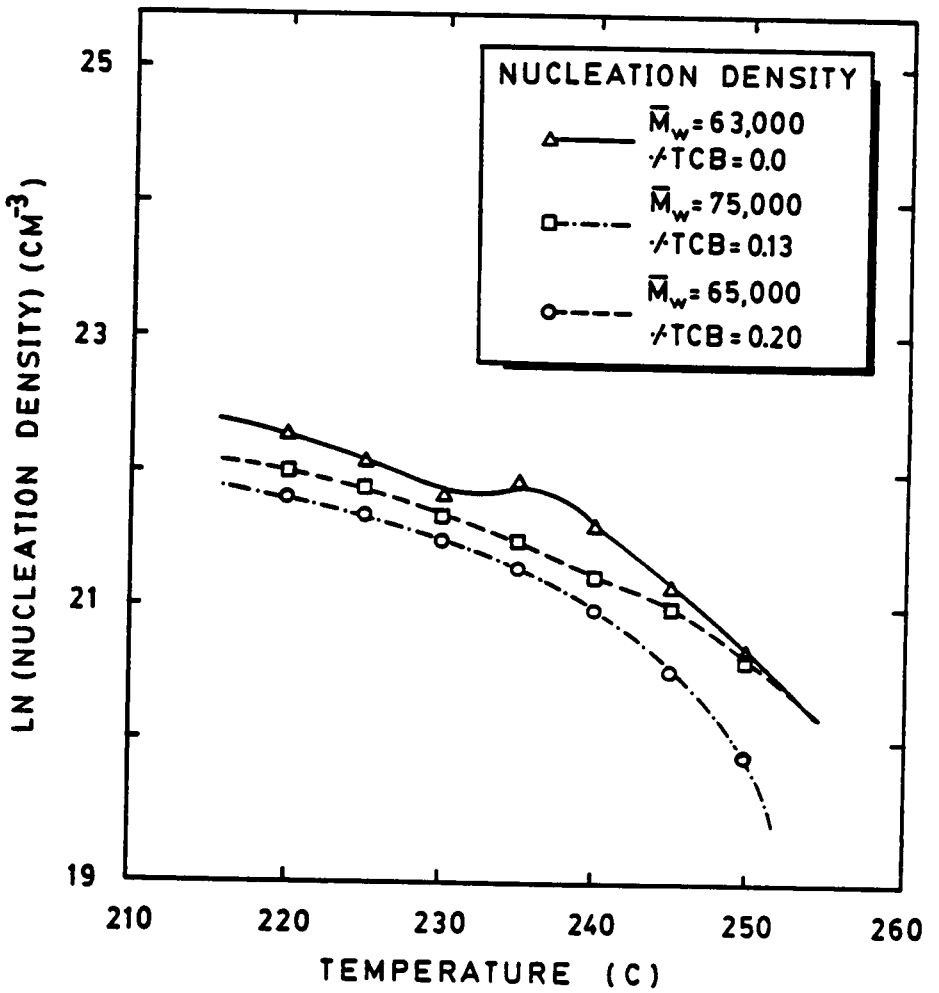


**Figure 42.** Graph of nucleation density as a function of crystallization temperature for PPS crystallized from the melt with different branching agent content.

sents the usual increasing trend with increasing crystallization temperature. PPS00 and PPS13 have very similar values of $\Delta H_c$. However, PPS20 displays somewhat lower values at higher crystallization temperatures, indicating that the crystalline content of branched PPS is lower than that of linear PPS. Furthermore, the perfection of the crystalline phase in branched PPS is not as high as that of linear PPS. This is reflected by the values of the equilibrium melting points determined in Fig. 44. Linear PPS presents a $T_m^0$ of 312°C, PPS13 has a $T_m^0$ of 304°C, and PPS20 (with higher concentration of branches) shows a $T_m^0$ of 301°C. A similar monotonic decrease of measured melting temperatures with increasing branch concentration was observed in LLDPE by Mandelkern and Maxfield (160). The equilibrium melting temperature is an indication of the perfection of the crystals formed. Higher melting points indicate higher perfection of the crystals. Therefore, perfection of the crystals decreases as the TCB content increases in PPS. Since the branch points would not fit in the crystal lattice, they would cause disruption of the crystal order and a decrease of the crystalline content. Kawai et al. (161) found results supportive of this argument when studying solution grown crystals of alkyl-branched polyethylene by x-ray diffraction. These authors indicated that the overall amorphous fraction found on solution grown crystals of branched polyethylene was larger than that of linear polyethylene. In addition, these same authors reported that the branches seemed to concentrate in the amorphous fraction of crystals and within the crystal defects. Voight-Martin et al. (162) reported that in hydrogenated polybutadienes (ethyl branched samples) the lamellar structure deteriorates as the concentration of ethyl branches increases. This deterioration produces the disappearance of the lamellar character at a concentration of 4.5 mole % of ethyl branches. Furthermore, at the same molecular weight, a branched polymer has more chain ends per molecule which will contribute to lower the crystallinity content. Therefore, it seems reasonable to expect lower values of the heat of crystallization for PPS with higher trichlorobenzene content.

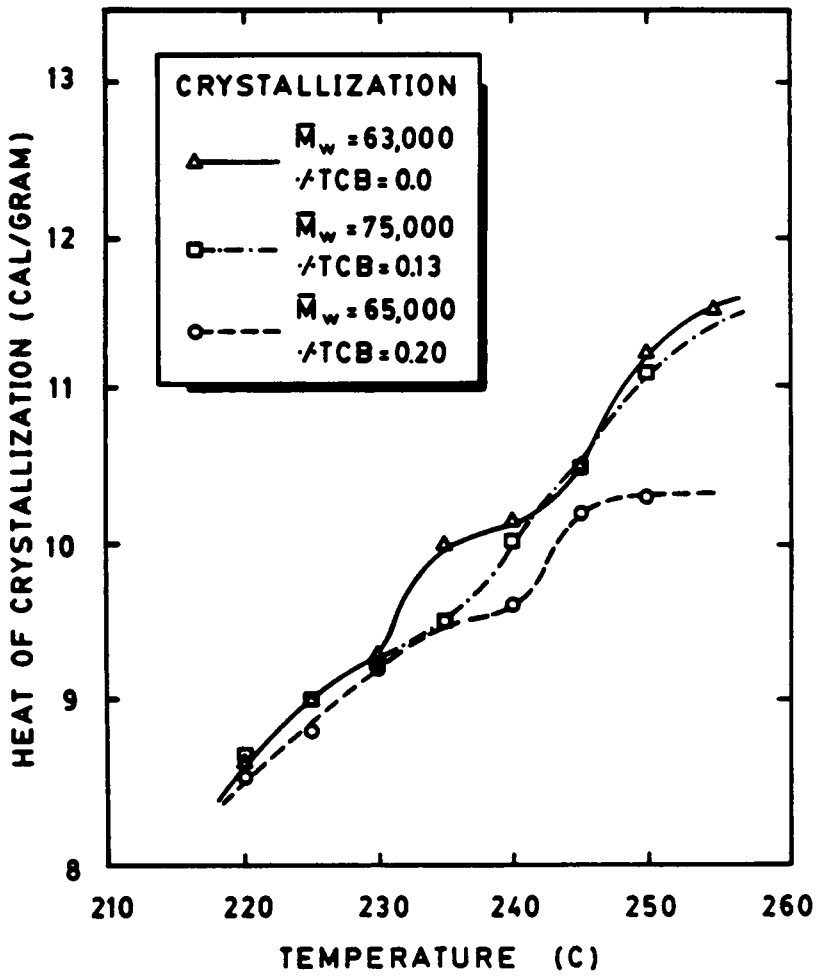


**Figure 43.** Heat of crystallization as a function of crystallization temperature for PPS crystallized from the melt for samples with different branching agent content.

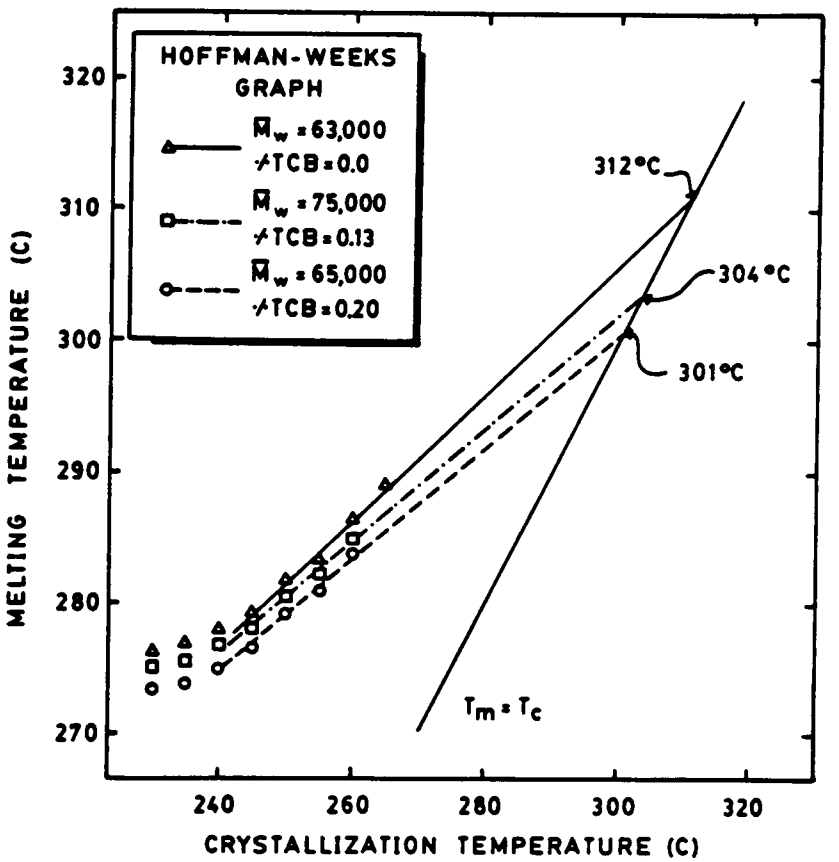


**Figure 44.** Hoffman-Weeks plots utilized to determine the thermodynamic melting points of PPS with different trichlorobenzene content.

## 5.3 EFFECT OF THE CHEMICAL NATURE OF THE ENDGROUP COUNTER-ATOM

The synthesis process of Campbell (25) was described in Chapter 2. This process comprises the preparation of sodium sulfide from aqueous sodium hydrosulfide and sodium carbonate in a polar solvent that contains an alkali-metal carboxylate or phenoxide; after water removal, this mixture is reacted with p-dichlorobenzene in a polar solvent at high temperature. The alkali-metal salt apparently "moderates" the polymerization process, presumably by reacting with sodium sulfide to form the species that initiates the polymerization reaction. Due to the reaction process, carboxylate or phenoxide end-groups would be expected in PPS synthesized by this method as alkali-metal salts. The presence of ionic end-groups has been found to affect the crystallization behaviour of bisphenol-A polycarbonate and polyethylene terephthalate (167,168). In these two cases, not only the nucleation and growth steps were affected by the presence of the ionic species, but also the morphology of the system. In view of this work, a systematic investigation of the effect of the endgroup counter-atom on the kinetics of crystallization of PPS is addressed in this section.

Figure 45 presents the linear crystal growth rate data corresponding to PPS with different endgroup counter-atoms. Although the effect of the counter-atom is small, the small standard deviation in the growth rate reproducibility indicates that the different G values are significant. The decreasing order of linear crystal growth rates is calcium > hydrogen > zinc > sodium. At this point, this ordering of the crystal growth rates is not understood. One might argue that there is a molecular weight increase due to chain extension by means of the ionic endgroups. In this respect, a highly electropositive cation would be expected of causing a more important effect. For example, sodium would form strong ionic bonds with the phenoxide endgroups. Similarly, calcium would also be able to form strong ionic bonds. Furthermore, since calcium is divalent, it might be able to cause chain extension to a greater degree than sodium

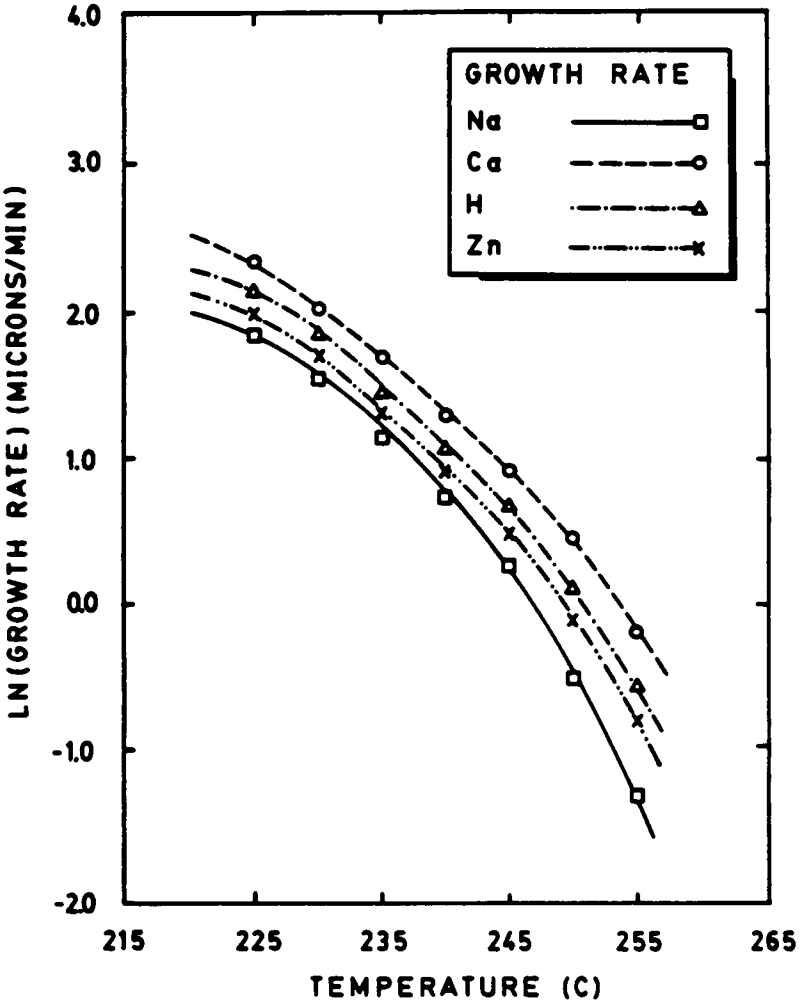


**Figure 45.** **Relationship between crystal growth rate and crystallization temperature for PPS crystallized from the melt as a function of the chemical nature of the endgroup counter-atom.**

producing slower crystal growth rates. However, PPSNa presents the lowest crystal growth rates and PPSCa shows the fastest crystal growth rates. Therefore, such an argument is not a plausible explanation of the crystal growth rates observed. Quantitatively, the crystal growth rates corresponding to PPSCa are higher than those of PPSNa by a factor of 2 on the average. Similarly, PPSH has growth rates 1.6 times faster than PPSNa, and crystal growth rates corresponding to PPSZn are 1.4 times faster than those of PPSNa. Since crystal growth rates represent information on the diffusion events occurring during crystallization, the data indicate that diffusion is facilitated in the case of PPS containing calcium, hydrogen and zinc counter-atoms. The growth rate values of PPSNa and those of PPS that has not undergone the ion-exchange processes (previous sections) are about the same. In other words, the linear crystal growth rate was not affected by the ion-exchange process. However, the nature of the endgroup counter-atom seems to affect the crystal growth rates when compared to the "control" PPS which contains the Na counter-atom. At this point, it is important to state a comment with regards to the morphology of PPS in comparison to that of polycarbonate reported by Bailly et al. (168). These authors indicated that the morphology of polycarbonate containing ionic end-groups consisted of multilamellar crystals dispersed in the amorphous matrix, with no trace of higher order organization or superstructure. In contrast, in the present case of PPS, the samples present the usual spherulitic superstructure previously observed.

Figure 46 shows a graph of the normalized crystalline content of PPSH crystallized from the melt as a function of the logarithm of time, and an Avrami plot. The Avrami plot in part b) of Fig. 46 indicates that the DSC data follow very well an Avrami equation for the overall rate of bulk crystallization. Moreover, Fig. 47 presents the values of the Avrami exponent , n, as a function of the crystallization temperature. The values of n are all in the vicinity of 3, except for PPSH that has lower values, on the order of 2.6. These lower values may be attributed to growth that is not three dimensional. Consider Fig. 26 which presents a schematic representation of the development of a spherulite. The presence of sheaf-like structures, such as that shown in step 4 of Fig. 26 would produce a decrease of the Avrami exponent from the value

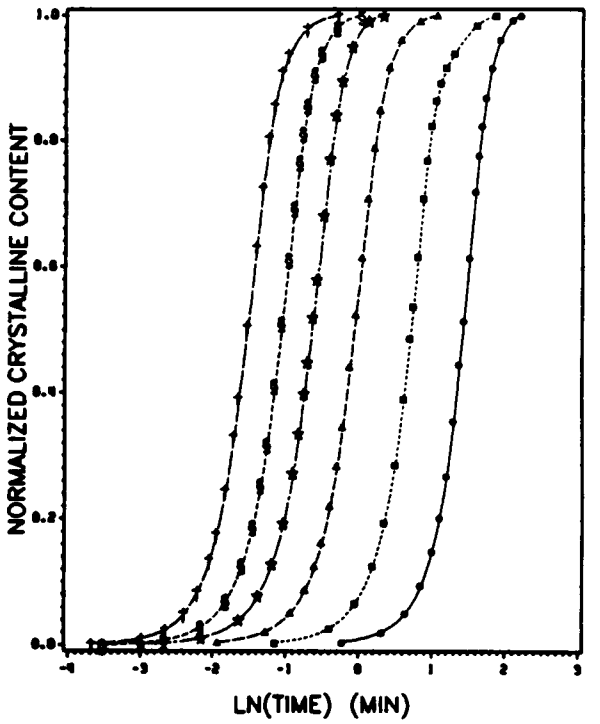


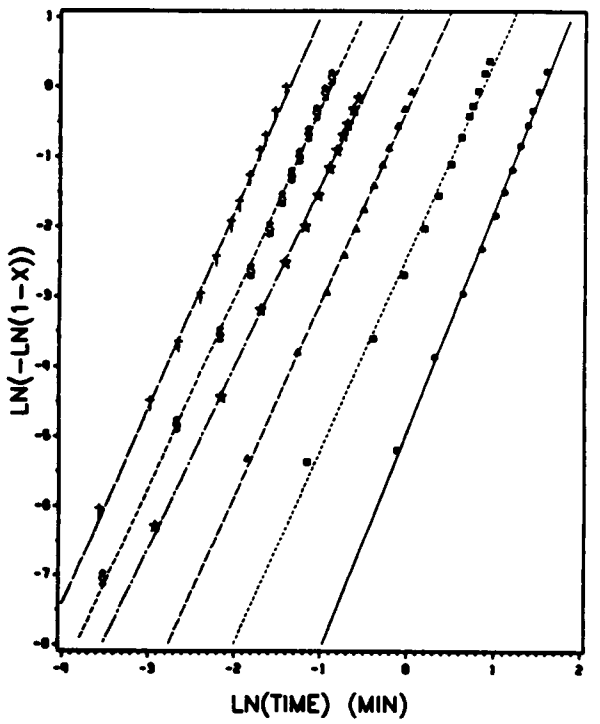


**Figure 46. Crystallization isotherms corresponding to PPSH:** a) Normalized crystalline content as a function of ln(time). b) Avrami plot. • T=255°C; ▪ T=250°C; ▲ T=245°C; ★ T=240°C; § T=235°C; † T=230°C.

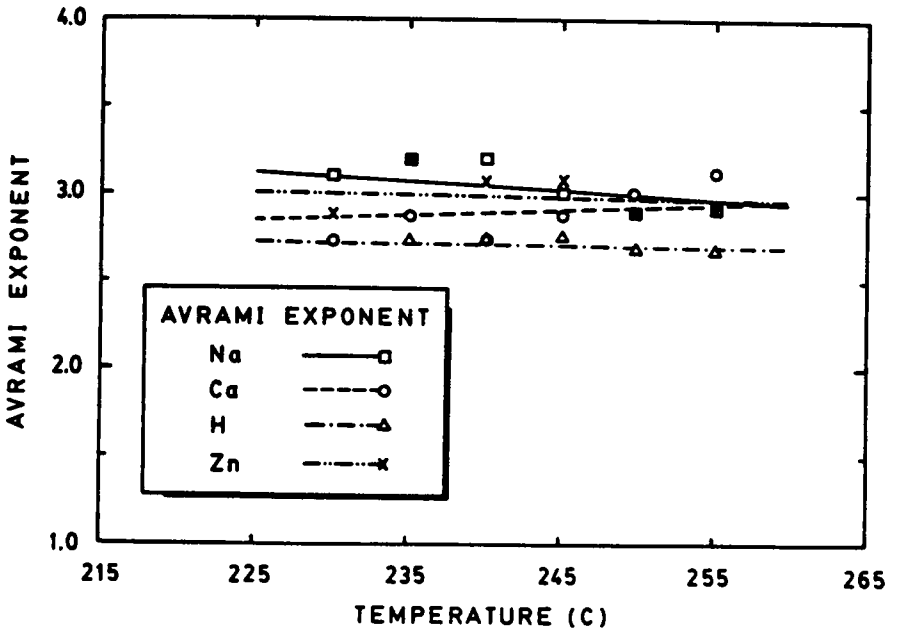


**Figure 47.** **Avrami exponent as a function of the crystallization temperature for PPS with different endgroup counter-atoms crystallized from the melt.**

of 3, even if such structure is 3-dimensional in nature. Therefore, the presence of this type of structure would contribute to decrease n. However, observations in the optical microscope indicated the formation of spherulitic-like textures in PPSH as well as in the other polymers. Nevertheless, there is another possible cause of a somewhat lower Avrami exponent. It has been shown that n may be lowered as much as 0.3 due to the impossibility of achieving a constant volume transformation, an assumption imposed in the derivation of Eq. (5.2) (131).

Figures 48a, 49a, and 50a display plots of the logarithm of K as a function of the crystallization temperature corresponding to PPSH, PPSCa, PPSZn and PPSNa. By following a third-order polynomial, the rate maxima are found at 180°C, in agreement with values reported previously (52,53). The overall rate of bulk crystallization is also affected by the nature of the endgroup counter-atom. However, the order of decreasing K is different than that observed for the crystal growth rates. The decreasing order is PPSH > PPSZn > PPSCa > PPSNa. PPSNa remains the slowest crystallizing polymer. PPSCa has values of overall rate of bulk crystallization 1.6 higher than those of PPSNa; K corresponding to PPSZn is 2.1 times higher than PPSNa; and PPSH presents a overall rate of bulk crystallization that is 17-fold faster than that of PPSNa! Similarly, the crystallization half-times of PPSH, PPSCa, PPSZn and PPSNa in part b) of Figs. 48, 49, and 50 present the corresponding trends. In addition, the values of K corresponding to PPSNa are 65 times higher ,on the average, than those of PPS that has not undergone the ion-exchange process (previous sections). Since the linear crystal growth rates are about the same for these two polymers, the data on overall rate of bulk crystallization suggest that nucleation density is playing an important role. Indeed, this is the case. Figure 51 shows plots of the logarithm of nucleation density as a function of crystallization temperature for samples crystallized from the melt. The nucleation density corresponding to PPSNa is 20 times higher than that of PPS that has not undergone the ion-exchange processes. Furthermore, the nucleation density of PPSNa remains fairly constant in the range of temperature studied. PPSH presents the highest nucleation density, about 8 times higher than PPSNa. PPSZn and PPSCa have nucleation densities lower than that of PPSNa, with PPSCa

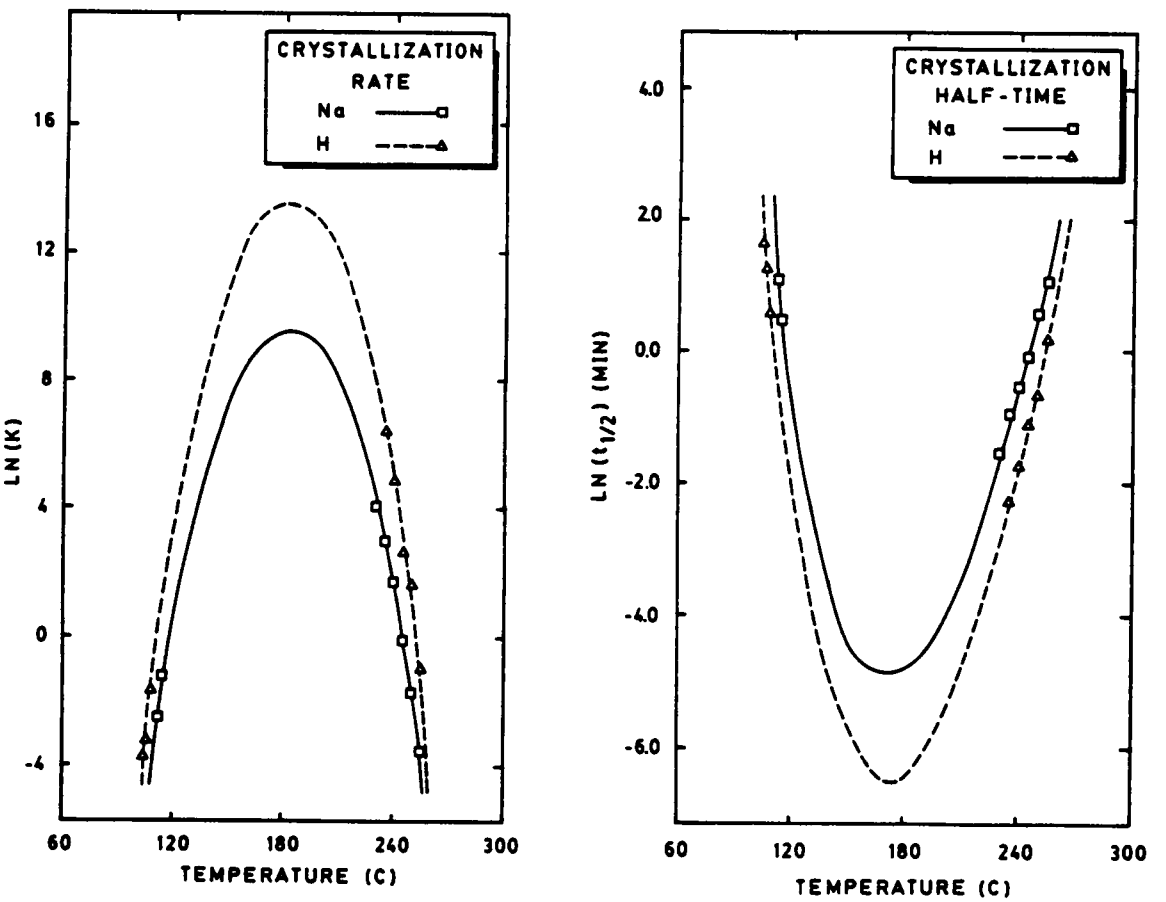


**Figure 48.** **Kinetics data determined from the Avrami analysis for PPSH and PPSNa:** a) Relationship between rate constant K and crystallization temperature. b) Relationship between crystallization half-time and crystallization temperature.

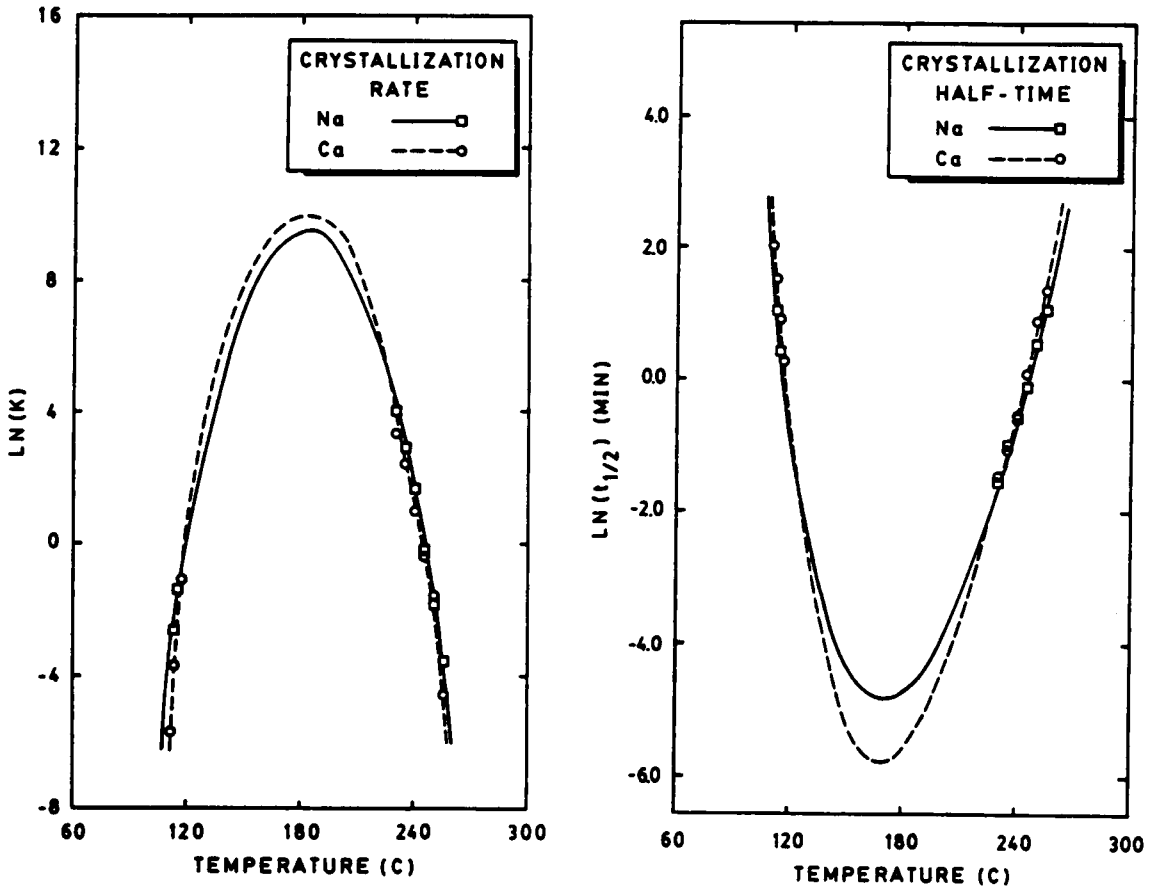


**Figure 49.** **Kinetics data determined from the Avrami analysis for PPSCa and PPSNa:** a) Relationship between rate constant K and crystallization temperature. b) Relationship between crystallization half-time and crystallization temperature.

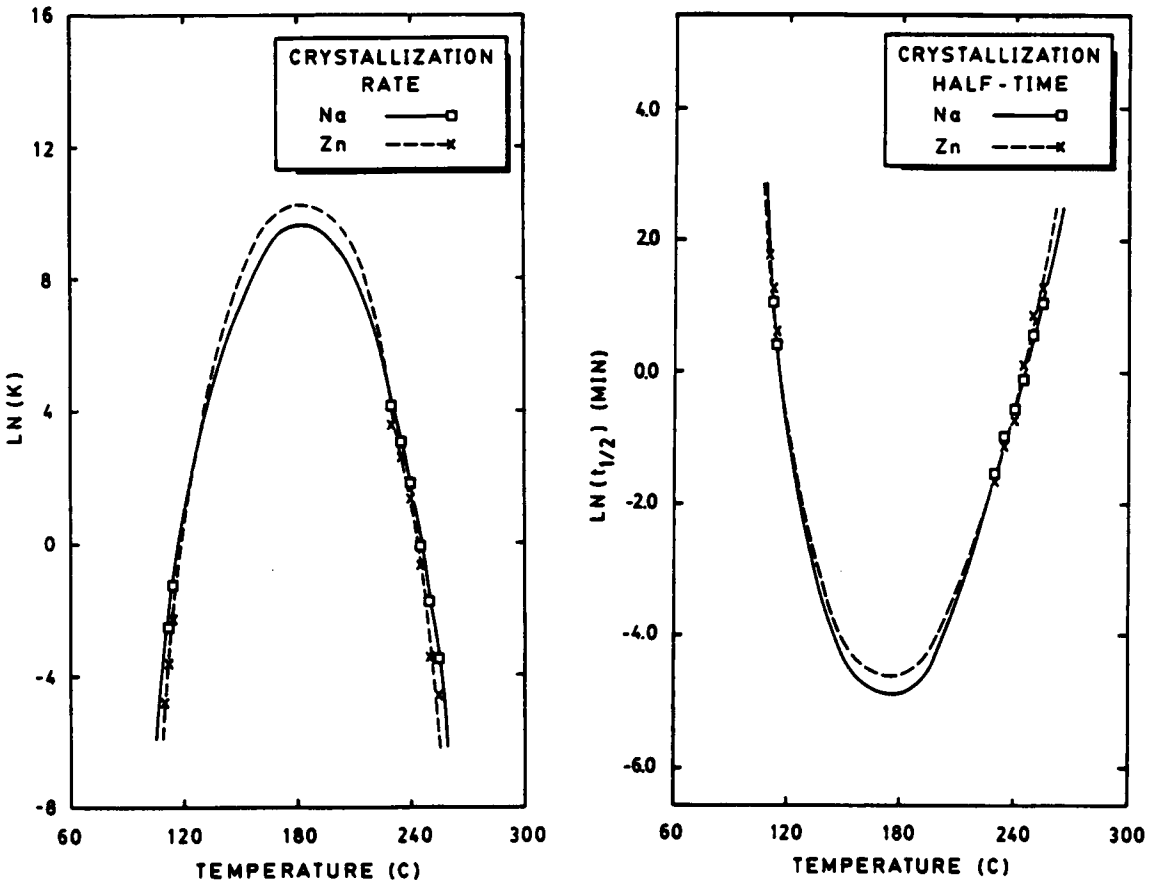


**Figure 50.** **Kinetics data determined from the Avrami analysis for PPSZn and PPSNa:** a) Relationship between rate constant K and crystallization temperature. b) Relationship between crystallization half-time and crystallization temperature.

as the lowest one. Such an important effect of ionic endgroups on the nucleation density was previously observed in sodium carboxylate-terminated poly (ethylene terephthalate) (PET) (167), and sodium phenoxide-terminated bisphenol-A polycarbonate (PC) (168). Legras et al. (167) indicated that the ionic end-groups of PET were aggregated in a separate phase in the polymer melt. These aggregates seemed to be the true nucleating species of the crystallization. In the case of polycarbonate, Bailly et al. (168) reported that both, nucleation and growth were affected by the presence of ionic chain ends. However, in these cases, there are chemical reactions occurring. PET and PC were shown to undergo a series of reactions including chain scission and chain rebuilding (167,168) that do not occur in PPS. Nevertheless, in none of these cases was the effect of the counter-ion studied. Therefore, it seems that the present report is rather unprecedented.

Figure 52 displays the overall heat of bulk crystallization plotted as a function of crystallization temperature for samples crystallized from the melt. The usual increasing trend with increasing temperature is observed. PPSNa, PPSZn, and PPSCa present about the same values of $\Delta H_c$. than PPS that has not undergone ion-exchange treatment. However, PPSH has values of $\Delta H_c$ that are 15% lower indicating that it crystallizes to a lesser extent than PPSNa, PPSZn and PPSCa. Legras et al. (167) and Bailly et al. (168) reported that the crystallinity of sodium carboxylate-terminated PET and sodium phenoxide-terminated PC were largely exceeding the limiting values observed in the polymers that did not have the ionic endgroups. If the ionic character of the endgroup is considered as one of the factors regulating the attainable final crystallinity, it is reasonable to find PPSH with the lowest heat of crystallization, since PPSH would have the lowest ionic character of the endgroups in the samples studied. Indeed, the author does not have any further explanation of the influence of the counter-atom on crystallization behaviour at this time. However, it is clear that the effect is present and it is reproducible.

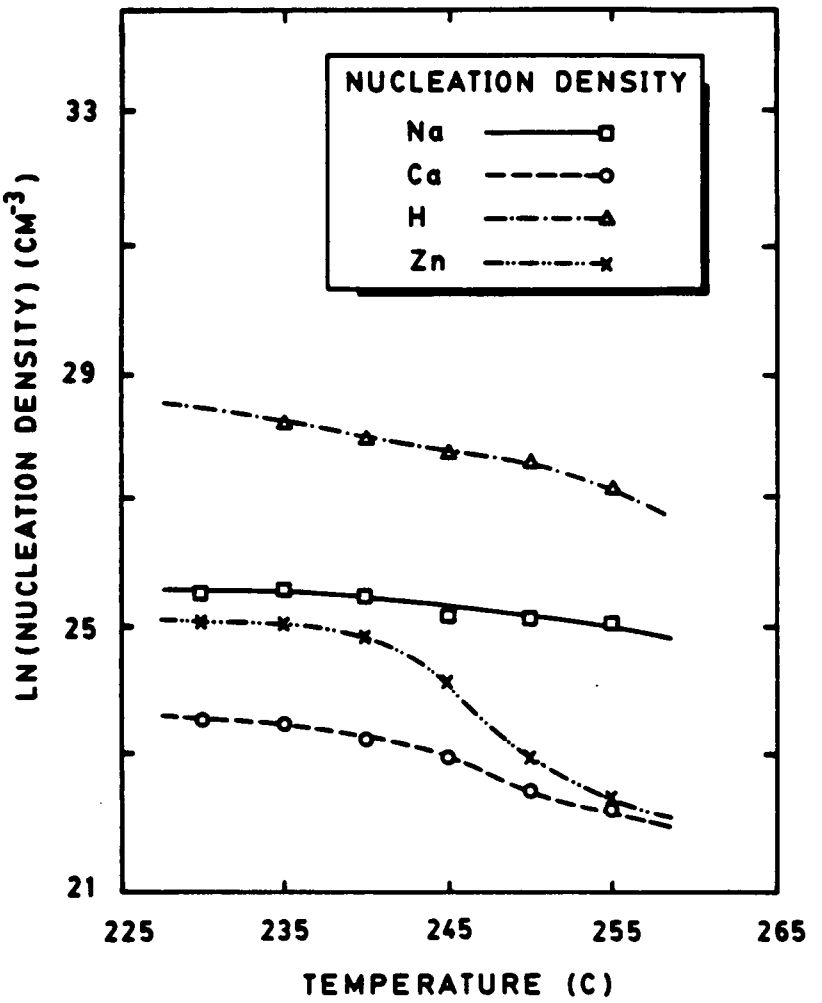


**Figure 51.** Plot of nucleation density as a function of the crystallization temperature for samples crystallized from the melt that contain different endgroup counter-atoms.

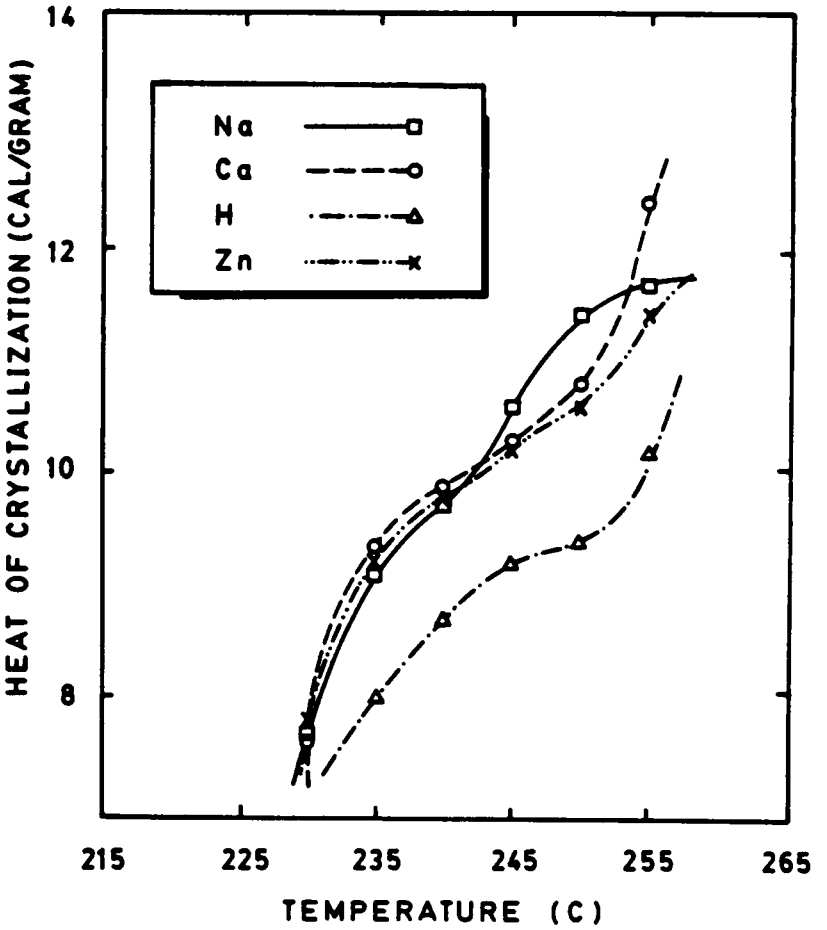


**Figure 52.** Heat of crystallization as a function of crystallization temperature corresponding to PPS materials with different endgroup counter-atom

# CHAPTER VI

# NON-ISOTHERMAL CRYSTALLIZATION OF PPS

In previous chapters, the crystallization behaviour of PPS was studied by isothermal methods. The effects of molecular weight, branching agent content and chemical nature of the endgroup counter-atom on the kinetic parameters were studied by means of the Avrami equation and crystal growth rates. However, from a technological point of view, the non-isothermal crystallization behaviour of polymers is of great importance since most of the processing techniques occur under non-isothermal conditions. In addition, isothermal measurements are often restricted to narrow temperature ranges because the response time of the measuring instrument becomes comparable to the overall time for crystallization. Consequently, non-isothermal experiments can be complementary to the understanding of the crystallization behaviour of polymers. Therefore, this chapter will be dedicated to the study of the non-isothermal crystallization of PPS, to complement the isothermal data discussed in previous chapters. The different methods available to study the non-isothermal crystallization kinetics of polymers will be discussed and the kinetic parameters of PPS will be determined by a non-isothermal method. Furthermore, these parameters will be compared with those obtained isothermally.

## 6.1 METHODS OF ANALYSIS

Only a few methods have been developed to study the kinetics of non-isothermal crystallization (169-171). The theory of those pertinent to this study will be reviewed in this section. The first to be discussed is the theory of Ziabicki (169) which assumes that the crystallization of polymers can be represented by first order kinetics,

$$\frac{dx}{dt} = (1 - x)K(T) \tag{6.1}$$

where x represents the normalized crystalline content and K(T) is a rate constant dependent only on temperature. As pointed out by Ziabicki, Eq. 6.1 neglects all the nonsteady-state effects and also the variation of the crystallization rate constant in isothermal steady-state conditions. Therefore, the rate constant K(T) may be considered an average rate constant for a given temperature. Based on inspection of the shape of plots of K(T) versus temperature, Jeziorny (172) also assumed that K(T) is represented by a Gaussian equation,

$$K(T) \cong K_{max} \exp[-4 \ln 2(T - T_m)^2/D^2] \tag{6.2}$$

where $K_{max}$ is the value of K corresponding to $T_{max}$, the temperature at the maximum of the crystallization exotherm; D is the width of the crystallization exotherm at half height; and $T_m$ is the melting temperature of the polymer. Equation 6.2 allows the calculation of C, a parameter known as the "kinetic crystallizability",

$$C = \int_{T_g}^{T_m} K(T)dT = (\pi/\ln 2)^{1/2} K_{max} D/2 \tag{6.3}$$

The "kinetic crystallizability" would characterize the degree of crystallization per unit cooling rate obtained over the crystallization range $T_m - T_g$, and consequently it would characterize the kinetics of non-isothermal crystallization. The parameter C would serve as a comparative

measure of the crystallizability of various materials when non-isothermal crystallization occurs. In particular, the higher C is, the larger the degree of crystallinity is at the same cooling rate. Furthermore, the higher C is, the higher is the cooling rate necessary to quench a melt to the glassy state without appreciable crystallization in the course of cooling. As examples, Ziabicki (169) indicated that polymers such as i-polystyrene with C=0.15 and poly(ethylene terephthalate) with C=0.53-1.0 can hardly crystallize upon cooling, except on slow cooling. However, polymers such as nylon 6.6 with C=133, and i-polypropylene with C=33 can crystallize upon rapid cooling. Therefore, the "kinetic crystallizability", C, would characterize the non-isothermal crystallization process. This theory was utilized by Jeziorny (172) to study the nonisothermal crystallization of Poly (ethylene terephthalate) by differential scanning calorimetry (DSC). Similarly, this method was used to investigate the crystallization of PET/Polycarbonate (PC) blends (173). Jo and Kim (173) found that the calculated kinetic crystallizability, C, decreased as the concentration of PC increased in the blend, indicating that the rate of crystallization decreased with increasing concentration of PC. However, the kinetic crystallizability does not allow a direct comparison with kinetic parameters determined by other methods. Therefore, this method was not utilized in the present study.

Harnisch and Muschik (170) also developed a method to determine the Avrami exponent from non-isothermal DSC experiments. The method derives from the well known Avrami equation,

$$X(t) = 1 - \exp(-Kt^n) \tag{6.4}$$

where X(t) is the crystalline fraction, K is a rate constant dependent on temperature, and n is the Avrami exponent. Equation 6.4 is rewritten in terms of the time derivative of X at constant temperature T, $x' = (\partial x/\partial t)_T$,

$$\ln \frac{x'}{1-x} = (n-1)\ln t + \ln(nK) \qquad (T = constant) \tag{6.5}$$

For a non-isothermal situation, the time derivative of x is given by,

$$\dot{x}(t, T) = dx/dt = (\frac{\partial x}{\partial t})_T + (\frac{\partial x}{\partial T})_t \frac{dT}{dt} \quad (6.6)$$

The second term on the right-hand side of Eq. 6.6 is usually regarded as negligible, an assumption that has to be confirmed. If indeed this assumption is correct, then Eq. 6.6 is reduced to the following,

$$\dot{x}(t, T) = \frac{dx}{dt} \cong (\frac{\partial x}{\partial t})_T = x' \quad (6.7)$$

and x′ in Eq. 6.5 can be substituted by $\dot{x}$. Calculation of the Avrami exponent would, then, imply the analysis of crystallization at two different heating or cooling rates ( $\varphi_1$ and $\varphi_2$). Values of $x_i(T_c)$ and $\dot{x}(T_c)$ can be extracted from the DSC thermograms:

1. x(T), the crystalline fraction, is calculated by integrating partial areas of the DSC exotherm.

2. $\dot{x}$(t), the derivative of x, represents the dH/dT value of the exothermic curve; therefore, it can be obtained by reading the value on the dH/dT scale of the DSC plot.

To determine the Avrami exponent n, the values of x(T) and $\dot{x}$(t) obtained are introduced in Eq. 6.5 as follows,

$$\ln \frac{\dot{x}_1}{1 - x_1} = (n - 1) \ln t_1 + \ln (nK) \quad (6.8a)$$

$$\ln \frac{\dot{x}_2}{1 - x_2} = (n - 1) \ln t_2 + \ln (nK) \quad (6.8b)$$

Substracting Eq. 6.8a from 6.8b and substituting $\varphi_1/\varphi_2$ for $t_1/t_2$ , an equation results to determine the Avrami exponent, n, as was written by Harnisch and Muschik (170),

$$n = 1 + \left( \ln \frac{\dot{x}_1}{1 - x_1} - \ln \frac{\dot{x}_2}{1 - x_2} \right) / \ln (\varphi_2/\varphi_1) \qquad \text{at } T = T_c \tag{6.9}$$

This equation has been successfully used to determine n in polyethylene and polypropylene, and their values compared well with those determined isothermally (170,174). However, the method presents some possible limitations to its applicability: 1) the Avrami equation is applicable, 2) the condition that the enthalpy of the transformation is independent of temperature in the temperature range of analysis, and 3) the heat of fusion of the polymer needs to be known to correct the values of x, since polymers are not 100% crystalline. This last limitation precluded the use of this method for PPS, since the heat of fusion of 100% crystalline of PPS has not been determined.

A third and rather simple method to determine the Avrami exponent from non-isothermal DSC experiments was developed by Ozawa (171) as an extension of the theory of Evans for isothermal crystallization (128). The Ozawa model assumes that crystallization occurs under a constant cooling rate $\varphi$ , and that crystallization originates from a distribution of nuclei that grow as spherulites with constant radial growth rate at a given temperature. Through these assumptions, Ozawa derived an expression for the volume fraction of untransformed material,

$$1 - x(T) = \exp\{ - \frac{4\pi}{\varphi^3} \int_{T_m^0}^{T} N(\theta)[U(T) - U(\theta)]^2 G(\theta) d\theta \} \tag{6.10}$$

where x(T) is the volume fraction of growing spherulites at temperature T, $\varphi$ is the constant cooling rate, N($\theta$) is the nucleation density, i. e., the number of nuclei per unit volume activated between temperatures $T_m^0$ and $\theta$, $T_m^0$ is the equilibrium melting temperature, G($\theta$) is the spherulite radial growth rate and U(T) is a function of G($\theta$),

$$U(T) = \int_{T_m^0}^{T} G(\theta) d\theta \tag{6.11}$$

Amongst other terms, Eq. 6.10 depends on the type of nucleation that takes place during crystallization; therefore, instantaneous nucleation and nucleation sporadic in time have to be considered. In the former case, the nucleation density $N(\theta)$ is independent of time, and Eq. 6.10 only depends on the temperature $\theta$; consequently, $N(\theta)$ is independent of the cooling rate $\varphi$. Taking the logarithm on both sides of Eq. 6.10 two times, it follows that

$$\ln\{-\ln[1-x(T)]\} = \ln 4\pi + \ln\left|\int_{T_m}^{T_0} N(\theta)[U(T)-U(\theta)]^2 G(\theta)\,d\theta\right| - 3\ln|\varphi| \qquad (6.12)$$

At a constant temperature, the integral in Eq 6.12 is a constant, $\chi$, called the "cooling crystallization function", and Eq. 6.12, then is reduced,

$$\ln\{-\ln[1-x(T)]\} = \chi_i - 3\ln|\varphi| \qquad (6.13)$$

For sporadic nucleation, the nucleation density, $N(\theta)$, is a function of time and temperature. As a consequence, $N(\theta)$ has to be assumed to follow a predetermined function of time. For example, $N(\theta)$ is usually assumed to be proportional to time, i. e., the nuclei appear at a constant rate per unit volume, $\dot{N}(\theta)$. If this is the case, Eq 6.12 can be written as

$$\ln\{-\ln[1-x(t)]\} = \ln 4\pi + \ln\left|\int_{T_m}^{T_0}\left[\int_{T_m}^{\theta}\dot{N}(u)\,du\right][U(T)-U(\theta)]^2 G(\theta)\,d\theta\right| - 4\ln|\varphi| \qquad (6.14)$$

Similar to Eq. 6.13, at a given temperature, the integral in Eq. 6.14 is a constant, $\chi_s$, therefore, Eq. 6.14 reads,

$$\ln\{-\ln[1-x(t)]\} = \chi_s - 4\ln|\varphi| \qquad (6.15)$$

In a general form, Eqs. 6.13 and 6.15 can be written as follows

$$\ln\{-\ln[1-x(t)]\} = \chi - n\ln|\varphi| \qquad \text{at } T = \text{constant} \qquad (6.16)$$

where n represents the well known Avrami exponent. Consequently, Eq. 6.16 allows the determination of the Avrami exponent in terms of the cooling rate and the fraction of crystallized material.

Two factors were neglected by Ozawa in the derivation of Eq. 6.16. The slow secondary ("post-Avrami") crystallization was not considered. This can lower the values of the Avrami exponent determined. However, since the crystallization process occurs under non-isothermal conditions, the slow secondary crystallization would be virtually nonexistent as the temperature decreases. The other factor disregarded in Eq. 6.16 is the fold-length of the polymer chain. The fold-length is a function of the crystallization temperature. Therefore, since the analysis is performed under non-isothermal conditions, the fold-length would be a variable that would need to be considered in the derivation of Eq. 6.16. Nevertheless, Ozawa (171) utilized this equation to study the non-isothermal crystallization of PET. This author found that PET followed Eq. 6.16. Moreover, values of the Avrami exponent in the range of 3.4-3.6 were in agreement with values obtained from isothermal crystallization. Polypropylene also followed the Ozawa equation over the cooling rate range of 0.5°C/min to 10°C/min (175). The Avrami exponents found ranged from 2.55 to 3.30 which seemed to be in fair agreement with values of 3 determined from isothermal crystallization. Eders and Wlochowicz (175) also reported that the cooling crystallization function ($\chi$) followed an exponential function of temperature. However, Monnase et al. (176,177) observed that the Avrami exponent was a function of temperature. These authors reported that n decreased from 4 at 107-116°C to about 3 at 122-129°C, with intermediate values in the 116-122°C temperature range. This variation of n was attributed to a change in the nucleation behaviour. At low temperatures, nucleation was sporadic in time; whereas, at high temperatures, nucleation was instantaneous. These same authors analyzed the nucleation density as a function of time at different temperatures. Indeed, at low temperatures (below 120°C), the number of nuclei increased during the whole crystallization time. However, at temperatures above 123°C, the number of nuclei reached a constant value at the beginning of crystallization. The Ozawa equation was also utilized to study the non-isothermal crystallization of polyamide 6 from the glassy state (178). The crystallization process of polyamide 6 seemed to follow the Ozawa equation, i. e., straight lines were obtained when $\ln\{-\ln[1-x(t)]\}$ was plotted as a function of $\ln|\varphi|$. The Avrami

exponent, however, decreased continuously from 1.8 to 0.5 in the temperature range from 56°C to 66°C.

Contrary to all the cases presented, Eq. 6.16 did not conform to non-isothermal crystallization data of polyethylene (175). Eder and Wlochowicz (175) attributed the deviation from the Ozawa equation to factors such as secondary crystallization, dependence of lamellar thickness on crystallization temperature, and occurrence of both sporadic and predetermined nucleation. However, it is worth commenting that secondary crystallization would not be expected to be an important factor in the the non-isothermal crystallization of PPS. In previous studies of the isothermal crystallization of PPS, it was observed that secondary crystallization did not have an important contribution to the crystallinity of PPS (179). Similarly, the occurrence of sporadic and predetermined nucleation would not affect the validity of Ozawa's equation; it would only affect the value of the Avrami exponent.

Due to the simplicity of the method of Ozawa to analyze the non-isothermal data, and the ease of comparison of the parameters obtained with those determined from isothermal experiments, Eq. 6.16 was utilized to analyze the non-isothermal crystallization of PPS.

## 6.2 EXPERIMENTAL

The materials utilized in this study comprise PPS with various molecular weights and branching agent content, as listed in Table 9. The results obtained for these samples can be directly compared with the values determined from isothermal experiments.

A Perkin Elmer DSC-4 was utilized for the thermal treatment and data gathering. The sample crystallizations were performed at constant cooling rate after being held in the molten state at 320°C for 4 minutes. As expressed before, the short residence time in the melt was

**Table 9. Characteristics of samples utilized to study the non-isothermal crystallization kinetics of PPS.**

| Sample Designation | $<M_w>$ | Branching Agent Content (% by weight) |
|---|---|---|
| PPS24 | 24,000 | 0.0 |
| PPS49 | 49,000 | 0.0 |
| PPS63 | 63,000 | 0.0 |
| PPS13 | 75,000 | 0.13 |
| PPS20 | 65,000 | 0.20 |

utilized to avoid curing reactions. The crystallization exotherms were recorded at selected cooling rates: 2.5, 10, 15, 20, 25, 30, 35, 40°C/min.

## 6.3 RESULTS AND DISCUSSION

Due to the non-isothermal nature of the experiments, the temperature scale needs to be corrected for the temperature lag existing between the sample and the calorimeter furnace. This temperature lag comprises the thermal gradient inside the sample and the temperature lag between the bottom of the sample and the calorimeter furnace. The former term was previously calculated for a 0.3mm thick polypropylene sample during an 80°C/min cooling by Monasse and Haudin (177). These authors estimated a 1°C maximum thermal gradient under those conditions. Assuming that a similar value would be obtained for PPS, and comparing it with the temperature lag between sample bottom and calorimeter furnace (10.8°C), the thermal gradient inside the sample can be neglected. Therefore, a temperature calibration as a function of cooling rate is required. This was achieved by calibrating the DSC with indium standard at various scanning rates.

The data treatment, then, involves calculating x(T) from the measurement of partial areas of the exotherms obtained upon cooling crystallization. Furthermore, the partial areas are normalized by specimen mass and cooling rate to allow comparison between the different curves. The calculated amorphous fraction [1 - x(T)] is plotted as a function of temperature for the different cooling rates as shown in Fig. 53 for PPS49. Values of the amorphous fraction at a given temperature are taken from these plots at each cooling rate. Then, the double logarithm of the amorphous fraction $\ln\{-\ln[1 - x(t)]\}$ at constant temperature is plotted as a function of the cooling rate. If Eq. 6.16 is valid, the curve corresponding to each temperature should

be a straight line. The slope would give the Avrami exponent and the intercept determines the value of the cooling crystallization function.

Figure 53 presents plots of the amorphous fraction as a function of temperature for PPS49 crystallized non-isothermally at various cooling rates. The effect of the different cooling rates is observed in these plots corresponding to PPS49. The higher the cooling rate, the lower the temperature range at which the crystallization occurs. At each cooling rate, crystallization takes place at temperatures above the point of maximum crystallization rate (~180°C); therefore, the transformation is controlled by nucleation. At slow cooling rates, there is sufficient time to activate nuclei at higher temperatures. On the contrary, at faster cooling rates, the activation of nuclei occurs at lower temperatures. Consequently, crystallization nucleates at higher temperatures when the polymer samples are cooled at slower scanning rates. Figure 53 also shows the limits of cooling rates utilized in this study. The lower limit is 2.5°C/min and the upper one is 40°C/min. The former is determined by the sensitivity of the differential scanning calorimeter utilized. At cooling rates lower than 2.5°C/min, the signal output presents noise due to a lower sensitivity of the calorimeter; consequently, the data is not accurate. The upper limit is established by the limiting heat transfer. Analyzing Fig. 53, it is observed that the temperature gap between successive curves at different cooling rates decreases as the cooling rate increases. Crystallizations performed at higher cooling rates tend to occur at the same temperature range as those obtained at 40°C/min, indicating that the higher cooling rates are not effective in lowering the temperature of the onset of crystallization. Another important characteristic of Fig. 53 is the shape of the curves. All the curves of amorphous fraction versus temperature have approximately the same shape and can practically be superimposed on one another. This would indicate that in the range of cooling rates and temperatures investigated, the mechanism of crystallization does not change. In other words, only the retardation effect of cooling rate on the crystallization is observed in these curves.

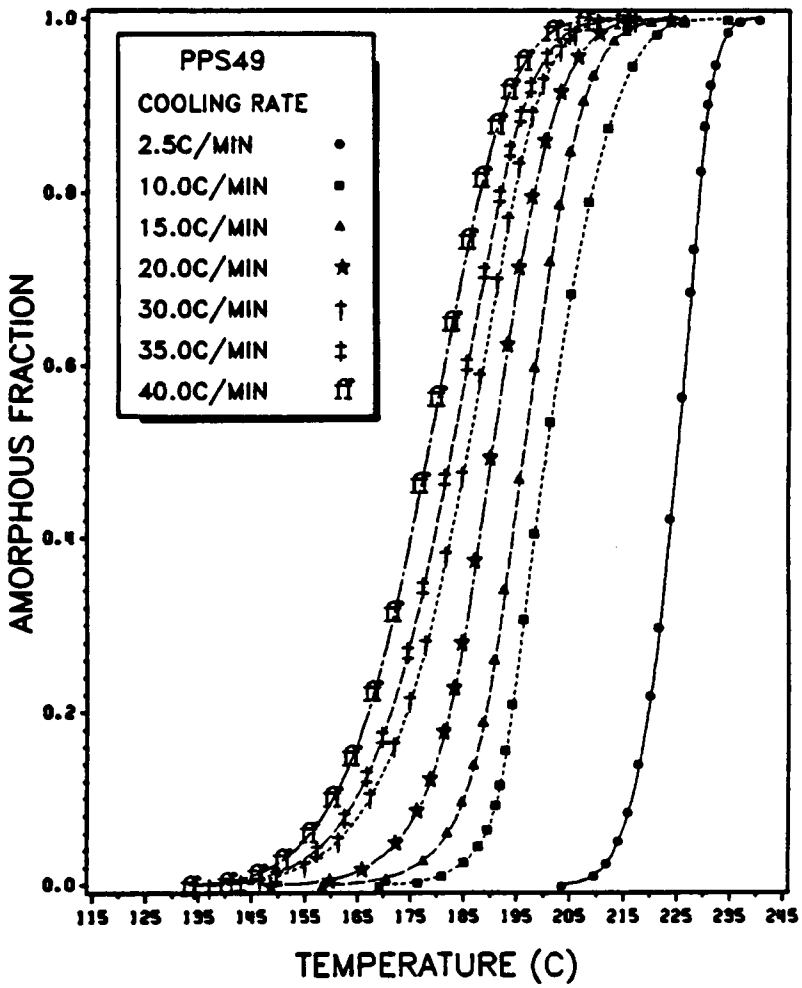


**Figure 53.** Plot of amorphous fraction as a function of temperature for PPS49 crystallized non-isothermally at various cooling rates.

Figures 54-58 present plots representative of the Ozawa equation (Eq. 6.16) for PPS24, PPS49, PPS63, PPS13, and PPS20; i. e., plots of $\ln\{-\ln[1 - x(t)]\}$ as a function of $\ln|\varphi|$ at constant temperature. If Eq. 6.16 is valid, the curve corresponding to each temperature should be a straight line. Indeed, Figs 54-58 indicate a very good agreement between the experimental results and the theoretical treatment of Ozawa (171). In addition, it should be noted that branching does not affect the behaviour of PPS when it is crystallized non-isothermally. Samples PPS13 and PPS20 were synthesized containing 0.13% and 0.20% by weight of branching agent trichlorobenzene, which presumably introduces long-chain branches. The Ozawa plots corresponding to PPS13 and PPS20 are presented in Figs. 57 and 58. It is noted that the plots are straight lines, following Eq. 6.16. The data corresponding to linear and branched PPS, then, conforms with the theoretical treatment of Ozawa (171). Consequently, Eq. 6.16 can be utilized to calculate the Avrami exponents of non-isothermally crystallized PPS. As expressed above, the Avrami exponent is the slope of the $\ln\{-\ln[1 - x(t)]\}$ versus $\ln|\varphi|$ curve, and the intercept of this straight line provides the cooling crystallization function. For the determination of the Avrami exponent, amorphous volume fractions higher than 0.5 were utilized. At lower fractions, the effect of impingement and truncation of spherulites can become very important. If impingement and truncation occur, the overall rate of crystallization is decreased and the mechanism of crystallization can change; ultimately, the value of the Avrami exponent decreases. Therefore, utilizing values of the amorphous fraction higher than 0.5 avoids the problem mentioned. The values of the Avrami exponent determined by this method are plotted in Fig. 59 as functions of temperature. The Avrami exponent has values between 2.3 and 3.0. In the case of PPS13 and PPS20, n is equal to 2.4 on the average. This value is slightly lower than those obtained isothermally by the method of Avrami (3.0 and 2.8, respectively). PPS63 has a higher value of n, in the order of 2.8 on the average, with no systematic variation with temperature. Furthermore, n is in very good agreement with that determined isothermally (3.0). However, the Avrami exponents determined for PPS24 and PPS49 present an increasing trend with temperature. This trend is more pronounced in PPS24. The Avrami exponent of PPS24 increases from 2.4 at 220°C to 3.0 at 230°C. This phenomenon was

not observed when the crystallization of PPS24 was studied isothermally. The latter case showed an Avrami exponent of ~2.5 that was attributed to the presence of sheaflike superstructures that lower the value of n. These structures were presumed present due to the fast crystallization rate of PPS24 that did not allow their full development into spherulites. A possible explanation of the present experiment is that due to the non-isothermal nature of the experiment, the overall crystallization rate would increase as the temperature is decreasing. This may provoke the incidence of impingement effects that would lower the values of n.

The cooling crystallization function, $\chi$, was also determined for each temperature from the intercept of the plot of $\ln\{-\ln[1 - x(t)]\}$ versus $\ln|\varphi|$. Such values are presented in Fig. 60 as functions of temperature. The cooling crystallization function shows a decreasing trend with increasing temperature for every polymer sample. This is in agreement with data on PET presented by Ozawa (171). This author showed that $\chi$ decreased with increasing temperature. Polypropylene also presented a similar trend (175). However, the significance of $\chi$ has not been discussed. Figure 60 shows that the linear PPS samples, PPS24, PPS49 and PPS63, have higher values of $\chi$ than the branched samples PPS13 and PPS20, at a given temperature. In addition, considering the decreasing trend, the values corresponding to PPS24 at high temperature are higher than those PPS49 and PPS63 would have. Therefore, the author believes that the cooling crystallization function, $\chi$, is related to the overall rate of bulk crystallization in the sense that it may give an indication of how fast the non-isothermal crystallization occurs.

In summary, the theory of Ozawa has been shown to be a good method to analyze data corresponding to non-isothermally crystallized PPS. Equation 6.16 conformed very well to the DSC data of PPS, allowing the determination of the Avrami exponent. In general, the Avrami exponents determined by this method were in agreement with values obtained by means of isothermal techniques. In addition, the analysis of Ozawa allowed the study of the crystallization behaviour of PPS in a wider temperature range, indicating that this technique can be a complementary tool for the investigation of the crystallization of polymers.

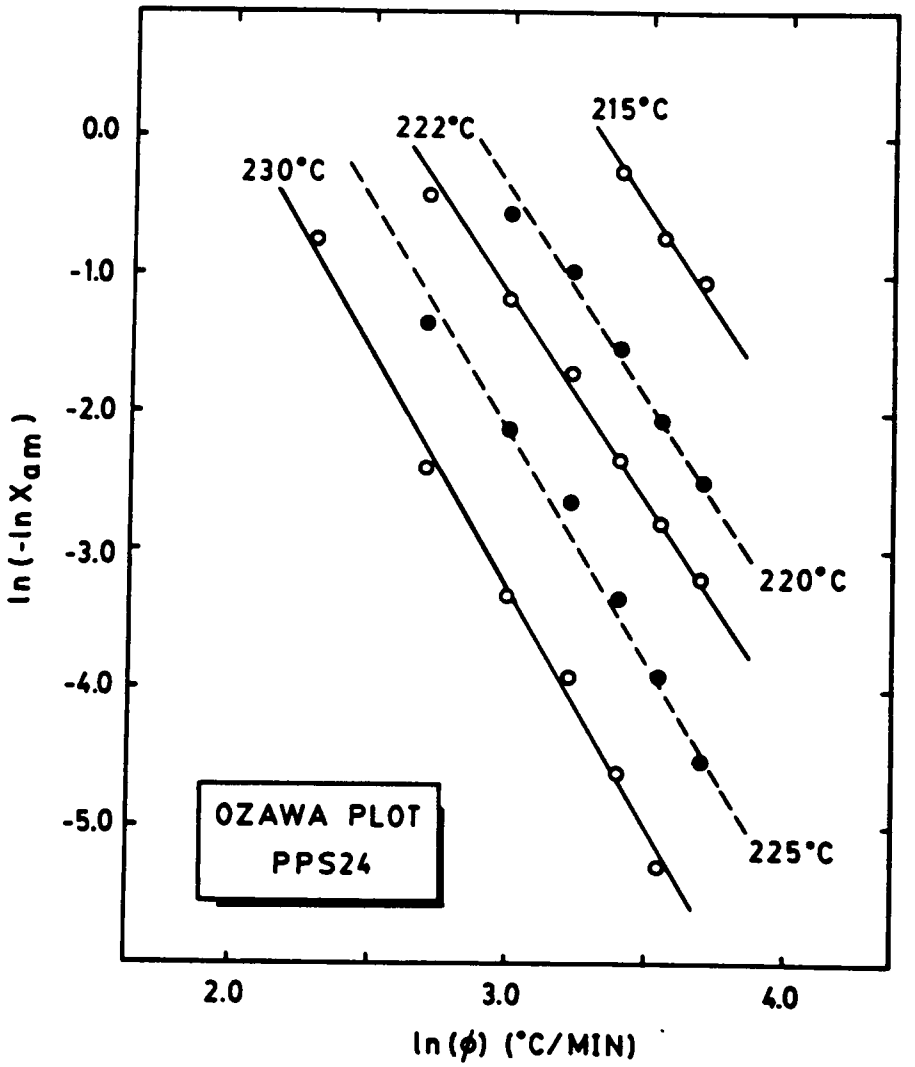


**Figure 54.** Plot of ln{-ln[1 - x(t)]} as a function of ln φ at various temperatures corresponding to PPS24.

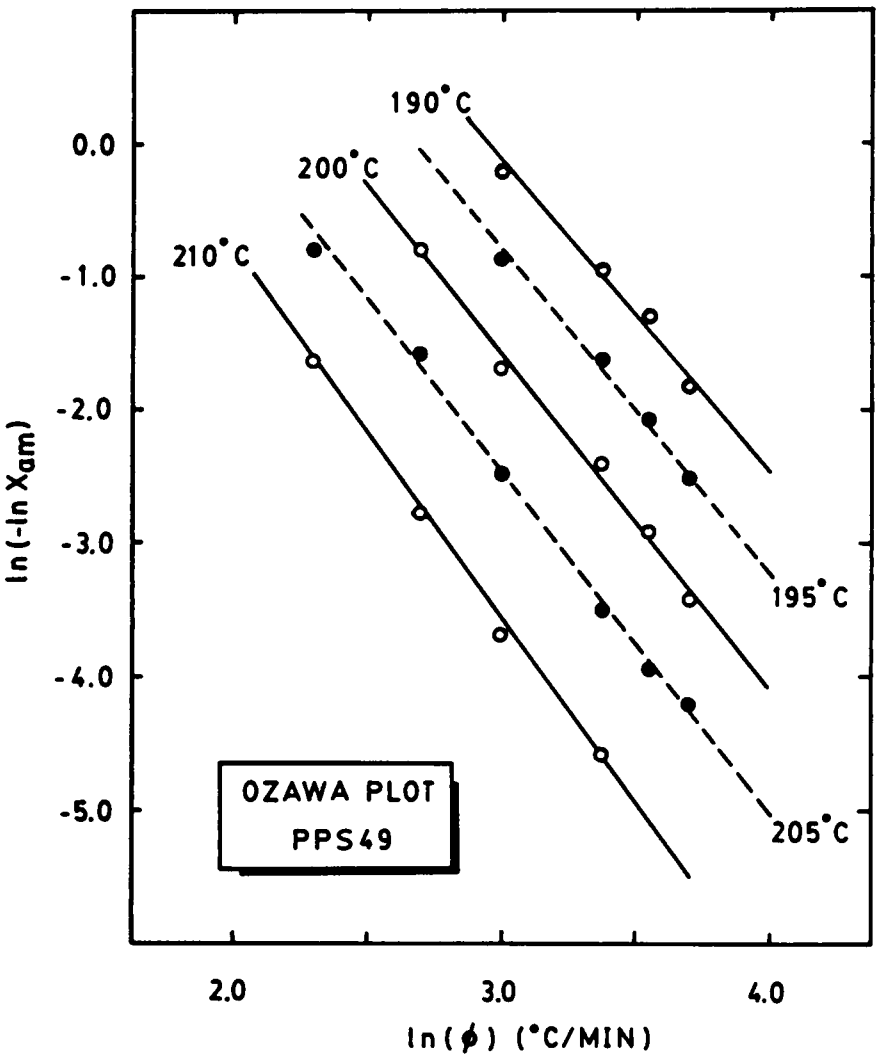


**Figure 55.** Plot of ln{-ln[1 - x(t)]} as a function of ln φ at various temperatures corresponding to PPS49.

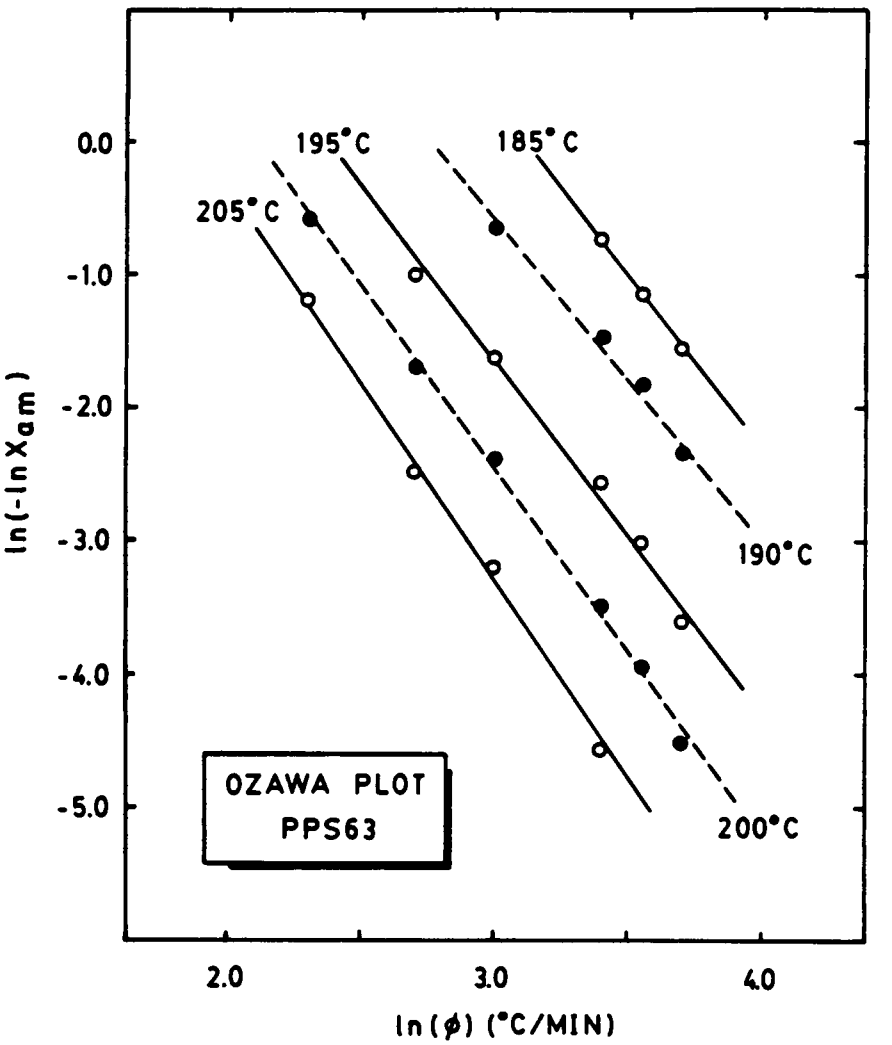


**Figure 56.** Plot of ln{-ln[1 - x(t)]} as a function of ln φ at various temperatures corresponding to PPS63.

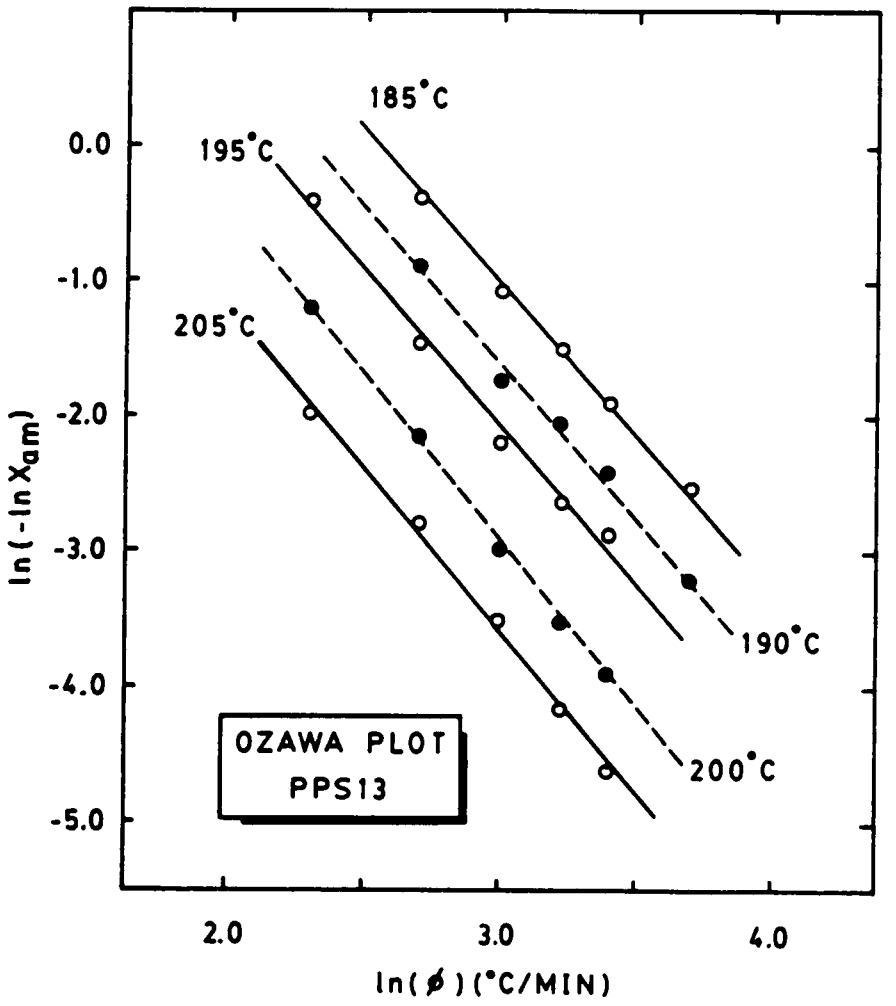


**Figure 57.** Plot of ln{-ln[1 - x(t)]} as a function of ln φ at various temperatures corresponding to branched PPS13.

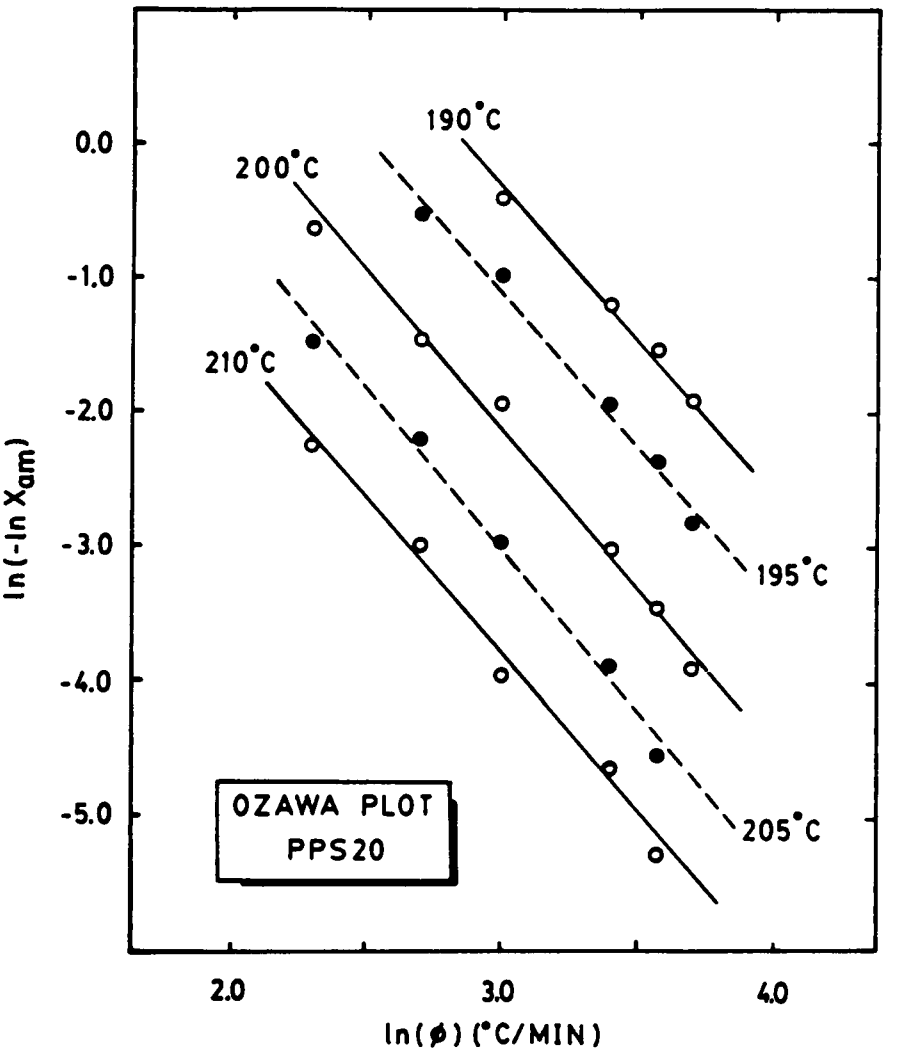


**Figure 58.** Plot of ln{-ln[1 - x(t)]} as a function of ln φ at various temperatures corresponding to branched PPS20.

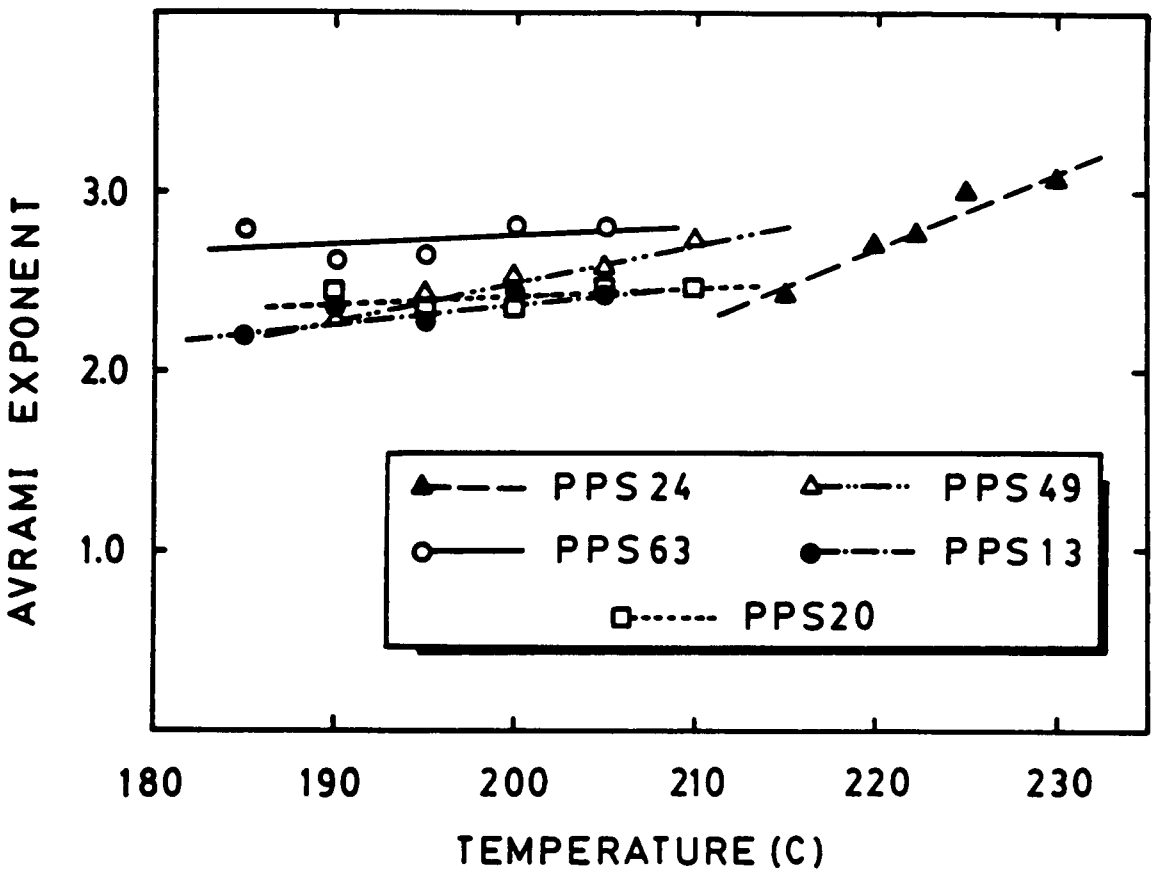


**Figure 59.** Plot of the Avrami exponent determined from Eq. 6.16 as a function of temperature corresponding to various PPS samples.

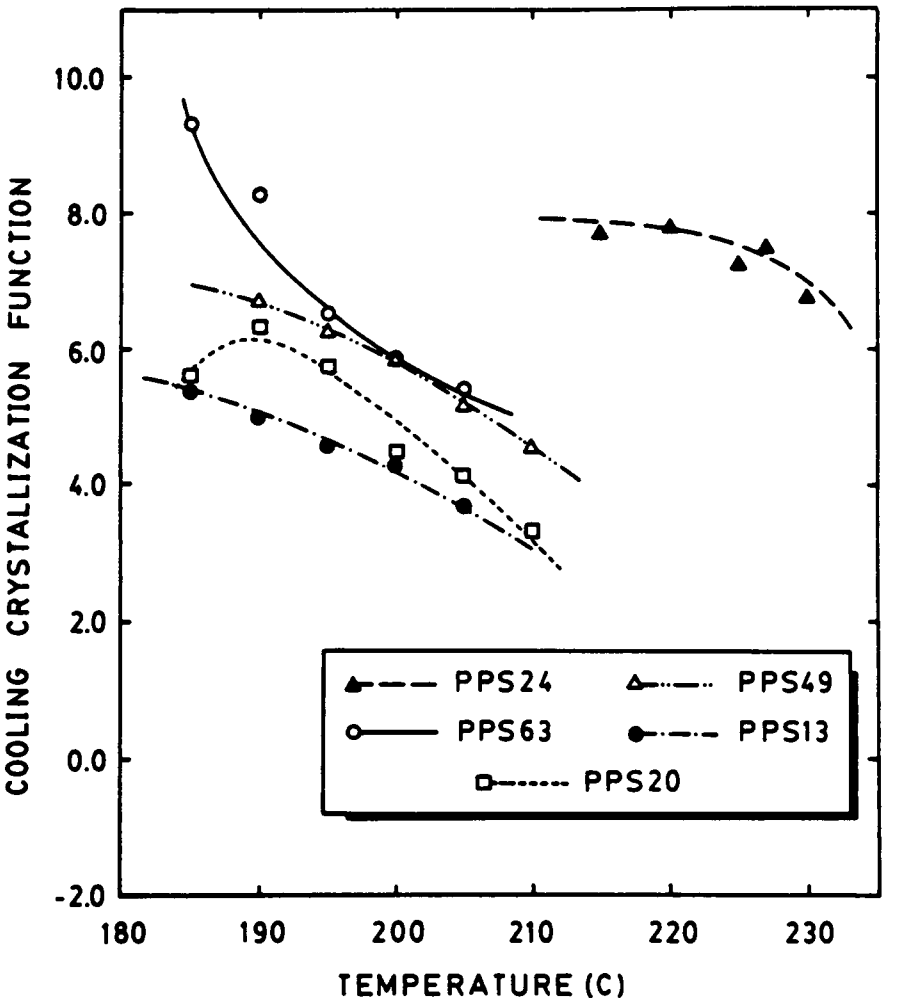


**Figure 60. Plot of the cooling crystallization function, $\chi$, as a function of temperature.**

# CHAPTER VII

# ON THE MORPHOLOGICAL TEXTURES OF POLY(PHENYLENE SULFIDE)

## *7.1 INTRODUCTION*

The study of the morphology of semicrystalline polymers involves three levels of structure. The first one is concerned with the crystal unit cell (2-20Å in magnitude). At this level, the spatial arrangement of the atoms of the polymer chains are determined by scattering techniques such as wide angle x-ray scattering (WAXS) and electron diffraction. The second level of structure often consists of folded chain lamellar crystals generally 50-300Å in thickness. As expressed in Chapter 3, the lamellae are entities in which the polymer molecules are folded with the chain axis generally in the direction of the lamellar thickness. The lamellar thickness is a characteristic dimension that represents the average polymer chain length between chain folds. The lamellar thickness can be determined by scattering techniques such as small angle x-ray scattering (SAXS), transmission electron microscopy (TEM), and in some cases by Raman spectroscopy. The third level of structure is concerned with the superstructure of the semicrystalline polymer (on the order of microns in magnitude). At this level, the arrangement

of the lamellar crystals (or the absence of them) and the amorphous phase determines whether the final superstructure is spherulitic, axialitic, dendritic, random, etc. This level of structure is usually studied by optical microscopy, electron microscopy and small angle light scattering. Utilization of electron microscopy often includes another experimental method to differentiate amorphous and crystalline phases. For example, in TEM staining techniques, and shadowing techniques are often utilized. Similarly, in scanning electron microscopy (SEM) other techniques have been utilized (180-196).

Chemical etching or selective solvent washing has long been used for purposes of enhancing contrast in scanning electron microscopy investigations. Particularly, in the area of polymer morphology, either technique is utilized to selectively degrade or dissolve one phase or component in multiphase and multicomponent systems. Subsequently, characterization of the remaining morphological structure is facilitated by microscopy.

By far, etching solutions based on mineral acids have been the most widely used for the enhancement of the morphology of semicrystalline polymeric materials. For example, cellulose microcrystals suitable for transmission electron microscopy have been prepared by hydrolysis with hydrochloric and sulphuric acid solutions(180). Individual lamellae of melt crystallized polyethylene have been observed by attack of the bulk structure with fuming nitric acid (181,182). The same etching technique was used by Ward and Williams (183) to degrade bulk polyethylene and to study the degradation products by gel permeation chromatography.

Other polyolefins have been treated with potassium permanganate solutions in concentrated sulphuric acid. Olley, Hodge and Bassett (184) developed such a permanganic etchant for polyolefines. This reagent was used to etch polyethylene, i-polypropylene and i-poly(4-methylpentene-1). This etching agent was found to discriminate not only between amorphous and crystalline material, but also 'between lamellar orientations. Fitchmun and Newman (186) set forth another oxidative etching agent for isotactic polypropylene. The technique consisted of swelling the samples in an aqueous solution of turpentine (10%) and a

surfactant at 70°C, prior to oxidation with a 20% sulphuric acid solution saturated with chromium trioxide. Good enhancement of the surface crystalline features of i-polypropylene was obtained.

Carter and Wilkes (186), and Fischer et al. (187) have utilized basic hydrolytic media to enhance morphological features on copolymers of glycolic-lactic acid, and lactic acid, respectively. Koenig and Agboatwalla (188) have also used a basic hydrolytic reagent to attack single crystal mats of poly(hexamethylene adipamide).

In other instances, selective dissolution has been used. Reding and Walter (189) have followed changes in the size and structure of spherulites in molded polyethylene specimens by selective dissolution with hot carbon tetrachloride, toluene or benzene. Preferential dissolution with carbon tetrachloride vapor was used by Muccigrosso and Phillips (190) to study the morphology of crosslinked polyethylene cable insulation. Xylene has also been used for selectively dissolving amorphous polyethylene and polypropylene to enhance their crystalline textures (191). Atactic polystyrene has been selectively dissolved from isotactic polystyrene with methyl ethyl ketone (192). Chu and Wilkes (193) utilized a contact etching technique with n-propylamine to selectively degrade and dissolve amorphous poly(ethylene terephthalate), poly(tetramethylene terephthalate) and poly(ethylene 2,6-naphthalate). A variety of films and fibers with different thermal and mechanical histories were treated with this reagent to achieve a good degree of crystalline texture enhancement.

Another kind of etching technique or selective degradation for the development of morphological contrast is the use of a glow discharge or ion beam radiation to selectively degrade the polymer. Examples of this type of experiments have been reported by Anderson and Holland (194), Spit (195), and more recently, by Nishimura et al. (196). Anderson and Holland (194) utilized argon ion bombardment to prepare fibers of nylon 66 and poly(ethylene terephthalate) for observation under the transmission electron microscope. Spit (195) used an oxygen glow discharge to prepare regenerated cellulose fibers. A selective degradation

of the amorphous regions seemed to have been obtained under the experimental conditions used. More recently, Nishimura et al. (196) used an oxygen plasma etching for preparation of samples for SEM observation.

In the present chapter, the author reports on the search of a suitable etching system for the observation of morphological textures in poly(phenylene sulfide). One of the objectives is the development of a technique that would allow the investigation of the crystalline morphology of PPS. In particular, the study of the morphology of PPS in carbon fiber composites is of interest. Given the excellent chemical resistance of poly(phenylene sulfide) (11), it seems a rather difficult task. However, the utilization of two etching techniques is reported here displaying various degrees of success. One technique, chromic acid etching, is based on the recent work of Zeng and Ho (38), while the second one is performed with anhydrous aluminum chloride. This last etching technique was developed by extensive modification of a patent of T. W. Johnson (66). In this patent, Johnson reports on a technique to completely degrade poly(phenylene sulfide) for the determination of the fiber content in composites based on this polymer. In the present study, the author extensively modifies the technique to achieve a good degree of crystalline texture enhancement and observe the superstructures developed by PPS upon crystallization.

## *7.2 EXPERIMENTAL*

Ryton® V-1 grade poly(p-phenylene sulfide) was used in the study. Thin films were prepared by pressing the polymer at 310°C and 2000 psi. The films were maintained at that temperature for three minutes and quenched in ice water. The film thickness was in the order of 0.003 in. The samples were crystallized from the melt in a heating stage under a nitrogen purge as follows. The films were introduced in the heating stage at 310°C and maintained at

that temperature for 2 min. Then, the temperature was lowered to 255°C and the films were isothermally crystallized at that temperature for 90 min. Several criteria were considered to select this sample preparation method. As was mentioned in Chapter 2, PPS is susceptible of undergoing curing reactions at high temperatures, in the presence of oxygen. These reactions may involve chain extension, branching and crosslinking. It was also mentioned that the morphology of PPS can be affected by these curing reactions. Therefore, the temperature and time of sample preparation needed to be minimized without compromising the formation of superstructure. In addition, a nitrogen purge was utilized to reduce the rate of the curing reactions to a minimum. Maintaining PPS at 310°C for 2 min in the melt provided a low nucleation density; thus, large spherulites could be formed. Similarly, a crystallization temperature of 255°C allowed the nucleation and growth of spherulites very suitable for microscopy observations.

The crystallized films were subsequently subjected to the etching procedures described below. The etched films were observed under the scanning electron microscope after metallization by sputter coating. An ISI Super 3-A and a Cambridge S200 scanning electron microscopes were utilized.

An uniaxial PPS/C fibre composite furnished by Phillips Petroleum Co. was also subjected to the aluminum chloride etching technique.

### 7.2.1 Chromic Acid Etching Technique

The etching reagent was prepared by dissolving potassium dicromate in a 1M sulphuric acid solution until saturation was achieved at 60°C. The solution was placed in a flask equipped with a condenser tube and a magnetic stirring bar. The flask containing the solution was placed in an oil bath set at 100°C allowing temperature stabilization for 20 min. After-

wards, the crystallized samples were introduced into the solution. Etching times were varied from two to five hours. Samples taken out of the etching solution were rinsed for 10 min in water, dried for 24 h in a vacuum-oven at 50°C and prepared for SEM observation.

### 7.2.2 Aluminum Chloride Etching Technique

Anhydrous aluminum chloride suspensions were prepared in reagent grade toluene under a nitrogen environment. A three-neck round bottom flask was utilized to carry out the reactions. The flask containing the suspension was placed in an oil bath and stirred for 3 min under a fume hood. Temperatures of the oil bath of 55°C, 45°C or 35°C were used. Several $AlCl_3$ concentrations were tested, 3%, 1.5%, and 0.8% by weight. As will be shown in the following sections, a temperature of 35°C and an $AlCl_3$ concentration of 0.8% by weight are the best conditions for texture enhancement.

The crystallized samples were introduced into the suspension by means of a holder and maintained in the stirred suspension from 3 to 10 min. During the whole procedure, nitrogen was purged through the system to decrease the effect of air moisture on the aluminum chloride reactivity.

After etching, the films were immersed in methanol for 30 seconds, rinsed in acetone for several minutes, dried at room temperature for 24 h, and prepared for SEM observation.

## 7.3 RESULTS AND DISCUSSION

### 7.3.1 Chromic Acid Etching

Figure 61 illustrates a micrograph of a PPS sample that was isothermally crystallized at 255° for 90 min without any etching treatment. Spherulitic superstructure is noticed, with the spherulite average diameter of 50μm. However, no fine texture can be perceived in this specimen at high magnification, indicating the need for a technique to enhance the contrast.

Figure 62 shows samples etched with the chromic acid reagent. Insert (a) of this figure presents an amorphous PPS sample that has been etched with the reagent for 2.5 h. The typical porous structure of corroded amorphous materials is observed, suggesting that it has little resistance to this environment. On the other hand, the crystallized samples show a different behaviour (Fig. 62-b and c). It is clear that the amorphous material has been selectively removed to some extent and the crystalline material displays a greater resistance towards the chromic acid attack. In addition to a better definition of the spherulitic superstructure, this etching procedure brings out a finer structure present in the spherulites.

Three dimensionally developed spherulites are present in addition to some that are two dimensional. The latter have nucleated somewhat below the free surface of the film and have undergone typical spherulitic growth. As the diameter increased, the spherulitic growth has terminated at the film surface and growth has essentially continued in two dimensions in the plane of the film until impingement occurred. A high magnification micrograph in Fig. 62b shows the radial texture of the spherulites. Furthermore, in Fig. 62c, considering a fully developed spherulite, a layered structure is noticed that akin to the radial texture would indicate a sheaf-like type of growth as explained in the model for spherulitic growth proposed by Keith (197). This author stressed the importance of fractionation and "impurity" segregation in the crystallization of polymers from the melt. By impurities, Keith referred to low molecular weight

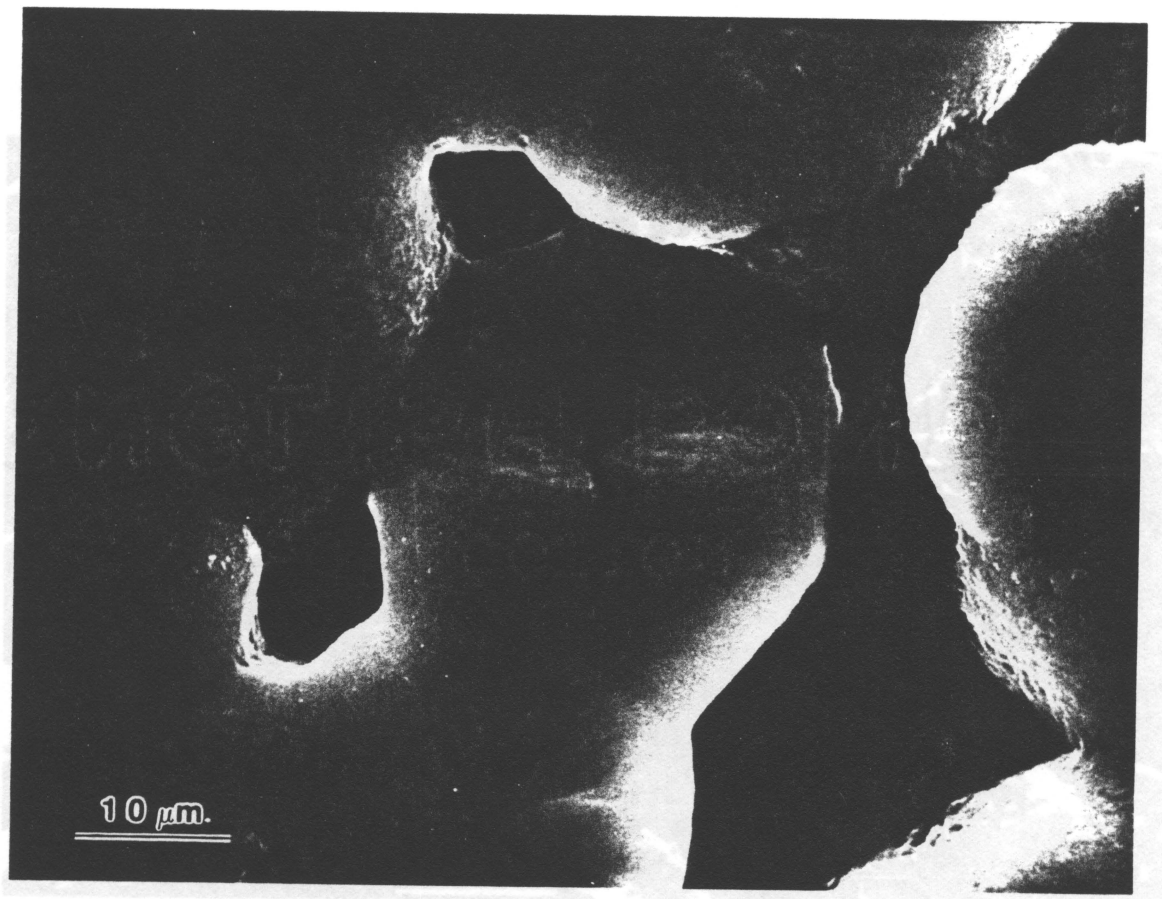


**Figure 61. PPS isothermally crystallized at 255°C:** Unetched film surface. Magnification: 3000X.

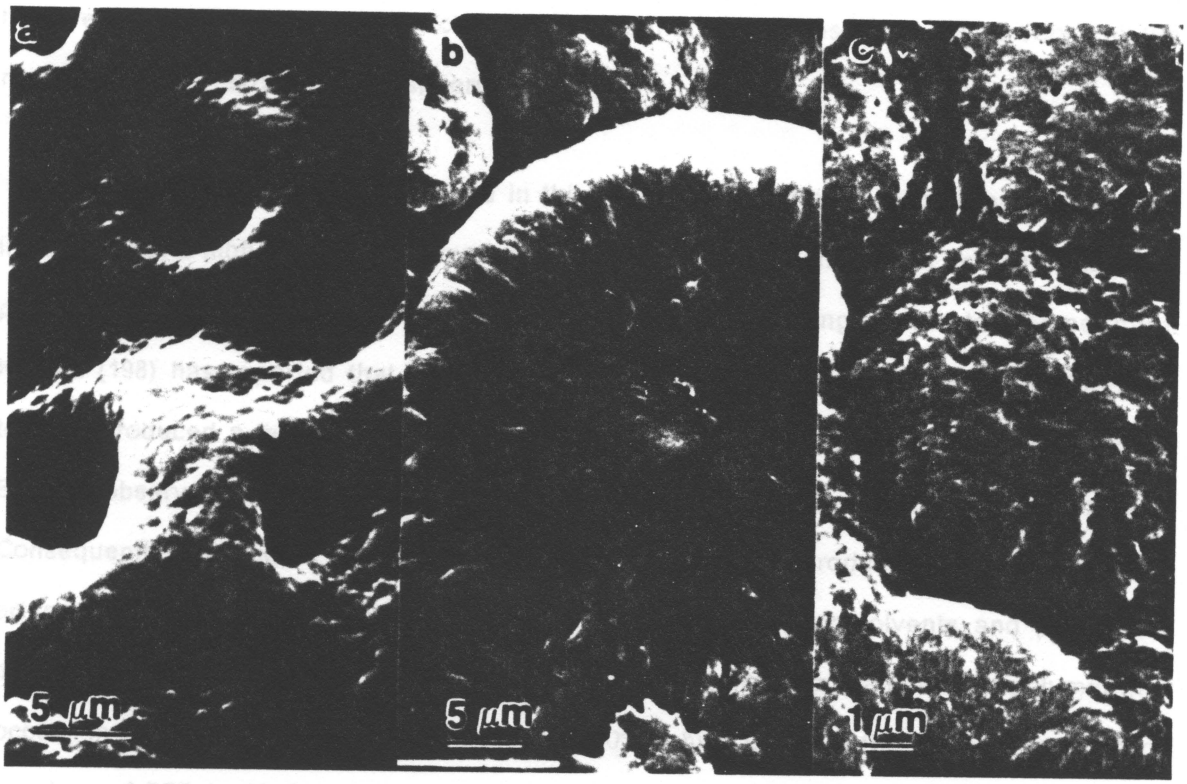


**Figure 62. PPS etched with chromic acid at 100°C:** (a) amorphous, etched for 2.5hs; M:3500X; 25° stage tilt; (b) semi-crystalline, etched for 4.5hs; M:3000X; (c) semi-crystalline, etched for 3.0hs; M:4500X.

polymer chains, stereoirregular molecules and generic impurities. These "impurities" rejected from crystallization would accumulate in the neighbourhood of the growing fronts of lamellar crystals provoking the formation of "cellular" growth fronts, and ultimately the development of crystals possessing fibrous habit. As crystallization proceeds, the impurities would be rejected to the sides of the fibrillar entities producing amorphous interfibrillar regions. Therefore, the spherulites would consist of radiating arrays of fibers that start at a central point (nucleating site). This kind of texture can be noticed in Fig. 62b with chromic acid etching; however, the aluminum chloride etching technique that will be described shows very well the radiating fibrous textures of the spherulites.

Comparison of the results obtained in this investigation with those of Zeng and Ho (38) indicates that a higher degree of morphological texture enhancement can be achieved in the present work. However, there is the problem of performing etching at elevated temperature. Kubota (198) has reported that exposure of polyethylene to boiling carbon tetrachloride or toluene produced a thin layer of new structure developed as a result of the vapor etching. Similar observations were made by this same author on polypropylene etched with xylene. Consequently, etching of crystalline polymers without the introduction of morphological artifacts seems to be possible only by utilizing sufficiently poor solvents and performing etching at temperatures well below those where significant reorganization of the polymer may occur. In our case, etching was performed at 100°C which is above the glass transition temperature of PPS (~85°C). Therefore, some further reorganization of the polymer can occur during etching. That is, some morphological artifacts may have been introduced by etching performed at 100°C. No artifacts such as overgrowths of precipitated polymer are noticed in the etched samples probably due to the non-solvent characteristics of the etching solution utilized. However, observation of Fig. 62a indicates the presence of a regular fine structure that resembles very small spherulites. Since that PPS sample was an amorphous film, the formation of the small spherulites may have occurred during the etching procedure performed at 100°C. This fact, in addition to not having achieved an outstanding degree of texture en-

hancement lead the author to the development of the anhydrous aluminum chloride etching technique.

### 7.3.2 Aluminum Chloride Etching

Figure 63 presents a micrograph of a PPS crystalline film after etching with the aluminum chloride reagent at a concentration of 3% by weight of anhydrous aluminum chloride. The etching temperature was 55°C and the etching time was 6 min. It is immediately noticed the stronger attack of this reagent as compared to the chromic acid etching reagent. For the $AlCl_3$ case, *the etching time is reduced by a factor of 30* . In addition, at this concentration and temperature, the attack is not selective at all. The amorphous fraction as well as the crystalline fraction have been attacked. Insert (a) shows that the attack is very strong particularly on the spherulites that have stopped three dimensional growth at the film surface. However, fully grown spherulites (complete three dimensional growth) do not show such a strong attack. Figure 63b presents a higher magnification micrograph of a fully developed spherulite that shows a crack presumably due to the effect of the etching reagent. The morphology of the amorphous material is different from that observed after chromic acid etching. In the $AlCl_3$ case, the amorphous material has the appearance of crumbs. This indicates, once more, the stronger nature of the anhydrous aluminum chloride etching as compared to the chromic acid one.

Reducing the concentration of aluminum chloride by a factor of two and the etching temperature to 45°C somewhat improved the situation. At this concentration of etching reagent and temperature, the attack was more selective, producing better detail of the spherulitic textures. However, the texture enhancement achieved was not sufficient for observation of the morphological textures.

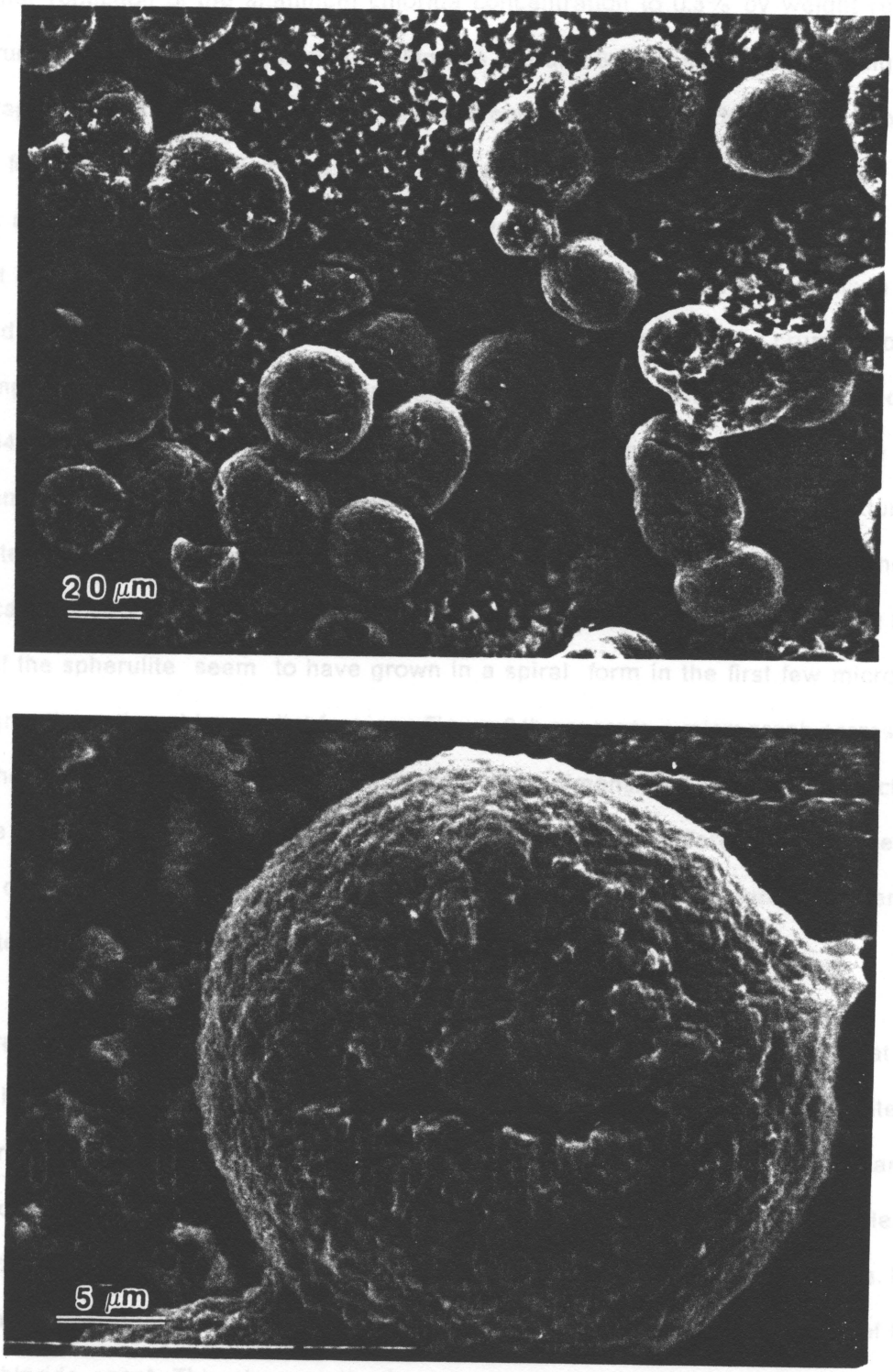


**Figure 63. PPS crystallized at 255°C etched with aluminum chloride at 55°C:** $AlCl_3$ concentration: 3% by weight. Etching time: 6 min. (a) Magnification: 500X. (b) Magnification: 3000X.

Further reduction of the aluminum chloride concentration to 0.8% by weight revealed a finer structure present in the spherulites. Figures 64a and 64b present two scanning electron micrographs of films etched with this reagent at a concentration of 0.8% and at a temperature of 35°C for 5 min. *The etching time is reduced by a factor of 36* when compared with the chromic acid etching time. The attack is very selective, degrading amorphous PPS at a fast rate, but leaving the crystalline texture intact for this etching period. The amorphous material observed in the background of these figures also has the appearance of crumbs confirming the stronger nature of the anhydrous aluminum chloride etching technique mentioned earlier. Figure 64a shows a spherulite that has nucleated somewhat below the film surface and has undergone spherulitic growth until the film surface was reached. A fine radial texture of the spherulite is now well accentuated by the aluminum chloride etching procedure. The higher magnification insert presents the center of the disk-like spherulite. "Fibrils" growing from the center of the spherulite seem to have grown in a spiral form in the first few microns, with further growth continued in a radial fashion. Figure 64b presents a micrograph corresponding to a spherulite that has undergone the typical three-dimensional growth, in which a fine structure is also observed. However, the structure is somewhat different as expected, since the end of the growing fibrils is observed. In this case, a nodular texture is present at the spherulite growth surface.

Figure 65 shows a spherulite that has nucleated and grown in three dimensions at the film surface. In this case, the growing front is also observed as in Fig. 64b. This spherulite seems to present a finer structure than that of Fig. 64. However, the features are very similar. In Fig. 65, the volume filling characteristics of the PPS spherulites can be observed very clearly. As the micrograph depicts it, there is a large fraction of empty volume in the spherulites. In those voids, amorphous polymer was presumably present, and was removed by attack of the aluminum chloride agent. This stresses the important concept that spherulitic superstructures are not completely crystalline; i. e., there is amorphous material also present inside the superstructure.

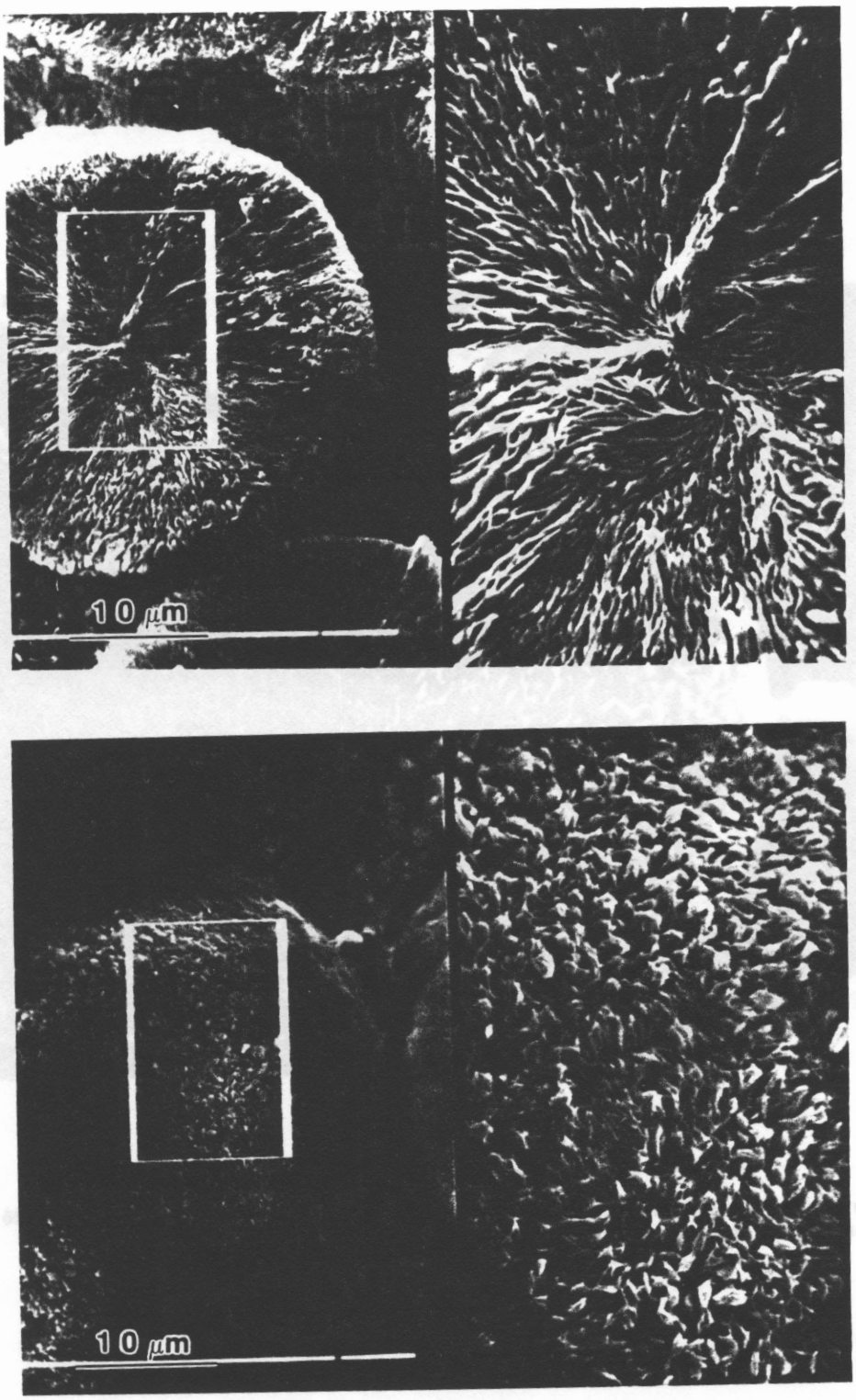


**Figure 64.** **PPS isothermally crystallized at 255°C etched with aluminum chloride reagent at 35°C:** (a) 2-dimensional spherulite. 30° stage tilt. Magnification: 2000X, 6000X. (b) 3-dimensional spherulite. 10° stage tilt. Magnification: 2000X, 6000X.

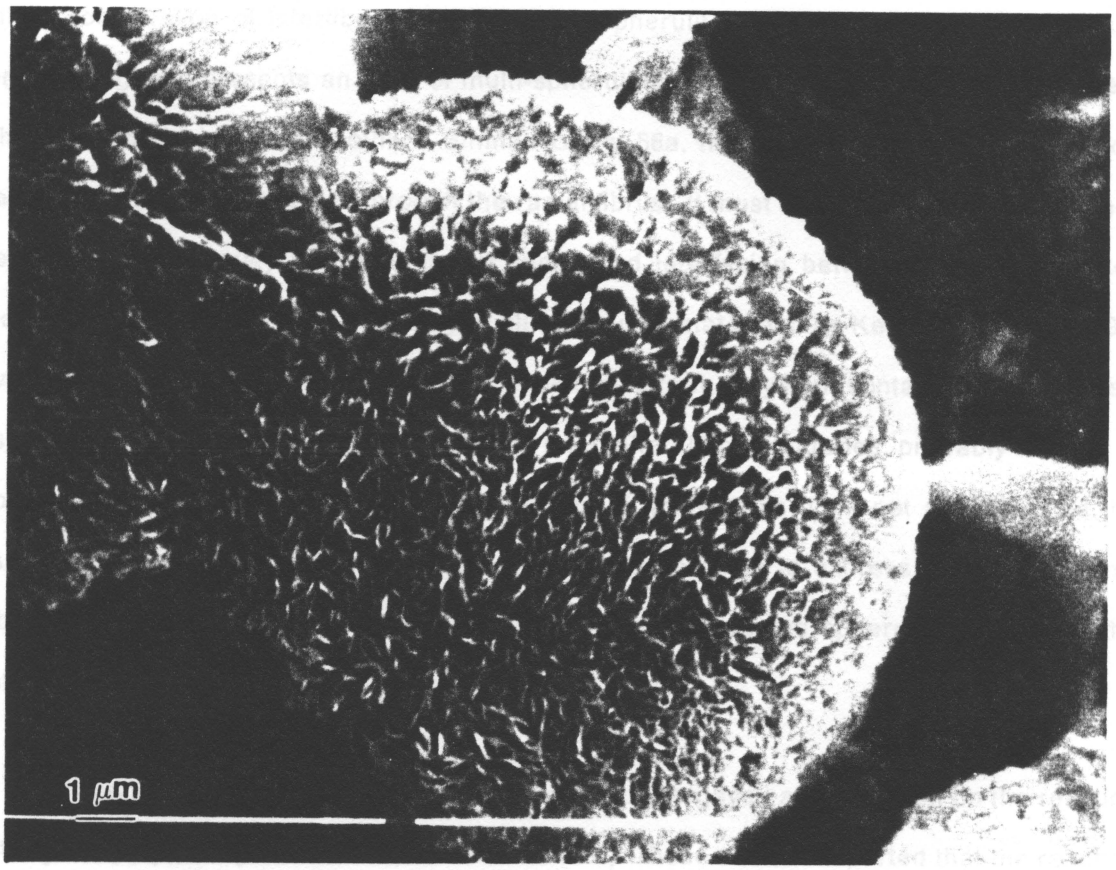


**Figure 65.** **PPS isothermally crystallized at 255°C etched with aluminum chloride reagent at 35°C:** 3-dimensional spherulite showing a very fine structure. Notice the volume filling characteristics of the spherulite. Magnification: 7000X.

Figure 66a shows two spherulites that have impinged into one another. The higher magnified region indicates that the interface between these spherulites is not very well defined. Indeed, these micrographs suggest that there is a good interfacing of the crystalline fibrils of one spherulite with those of the neighbouring one. In particular, after removing the interfibrillar material with chemical etching, general connectivity of the fibrils is observed, as well as continuation of interfibrillar voids of one spherulite into the neighbouring one. Furthermore, Fig. 66b presents an area of multi-spherulitic impingement. Four spherulites seem to have impinged into one another. Similar to Fig. 66a, there is a clear indication of good interfacing between spherulites through the radial fibrils. It must be mentioned that the author does not wish to convey the thought that such good interfacing between spherulites takes place at every interspherulitic boundary of all spherulitic materials. As Keith and Padden (199) have shown, when spherulitic superstructure develops from a system containing "impurities", this impurities will usually be concentrated at interspherulitic boundaries, probably leading to poor connectivity of fibrils across the boundaries. However, this does not appear to be the case in the system reported here. Therefore, the author wishes to express that there seems to be considerable interfacing of the crystalline fibrils of impinged spherulites *only* for the system discussed here.

At this point it is of interest to describe the study of Sergeyev and Nedelkin on the reaction of $AlCl_3$ and poly(phenylene sulfide) in benzene (200). These authors reported that the reaction of PPS with $AlCl_3$ at room temperature in suspension in benzene produced the degradation of PPS to form diphenyl sulfide. Mass spectral analysis also indicated the formation of other by-products. In particular, the conditions in which the reaction was carried out seemed to have had a major role in determining the reaction products. For example, with reaction temperatures of 80°C, 3% of thianthrene seemed to have been produced. Further increase in the temperature to 200-250°C resulted in the production of polymers with different chemical structure than PPS. At this temperature, the process included distillation of benzene, liberation of HCl and $H_2S$, and formation of a partially soluble polymer with decomposition temperature

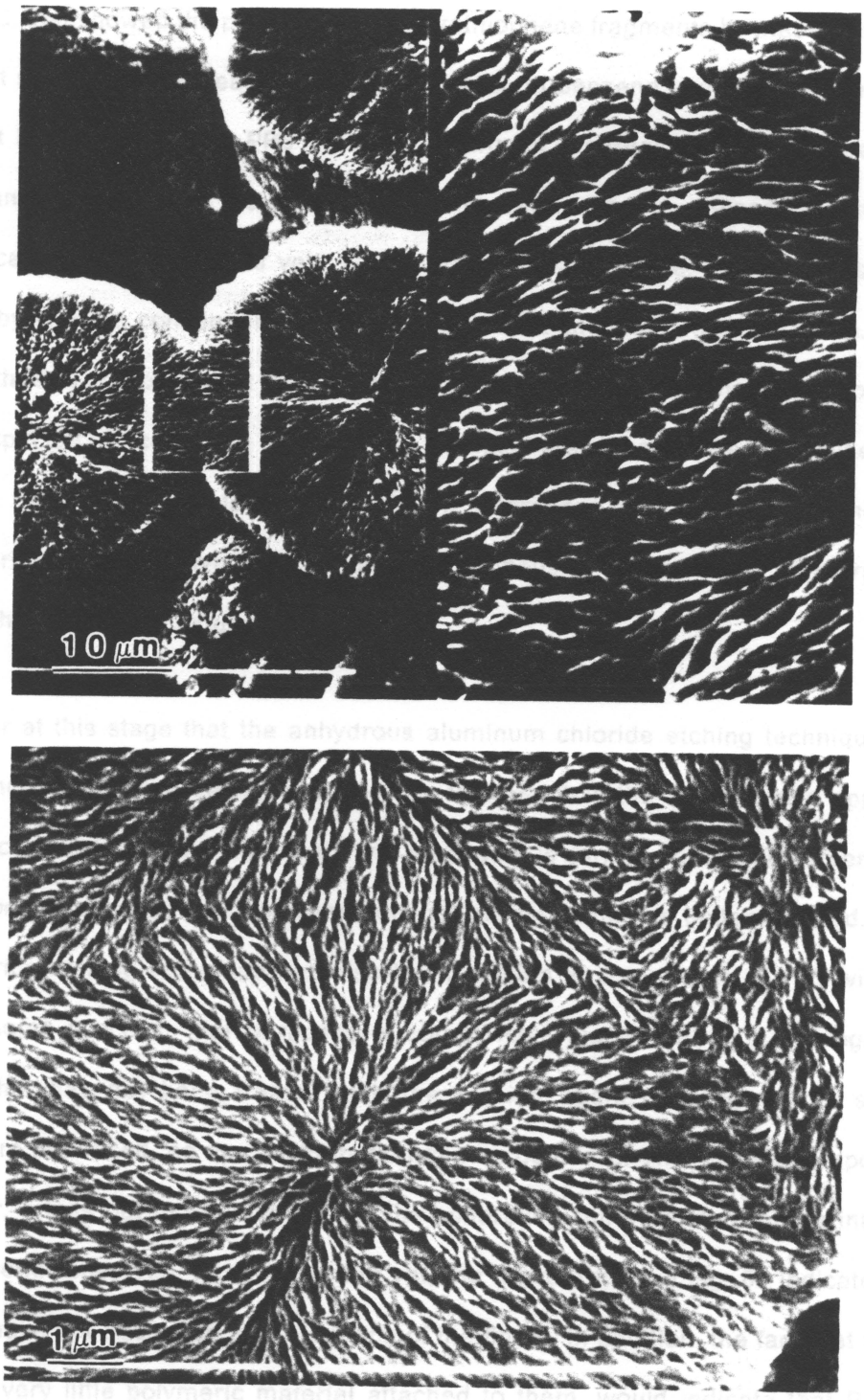


**Figure 66. Impinging spherulites in PPS crystallized at 255°C:** Film surface etched with aluminum chloride reagent at 35°C. (a) Two impinging spherulites. Stage tilt 30° Magnification: 1500X, 7500X. (b) Area of multi-spherulitic impingement. Magnification: 10000X.

above 500°C, that showed the presence of dibenzothiophene fragments by mass spectrometry. Therefore, it seems that the reaction of PPS with $AlCl_3$ in benzene is very dependent on temperature. At low temperatures, PPS would be destroyed; whereas at high temperatures, degradation and condensation would occur. The reaction scheme utilized to enhance the morphological textures of PPS is very similar. In the present case, the solvent benzene is substituted by toluene; consequently, a very similar reaction series may take place. Since the etching method is performed at low temperature (35°C), the depolymerization of the PPS would be expected to occur. Due to the higher chemical resistance of the crystalline polymer, the reaction rate is expected to be higher at the amorphous phase. Therefore, the reaction allows the preferential depolymerization of the amorphous PPS to enhance the morphological features of the crystalline textures.

It is clear at this stage that the anhydrous aluminum chloride etching technique gives a better enhancement of fine details of spherulitic textures than the chromic acid approach. In addition, since the aluminum chloride etching procedure is carried out at low temperature, the problem of possible reorganization of the polymer during etching is better avoided. This aluminum chloride etching technique has also been applied to composites of PPS with carbon fibers with some success. For purposes of comparison, Fig. 67 shows a micrograph of a composite that has not been treated with the etching agent. Although some spherulitic superstructure is noticed, no more information can be gathered. The treated composite (Fig. 68), however, brings out more information. The spherulitic superstructure of the interfibrillar material is better observed. More important yet, the micrographs in Fig. 68 indicate that the spherulites have not nucleated at the surface of the fibers. In addition, the fact that the fibers appear with very little polymeric material attached to them, would indicate that PPS has a structure close to the fiber interface that can not resist the reagent attack. That is, PPS is either amorphous at the interface, or the crystalline structure does not have such a good chemical resistance as the spherulitic material. In any case, these observations lead to the

conclusion that fiber surface preparation is an important factor that has to be considered to provide good interfacial adhesion.

To summarize, several points can be stated, based on the experimental observations described previously. First, a better degree of texture enhancement was obtained with the chromic acid reagent in the present study than in that performed by Zeng and Ho (38). Second, selective attack of amorphous PPS was achieved with the aluminum chloride etching reagent. This etching agent enhanced the morphological textures to an even greater extent than the chromic acid reagent. Lastly, the author is confident that the aluminum chloride etching technique will likely be a very useful tool to utilize for the study of the PPS morphology in its fiber composites; in the following chapter, this technique will be utilized to study carbon fiber composites containing very few carbon fibers. In addition, it is believed that this technique will also be useful to prepare samples for STEM or TEM observation.

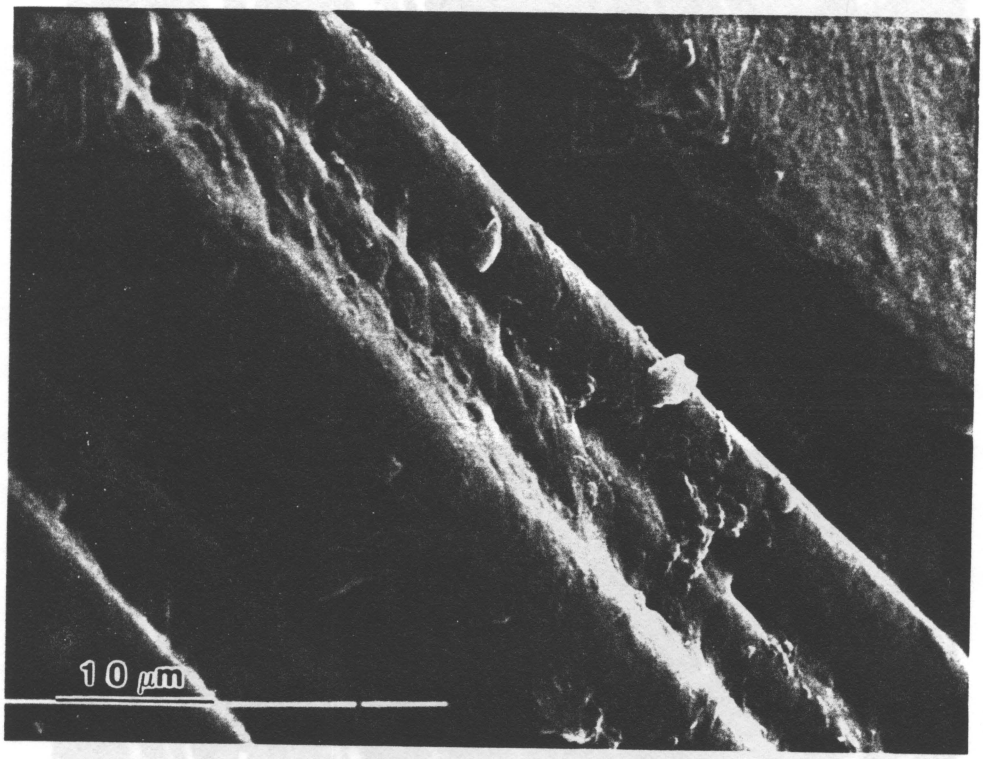


**Figure 67. PPS/C fiber composite unetched:** Stage tilt: 45°. Magnification: 2000X.

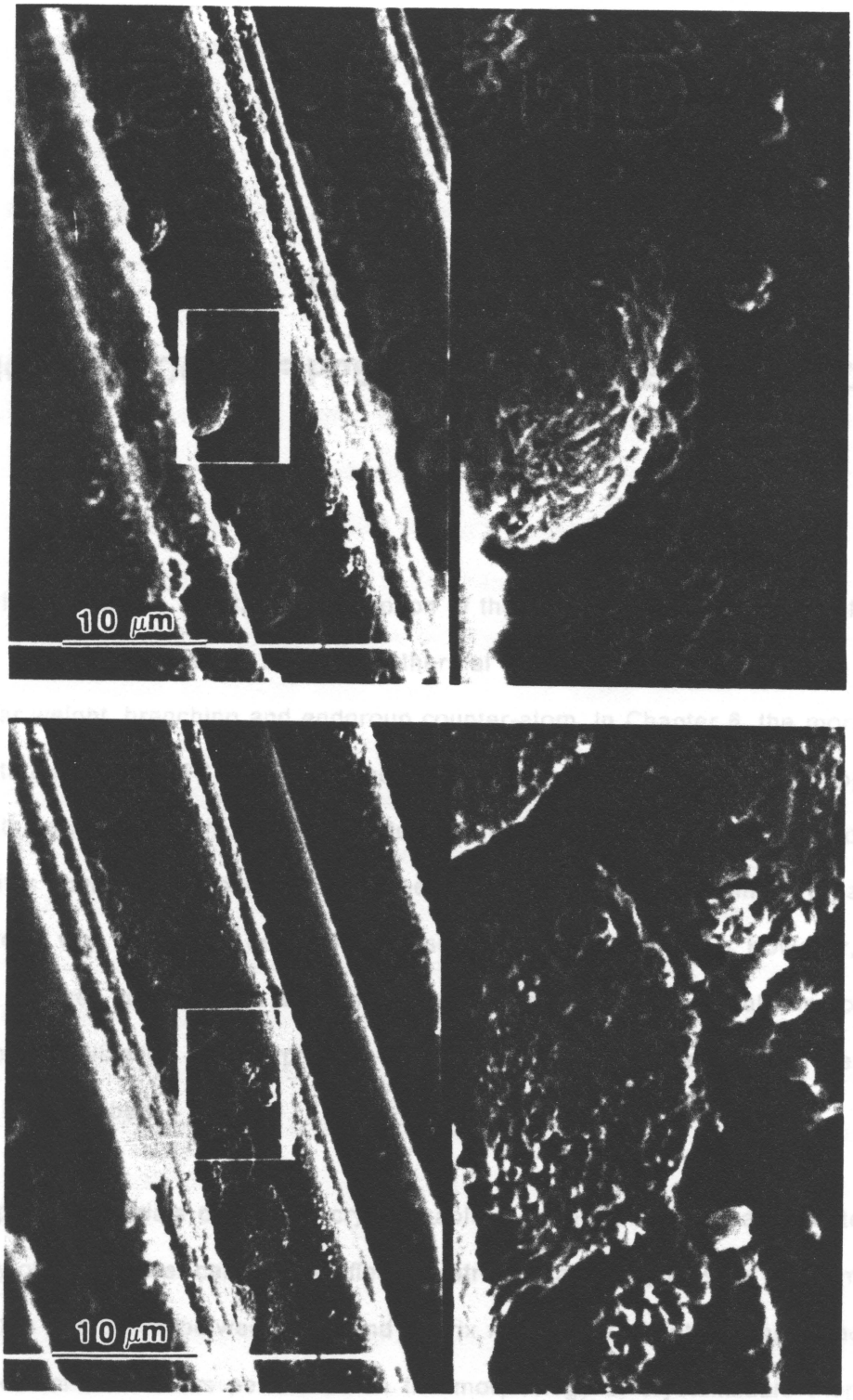


**Figure 68. PPS/C fiber composite etched with aluminum chloride reagent at 35°C:** Aluminum chloride concentration: 1% by weight. Etching time: 4 min. Stage tilt 45°. Magnification: 2000X, 10000X.

# CHAPTER VIII

# THE MORPHOLOGY OF PPS IN CARBON FIBER COMPOSITES

In previous chapters, a detailed description of the kinetics of crystallization of PPS was presented; quiescent isothermal and non-isothermal crystallization was studied as a function of molecular weight, branching and endgroup counter-atom. In Chapter 6, the morphological superstructures of neat PPS were described utilizing scanning electron microscopy in conjunction with an aluminum chloride etching technique. In this chapter, the morphology of PPS in composites containing carbon fibers will be discussed, although not in as great a detail since this topic was not viewed as the primary subject of this dissertation. However, since the interaction between carbon fibers and the matrix polymer can be of particular importance regarding the crystallization and morphology of PPS, some cursory investigations were carried out as will be described.

In composite materials containing crystallizable thermoplastics as matrix materials, the morphology of the polymer can greatly affect the strength and toughness of the composite. In particular, the interaction between fiber and matrix material is of critical importance. In this respect, most of the studies performed on the morphology of crystallizable thermoplastic composites are concerned with establishing whether the reinforcing fibers can heterogeneously nucleate crystallization of the polymer matrix. If the heterogeneous

nucleation density on the fibers is high, a transcrystalline morphology will develop. Under these circumstances, the lamellae which grow from the fiber surface can propagate in only one direction (normal to the surface) since lateral growth is restricted by neighboring lamellae. A cylindrically symmetric superstructure is formed around the fiber. This phenomenon has been observed in a variety of polymer systems against carbon fibers (120-123), glass fibers (201) and thermoplastic fibers (202-204).

Reports on the effect of transcrystallinity on the properties of composites are contradictory. For example, Lee and Porter (122) stated that the transverse toughness (normal to the fiber long axis) of PEEK/C fiber composites was higher for samples that presented transcrystallinity due to an increase of the fiber-matrix bond strength. However, the interfacial shear strength of nylon 66/C fiber composites was shown to decrease 25% when transcrystallinity develops, indicating that fiber-matrix bond strength is reduced in the case of transcrystallinity (206). Similarly, determination of critical fiber length in this same system indicated that the interfacial bond strength of samples having transcrystallinity was lower than those having no significant interfacial morphology (206). Huson and McGill (205) reported that transcrystallinity generated in polypropylene/copper fiber composites produced an increase in the elongation at yield. In a different context, Kwei et al. (207) studied the dynamic mechanical properties of polyethylene and polypropylene containing transcrystalline regions of different thicknesses. Samples tested in a direction perpendicular to the growth direction of transcrystallinity showed that the storage modulus decreased as the thickness of the transcrystalline regions decreased. Moreover, these same authors fitted the experimental data with a model in "parallel" in which the modulus of the transcrystalline region is higher than that of the bulk polymer.

Reports on the conditions that may induce transcrystallinity are as contradictory as those on the effect of transcrystallinity on the properties of composites. Several factors have been suggested as influencing the formation of transcrystalline regions. These include chemical composition of the substrate (208,209), the crystalline morphology of the substrate (212), the

topography of the fibers (213), the adsorption of heterogeneous nucleants present in the bulk of the polymer matrix (206), and the processing conditions. It was indicated that similarity of chemical composition between polymer and substrate surface was a necessary condition for nucleation (208,209). Similarly, it was stated that a crystalline substrate was necessary to nucleate transcrystallinity (210) and that close match between the crystal lattice parameters of substrate and polymer was also needed (211). In addition, a high surface energy substrate seemed to be of importance in nucleating transcrystallinity (212). However, Campbell and Qayyum (204) showed that chemical similarity was not a critical factor. They found that polyester and nylon fibers (polar) could nucleate transcrystallinity in polypropylene (non-polar) having no chemical similarity. Furthermore, the need of a high surface energy substrate was not important, since polyester fibers with lower surface energy could also nucleate transcrystallinity. Similar conclusions were reached by Chatterjee et al. (209) and Gray (214). It was also shown that the crystalline morphology of the substrate was not important. Chatterjee et al. (209) reported that a close match of crystal lattice parameters between substrate and crystallizing polymer was not a necessary condition. Moreover, crystallinity of the substrate was also shown to be an unnecessary condition, since glass fibers (that are amorphous) also induced transcrystallization in polypropylene (201,214).

The ongoing discussion makes clear that the understanding of transcrystallinity is not very precise; however, since the morphology of crystallizable polymers is highly dependent on processing conditions, transcrystallization is bound to be affected by the processing conditions applied to the composite material. In this respect, several reports indicate that melting temperature, time in the melt, crystallization conditions and external stresses can have some effect on the nucleation of transcrystallinity (122,123,201,209,215). Fitchmun and Newman (215) stated that rapid cooling rates and high crystallization temperatures promoted transcrystallinity in polyethylene molded against poly (ethylene terephthalate). On the contrary, Chatterjee et al. (209) showed that with increasing crystallization temperatures the surface morphology of a series of polymers against a series of substrates changed from

transcrystalline to spherulitic. Tung and Dynes (123) reported that slow cooling rates favored the formation of transcrystallinity in PEEK/carbon fiber composites; and Lee and Porter (122) indicated that as the time in the melt of PEEK/C fiber composite increased from 0.5 hr to 4 hr, the final PEEK morphology changed from having no transcrystallinity to the development of a very thick transcrystalline region. Furthermore, transcrystallinity can be promoted by crystallizing under a temperature gradient. For example, Kwei et al. (207) utilized a temperature gradient across the thickness of polyethylene and propylene melts to originate transcrystalline regions of variable thickness. Apparently, the effect of processing conditions are also contradictory, and they seem to be particular to each system studied. Therefore, the author started a program to investigate the effect of processing conditions, carbon fiber kind, and fiber surface treatment on the morphology of PPS in PPS/C fiber composites containing few fibers. The details of this cursory study will now be presented.

## *8.1 EXPERIMENTAL*

Commercial grade Ryton V1 poly(phenylene sulfide) from the Phillips Petroleum Company was utilized as the matrix material. The weight average molecular weight was 32,400. A second Poly (phenylene sulfide) with $<M_w>$ = 63,000 was also used to study the effect of molecular weight on the morphology of PPS in PPS/C fiber composites.

The carbon fibers were generously provided by Dr. T. Devilbiss of the Chemistry Department at Virginia Tech. The carbon fibers utilized are poly(acrylonitrile)-based fibers, and are considered to be high-strength low-modulus carbon fibers. The fibers included XAU fibers manufactured by Courtaulds, AU4 fibers manufactured by Hercules Aerospace Magna, and T300U fibers manufactured by Union Carbide. These fibers are all finish free, that is, they did

not undergo surface treatments by the manufacturer. In addition, Devilbiss also provided the author with well characterized fibers that were anodized in NaOH and in $H_2SO_4$ electrolytes.

Several factors contributed to the selection of these fibers. The fibers were well characterized in terms of the surface characteristics. For example, the surface roughness was found to increase in the order AU4 < XAU < T300U (216) and the surface topography was not affected by the anodization methods. Furthermore, Devilbiss (216) reported that the interfacial shear transfer coefficients (ISTC) in composites with bisphenol-A polycarbonate, bisphenol-A polysulfone and polyetherimide were increased by the anodization process on the fibers. In other words, the anodization processes seemed to have improved the adhesion of fibers to the thermoplastic matrices. Therefore, one can speculate that these surface treatments may affect the formation of transcrystallinity. The fibers utilized, then, allowed the study of the effect of fiber kind, surface topography and surface treatment of the fiber on the nucleation of transcrystallinity in PPS. Furthermore, the effect of processing conditions on nucleation at the fiber surface could also be analyzed.

Prior to preparation of the samples, all the fibers were dried at 120°C in a vacuum oven for 24hr. Composites with very few fibers were prepared by placing a few carbon fibers between two polymer films in a microscope slide and set in the heating stage of a Zeiss polarized optical microscope. The samples were heated to the melt; in the melt, some pressure was applied to the cover glass to obtain a homogeneous thin film. The composites were maintained at 315°C for 4 min. For isothermal crystallizations the samples were quenched rapidly to the crystallization temperature. For non-isothermal crystallizations, the composites were cooled at constant cooling rates. A nitrogen purge through the system was maintained during the whole procedure. Crystallization was followed by taking photographs with a 35mm camera attached to the microscope. Each crystallization was reproduced at least twice.

## 8.2 RESULTS AND DISCUSSION

Figures 69 and 70 present the effect of crystallization conditions on the morphology of PPS/T300U carbon fiber composite. In Fig. 69, the effect of isothermal crystallization temperature is shown. Samples crystallized at 245°C, 220°C, 200°C, and 180°C are included. In this figure, the thermal history prior to crystallization is the same for every specimen. Therefore, the differences observed can only be attributed to the different crystallization temperatures. The T300U fiber seems to heterogeneously nucleate the crystallization of PPS. Figure 69a presents a row of spherulites that have nucleated at the fiber surface when crystallization was performed at 245°C. However, the nucleation density on the fiber is not as high to produce transcrystalline regions. Nevertheless, a few comments need be made at this point. Nucleation does not occur preferentially on the fiber. In the nucleation process, there is a competition between nucleating sites on the fiber surface and nucleating sites in the bulk of the polymer matrix. When the competition is highly favorable to the fibers, transcrystallinity develops. At 245°C, the nucleation density seems to be very similar in the bulk and at the fiber surface. Consequently, nucleation on the fiber is observed, but the nucleation density is too low to create transcrystallinity.

The spherulitic size indicates a bimodal distribution of sizes. There are spherulites with radius of approximately 60μm and 40μm. In addition, the size of the spherulites that nucleated at the fiber is the same as that of spherulites nucleated in the bulk of the polymer. Since the radial growth rate of spherulites nucleated in the bulk is the same as that of spherulites nucleated onto the fiber surface, the similar sizes indicate that nucleation occurred simultaneously on the fiber surface and in the bulk polymer, confirming the lack of preference for nucleation at the fiber surface.

Lowering the crystallization temperature affects the balance observed at 245°C. At lower temperatures, the nucleation density increases in the bulk and at the fiber surface. However,

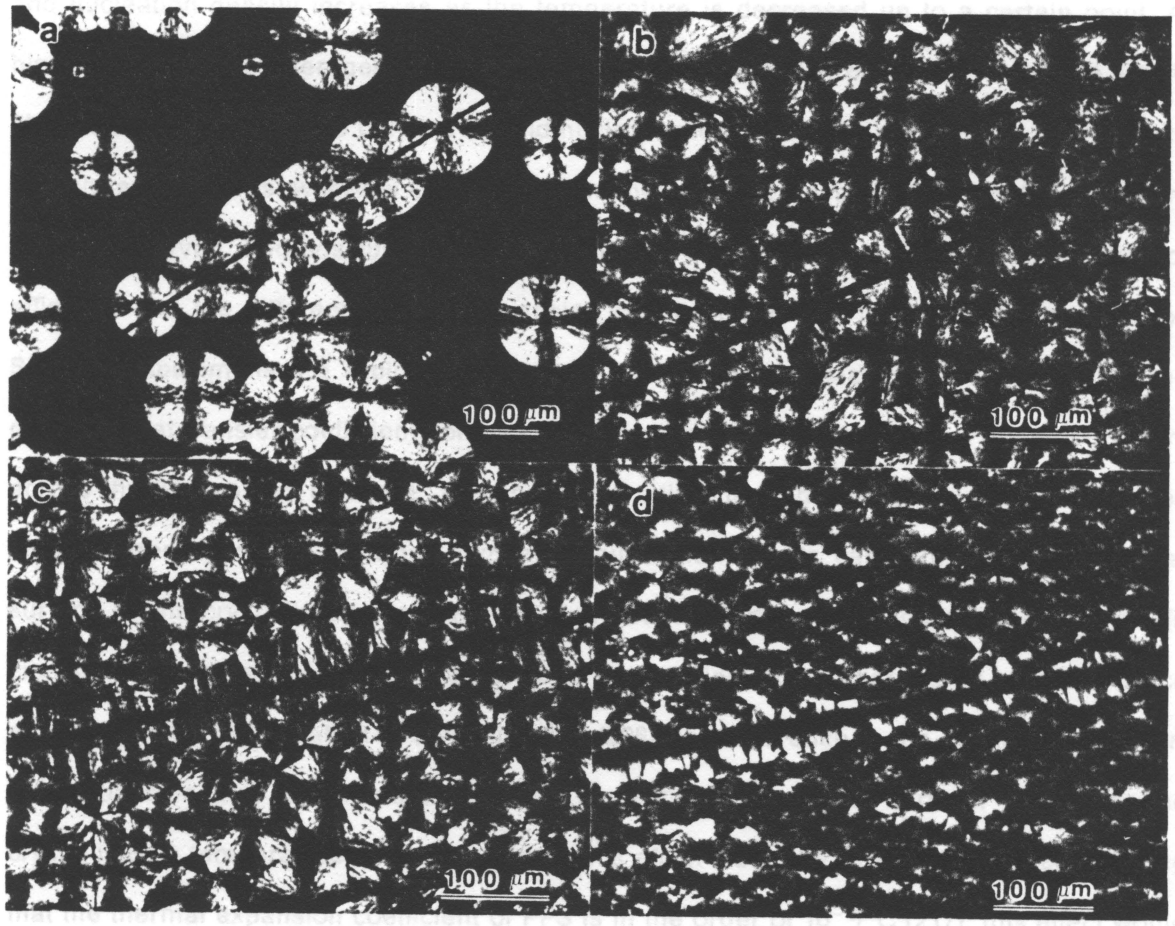


**Figure 69. Effect of crystallization temperature on the morphology of PPS/T300U carbon fiber composite:** (a) T = 245°C; (b) T = 220°C; (c) T = 200°C; (d) T = 180°C.

it is clearly seen in Fig. 69 that a transcrystalline region has developed when crystallization was performed at 200°C. That is, PPS is nucleating more efficiently on the fiber surface than in the bulk of the polymer. The traditional nucleation theory indicates that the nucleation rate and nucleation density increases as the temperature is decreased up to a certain point. At high temperatures, heterogeneous nucleation will be favored; in particular, since the T300U fiber can nucleate PPS, the polymer should nucleate more preferentially onto the fiber surface at high temperatures, whereas bulk nucleation should be depressed. Nevertheless, the contrary is observed. Two possible explanations may be extended: the different heat transfer coefficients and the different thermal expansion coefficients of the fiber and polymer matrix. Since the specimens are rapidly cooled from 315°C to the crystallization temperature, the different heat transfer coefficients of the carbon fiber and PPS may induce a thermal gradient across the fiber-matrix interface. This thermal gradient is higher at the lower crystallization temperatures; therefore, a larger number of nucleation events can take place at the fiber surface as the crystallization temperature decreases. Furthermore, the difference in coefficients of thermal expansion would create a stress gradient at the fiber-matrix interface. Since stress can induce nucleation of crystallization (206), the difference in the coefficients of thermal expansion may contribute to produce nucleation at the fiber surface. The lower the crystallization temperature, the more critical this effect would be. Nevertheless, considering that the thermal expansion coefficient of PPS is in the order of $10^{-5}$/°C (217), this effect would be of minimum importance. Therefore, the difference in heat transfer coefficients would contribute to generate the morphology changes associated with the different crystallization temperatures observed in Fig. 69.

Figure 70 presents micrographs corresponding to samples that were crystallized non-isothermally at selected cooling rates. The cooling rate clearly affects the nucleating ability of the fiber. The results are in slight contradiction with the ones shown in Fig. 69. As the cooling rate is decreased from 60°C/min to 2°C/min, the nucleation density at the fiber surface increased. At a cooling rate of 10°C/min, an almost transcrystalline region can be observed

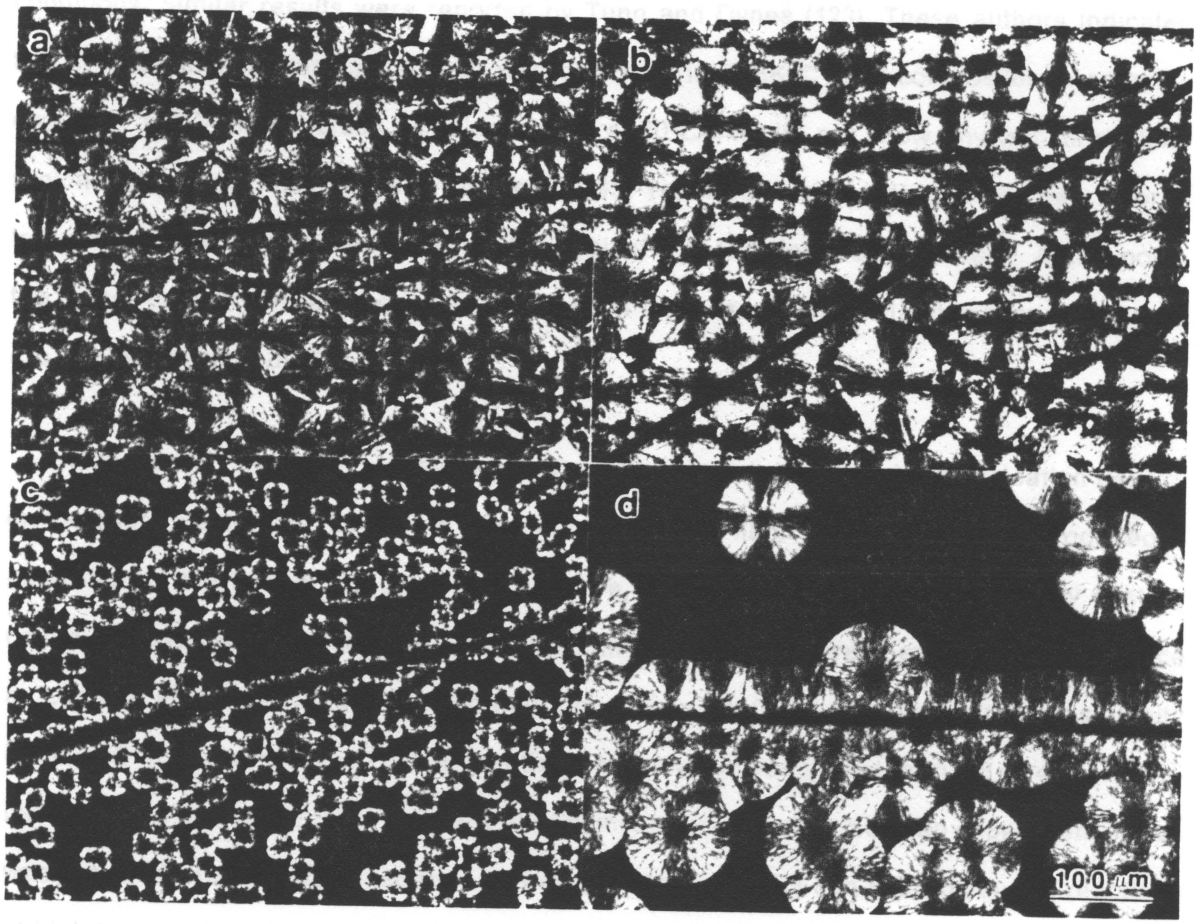


**Figure 70. Effect of crystallization cooling rate, φ, on the morphology of PPS/T300U carbon fiber composite:** (a) φ = 60°C/min; (b) φ = 30°C/min; (c) φ = 10°C/min; (d) φ = 2°C/min.

and at 2°C/min, a transcrystalline region of about 100μm in diameter is generated. In this case, the difference in heat transfer coefficient can not be invoked, since transcrystallization occurs at the lowest cooling rate where the fiber and matrix are closer to thermal equilibrium conditions. Similar results were reported by Tung and Dynes (123). These authors indicated that well developed transcrystallinity was observed in PEEK/C fiber composites in samples cooled at 1.5°C/min; whereas samples cooled at 70°C/min did not show any transcrystalline regions. However, Fitchmun and Newman (215) reported that rapid cooling rates favored transcrystallization of polyethylene molded against poly (ethylene terephthalate). At this point, the author does not have reasonable explanation for these phenomena; however, the results are very much reproducible.

Since transcrystallization is favored by conditions which induce a high nucleation density on the substrate surface, there is a competition between fiber nucleation and heterogeneous nucleation in the bulk of the polymer. Therefore, melting conditions that completely destroy crystal embryos will favor transcrystallization. In this context, there is experimental evidence by Lee and Porter (122) that indicated that longer times in the melt induced transcrystallinity in PEEK/C fiber composites. The melting time in that work was varied from 0.5 to 4 hr. A similar effect is expected to occur in PPS/C fiber composites. However, such an experiment series was not conducted. As was described in previous chapters, PPS can undergo curing reactions at high temperature that change the chemical structure of PPS. Since the author's aim was to better understand the phenomenon of transcrystallinity, such a change in chemical structure would only complicate the matter. Therefore, the experiment series was not performed.

In Chapter 5, it was reported that the nucleation density of PPS was higher for higher molecular weight PPS. If nucleation density is very high in the bulk of the high molecular weight polymer, one can speculate that transcrystallinity would not be favored. Figure 71 shows micrographs of PPS/C fiber composites prepared with PPS of different molecular weights crystallized by cooling at 2°C/min. Inserts (a) and (c) of Fig. 71 corresponds to PPS with weight average molecular weight of 32,400 at two two different magnifications. It is obvi-

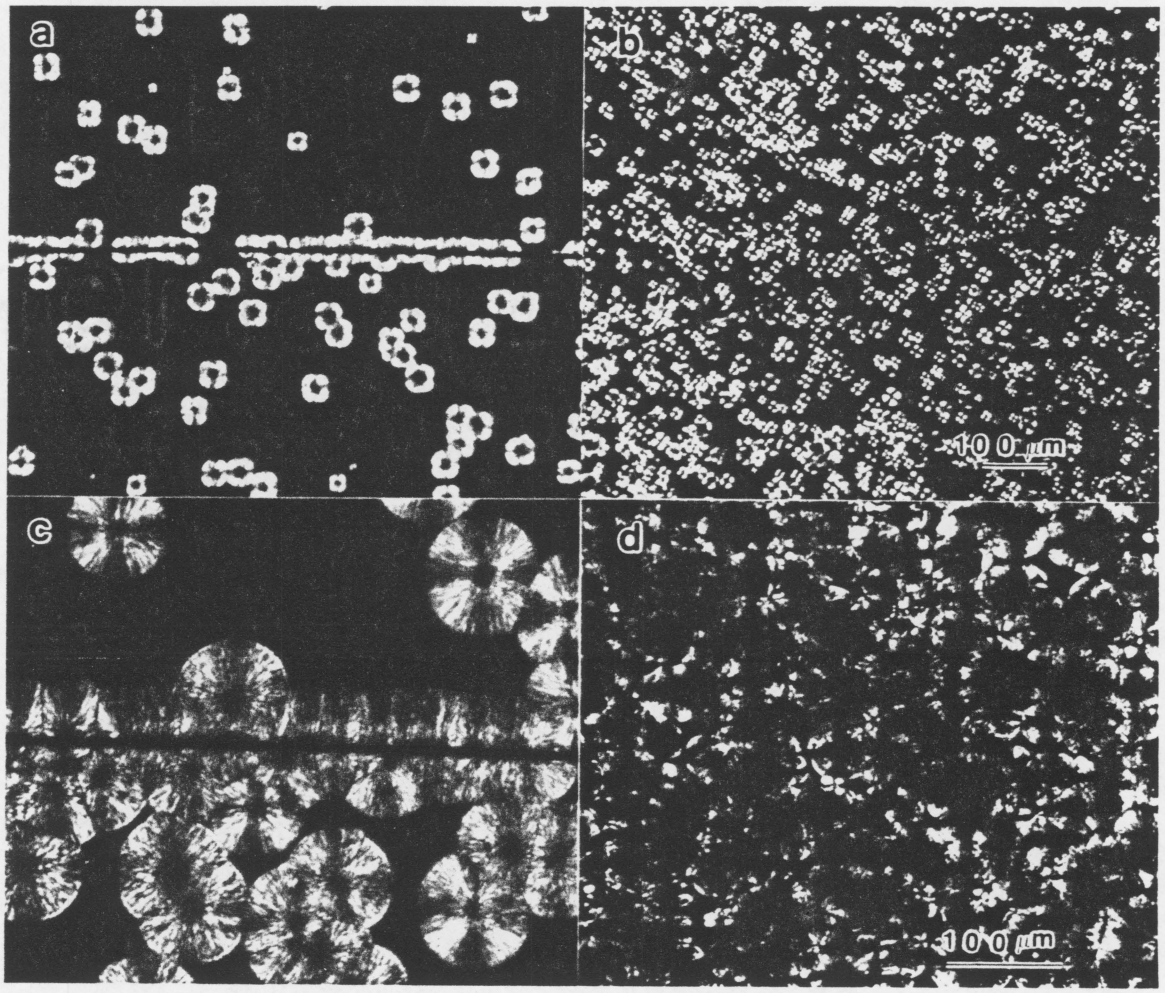


**Figure 71. Effect of polymer molecular weight on the morphology of PPS/T300U carbon fiber composite:** (a) and (c) $< M_W >$ = 32400; (b) and (d) $< M_W >$ = 63000.

ous that transcrystallization occurs. Inserts (b) and (d) present micrographs of specimens with PPS of weight average molecular weight of 63,000 at two different magnifications. No nucleation is observed at the fiber surface in these specimens, which would confirm the speculation mentioned above. Folkes et al. (202) reported that as the melt flow index of polypropylene increased from 1.5 to 22, the nucleation along polyester fibers decreased until no transcrystallinity was observed. Since the melt flow index is inversely related to the molecular weight of the polymer, this implies that the nucleation density on the fiber decreases as the molecular weight of the polymer increases, similar to the results presented in this report. Furthermore, Folkes et al. (202) proposed that adsorption of the polymer molecules on the fiber surface would occur through deposition of chain ends onto the fiber surface. As low molecular weight polymers posses more chain ends, they would nucleate more efficiently on the fiber surface than polymers of high molecular weight. This speculation is in agreement with the experimental results presented in this report. However, in the present case, neat PPS with $<M_w>$ = 63,000 shows a very high nucleation density probably due to heterogeneities present in the melt that nucleate crystallization more efficiently in the bulk as opposed to nucleation on the fiber.

Figure 72 shows micrographs corresponding to samples that contain different carbon fibers that were crystallized by cooling at 2°C/min. There seems to be a decreasing trend in the nucleation efficiency of the carbon fibers in the order T300U > XAU > AU4 which follows Fig. 72a-c respectively. The fiber kind is the only variable in this series of micrographs; therefore, the different nucleating efficiencies of the carbon fibers might be attributed to the chemical composition of the fiber surface, the crystalline morphology and topography of the fiber surface, and the surface energy of the fiber. The total surface energies of the carbon fibers determined by Devilbiss (216) are 42 erg/cm$^2$ for T300U, 56 erg/cm$^2$ for AXU, and 46 erg/cm$^2$ for AU4 fibers. There is no trend relating the nucleating efficiency of the fibers and their total surface energies. Since PPS is not a very polar polymer, it may be instructive to look at the dispersive component of the surface energies. The values are 33 erg/cm$^2$ for T300U, 33

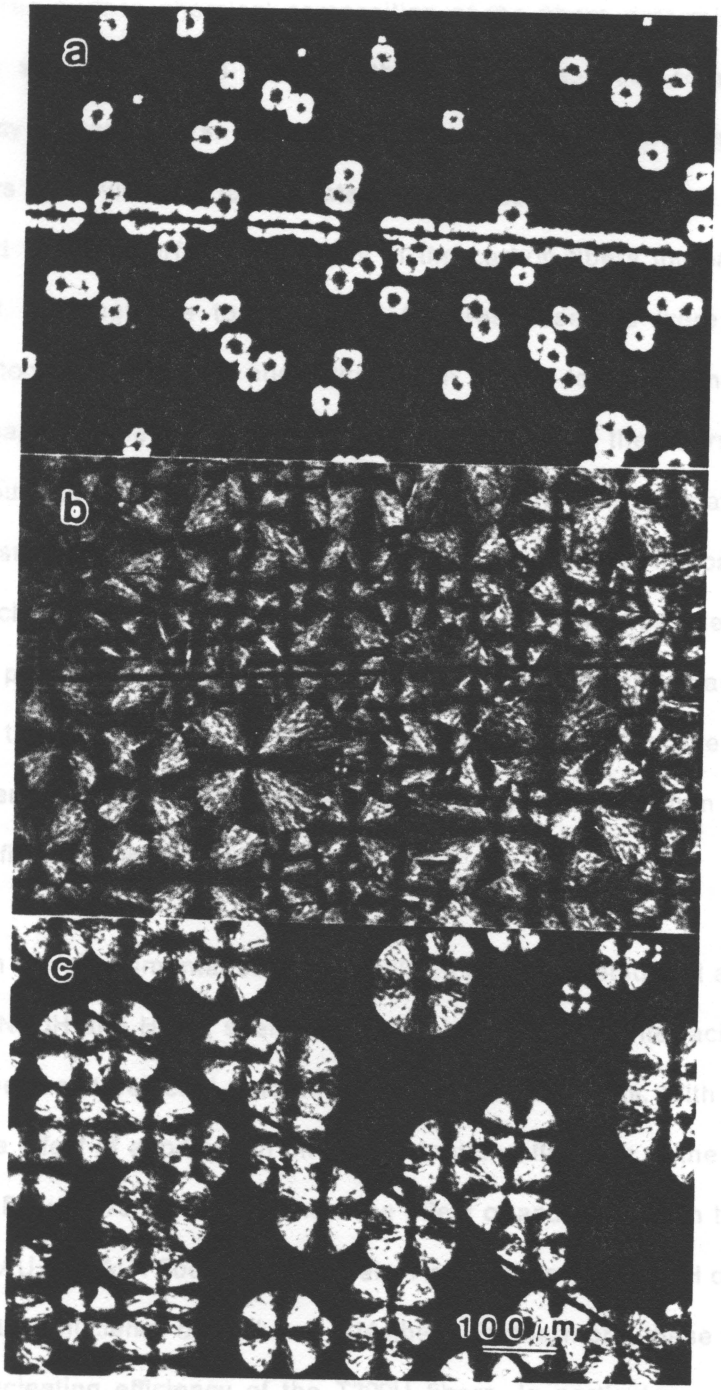


**Figure 72. Effect of carbon fiber type on the morphology of PPS/carbon fiber composite:** (a) T300U; (b) XAU; (c) AU4.

erg/cm² for XAU, and 28 erg/cm² for AU4 (216). However, these values do not reveal any relationship either. The surface chemical composition of the fibers determined by XPS (216) does not indicate any relationship between the surface chemical composition and the nucleating efficiency of these fibers. As stated earlier, scanning electron microscopy studies of the carbon fibers by Devilbiss (216) indicated differences in the surface roughness of the fibers. He reported that the surface roughness of the carbon fibers increased in the order AU4 < XAU < T300U. Although the topographical features observed were in the order of 0.2μm, seemingly too large to affect nucleation at an atomic level, the increasing trend in roughness is the same as the increasing nucleating efficiency of the fibers. Therefore, it is apparent that the surface topography of the fibers may influence the nucleation of PPS at the fiber surface. The surface roughness at an atomic level would be of importance here. High energy features such as dislocations have been proposed as nucleating sites in metals. If the T300U carbon fiber presents more surface defects of high surface energy than the other fibers, then nucleation on the surface of the T300U fibers would be more favorable than in the other carbon fibers. Determination of the specific surface area by gas adsorption techniques might prove useful in confirming this statement.

As expressed in the experimental section, Devilbiss (216) indicated that anodization of the carbon fibers with NaOH and $H_2SO_4$ seemed to have improved the interfacial bond strength between carbon fibers and selected amorphous thermoplastic resins. With this in mind, the author analyzed the effect of anodization on the nucleation efficiency of the T300U, XAU and AU4 carbon fibers. Figures 73, 74 and 75 show the effect of anodization on the nucleation efficiency of T300U, XAU and AU4 fibers, respectively. Anodization with NaOH or $H_2SO_4$ does not improve the nucleating efficiency of XAU and AU4 fibers. Furthermore, these treatments seem to decrease the nucleating efficiency of the T300U fibers. In particular, anodization of the T300U fibers in NaOH electrolyte is very effective in decreasing the nucleating ability of this fiber. The interesting point is that the anodization methods did not change the surface topography at a microscopic level (216). Therefore, there may be another controlling factor. The

total surface energies of the T300U fibers were reported to increase from 42 erg/cm$^2$ to 57 erg/cm$^2$ (216). This increase was fully due to an increase of the polar component of the surface energy from 10 erg/cm$^2$ to 24 erg/cm$^2$. Since PPS is a rather non-polar polymer, the increased polarity of the carbon fiber surface may affect the interaction between fiber and matrix; consequently, decreasing the nucleating efficiency of the T300U carbon fibers. The T300U fibers anodized in $H_2SO_4$ electrolyte presented some nucleation at the fiber surface. The nucleation density, however, was slightly lower than that for the untreated fiber (Fig. 73). The $H_2SO_4$ anodization increased the polar component of the surface energy by only a 20%. Therefore, for the T300U carbon fibers there seems to be an inverse relationship between the nucleating efficiency of the fibers and the value of the polar component of the surface energy; i.e., the higher the polar component of the surface energy, the lower the nucleating efficiency of the carbon fibers.

Figure 76 shows the effect that strain can have in inducing transcrystallinity on a specimen containing XAU fibers that were anodized in NaOH electrolyte. Figure 76a shows the "control" specimen, that is, a specimen that did not present any nucleation at the fiber surface. Insert (b) presents a specimen in which the carbon fiber was pulled with tweezers at a temperature of 270°C while the specimen was cooled at 2°C/min. The effect is clear, the shear strain induced in the melt by the pulled fiber produced local orientation of the polymer melt and induced a very high nucleation density at the fiber surface that lead to transcrystallization. It is interesting to observe in insert (b) that there is another fiber that was not pulled. This fiber does not present any nucleation events on its surface, making evident the effect of strain on generating transcrystallinity. Similar effects have been previously observed in polypropylene/glass fiber composites (201,214).

Considering the high concentration of fibers usually used in composite materials, the effect discussed in the previous paragraph can be of major importance in determining the morphology at the fiber-matrix interface. In particular, in molding operations there may be shearing flow generated at the fiber-matrix interface that can be very important in defining the

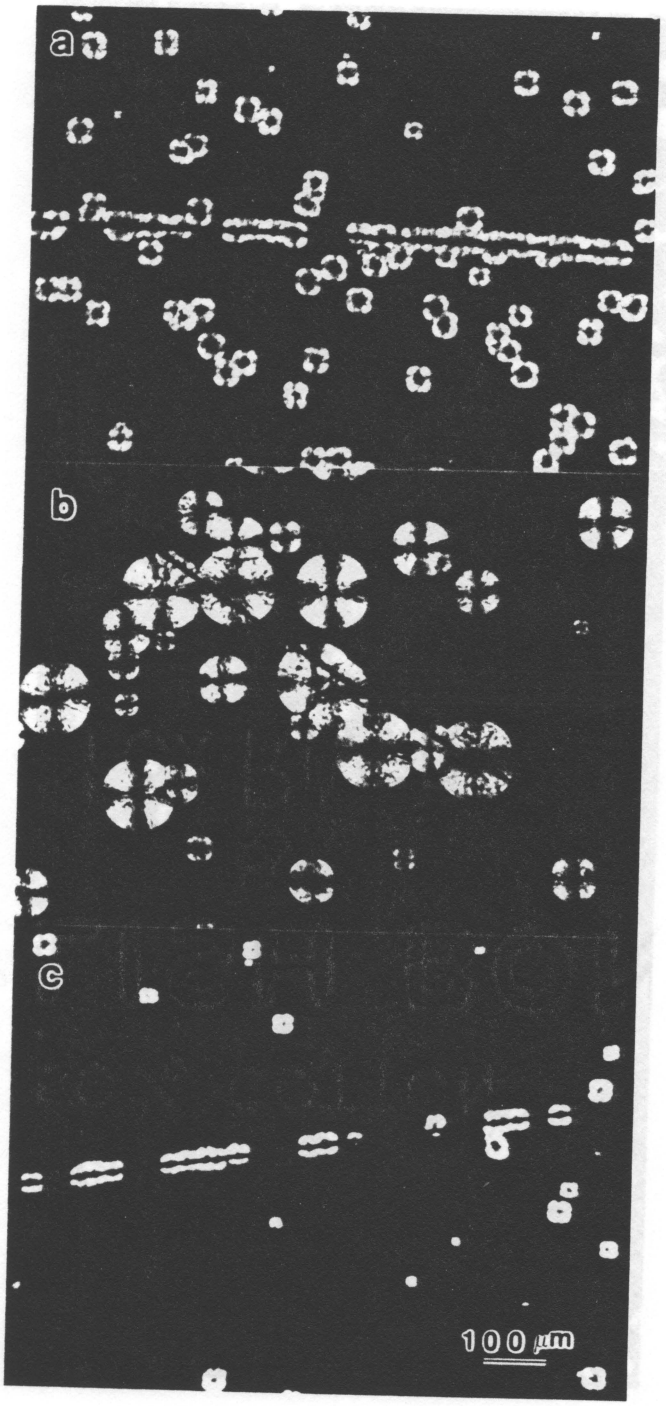


**Figure 73.** **Effect of fiber surface anodization on the morphology of PPS/T300U carbon fiber composite:** (a) untreated; (b) NaOH anodization; (c) $H_2SO_4$ anodization.

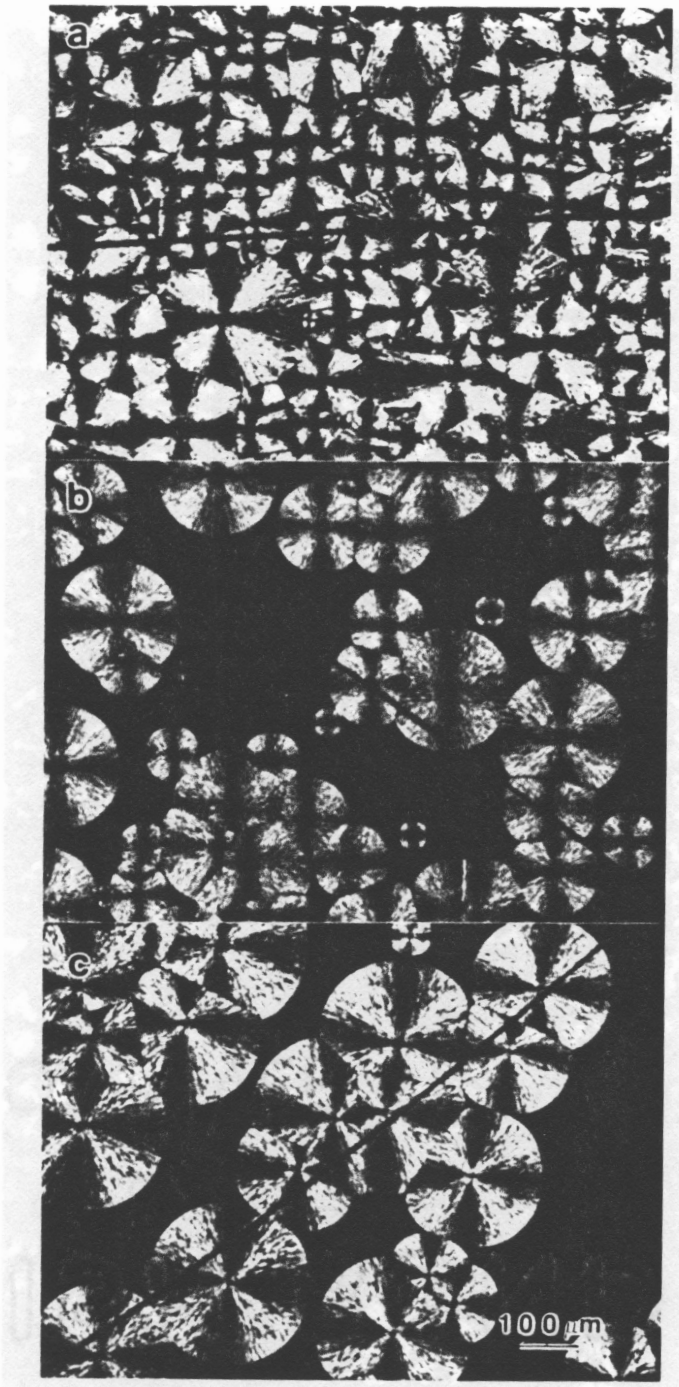


**Figure 74. Effect of fiber surface anodization on the morphology of PPS/XAU carbon fiber composite:** (a) untreated; (b) NaOH anodization; (c) $H_2SO_4$ anodization.

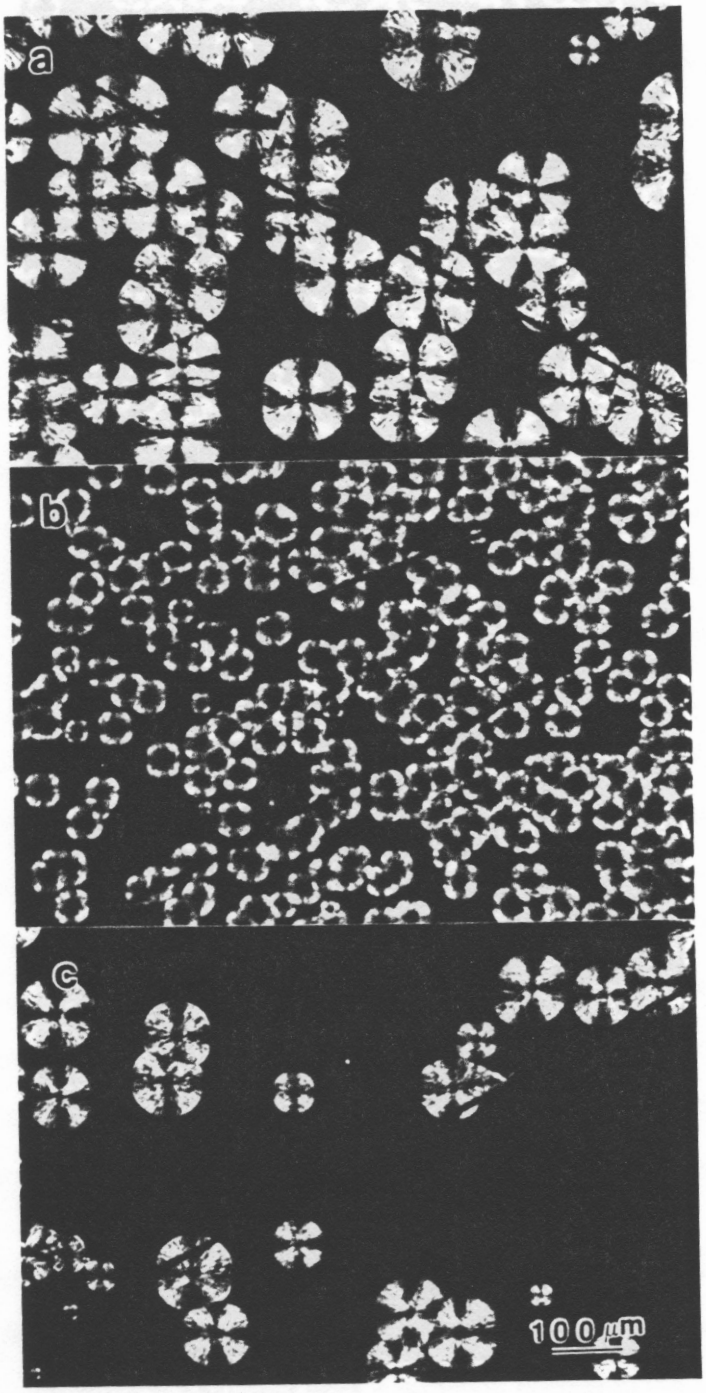


**Figure 75. Effect of fiber surface anodization on the morphology of PPS/AU4 carbon fiber composite:** (a) untreated; (b) NaOH anodization; (c) $H_2SO_4$ anodization.

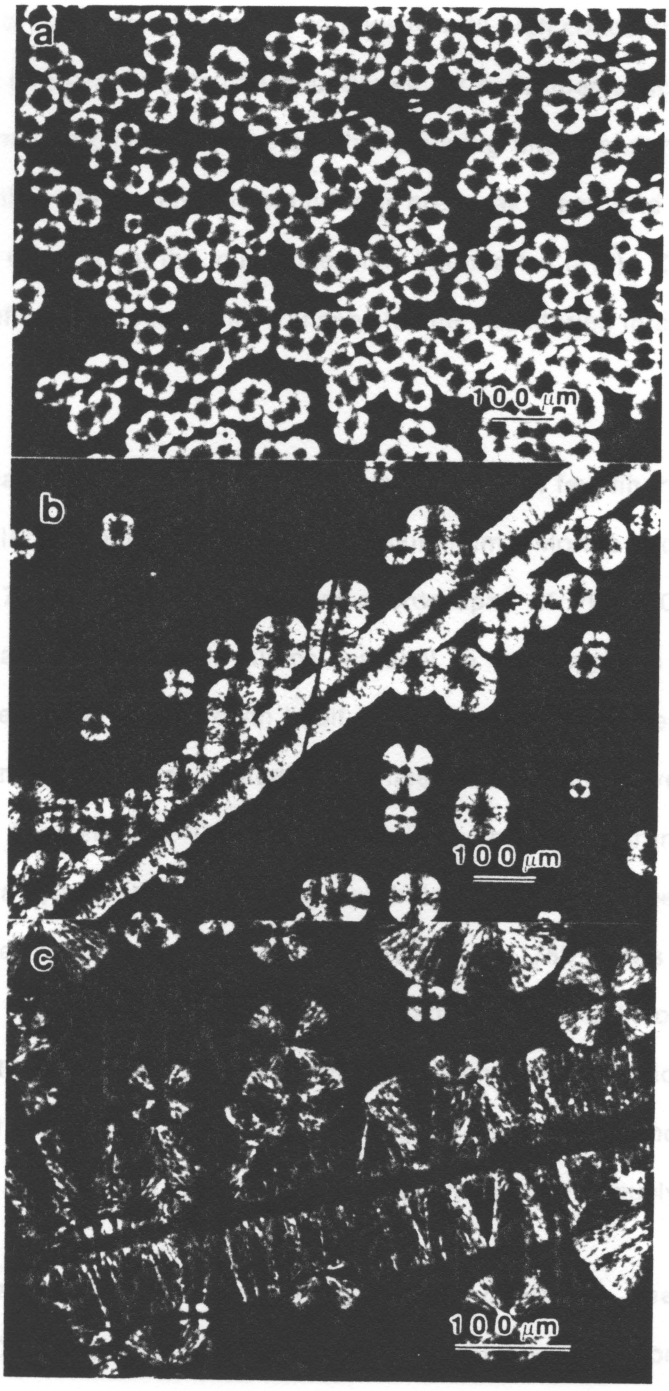


**Figure 76. Effect of strain on the morphology of PPS/NaOH anodized XAU carbon fiber composite:** (a) no strain; (b) fiber pulled; (c) fiber pulled.

local morphology around fibers, and in turn affect the properties of the composite. In this respect, the presence of transcrystallinity in a composite with high concentration of fibers raises questions about the inter-transcrystalline boundaries. At high fiber concentration, the transcrystalline regions may impinge into one another creating inter-transcrystalline boundaries (Fig. 77). It is known that inter-spherulitic boundaries are weak areas, and that under long term testing, microcracks originate at the inter-spherulitic boundaries (218). Consequently, a similar weak boundary effect may occur with transcrystalline boundaries in composites with high fiber concentration.

The morphological features of PPS/C fiber composites with few fibers were also studied utilizing scanning electron microscopy and the aluminum chloride etching technique described in Chapter 7. Figure 78 presents two micrographs of PPS/T300U composite. The micrographs were taken at an angle almost parallel to the long axis of the fiber. These micrographs show very clearly the growth habit of the transcrystalline region. The "fibrils" of the transcrystalline region have nucleated at the fiber surface and have grown radially, or perpendicular to the fiber surface. This figure effectively shows that transcrystallinity developed on a fiber has a cylindrically symmetric morphology around the fiber as long as it does not impinge with other crystallizing regions. Furthermore, Fig. 78b shows the impingement of the transcrystalline region with a spherulite nucleating in the bulk of the polymer. The boundary can be noticed, however, there seems to be very good connectivity of the "fibrils" of the spherulite and those of the transcrystalline region. This phenomenon may be of importance and perhaps it may reduce the effect of weak boundaries previously discussed.

Another view of a transcrystalline region is presented in Fig. 79. These micrographs represents a PPS/T300U composite after etching with the alumimum chloride reagent. In this case, the polymer composite is observed from a direction normal to the long axis of the fiber. Two important features are observed. The radial growth habit is clearly seen in this micrograph. The "fibrils" extend perpendicular to the fiber surface in a radial fashion. The other feature concerns the presence of weak boundaries between spherulites and transcrystalline

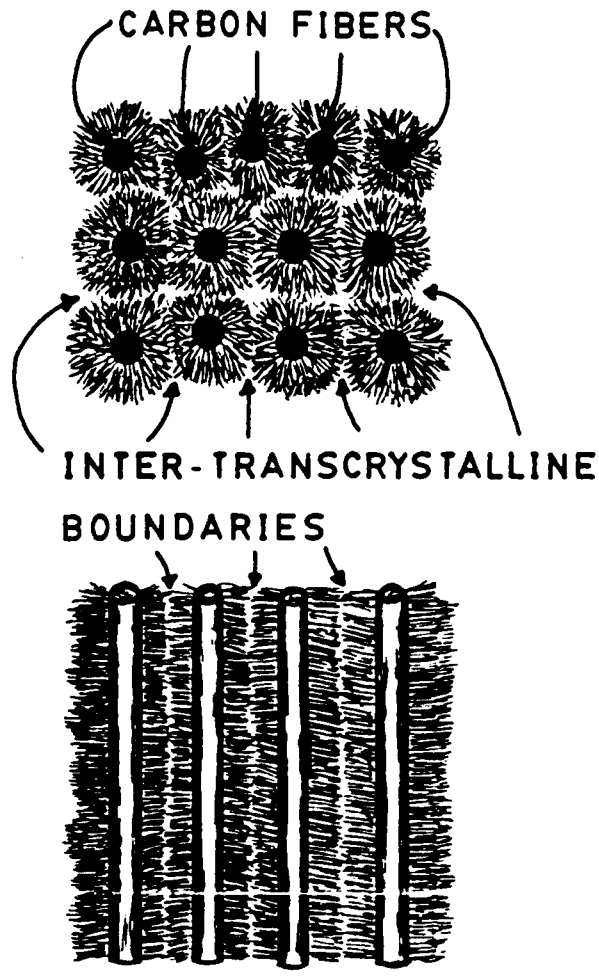


**Figure 77.** Schematic representation of impinged transcrystalline regions developed on carbon fibers.

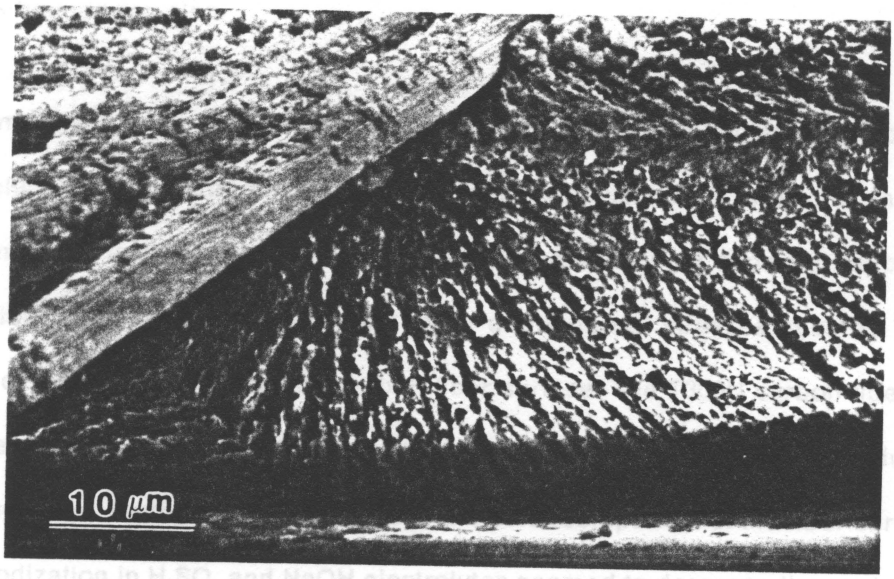


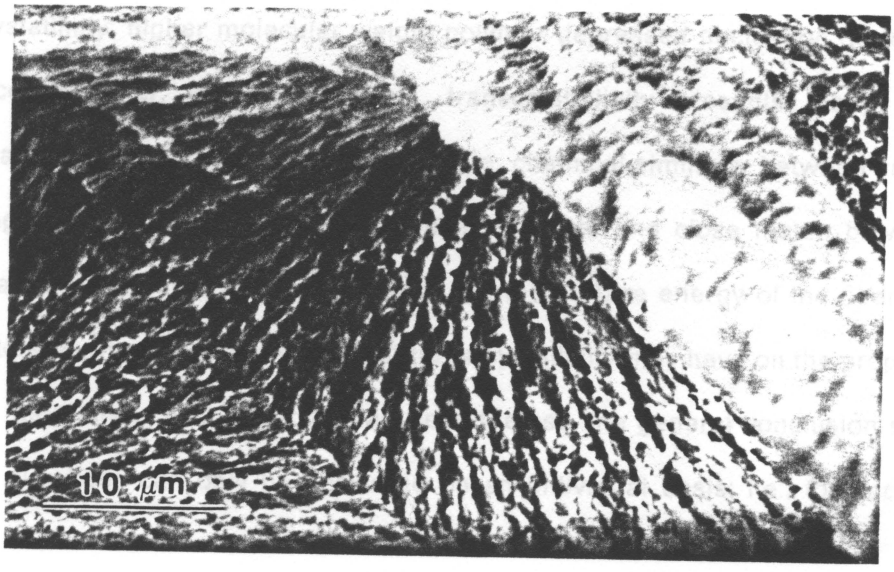


**Figure 78. SEM micrographs of PPS/T300U carbon fibers etched with aluminum chloride reagent.**

regions. These boundaries seemed to be attacked more strongly than the spherulitic or transcrystalline regions. Therefore, these boundaries are at least weak for the attack of aluminum chloride agent. Nevertheless, as expressed before, they are expected to be mechanically weak boundaries also.

In summary, the experimental results described in this section indicate the complexity involved in elucidating the controlling factors of transcrystallization. It is evident that there are several controlling factors. Indeed, the processing conditions were shown to be crucial. Low crystallization temperatures, slow cooling rates and external stresses seemed to favor the nucleation of transcrystallinity on the carbon fiber surface. The T300U carbon fibers from Union Carbide were the most effective in nucleating transcrystallinity presumably due to higher surface roughness. Furthermore, increases in the polar component of the fiber surface energy through anodization in $H_2SO_4$ and NaOH electrolytes seemed to decrease the nucleating ability of the T300U carbon fibers. The molecular weight of the polymer also affected the nucleation of transcrystallinity; higher molecular weight polymer depressed nucleation on the carbon fiber surface. However, in general terms, transcrystallinity presents many unanswered questions and topics of controversy. For example, chemical similarity between substrate and crystallizing polymer, the need of a crystalline substrate and close match between crystal lattice parameters of substrate and polymer, and the surface energy of the fiber are controversial factors. Furthermore, the effect that transcrystallinity may have on the properties of the composite materials is also controversial. Nevertheless, the general conclusion seems to be that these questions can only be answered on an individual basis; i.e., for each particular system.

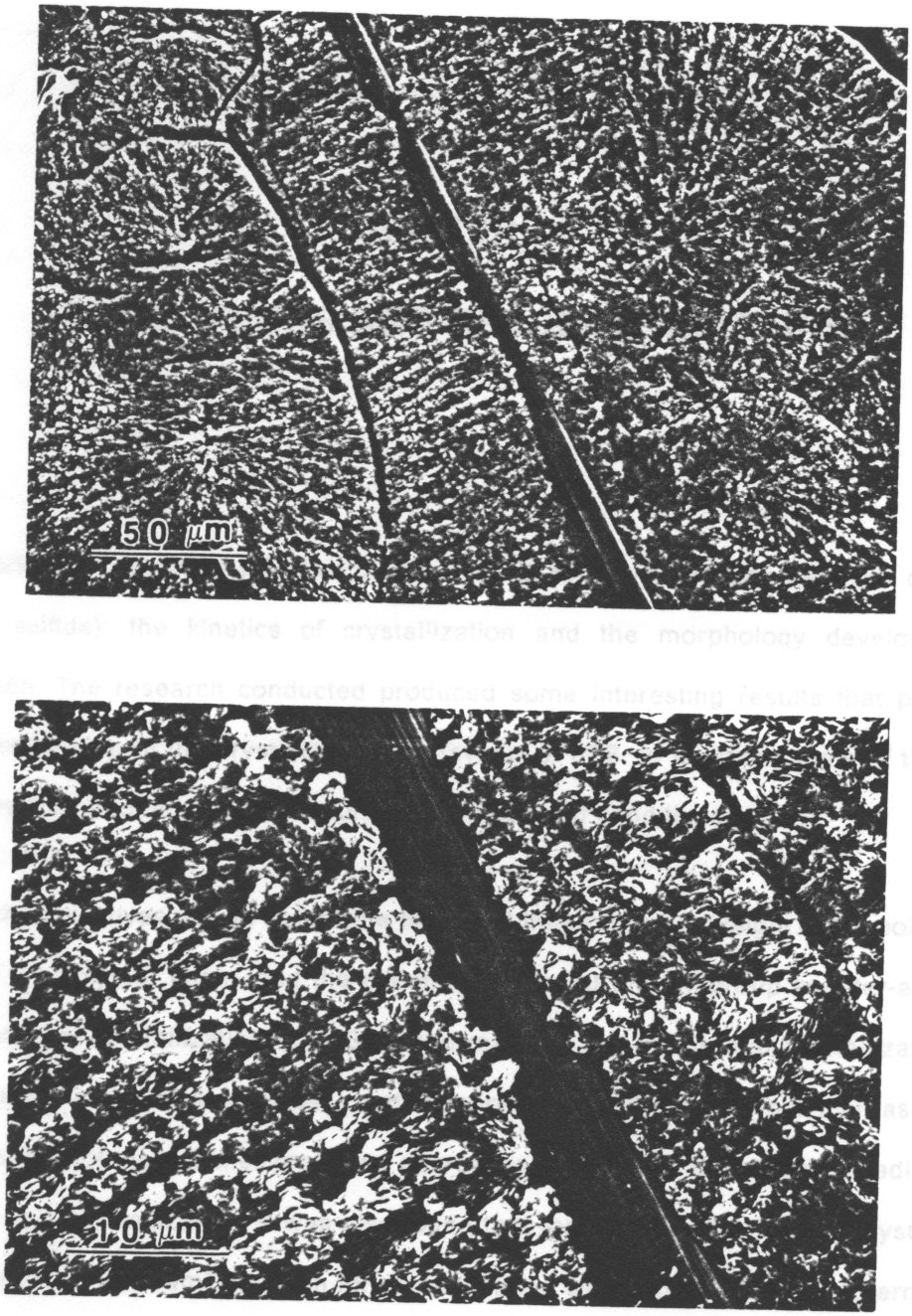


**Figure 79. SEM micrographs of PPS/T300U carbon fibers etched with aluminum chloride reagent.**

# CHAPTER IX

# CONCLUSIONS AND RECOMMENDATIONS

This work was concerned with two major areas of the crystallization behavior of poly (p-phenylene sulfide): the kinetics of crystallization and the morphology developed upon crystallization. The research conducted produced some interesting results that provided a better understanding of the crystallization behaviour of PPS. In addition, some of the results can be translated into more efficient control of processing conditions.

One of the objectives was to determine the effect that molecular weight of the polymer, the topology of the polymer chain, and the chemical nature of the endgroup counter-atom have on the kinetics of crystallization of PPS. Isothermal and non-isothermal crystallization techniques were utilized. The isothermal crystallization results indicated that increases in the molecular weight of the polymer produced decreases of the rates of spherulitic radial growth and overall bulk crystallization. It was also found that the overall rates of bulk crystallization followed the general Avrami equation for crystallization with exponent $\sim 3$. Furthermore, low molecular weight PPS presented a much lower nucleation density than PPS with higher molecular weight. The spherulitic radial growth rates were analyzed in terms of theoretical equations proposed to explain the molecular weight dependence of the growth rate. It was found that the logarithm of the radial growth rate was a linear function of the logarithm of the

number average molecular weight proposed by Cheng and Wunderlich ( ). However, the molecular weights available were limited. Therefore, further investigation in this area would include the gathering of crystallization data for a wider range of molecular weights of PPS. This would allow the performance of a more complete statistical analysis to test the models analyzed previously.

The effect of topology of the polymer chain was studied with samples that were synthesized with different concentrations of branching agent trichlorobenzene (TCB) in the reaction vessel. An increase of the concentration of branching agent produced decreases in the radial spherulitic growth rates and overall rate of bulk crystallization. The overall rate of bulk crystallization followed a simple Avrami equation for bulk crystallization with exponent $\sim 3$. This is in contrast with results previously reported for linear low density polyethylene (LLDPE). In the latter case, it has been reported that crystallization rates did not follow a simple Avrami equation, and values of the Avrami exponent were as low as unity (163-165). This contrast was attributed to the fact that PPS seems to have long branches as opposed to the short branches that LLDPE has. In this respect, it would be interesting to study the changes in the morphology of branched PPS as branch content increases. This kind of investigation would require the use of solid state nuclear magnetic resonance (NMR) or high temperature solution NMR to characterize the concentration of branches and possibly their distribution on the polymer chain. NMR measurements have been precluded to date due to the high insolubility of PPS at room temperature. PPS is soluble only at high temperatures (200°C). Therefore, it is very difficult to find an appropriate solvent to perform the NMR experiments. Although the long spacing determined by small angle x-ray scattering was found to be the same for linear PPS and PPS containing 0.2% by weight of TCB, the lamellar thickness is expected to decrease as branch concentration increases. Then, the lamellar thickness may be determined as a function of branch concentration utilizing small angle x-ray scattering (219) and transmission electron microscopy. Furthermore, the crystal perfection can also be studied by x-ray diffraction techniques to determine if the branching points are distorting the crystal lattice. Such an effect has

been observed in branched polyethylene (LDPE). It has been found that branches longer than butyl groups can be incorporated into the crystal lattice of branched polyethylene (220). The incorporation of branches causes an expansion of the crystalline lattice that can be detected by determining the lattice parameters by means of wide angle x-ray scattering experiments. Therefore, it may be interesting to investigate whether the branch points in PPS are included in the crystalline lattice as defects, similar to what happens in branched polyethylene.

The presence of branches in PPS also decreased the nucleation density in the polymer, the heat of crystallization and the thermodynamic melting point, indicating that the crystalline content and crystal perfection of the branched polymer are lower than those of the linear PPS. These results may have some importance in the thermoplastic composites area. One problem that highly crystalline matrices have is their brittleness after crystallization. Perhaps, upon addition of branched polymer into PPS matrices for carbon fiber composites may help reduce the crystallinity of the matrix to a certain extent. This might reduce some of the brittleness problem without affecting the high chemical resistance that characterizes PPS.

The chemical nature of the endgroup conter-atom was found to affect the crystallization rates and nucleation densities of PPS. The spherulitic radial growth rates decreased in the order of counter-atom calcium > hydrogen > zinc > sodium. These results are not fully understood. It can be argued that there is a molecular weight increase due to chain extension by means of the ionic endgroups. In this respect, a highly electropositive cation would be expected of causing a more important effect. For example, sodium would form strong ionic bonds with the endgroups. Similarly, calcium would also be able to form strong ionic bonds. Moreover, since calcium is divalent, it might be able to cause chain extension more efficiently than sodium producing a slower crystal growth rate. The experimental results, however, present the reverse trend. Therefore, this is not a plausible explanation. The overall rates of bulk crystallization decreased in the order hydrogen > zinc > calcium > sodium. Consequently, the nucleation density played an important role. Indeed, results indicated that the nucleation densities varied in decreasing order as hydrogen > sodium > zinc > calcium. The author does

not have a full understanding of the effect of endgroup counter-atom on the crystallization behavior of PPS; however, the results are quite reproducible. Further experimentation is required to acquire a better understanding of these results. Two variables would need to be investigated: (1) the effect of the ionic character of the endgroup-counteratom bond, and (2) the effect of the oxidation state of ionic counter-atoms. For example, (1) may be studied utilizing lithium as a counter-atom. Lithium would form bonds with ionic character in between those of hydrogen and sodium. The second effect may be investigated using counter-atoms of similar ionic character but different oxidation states, perhaps sodium, calcium and ferric counterions would serve the purpose.

Since most polymer processing operations occur under non-isothermal conditions, the non-isothermal kinetics of crystallization of PPS were investigated. The non-isothermal crystallization of PPS indicated that non-isothermal DSC data can be analyzed by the model proposed by Ozawa (171). This model allowed the determination of the Avrami exponent under non-isothermal conditions. The values of n obtained were in agreement with values determined by means of isothermal methods. Moreover, the analysis of Ozawa permitted the study of the crystallization behavior of PPS in a wider temperature range, indicating that this technique can be a complementary tool for the investigation of the crystallization of polymers.

The morphological superstructures of PPS were investigated utilizing a chromic acid and an aluminum chloride etching technique. The latter one demonstrated a higher degree of texture enhancement by rapidly degrading amorphous PPS. This technique highlighted the fine structure present in the spherulitic material. It allowed the observation of the spherulitic growth habit and the "interconnectivity" between impinged spherulites. Furthermore, it proved useful in the study of the morphology of PPS in composite materials with carbon fibers. Another application of this technique that may be attempted is the preparation of samples for transmission electron microscopy or scanning transmission electron microscopy. In this respect, the investigation of the morphological structure of strain induced crystallized PPS would be of special interest since PPS is utilized in fibers and films.

The morphology of PPS in composite materials containing few carbon fibers were analyzed utilizing optical microscopy. In particular, a few variables that affect the formation of transcrystallinity were identified. It was found that low crystallization temperatures, slow cooling rates, low molecular weight of PPS and stresses favored the nucleation of transcrystallinity at the carbon fiber surface. T300U carbon fibers from Union Carbide were the most effective in nucleating transcrystallinity. Fiber anodization in $H_2SO_4$ and NaOH electrolytes decreased the nucleating ability of the fibers possibly due to an increase of polarity at the fiber surface. Utilization of the aluminum chloride etching technique in conjunction with scanning electron microscopy confirmed that PPS was nucleating at the fiber surface. It also showed the radial growth habit and cylindrical symmetry of the transcrystalline regions. Further investigation in this area would involve the application of the crystallization conditions indicated in this study to composite materials with high fiber concentration. Their morphology would then be studied by utilizing the aluminum chloride etching technique and scanning electron microscopy. Finally, the effect of transcrystallinity on the properties of the composites would be analyzed to establish correlations between structure and properties.

# REFERENCES CITED


1. M. P. Grenvesse, Bull. Soc. Chim. 17, 599 (1898).
2. A. D. Macallum, J. Org. Chem. 13, 154 (1948).
3. R. W. Lenz and W. K. Carrington, J. Polym. Sci. 41, 333 (1959).
4. R. W. Lenz and C. E. Handlovits, J. Polym. Sci. 43, 167 (1960).
5. R. W. Lenz, C. E. Handlovits, and H. A. Smith, J. Polym. Sci. 58, 351 (1962).
6. J. T. Edmonds, Jr., and H. W. Hill, Jr., U.S. Patent 3,354,129 to Phillips Petroleum Company (November 1967).
7. J. F. Geibel, Personal Communication.
8. C. J. Stacy, J. Appl. Polym. Sci. 32, 3959 (1986).
9. R. T. Hawkins, Macromolecules 9, 189 (1976).
10. W. D. Powell, Spec. Plast. Educ., Tech. Pap., Annu. Pac. Tech. Conf., 2nd, 268 (1976).
11. H. W. Hill, Jr., and D. G. Brady, Polym. Eng. Sci. 16, 832 (1976).
12. J. N. Short and H. W. Hill, Jr., Chem. Tech. 2, 481 (1972).
13. T. C. Clarke, K. K. Kanazawa, V. Y. Lee, J. F. Rabolt, J. R. Reynolds, and G. B. Street, J. Polym. Sci.: Polym. Phys. Ed. 20, 117 (1982).
14. J. E. Frommer, R. L. Elsenbaumer, H. Eckhart, and R. R. Chance, J. Polym. Sci.: Polym. Letter. Ed. 21, 39 (1983).
15. J. J. B. Deuss, Rec. Trav. Chim. 28, 136 (1909).
16. T. P. Hilditch, J. Chem. Soc. 97, 2579 (1910).
17. H. B. Glass and E. E. Reid, J. Am. Chem. Soc. 51, 3428 (1928).
18. B. Hortling and J. Lindberg, Makromol. Chem. 179, 1707 (1978).
19. D. G. Brady, J. Appl. Polym. Sci.: Appl. Polym. Symp. 36, 231 (1981).
20. C. R. Rajan, S. Ponrathman, and V. M. Nadkarni, J. Appl. Polym. Sci. 32, 4479 (1986).

21. S. Radhakrishnan, C. R. Rajan, and V. M. Nadkarni, J. Mater. Sci. 21, 597 (1986).

22. W. D. Reents, Jr., and K. L. Kaplan, Polymer 23, 310 (1982).

23. D. R. Battiste, R. D. Cody, and C. E. Brown, Preprint.

24. G. Montaudo, C. Puglisi, E. Scamporrino, and D. Vitalini. Macromolecules 19, 2157 (1986).

25. R. W. Campbell, U.S. Patent 3,919,177 to Phillips Petroleum Company (November 1975).

26. R. S. Shue, Dev. Plast. Technol. 2, 259 (1985).

27. H. W. Hill, Jr., Ind. Eng. Chem. Prod. Res. Dev. 18, 4 (1979).

28. W. Koch and W. Heitz, Makromol. Chem. 184, 779 (1983).

29. M. Wejchan-Judek and E. Rogal, Polym. Comm. 25, 53 (1984).

30. M. Wejchan-Judek, Polym. Bull. 15, 141 (1986).

31. L. Kreja, A. Warszawski, and W. Czerwinski, Angew. Makromol. Chem. 141, 77 (1986).

32. A. B. Port and R. H. Still, Polym. Deg. Stab. 1, 133 (1979).

33. M. Novi, G. Petrillo, and M. L. Sartirana, Tetrahedron Lett. 27, 6129 (1986).

34. J. O. Reed and R. D. Mathis, a) Eur. Pat. 94092 to Phillips Petroleum Co. (November 1983). b) U.S. Patent 4,478,969 to Phillips Petroleum Co. (October 1984).

35. H. W. Hill, Jr., and D. G. Brady, "Encyclopedia of Chemical Technology", 18, 793 (1982).

36. M. Wejchan-Judek and A. Zuk, Polym. Deg. Stab. 11, 55 (1985).

37. D. G. Brady, J. Appl. Polym. Sci. 20, 2541 (1976).

38. H. Zeng and G. Ho, Angew. Makromol. 127, 103 (1984).

39. S. G. Joshi and S. Radhakrishnan, Thin Solid Films 142, 213 (1986).

40. V. A. Sergeyev, V. K. Shitikov, V. I. Nedel'kin, A. A. Askadskii, K. A. Bychko, G. L. Slonimskii, and V. V. Korshak, Polym. Sci. USSR 19, 1494 (1977).

41. R. M. Black, C. F. List and R. J. Wells, J. Appl. Chem. 17, 269 (1967).

42. N. S. J. Christopher, J. L. Cotter, G. J. Knight, and W. W. Wright, J. Appl. Polym. Sci. 12, 863 (1968).

43. H. W. Hill, Jr., and J. T. Edmonds, Jr., Adv. Chem. Ser. 129, 80 (1973).

44. S. Tsunawaki and C. C. Price, J. Polym. Sci. A2, 1511 (1964).

45. B. J. Tabor, E. P. Magré, and J. Boon, Eur. Polym. J. 7, 1127 (1971).

46. J. Garbarczyk, Polymer Comm. 27, 335 (1986).

47. A. J. Waddon, M. J. Hill, A. Keller, and D. J. Blundell, J. Material Sci., submitted.

48. T. P. H. Jones, G. R. Mitchell, and A. H. Windle, Colloid Polym. Sci. 261, 110 (1983).

49. C. Anton, M. R. Mackley, and S. B. Solbai, Polym. Bull. 17, 175 (1987).

50. A. Uemura, S. Isoda, M. Tsuji, M. Ohara, A. Kawaguchi, and K. Katayama, Bull. Inst. Chem. Res., Kyoto Univ., Vol. 64, 66 (1986).

51. M. Ito and R. S. Porter, J. Polym. Sci.: Polym. Phys. Ed. 23, 245 (1985).

52. J. P. Jog and V. M. Nadkarni, J. Appl. Polym. Sci. 30, 997 (1985).

53. A. J. Lovinger, D. D. Davis, and F. J. Padden, Jr., Polymer 26(11), 1595 (1985).

54. J. D. Hoffman, G. T. Davis, and J. I. Lauritzen, Jr., in "Treatise in Solid-State Chemistry", Ed. N. B. Hannay, Plenum Press, New York, 1976 Vol. 3, Ch. 7.

55. J. D. Hoffman, Polymer 24, 3 (1983).

56. R. V. Jones and H. W. Hill, Jr., Adv. Chem. Ser. 140, 174 (1975).

57. C. L. Markert, H. E. Blair, and P. G. Kelleher, Therm. Anal., Proc. Int. Conf. 7th, Vol. 2, 1362 (1982), Ed. B. Miller, Wiley, Chichester UK.

58. R. M. Lum, Polym. Prepr., Am. Chem. Soc., Div. Polym. Chem. 18(1), 761 (1977).

59. B. Hortling, Makromol. Chem. 178, 2185 (1977).

60. G. F. L. Ehlers, K. R. Fisch, and W. R. Powell, J. Polym. Sci.: Part A1, 7, 2955 (1969).

61. L. W. Shacklette and J. E. Toth, J. Chem. Soc., Chem. Commun. 20, 1159 (1983).

62. K. Udipi, Polym. Prepr., Am. Chem. Soc., Div. Polym. Chem. 28(1), 217 (1987).

63. A. Kaul, Polym. Prepr., Am. Chem. Soc., Div. Polym. Chem. 28(1), 229 (1987).

64. J. N. Murray, Soc. Plast. Eng., Tech. Pap. 22, 259 (1976).

65. V. C. Vives, J. S. Dix, and D. G. Brady, ACS Symp. Ser. 229, 65 (1983).

66. T. W. Johnson, U.S. Patent 4,426,500 to Phillips Petroleum Company.

67. A. Eisenberg and B. Cayrol, J. Polym. Sci.: Part C 35, 129 (1971).

68. S. J. Rigby and D. Dew-Hughes, Polymer 15, 639 (1974).

69. S. Schlick and B. R. McGarvey, Polym. Comm. 25, 369 (1984).

70. R. F. Boyer, Polym. Eng. Sci. 8, 161 (1968).

71. C. E. Brown, I. Khoury, M. D. Bezoari, and P. Kovacic, J. Polym. Sci.: Polym. Chem. Ed. 20, 1697 (1982).

72. K. Yoshino, M. S. Yoon, M. Ozaki, S. H. Kim, Y. Inuishi, and J. Kyokane, Jpn. J. Appl. Phys.: Part 1, 22(10), 1510 (1983).

73. S. Saito, T. Tsutsui, S. Tokito, T. Hara, and H. Chin, Polymer J. 17, 209 (1985).

74. T. Tsutsui, N. Nitta, and S. Saito, J. Appl. Phys. 57, 5367 (1985).

75. K. Yoshino, M. S. Yun, M. Ozaki, and Y. Inuishi. Jpn. J. Appl. Phys.: Part 2, 23(1), 55 (1984).

76. Y. Takai, M. Inoue, A. Shibata, T. Mizutani, and M. Ieda. Jpn. J. Appl. Phys.: Part 1, 23(1), 1614 (1984).

77. Y. W. Park, M. A. Druy, C. K. Chiang, A. G. MacDiarmid, A. J. Seeger, H. Shirakawa, and S. Ikeda, J. Polym. Sci.: Polym. Lett. Ed. 17, 195 (1979).

78. D. M. Ivory, G. G. Miller, J. M. Sowa, L. W. Shackelette, R. R. Chance, and R. H. Baughman, J. Chem. Phys. 71, 1506 (1979).

79. K. K. Kanazawa, A. F. Diaz, R. H. Geiss, W. D. Gill, J. F. Kwak, L. A. Logan, J. F. Rabolt, and G. B. Street, J. Chem. Soc.: Chem. Comm. 854 (1979).

80. J. F. Rabolt, T. C. Clarke, K. K. Kanazawa, J. R. Reynolds, and G. B. Street, J. Chem. Soc.: Chem. Comm. 347 (1980).

81. R. R. Chance, L. W. Shacklette, G. G. Miller, D. M. Ivory, J. M. Sowa, R. L. Elsenbaumer, and R. H. Baughman, J. Chem. Soc.: Chem. Comm. 348 (1980).

82. R. L. Elsenbaumer, L. W. Shacklette, J. W. Sowa, and R. H. Baughman, Mol. Cryst. Liq. Cryst. 83, 229 (1982).

83. R. R. Chance, L. W. Shacklette, H. Eckhardt, J. M. Sowa, R. L. Enselbaumer, D. M. Ivory, G. G. Miller, and R. H. Baughman, Polym. Sci. Technol. 15 (Conductive Polymers), 125 (1981).

84. L. W. Shacklette, R. L. Elsenbaumer, R. R. Chance, H. Eckhardt, J. E. Frommer, and R. H. Baughman, J. Chem. Phys. 75, 1919 (1981).

85. N. S. Murthy, R. L. Elsenbaumer, J. E. Frommer, and R. H. Baughman, Synth. Met. 9(1), 91 (1984).

86. R. L. Elsenbaumer and L. W. Shacklette, J. Polim. Sci.: Polym. Phys. Ed. 20, 1781 (1982).

87. S. K. Tripathy, D. Kitchen, and M. A. Druy, Macromolecules 16, 190 (1983).

88. J. E. Frommer, R. L. Elsenbaumer, H. Eckhardt, L. W. Shacklette, and R. R. Chance, Polym. Prepr., Am. Chem. Soc., Div. Polym. Chem. 23(1), 107 (1981).

89. J. E. Frommer, R. L. Elsenbaumer, H. Eckhardt, and R. R. Chance, J. Polym. Sci.: Polym. Lett. Ed. 21, 39 (1983).

90. H. Reiss and W. D. Murphy, J. Phys. Chem. 89, 2596 (1985).

91. J. E. Frommer, R. L. Elsenbaumer, and R. R. Chance, Org. Coat. Appl. Polym. Sci. Proc. 48, 552 (1983).

92. H. Shimizu, Y. Tanabe, and H. Kanetsuna. Polymer J. 18, 367 (1986).

93. D. R. Rueda, T. A. Ezquerra, M. E. Cagiao, F. J. Balta-Calleja, and J. Alonso-Lopez, Mol. Cryst. Liq. Cryst. 118, 263 (1985).

94. K. F. Schoch, Jr., Polym. Prepr., Am. Chem. Soc., Div. Polym. Chem. 25(2), 278 (1984).

95. S. Kazama, K. Arai, and Maekawa, Synth. Met. 15(4), 299 (1986).

96. K. F. Schoch, Jr., J. F. Chance, and K. E. Pfeiffer, Macromolecules 18, 2389 (1985).

97. M. Rubner, P. Cukor, H. Jopson, and W. Deits, J. Electron. Mater. 11, 261 (1982).

98. S. Tokito, T. Tsutsui, and S. Saito, Polymer J. 17, 959 (1985).

99. M. Kawano, S. Shichijyo, T. Horiuchi, K. Matsushige, and T. Takemura, Jpn. J. Appl. Phys.: Part 1, 23(8), 979 (1984).

100. J. Tsukamoto and K. Matsumura, Jpn. J. Appl. Phys.: Part 2, 23(8), 584 (1984).

101. M. S. Yun and K. Yoshino, J. Appl. Phys. 58, 1950 (1985).

102. K. Yoshino, J. Kyokane, M. Ozaki, M. S. Yun, and Y. Inuishi, Jpn. J. Appl. Phys.: Part 2, 22(5), 289 (1983).

103. H. Mazurek, D. R. Day, E. W. Maby, J. S. Abel, S. D. Senturia, M. S. Dresselhaus, and G. Dresselhaus, J. Polym. Sci.: Polym. Phys. Ed. 21, 537 (1983).

104. B. Wasserman, M. S. Dresselhaus, G. Braunstein, G. E. Wnek, and G. Roth, J. Electron. Mater. 14(2), 157 (1985).

105. K. F. Schoch, Jr. and J. Bartko, Polymer 28, 556 (1987).

106. H. Zeng and K. Mai, Makromol. Chem. 187, 1787 (1986).

107. H. Zeng, G. He, and Y. Li, Gaofenzi Tongxun 2, 97 (1986).

108. H. Zeng, G. He, and G. Yang, Angew. Makromol. Chem. 143, 25 (1986).

109. T. E. Fisher and M. J. Balow, Plast. Eng. 39(4), 31 (1983).

110. V. M. Nadkarni and J. P. Jog, J. Appl. Polym. Sci. 32, 5817 (1986).

111. T. P. Murtha, C. C. Ma, A. South, J. H. Walker, and D. G. Brady, Natl. SAMPE Symp. Exhib. Proc. 29, 870 (1984).

112. A. Y. Lou, Natl. SAMPE Symp. Exhib. Proc. 30, 786 (1985).

113. C. Lhymn, J. Mater. Sci. Lett. 4, 1221 (1985).

114. C. Lhymn, J. Mater. Sci. Lett. 4, 1217 (1985).

115. C. Lhymn, J. Mater. Sci. Lett. 4, 1429 (1985).

116. C. Lhymn and J. M. Schultz, J. Mater. Sci. Lett. 4, 1244 (1985).

117. C. Lhymn, J. Mater. Sci. Lett. 5, 260 (1986).

118. C. C. M-Ma, J. E. O'Connor, and A. Y. Lou, SAMPE Q. 15(7), 12 (1984).

119. J. J. Hartness, SAMPE J. 20 (5), 26 (1984).

120. T. W. Johnson and C. L. Ryan, Int. SAMPE Symp. Exhib. 32, 1537 (1986).

121. F. N. Cogswell, Natl. SAMPE Symp. 28, 528 (1983).

122. Y. Lee and R. S. Porter, Polym. Eng. Sci. 26, 633 (1986).

123. C. M. Tung and J. P. Dynes, J. Appl. Polym. Sci. 33, 505 (1987).

124. P. H. Lindenmeyer, N. T. Gerken, and C. H. Sheppard, Int. SAMPE Tech. Conf. 18, 45 (1986).

125. B. Wunderlich, Macromolecular Physics, Vol. 2 "Crystal Nucleation, Growth, Annealing", Academic Press (1976).

126. F. Von Goler and G. Sachs, Z. Physik 77, 281 (1932).

127. W. A. Johnson and R. F. Mehl, Trans. Am. Inst. Mining Met. Engrs. 135, 416 (1939).

128. R. U. Evans, Trans. Faraday Soc. 41, 365 (1945).

129. M. Avrami, J. Chem. Phys. 7, 1103 (1939); J. Chem. Phys. 8, 212 (1940); J. Chem. Phys. 9, 177 (1941).

130. L. Mandelkern, "Crystallization of Polymers", McGraw-Hill, 1964, Ch. 8.

131. F. P. Price, J. Polym. Sci.: Part A 3, 3079 (1965).

132. I. H. Hillier, J. Polym. Sci.: Part A 3, 3067 (1965).

133. F. P. Price, J. Appl. Phys. 36, 3014 (1965).

134. J. D. Hoffman and J. I. Lauritzen, Jr., J. Res. Nat. Bur. Std., Phys. Chem. 65A, 297 (1961).

135. D. Y. Yoon and P. J. Flory, Disc. Faraday Soc. 68, 288 (1979).

136. J. D. Hoffman, C. M. Guttman, and E. A. DiMarzio, Disc. Faraday Soc. 68, 177 (1979).

137. Y. Fujiwara, J. Appl. Polym. Sci. 4, 10 (1960).

138. J. I. Lauritzen, Jr., and J. D. Hoffman, J. Appl. Phys. 44, 4340 (1973).

139. R. C. Allen and L. Mandelkern, Polymer Bull. 17, 473 (1987).

140. J. Martínez-Salazar, P. J. Barham, and A. Keller, J. Polym. Sci.: Polym. Phys. Ed. 22, 1085 (1984).

141. Z. Pelzbauer and A. Galeski, J. Polym. Sci.: Part C 38, 22 (1972).

142. E. J. Clark and J. D. Hoffman, Macromolecules 17, 878 (1984).

143. E. N. Dalal and P. J. Phillips, J. Polym. Sci.: Polym. Lett. Ed. 22, 7 (1984).

144. B. C. Edwards, J. Polym. Sci.: Polym. Phys. Ed. 13, 1387 (1975).

145. J. I. Lauritzen, Jr., and E. Passaglia, J. Res. Nat. Bur. Std. 71A, 261 (1967).

146. J. I. Lauritzen, Jr., E. A. DiMarzio, and E. Passaglia, J. Chem. Phys. 45, 4444 (1966).

147. I. C. Sanchez and E. A. DiMarzio, J. Chem. Phys. 55, 893 (1971).

148. C. Devoy and L. Mandelkern, J. Polym. Sci.: Part A2 7, 1889 (1969).

149. J. D. Hoffman and J. J. Weeks, J. Chem. Phys. 37, 1723 (1962).

150. J. H. Magill, J. Appl. Phys. 35, 3249 (1964).

151. E. G. Lovering, J. Polym. Sci.: Part C 30, 329 (1970).

152. J. D. Hoffman, Polymer 23, 656 (1982).

153. J. H. Magill and H. M. Li, Polymer 19, 416 (1978).

154. S. Z. D. Cheng and B. Wunderlich, J. Polym. Sci.: Polym. Phys. Ed. 24, 595 (1986).

155. Van Antwerpen, F., and van Krevelen, D. W., J. Polym. Sci.: Polym. Phys. Ed. 1972, 10, 2423.

156. Hoffman, J. D., and Weeks, J. J., J. Res. Natl. Bur. Standards 1962, 66A, 13.

157. Lauritzen, J. I., Jr., and Hoffman, J. D., J. Res. Natl. Bur. Standards 1960, 64A, 73.

158. D. R. Norton and A. Keller, J. Mater. Sci. 19, 447 (1984).

159. L. Mandelkern, M. Glotin, and R. A. Benson, Macromolecules 14, 22 (1981).

160. L. Mandelkern and J. Maxfield, J. Polym. Sci.: Polym. Phys. Ed. 17, 1913 (1979).

161. T. Kawai, K. Ujihara, and H. Maeda, Makromol. Chem. 132, 87 (1970).

162. I. G. Voight-Martin, R. Alamo, and L. Mandelkern, J. Polym. Sci.: Polym. Phys. Ed. 24, 1283 (1986).

163. G. R. Strobl, T. Engelke, E. Maderek, and G. Urban, Polymer 24, 1585 (1983).

164. E. Maderek and G. R. Strobl, Colloid & Polymer Sci. 261, 471 (1983).

165. W. Banks, M. Gordon, R. J. Roe, and A. Sharples, Polymer 4, 61 (1963).

166. G. R. Strobl, M. Schneider, and I. Voight-Martin, J. Polym. Sci.: Polym. Phys. Ed. 18, 1361 (1980).

167. R. Legras, C. Bailly, M. Daumerie, J. M. Dekoninck, J. P. Mercier, V. Zichy, and E. Nield, Polymer 25, 835 (1984).

168. C. Bailly, M. Daumerie, R. Legras, and J. P. Mercier, J. Polym. Sci.: Polym. Phys. Ed. 23, 751 (1985).

169. A. Ziabicki, Appl. Polym. Symp. 6, 1 (1967).

170. K. Harnisch and H. Muschik, Coll. Polym. Sci. 261, 908 (1983).

171. T. Ozawa, Polymer 12, 150 (1971).

172. A. Jeziorny, Polymer 19, 1142 (1978).

173. W. H. Jo and S. D. Kim, Polymer (Korea) 9, 537 (1985).

174. J. L. Acosta, M. C. Ojeda, E. Morales, and A. Linares, J. Appl. Polym. Sci. 32, 4119 (1986).

175. M. Eder and A. Wlochowicz, Polymer 24, 1593 (1983).

176. B. Monasse, J. M. Escleine, and J. M. Haudin, 29th Int. Symp. on Macromolecules, IUPAC Macro 83, Bucharest, Section IV, 146 (1983).

177. B. Monasse and J. M. Haudin, Coll. Polym. Sci. 264, 117 (1986).

178. W. Kozlowski, J. Polym. Sci.: Part C 38, 47 (1972).

179. L. C. López and G. L. Wilkes, Polymer, in press.

180. O. A. Battista, Am. Sci. 53, 151 (1965).

181. R. P. Palmer and A. J. Cobbold, Macromol. Chem. 74, 174 (1964).

182. A. Keller and S. Sawada, Macromol. Chem. 74, 190 (1964).

183. I. M. Ward and T. Williams, J. Macromol. Sci. Phys. B5(4), 693 (1971).

184. R. H. Olley, A. M. Hodge, and D. C. Bassett, J. Polym. Sci., Polym. Phys. Ed. 17, 627 (1979).

185. D. R. Fitchmun and S. Newman, J. Polym. Sci.: Part A2, 8, 1545 (1970).

186. B. K. Carter and G. L. Wilkes, in "Polymers as Biomaterials", Edited by S. W. Shalaby, A. S. Hoffman, B. D. Ratner and T. A. Horbett, Plenum Press, 1984.

187. E. W. Fischer, H. J. Sterzel, and G. Wegner, Kolloid Z. Z. Polymere 251, 980 (1973).

188. J. L. Koenig and M. C. Agboatwalla, J. Macromol. Sci.: Phys. B2(3), 391 (1968).

189. F. P. Reding and E. R. Walter, J. Polym. Sci. 38, 141 (1959).

190. J. Muccigrosso and P. J. Phillips, I.E.E.E. Trans. Electr. Insul. Vol.EI-13, No.3, 172 (1978).

191. G. W. Bailey, J. Polym. Sci. 62, 241 (1962).

192. B. C. Edwards and P. J. Phillips, Polymer 15, 351 (1974).

193. C. M. Chu and G. L. Wilkes, J. Macromol. Sci.: Phys. B10(4), 551 (1974).

194. F. R. Anderson and V. F. Holland, J. Appl. Phys. 31(9), 1516 (1960).

195. B. J. Spit, Polymer 4, 109 (1963).

196. H. Nishimura, T. Yarita, and M. Noshiro, Asahi Garasu Kankyu Hokoku 33(2), 151 (1983).

197. H. D. Keith, J. Polymer Sci. A2, 4339 (1964).

198. K. Kubota, J. Polym. Sci.: Part B 3, 545 (1965).

199. H. D. Keith, F. J. Padden, Jr., and R. G. Vadimsky, J. Appl. Phys. 24(12), 4585 (1971).

200. V. A. Sergeyev and V. I. Nedelkin, J. Polym. Sci.: Polym. Chem. Ed. 24, 3153 (1986).

201. A. Misra, B. L. Depoura, S. F. Xavier, F. D. Hartley, and R. H. Peters, Angew. Makromol. Chem. 113, 113 (1983).

202. H. J. Folkes and S. T. Hardwick, J. Mater. Sci. Lett. 3, 1071 (1984).

203. M. R. Kants and R. D. Corneliussen, J. Polym. Sci.: Polym. Lett. Ed. 11, 279 (1973).

204. D. Campbell and M. M. Qayyum, J. Polym. Sci.: Polym. Phys. Ed. 18, 83 (1980).

205. M. G. Huson and W. J. McGill, J. Polym. Sci.: Polym. Phys. Ed. 23, 121 (1985).

206. M. J. Folkes, S. T. Hardwick, and W. K. Wong, in "Polymer Composites", Ed. B. Sedlacek, W. de Gruyter & Co., Berlin (1986), p.33.

207. T. K. Kwei, H. Schonhorn, and M. L. Frisch, J. Appl. Phys. 38, 2512 (1967).

208. D. R. Fitchmun and S. Newman, J. Polym. Sci.: Part A-2 8, 1545 (1970).

209. A. M. Chatterjee, F. P. Price, and S. Newman, J. Polym. Sci.: Polym. Phys. Ed. 13, 2369 (1975).

210. D. Turnbull and B. Vonnegut, Ind. Eng. Chem. 44, 1292 (1952).

211. T. Bessel and J. B. Shortall, J. Mater. Sci. 10, 2035 (1975).

212. H. Schonhorn and F. W. Ryan, J. Polym. Sci.: Part A-2 6, 231 (1968).

213. B. Wunderlich, Macromolecular Physics, Vol. 1, Academic Press, New York (1973).

214. D. G. Gray, J. Polym. Sci.: Polym. Lett. Ed. 12, 645 (1974).

215. D. Fitchmun and S. Newman, J. Polym. Sci.: Polym. Lett. Ed. 7, 301 (1969).

216. T. A. Devilbiss, Doctoral Dissertation, VPI&SU (1987).

217. A. M. Ibrahim, T. K. Shah, L. J. Matienzo and J. D. Venables, SAMPE J., in press.

218. A. Lustiger, SAMPE J. 20(5), 13 (1984).

219. G. R. Strobl and M. Schneider, J. Polym. Sci.: Polym. Phys. Ed. 19, 1343 (1980).

220. M. Sanchez Cuesta, J. Martínez Salazar, and F. J. Baltá Calleja, Polymer Bull. 17, 23 (1987).

**The vita has been removed from the scanned document**